Strategies to enhance extracellular electron transfer rates in wild-type cyanobacterium *Synechococcus elongatus* PCC7942 for photo-bioelectricity generation

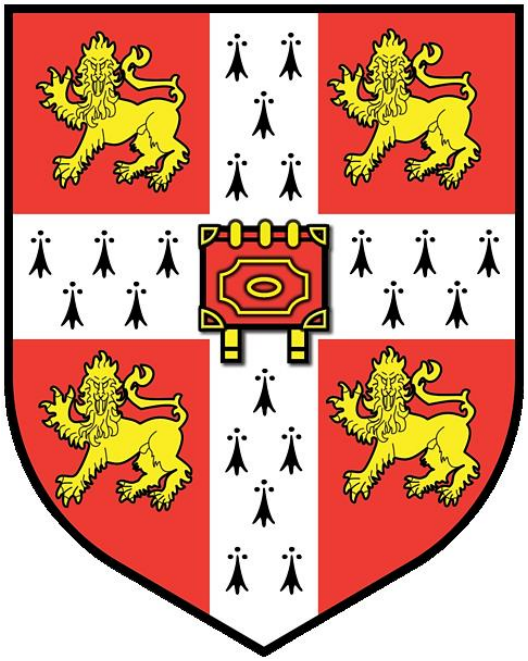

Arely Carolina Gonzalez Aravena

Department of Chemical Engineering and Biotechnology

University of Cambridge

This dissertation is submitted for the degree of
Doctor of Philosophy

September 2017
Churchill College

Strategies to enhance extracellular electron transfer rates in wild-type cyanobacterium *Synechococcus elongatus* PCC7942 for photo-bioelectricity generation

Arely Carolina Gonzalez Aravena

Abstract

The aim of this thesis is to enhance the extracellular electron transfer rates (exoelectrogenesis) in cyanobacteria, to be utilised for photo-bioelectricity generation in biophotovoltaics (electrochemical cell).

An initial cross comparison of the cyanobacterium *Synechococcus elongatus* PCC7942 against other exoelectrogenic cultures showed a hindered exoelectrogenic capacity. Nonetheless, in mediatorless biophotovoltaics, it outperformed the microalgae *Chlorella vulgaris*. Furthermore, the performance of *S. elongatus* PCC7942 was improved by constructing a more efficient design (lower internal resistance), which was fabricated with carbon fibres and nitrocellulose membrane, both inexpensive materials.

To strategically obtain higher exoelectrogenic rates, *S. elongatus* PCC7942 was conditioned by iron limitation and CO_2 enrichment. Both strategies are novel in improving cyanobacteria exoelectrogenesis. Iron limitation induced unprecedented rates of extracellular ferricyanide reduction (24-fold), with the reaction occurring favourably around neutral pH, different to the cultural alkaline pH. Iron limited cultures grown in 5% and 20% CO_2 showed increased exoelectrogenic rates in an earlier stage of growth in comparison to air grown cultures. Conveniently, the cultural pH under enriched CO_2 was around neutral pH.

Enhanced photo-bioelectricity generation in ferricyanide mediated biophotovoltaics was demonstrated. Power generation was six times higher with iron limited cultures at neutral pH than with iron sufficient cultures at alkaline pH. The enhanced performance was also observed in mediatorless biophotovoltaics, especially in the dark phase. Exoelectrogenesis was mainly driven by photosynthetic activity. However, rates in the dark were also improved and in the long term it appeared that the exoelectrogenic activity under illumination tended to that seen in the dark.

Proteins participating in iron uptake by an alleged reductive mechanism were overexpressed (2-fold). However, oxidoreductases in the outer membrane remain to be identified. Furthermore, electroactive regions in biofilms of *S. elongatus* PCC7942 were established using cyclic voltammetry. Double step potential chronoamperometry was also successfully tested in the biofilms. Thus, the electrochemical characterisation of *S. elongatus* PCC7942 was demonstrated, implying that the strategies presented in this thesis could be used to screen for cyanobacteria and/or electrode materials to further develop systems for photo-bioelectricity generation.

In memory of my father who always believed in me.

Preface

The work described in this PhD thesis was carried out in the Department of Chemical Engineering and Biotechnology at the University of Cambridge, between October 2013 and September 2017.

This dissertation is the result of my own work and includes nothing which is the outcome of work done in collaboration except as declared and specified in the text.

It is not substantially the same as any that I have submitted, or, is being concurrently submitted for a degree or diploma or other qualification at the University of Cambridge or any other University or similar institution. I further state that no substantial part of my dissertation has already been submitted, or, is being concurrently submitted for any such degree, diploma or other qualification at the University of Cambridge or any other University or similar institution.

This thesis contains 64,336 words and 99 figures.

Arely Carolina Gonzalez Aravena
Department of Chemical Engineering and Biotechnology
University of Cambridge
September 2017

Acknowledgments

I wish to acknowledge my supervisor Dr Adrian Fisher for all his support during my time as a PhD candidate. I also wish to acknowledge Dr Kamran Yunus for all his help and guidance.

I wish to acknowledge my family. To my husband Damian Brogden for his love and unconditional support, to my mother Nieves Aravena for always being there for me, to my brother Werner Gonzalez for being always a friend, and to the memory of my father Werner Gonzalez for being the inspiration he was for me.

I would like to thank my colleagues in the CREST group, especially my good friend Aazraa Oumayyah for the time shared, help and constant support. Also, to my good friends Antonio del Rio, Dongda Zhang, Fabio Fiorelli, Hassan Alderazi, Jana Weber and Parminder Kaur Heer, for their help and friendship.

I would like to thank my collaborators in NTU Singapore for helping me to carry out some of the work in this thesis. Also, to the staff in electronics, mechanical workshop, stores and technicians in the Department of Chemical Engineering and Biotechnology.

Finally, I would like to acknowledge Conicyt Becas Chile and Cambridge Trust for the financial support I received to pursue my PhD studies.

Contents

Glossary

Term	Description
Air cathode	Oxygen reducing cathode.
Anaerobic	The absence of oxygen.
Autotrophic	Organism with the ability to synthesise organic compounds from simple inorganic compounds such as carbon dioxide for its nutritional requirements.
Bioanode	Anode operated with microbial activity.
Biocathode	Cathode operated with microbial activity.
Biophotovoltaics	Electrochemical cell inoculated with oxygenic photosynthetic microorganisms in the anode.
Counter electrode	Auxiliary electrode for working electrode used for electrical current to flow.
Cyanobacteria	Phylum of bacteria (prokaryotic) capable of oxygenic photosynthesis. Also known as blue-green algae.
Exoelectrogen	Organism capable of exoelectrogenesis.
Exoelectrogenesis	Metabolic process to export electrons extracellularly.
Extracellular	Outside the cellular compartment delimited by the plasma membrane.
Heterotrophic	Organism dependent on external organic compounds for its nutritional requirements.
Mediatorless	In the absence of artificially added redox mediators.
Microalgae	Unicellular algae (eukaryotic), typically autotrophic organisms capable of oxygenic photosynthesis.

Microbial Fuel Cell	Electrochemical cell inoculated with exoelectrogens in the anode, in the cathode or in both.
Nanowire	Electrically conductive appendages in some microorganisms, they correspond to modified *pili* with electron transfer capacity.
Outer membrane	Biological membrane comprising the last semipermeable barrier in the cellular envelope of some bacteria (gram-negative).
Oxygenic	The generation of oxygen.
Photosynthesis	Metabolic process to convert light energy into chemical energy.
Plasma membrane	Biological membrane comprising the cellular envelope of any cell, separating the intracellular compartment with the extracellular environment.
Potentiostat	Electronic instrument that controls the potential of a working electrode against a reference electrode within an electrochemical cell.
Redox mediator	Redox compound shuttling electrons from the electron donor to the electrode.
Reference electrode	Electrode with stable constant potential (normal conditions).
Thylakoid membrane	Intracellular biological membrane found in cyanobacteria and in chloroplasts, containing enzymes for the light reactions in the photosynthetic process.
Working electrode	Electrode in which a reaction of interest occurs.

Nomenclature

Symbol	Description	Units
A	Area	m^2
C	Capacitance	F
D_o	Diffusion coefficient	$m^2\ s^{-1}$
E	Potential	V
E_{eq}	Equilibrium potential	V
E_F	Fermi level potential	V
E_{mf}	Electromotive force	V
E^o	Standard potential	V
E_p^a	Anodic peak potential	V
E_p^c	Cathodic peak potential	V
F	Faradays constant	$C\ mol^{-1}$
ΔG	Gibbs free energy	J
ΔG^o	Standard Gibbs free energy	J
i	Net electrical current	A
i_{mt}	Mass limited current	A
i_o	Exchange current	A
i_p^a	Anodic peak current	A
i_p^c	Cathodic peak current	A

$\mathbf{j_o}$	Diffusion flux	mol m^{-2} s^{-1}
k	Reaction rate constant	s^{-1}
n	Number of moles of electrons	-
OCP	Open circuit potential	V
pH	Measure of acidity or alkalinity, equal to minus $\log_{10}$ of the molar concentration of hydrogen ions	-
$\mathbf{P_{max}}$	Maximum power output	W
$\mathbf{P_{out}}$	Power output	W
Q	Charge	C
R	Universal gas constant	J K^{-1} mol^{-1}
$\mathbf{R_{int}}$	Internal resistance	Ω
$\mathbf{R_L}$	Resistance of the load	Ω
$\mathbf{R_S}$	Resistance of the source	Ω
[R] or [O]	Concentration of species R or O.	M
t	time	s
T	Temperature	K, ^oC
$\mathbf{V_{cell}}$	Voltage of the cell	V
$\mathbf{V_L}$	Voltage drop across the load	V
$\mathbf{V_S}$	Voltage of the source	V
$\mathbf{V_{max}}$	Enzymatic maximum rate of reaction	mol s^{-1}
W	Work	J

$\mathbf{x}$	Normal distance to the electrode	m
$\boldsymbol{\delta_o}$	Diffusion layer thickness	m
$\boldsymbol{\eta}$	Overpotential	V
$\boldsymbol{\eta_{act}}$	Activation overpotential losses	V
$\boldsymbol{\eta_{conc}}$	Concentration overpotential losses	V
$\boldsymbol{\eta_{ohm}}$	Ohmic overpotential losses	V
$\boldsymbol{v}$	Scan rate	$V\ s^{-1}$
$\boldsymbol{\pi}$	Reaction quotient	-
$\boldsymbol{\phi}$	Electrochemical potential	V

Acronyms

Acronym	Description
5%CO_2	5% CO_2 in air
20%CO_2	20% CO_2 in air
BM	Biomass
BPV	Biophotovoltaics
CA	Carbonic anhydrase (enzyme)
Chl	Chlorophyll
C_i	Inorganic carbon
CMM	CO_2 concentrating mechanism
DO	Dissolved oxygen
Fe lim/Fe(-)	Iron limited
Fe suff/Fe(+)	Iron sufficient
Fe(II)CN	Ferrocyanide
Fe(III)CN	Ferricyanide
FeCN-R	Ferricyanide reduction to ferrocyanide
MFC	Microbial fuel cell
O	Oxidised species
OCP	Open circuit potential
OD	Optical density

OM	Outer membrane
OMP	Outer membrane protein
pCO_2	Partial pressure of CO_2 in air
photo-MFC	Photosynthetic microbial fuel cell
PM	Plasma membrane
R	Reduced species
RuBisCo	Ribulose-1,5-bisphosphate carboxylase/oxygenase (enzyme)
SOD	Superoxide dismutase (enzyme)
TM	Thylakoid membrane

Chapter 1 Introduction

The necessity for sustainable processes in today's economy is one of the main challenges that engineers and scientists face. Carbon neutral operations are imperative in order to reduce and mitigate the enormous release of carbon dioxide (CO_2) to the atmosphere from the combustion of fossil fuels. It is now accepted that the fraction regarding anthropogenic CO_2 release has had a significant effect over the increment in greenhouse gases and consequently over climate change the planet undergoes, putting at risk ecosystems and human security.[1]

Furthermore, fossil fuels are a finite resource and future energy availability depends on the development of renewable energy sources (Figure 1-1). The most prominent renewable sources include solar, wind, biomass, hydro and geothermal.[2]

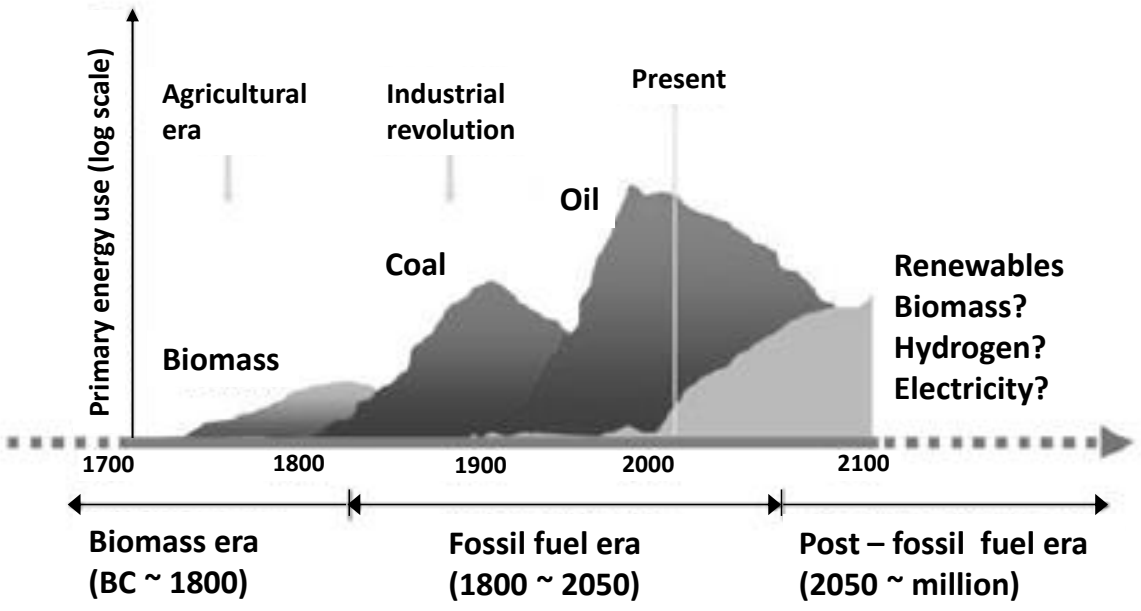

Figure 1-1. History of energy resources use and future prediction. Taken from Chang *et al*.[2]

Bioprocesses represent a carbon neutral alternative to deal with the ever demanding requirements of modern life. Nowadays, there is a serious agenda within the European Commission for Research & Innovation in moving towards a bio-based, resource-efficient and sustainable economy.[3] Bioeconomy is based on renewable biological resources, such as crops, forests, fish, animals and microorganisms

to produce food, biomaterials and bioenergy. The latter being of special interest because it is a potential source of clean renewable energy.

The focus of the investigation presented in this thesis is on light driven bioelectricity (photo-bioelectricity), generated in bioelectrochemical cells known as biophotovoltaics (BPV), a form of bioenergy. This thesis seeks to contribute to the understanding and improvement of photo-bioelectricity generation utilising wild-type cyanobacteria (photosynthetic bacteria). Within this context, the cyanobacterium *Synechococcus elongatus* PCC7942 was investigated in different platforms and conditions of growth, with the aim of finding conditions enhancing cyanobacterial extracellular electron transfer (exoelectrogenesis). The latter was characterised in its capacity to react with an artificial redox mediator and to react directly on the electrode surface. The importance of the photosynthetic activity in cyanobacterial exoelectrogenesis was also analysed.

To understand bioelectricity generation by whole microorganisms, microbial fuel cells (MFC) need to be examined, as these operate with well-known exoelectrogenic bacteria. In this thesis, MFCs are used as a point of comparison.

In this introductory chapter, a framework in bioenergy and bioelectrochemical systems is presented. The fundamental aspects regarding the technology, including the characterisation of electrochemical reactions and electrochemical cells operation, are then introduced. A review of the "state of the art" in bioelectrochemical cells (MFCs, photo-MFCs and BPVs) follows, with particular emphasis in BPV operation. Finally, a description of exoelectrogenesis and oxygenic photosynthesis in cyanobacteria are presented.

1.1 Bioenergy and photosynthetic bioprocesses

The energy generated through bioprocesses or bio-catalysed processes is known as bioenergy, a promising alternative to fossil fuels. Bioenergy can be generated as biomass, biofuels, biogas and bioelectricity.

Bioenergy is closely, but not exclusively, related to solar energy due to the catalytic capacity of photosynthetic organisms in converting solar energy into chemical energy, generating biomass through the capturing and fixation of CO_2. Solar energy has the highest potential in the renewable sector as the amount of energy that the sun provides to the earth is stratospheric, one hour of solar energy is more than the energy consumed in the world in one year (Table 1-1). Remarkably, the energy

fixed as biomass by photosynthetic organisms is six times higher than the world energy consumption, demonstrating the potential and efficacy of the photosynthetic process.[4]

Source/consumption	Energy [exajoules (10^{18} J) $year^{-1}$]
Solar energy	3,850,000
Energy fixed in photosynthesis	3,000
World consumption	500

Table 1-1. Solar energy comparison to biomass fixation and total world consumption.[4]

Biomass can be used directly or further processed to obtain a range of fuels. The combustion of biomass produces heat for immediate use and electricity (steam powered), while through conversion routes (gasification or pyrolysis), gas and liquid fuels can be obtained. These processes require high temperature (500 – 1000 °C), which reduces the energy efficiency of the product, but still they represent a promising renewable energy source.[5]

Alternatively, low temperature processing of biomass for fuel generation can be conducted through biochemical conversion. The fermentation of sugar by yeast can be used to produce bioethanol. The breakdown of organic matter by specialised methanogenic microorganisms in anaerobic biodigesters can be used to produce biomethane (biogas).[5] Dried cyanobacterial biomass can be used to feed an anaerobic biodigester, demonstrating the versatility of photosynthetic microorganism as an energy source.[6] Another emerging type of biogas is biohydrogen, generated by photo-biological fermentation, anaerobic fermentation, enzymatic and microbial electrolysis or a combination of these processes.[7] Additionally, oils from oil-rich biomass can be mechanically extracted and used directly or further processed to produce biodiesel.[5]

Biofuels (biodiesel or bioethanol) are alternatives to replace conventional fuels in current vehicle engines without major modifications. Biofuels from crops have high calorific content (Sunflower: 39.60 kJ/g – Rapeseed: 39.70 kJ/g) and are known as first generation biofuels. However, because of competing factors concerning arable land, food demand takes priority over biofuel demand, therefore second generation biofuels have received more attention, these are generated from non-feedstock crops (Switchgrass: 16.70 kJ/g), food waste and wood waste, to name a few. Third generation biofuels correspond to biofuels obtained from photosynthetic microorganisms (microalgae and cyanobacteria), representing a promising alternative. Not only do photosynthetic microorganisms have higher biomass yields per hectare, but they also do not compete with agricultural demand. Furthermore, photosynthetic microorganism can thrive in high CO_2 concentrations, offering an alternative to mitigate CO_2 emissions from industrial activity.[8]

Another form of bioenergy is bioelectricity, the main topic in this thesis, which is spontaneously generated in bioelectrochemical cells and occurs due to the electrocatalytic action of biological systems, including photosynthetic systems. Bioelectricity is generated *in vivo*, therefore it can be integrated with other photo-bioprocesses (Figure 1-2), for instance bioremediation and biodiesel production. Furthermore, bioprocesses using photosynthetic biomass are, in general, non-toxic, therefore they can be implemented in open field applications.

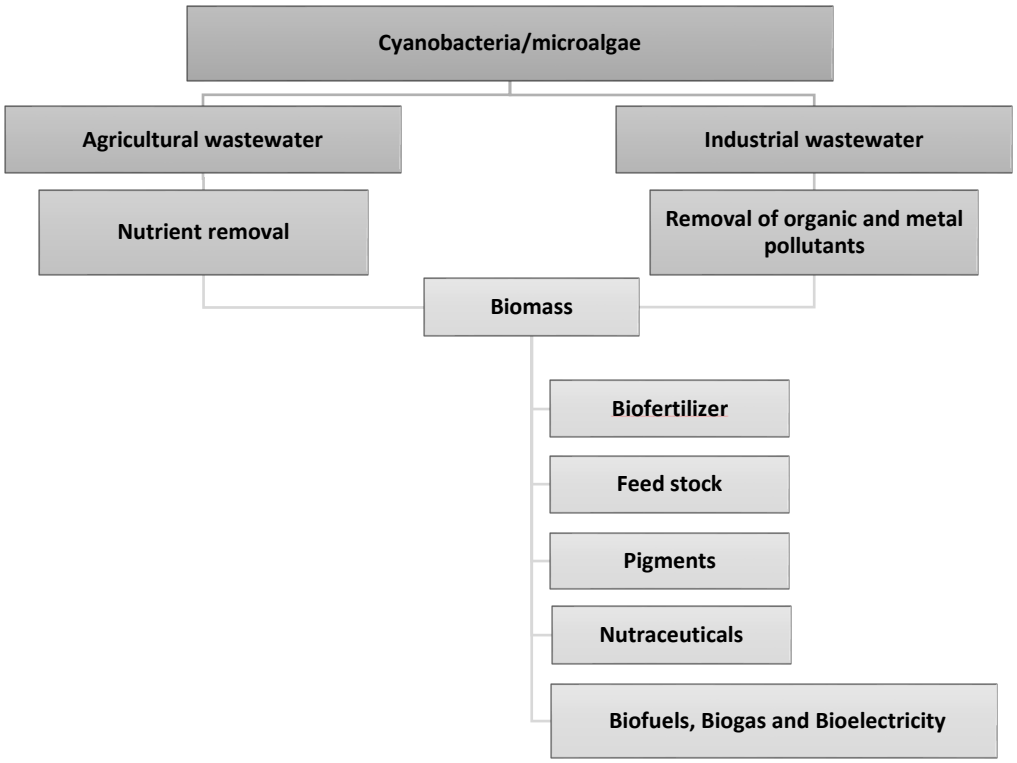

Figure 1-2. Biotechnological applications using photosynthetic microorganisms in an integrated view.[9]

1.2 Bioelectrochemical systems

Bioelectrochemistry deals with the electrochemical aspects of biology, that is to say biochemical reactions involving electron transfer, with an oxidation (electron lost) coupled to a reduction (electron gain).

Bioelectrochemical systems are technological platforms based on bioelectrochemical reactions occurring at the surface of an electrode. To engineer systems using biological substrates interacting with solid phase electrodes has become a fertile area of research, incorporating the disciplines of biochemistry, cell biology, electrochemistry, engineering and physics. The subject has received

attention from the "Science for Environment Policy" (information service from the European Commission), which provides the latest environmental policy-relevant research findings and reported in 2013 on the potential of bioelectrochemical systems for energy generation, wastewater treatment and valuable chemicals production.[10]

Bioelectrochemical systems can be used to spontaneously generate electricity (galvanic cell), a form of bioenergy; or oppositely, they can be utilised to force an electrical current driving a desired reaction (electrolytic cell), known as microbial electrolytic cells; both applications are the subject of numerous lines of research with the development of bioanodes and biocathodes for bioelectrochemical cells. The redox active biological substrates can be enzymes, subcellular structures (membranes or organelles) or whole microorganisms. The advantage of bioelectrochemical systems is that biological substrates replace expensive catalyst.

Bioelectrochemical cells using bioanodes with whole microorganisms as biocatalysts are known as microbial fuel cells (MFC), because a feed of organic load (carbon source, "fuel" for cellular activity) is required. Therefore, to maintain the efficiency of a MFC, a continuous feed, or at least semi-continuous, is necessary.[11,12] Alternatively, photosynthetic microorganisms have also been investigated, generating bioelectricity driven by light, with no fuel requirement. This type of bioelectrochemical cells are known as biophotovoltaics (BPV).[13,14] In this case, the biological electrochemical cell resembles in a better way a battery (close system). The performance of whole microorganisms as the electron donor varies according to their capacity of extracellular electron transfer. A full description of extracellular electron transfer and of bioelectricity generation by whole microorganism is presented in Section 1.3 and Section 1.5 respectively.

Enzymatic fuel cells have shown good performance and current densities in the order of 1 mW cm^{-2}, although the use of co-factors and redox mediators is in many cases necessary.[15] Glucose oxidases and dehydrogenases have been used in the bioanode of enzymatic fuel cell platforms.[15] Enzymes can also be used in the cathode of a bioelectrochemical cell, in this case catalysing the reduction of the electron acceptor, normally oxygen, and eliminating the requirement of an expensive catalyst, normally platinum. The two enzymes commonly used in oxygen biocathodes are laccases and bilirubin oxidases.[15,16] If well immobilised (meaning favourable orientation of the enzymatic active site onto the electrode) higher current densities can be achieved alongside higher stability.[16]

Similar to what has been described regarding MFCs, enzymatic fuel cells have their counterpart light driven platform, when the biocatalysis is performed by photosynthetic protein complexes. Light driven current by thylakoid membrane has been demonstrated. The thylakoids can interact directly with an

electrode, but currents are enhanced in the presence of electron shuttles (mediator).[17,18] In combination with a laccase cathode and using ferricyanide as a redox mediator in a photo-bioanode, Calkins *et al.*[17] reached photo-current densities of 68 μA cm^{-2} and a maximum power of 5.3 μW cm^{-2}, in a fully enzymatic, light driven electrochemical cell. Isolated photosystem II (PSII) has also been demonstrated to drive photo-currents in electrochemical cells.[19] However, higher power outputs were achieved by using thylakoids, possibly due to the stability of the enzymes and to multiple proteins with redox capacity within the membrane.[17] Moreover, photo-bioelectricity was produced using isolated chloroplasts, which were able of direct electron transfer to an electrode, but higher currents were obtained in the presence of mediators.[20]

The photosynthetic process holds such high value that researchers are after designing artificial photosynthesis (biomimetic). Recently, Majumdar *et al.*[21] discussed the viability of an integrated photo-anode with water splitting capacity coupled to enzymatic cathodes, generating currents in a sustainable way, although co-factors and materials remain a challenging cost.

Bioelectrochemical cells (whole microbe or enzymatic) can also be used in bioelectrolytic cells with a biological substrate in the anode, cathode or both. In this setup, the electrochemical cell is powered and a reaction occurs, therefore the system can be tailored to generate valuable products (bioelectrosynthesis). Hydrogen has been produced in the cathode of a microbial electrolytic cell (bioanode),[22] as well as in the biocathode of a microbial electrolytic cell (abiotic anode)[23]. Methane has also been generated in a microbial electrolytic cell, in this case both biocathode and bioanode inoculated with microorganisms.[24] Light driven electrochemical cells were also demonstrated to be useful in electrolytic systems, with hydrogen production in the cathode of a cell using a photo-driven bioanode catalysed by thylakoid membrane.[25] Hydrogen and methane are valuable fuels which can be used in an abiotic fuel cells or in combustion.

Regarding enzymatic electrochemical cells, the expense of the biocatalyst assembly involving production, extraction and purification of enzymes or membranes, besides the expense of co-factors and/or mediators, reduce the cost efficiency of the platform. Nonetheless, once enzymes or membrane fractions are obtained, electrodes can be assembled with a high biocatalyst density per surface area, implying that higher current densities can be achieved. Stability of enzymatic electrodes is another issue to overcome.[15] Whole microbe electrochemical cells involve a more complex biocatalysis, but microbes are self-replicating and self-repairing substrates, easing the operation and maintenance of the platform.

Finally, but no less important, a third bioelectrochemical system utilising electrodes exists, used in analytical studies of a given biological substrate, the latter is analysed in the working electrode of a three electrode system (described in Section 1.4.5).

1.3 Extracellular electron transfer: exoelectrogenesis

Extracellular electron transfer is a general term conveying the capability of a given microorganism to react electrochemically with an extracellular substrate, which works in both directions, uptake and export of electrons.

Originally bioelectricity catalysed by whole microorganisms, including cyanobacteria, was investigated with artificial mediators to shuttle electrons from intracellular processes out of the cell,[4,26–28] but the use of mediators intercepting directly the cellular metabolism disrupts the viability of the cells and the approach is not sustainable in time.

Later it was found that many microorganisms are capable of extracellular electron transport and by doing so, reducing or oxidising an extracellular substrate. The latter implies the ability of vertical electron transfer through biological membranes (cell envelope), or alternatively, secretion of redox active compounds. The process regarding export of electrons is known as exoelectrogenesis, while microorganisms with the capability to export electrons are known as exoelectrogens.

Geobacter sulfurreducens and *Shewanella oneidensis* are well-known exoelectrogenic microorganisms because of their capability to produce some of the highest current densities for pure cultures in MFC, reaching maximum power outputs in the order of 3,000 mW m^{-2}.[29,30]

Mechanisms employed by microorganisms for extracellular electron transfer vary (Figure 1-3). It has been found that outer membrane c-cytochromes exposure in *S. oneidensis* and *G. sulfurreducens* is a determining factor in the transference of electrons to an extracellular solid substrate.[31–33] It has also been reported the secretion of redox active compounds like riboflavins, which act as a natural redox mediator.[34,35] Additionally, the presence of electrically conductive nanowires (*pili*) on the outer surface of the bacterial wall has been described and found to be necessary for higher extracellular electron transport rates.[36–38] Microorganisms might utilise one or all of these electron transfer mechanisms, in the case of direct electron transfer from c-cytochromes and nanowires, a bacterial biofilm on the electrode is necessary. Furthermore, exoelectrogenic microorganisms can relay electrons in cell to cell interactions within a biofilm, very likely involving *pili* structures, demonstrating long distance electron

transfer. Currents densities are not only accounted by the catalytic activity of the first layer of bacteria in a biofilm.[39,40]

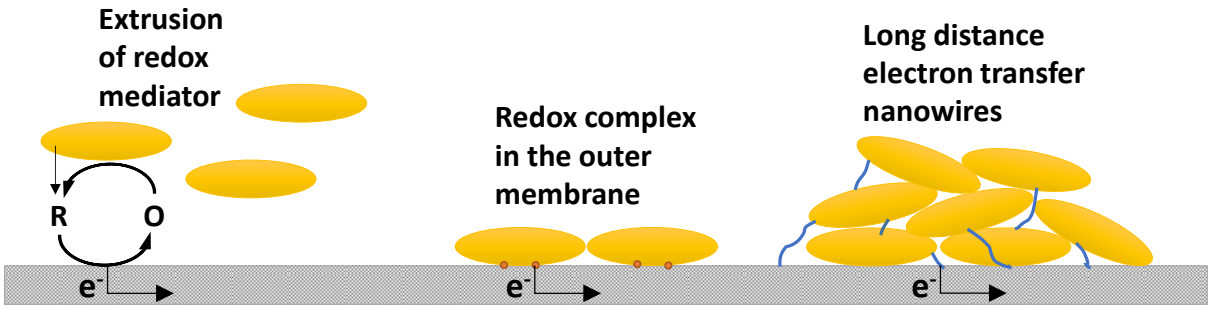

Figure 1-3. Schematics of extracellular electron transfer mechanism detected in redox active microorganisms.[31–33]

A good exoelectrogen like those mentioned, couples respiration, a major metabolic pathway, to extracellular electron acceptors, which can be intercepted with an electrode, thus good exoelectrogens are known as anode respiring bacteria.[41,42] However, there are other metabolic processes regarding exoelectrogenic activity. For instance, while iron oxide ($Fe(III)_2O_3$) serves as an electron acceptor in extracellular respiration (known as dissimilatory iron reduction),[41,43] extracellular electron transfer to iron oxides results in the dissolution of ferrous, readily available for iron uptake, this is known as assimilatory iron reduction.[43] The latter is a common strategy to solubilise iron, also involving extracellular electron transfer. Some processes related to cell signalling and immunology involve extracellular electron transfer as well.[44] Albeit, many exoelectrogenic processes are possibly not identified, for instance, photosynthetic cyanobacteria have been demonstrated to have exoelectrogenic capacity, but the metabolic processes driving exoelectrogenesis are not well understood.[45,46] In the case of poor exoelectrogens like cyanobacteria, soluble artificial redox mediators impermeable to the plasma membrane, therefore relying on extracellular electron transport and not disruptive to the cell viability, are utilised to facilitate exoelectrogensis.[47,48] Artificial redox mediators work in a similar way to natural redox mediators as pictured in Figure 1-3. If artificial mediators are not utilised, the system is referred as mediatorless.

1.4 Electrochemical characterisation of exoelectrogenic microorganisms

Many electrochemical techniques exist and several have been applied to biological systems.[49] In this section, the theoretical background and techniques relevant to the experimental work presented in this thesis are introduced, focusing on the electrochemical characterisation of redox reaction occurring at the electrode surface. Electrochemical cell characterisation is presented in Section 1.5.

1.4.1 Electrochemical reactions at the electrode interface

Electrochemical reactions are those involving electron transfer, with one reactant losing electrons (oxidation) and one reactant gaining electrons (reduction), these are known as half-reactions (Equation 1-1). Half-reactions do not occur independently, thus in general, electrochemical reactions are defined as redox reactions, and reactants as redox species. The reaction, oxidation or reduction, can occur between a given redox species and a solid conductive material, the electrode (Figure 1-4), as long as another complementary half-reaction occurs within the same system. Electron transfer occurs via quantum mechanical tunnelling between the electrode and reactant at the electrode surface (typical tunnelling distances are less than 2 nm).[50]

$$O + ne^{-} \leftrightarrow R$$

Equation 1-1. Redox half-reaction of the generic O/R redox species occurring on an electrode surface. *O*: oxidised state, *R*: reduced state and, and *n* is the number of electrons transferred.

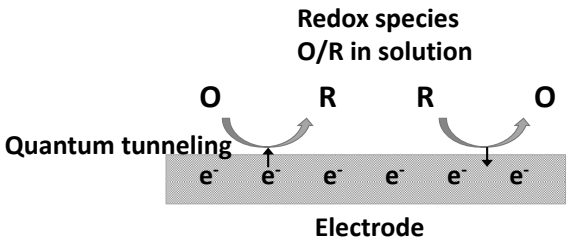

Figure 1-4. Redox reaction between the redox species O/R and the electrode.[50]

The electrochemical reaction between a redox species and an electrode occurs at the interface of two phases involving charge transfer. Initially, the uncharged phases will interact electrochemically and a net charge separation occurs creating a potential difference at the interface (Equation 1-2).

$$\Delta\phi_{m/s} = \phi_m - \phi_s$$

Equation 1-2. Potential difference across the electrode/solution interface. $\Delta\phi_{m/s}$: electrochemical potential in the interface metal/solution. ϕ_m: electrochemical potential in the metal, ϕ_s: electrochemical potential in the solution.

To measure the potential at the electrode interface, a complete circuit is necessary, in other words, the potential of a half-reaction can only be measured against the potential of another half-reaction (potential difference). A reference electrode has an invariant potential across its interface and the solution (under normal conditions). In practice, the potential difference is measured in an electrochemical cell with two half cells. The redox species of interest O/R is in one half-cell with a given electrode which is denominated as the working electrode, and the reference electrode is the second half-cell. Equation 1-3 shows the potential difference of O/R against a reference "*c*". As long as there is not net current flow, the O/R species in solution reach equilibrium and the electrode holds equilibrium potential (E_{eq}). Typical reference electrodes are the standard hydrogen electrode (SHE) and saturated silver/silver chloride (Ag/AgCl). By consensus, the potential of SHE is zero volt (V). Ag/AgCl is 0.29 V vs SHE.

$$E_{eq} = \Delta\phi_{m/s} + c$$

Equation 1-3. Potential difference between the working electrode and the reference electrode with constant potential *c*.

From the thermodynamics, the Nernst equation (Equation 1-4) establishes the half-reaction equilibrium potential for given conditions. The standard redox potential E^o is the potential at standard conditions when the concentration of both O and R at the electrode surface is the same as that in the bulk solution (equilibrium conditions). E^o is listed for many redox species against SHE. When concentrations of O and R are different, E_{eq} is determined from the standard potential E^o and the reactants/products ratio. While it is true that concentrations should be replaced by activities (a=*y*c,

where *y* is the activity coefficient and c is the concentration), at low concentration activity coefficients tend to be 1, thus values of activities tend to be the same as those of concentrations.

$$a)\ \Delta G = \Delta G^{O} + RTln\frac{[R]}{[O]}$$

$$b)\ E_{eq} = E^{O} - \frac{RT}{nF}ln\frac{[R]}{[O]}$$

Equation 1-4. a) Gibbs free energy for the redox half reaction (maximum work that can be derived from the reaction) and b) Nernst equation for the redox species O/R. Standard Gibbs free energy ΔG^{o} can be calculated from tabulated energies of formation. Standard redox potential ΔE^{o} is listed for many redox species. R: universal gas constant, n: moles of electrons and F: Faradays constant.

The potential of the working electrode can be altered with a potentiostat and monitored against the reference electrode. When the applied potential *E* is different to E_{eq} (voltage difference), the reaction proceeds and a net electrical current develops. A volt, the unit of voltage difference, corresponds to the energy required to move electrical charge. A third electrode, the counter electrode, is necessary in the system to allow the electrical current to flow, because for the reference electrode to maintain its invariant potential only a very low current should flow through. The electrical current established due to an applied potential away from E_{eq} can be in either direction, oxidation or reduction, depending on if *E* is higher or lower than E_{eq}.

When an electrode, generally a metal, is placed in a solution with redox active species, the electrochemical potential of electrons in each phase will reach equilibrium, implying that electrons flow between phases to equalise the Fermi energy levels. The Fermi energy level corresponds to the average energy of available electrons (*i.e.* transferable) in a given phase and is related to the chemical potential of electrons in that phase.[51] An applied potential over the electrode can raise or decrease the Fermi level (Figure 1-5). If a negative potential is applied (with respect to E_{eq}) and it is higher than the lowest unoccupied molecular orbital (LUMO) in the reactant O, electron transfer from the electrode to O is favourable to occur, then O is reduced to R. Likewise, if the applied potential is positive (with respect to E_{eq}), the electrode becomes an electron acceptor, then R is oxidised to O. By convention, oxidation currents (i_a) are positive and reduction currents (i_c) are negative.

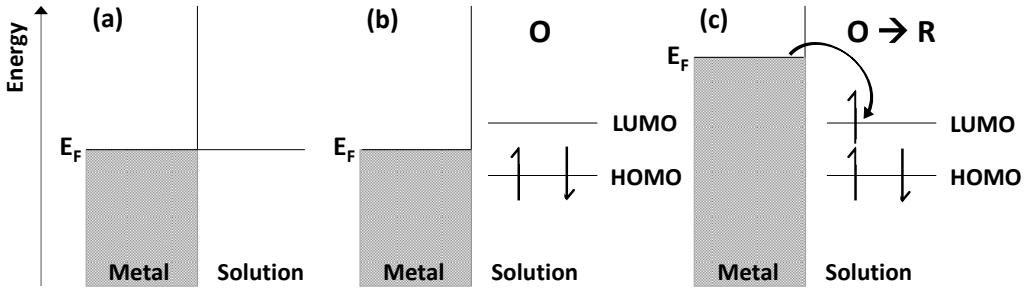

Figure 1-5. a) Fermi energy level of a metal (electrode) in solution, no applied potential, b) Fermi energy level is insufficient to drive the reduction of O, and c) an applied potential raised the Fermi energy level and is sufficient to drive the reduction of O to generate R. LUMO refers to the lowest unoccupied molecular orbital and HOMO to the highest occupied molecular orbital.[51]

The applied potential difference in respect to the equilibrium ($E - E^o$) is the overpotential η which can drive the system out of equilibrium, therefore the equations are often written as a function of η.

The Butler – Volmer equation describes the net current flowing at the electrode as a function of the overpotential (Equation 1-5 (a)). If the solution is well stirred, the Butler – Volmer equation is simplified as shown in Equation 1-5 (b).

$$a)\ \ i = i_o\left(\frac{[R]_o}{[R]_{bulk}}exp\left\{\frac{(1-\alpha)nF\eta}{RT}\right\} - \frac{[O]_o}{[O]_{bulk}}exp\left\{\frac{-\alpha nF\eta}{RT}\right\}\right)$$

$$b)\ \ i = i_o\left(exp\left\{\frac{(1-\alpha)nF\eta}{RT}\right\} - exp\left\{\frac{-\alpha nF\eta}{RT}\right\}\right)$$

Equation 1-5. Buttler – Volmer equation for net current flow in an electrode where electroactive species O/R react with exchange current i_o (net current zero) and as a result of an applied potential (overpotential), where a) concentrations [R] and [O] at the surface are different to those in the bulk solution and b) concentrations of [R] and [O] are equal at the surface and bulk solution. The fractional change ($0 \geq \alpha \geq 1$) reflects the sensitivity of the transition state to the drop in electrical potential between electrode and solution. When α is 0.5, the transition state lies intermediate between reactants and products.

i_o is the exchange current when no net current flows through, where anodic (oxidation) and cathodic (reduction) exchange currents (reaction) are happening at the same electrode. The magnitude of i_o determines if the variation of current in response to an overpotential is reversible (large i_o) or irreversible (small i_o), as shown in Figure 1-6. In reversible redox reactions a small overpotential is enough to drive a current. As the redox reactions are kinetically favourable, both processes occur, in the anodic and cathodic direction, with the resulting net current being anodic or cathodic depending

on the applied potential; while only at very high overpotentials the opposite process becomes negligible. Contrarily, irreversible redox reactions are not kinetically favourable and a large overpotential is needed to drive a net current, which can also be seen as a large activation energy that has to be overcome; when a net anodic or cathodic current develops, the opposite process is not occurring. The reversibility of a given redox reaction depends on the electrode material and the catalytic processes which might be involved.

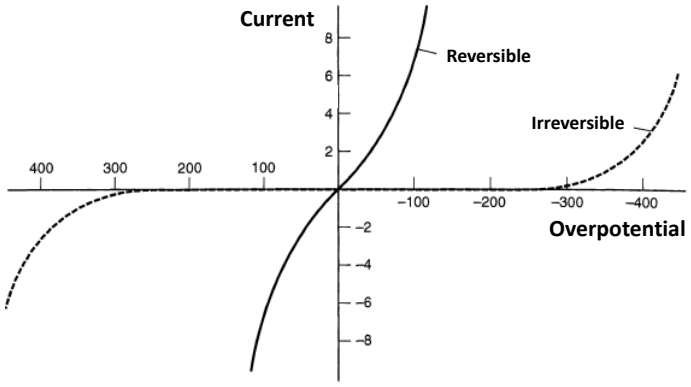

Figure 1-6. Activation overpotential required to deliver net current densities in reversible and irreversible systems.[51]

The applied potential generates electrostatic forces at the electrode surface attracting electrolyte ions, as well as dipole moments of the solvent, creating a phase different to that of the bulk solution. The concept of electrical double layer derives from the neutrality in the interface solid/solution.[51]

The formation of the electrical double layer creates a transient current due to a capacitor-like behaviour. The charge in a capacitor *Q* is proportional to the potential drop across the capacitor (Equation 1-6). In a capacitor, the proportionality constant *C* is known as the capacitance of the medium.

$$Q = C\Delta E$$

Equation 1-6. Charge in a capacitor with potential different ΔE and capacitance C.

If the applied potential is changed in time, the charge in the electrical double layer changes accordingly (Equation 1-7), which implies that an electrical current is created different to that induced by redox

reactions. The current due to the electrical double layer is named capacitive current, while the electrical current due to redox reactions is known as faradaic current.

$$i = \frac{dQ}{dt} = C\frac{dE}{dt}$$

Equation 1-7. Capacitive electrical current in the electrode due to changing the applied potential.

The net current induced by redox reactions (faradaic current) occurring at the surface of the electrode are not affected only by reaction kinetics as shown in the Butler – Volmer equation (Equation 1-5), but also by the transport rates of reactant from the bulk solution to the electrode surface and the transport of products away from the electrode surface towards the bulk solution. Furthermore, the process could involve additional steps regarding physical interaction and chemical reactions (not redox reactions) like adsorption, desorption, protonation and/or decomposition, which might be necessary for the electron transfer to occur.[49,51] Therefore, the dynamic process is the sum of all the kinetics and mass transport processes involved as pictured in Figure 1-7.

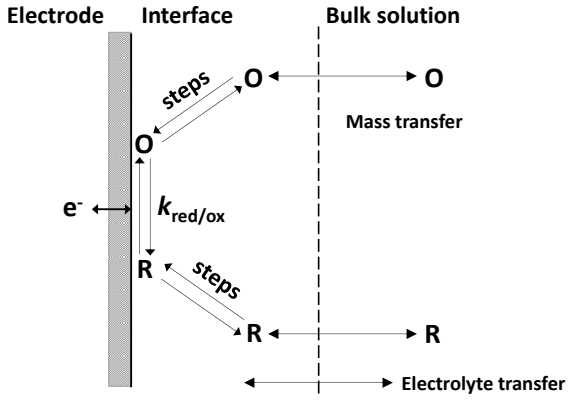

Figure 1-7. Schematics of processes involved in a redox species in solution reacting at the electrode surface. *k*: heterologous constant rate of reaction. Adapted from Zhao *et al.*[49]

If the net current is limited by mass transport, it means that the flux j_o of reactants reaching the electrode surface controls the process. Mass transport has three components, diffusion across a concentration gradient, migration along an electric field gradient, and convection.[50,51]

Under controlled conditions, mass transport is limited only by diffusion of the reactant species. Fick's first law (Equation 1-8), describes the diffusional flux j_o of a species, related to the concentration gradient and the diffusion coefficient. The negative sign indicates that mass flows down a concentration gradient, from high to low. The diffusion trajectory is assumed to be normal to the electrode surface. The flux j_o determines the current magnitude i_{mt} at the electrode.[50,51]

$$a)\ j_o(x,t) = -D_o \frac{\partial C_o(x,t)}{\partial x}$$

$$b)\ \frac{i_{mt}(x,t)}{nFA} = -D_o \frac{\partial C_o(x,t)}{\partial x}$$

Equation 1-8. Fick's first law of diffusional flux for a given species with concentration C_o at location x and time t. i_{mt} is the current magnitude limited by mass transfer.

1.4.2 Electrocatalysis by microorganisms

The processes described in the previous sections, involve conventional electrochemical systems where the reactant is in solution. In bioelectrochemical systems this can be the case if redox mediators, natural or artificial, are in solution, although there is an additional kinetic component in the reaction of the mediator at the cell surface. Thorne *et al.*[52] studied the system ferricyanide – *Synechocystis sp.* PCC6803 – ferrocyanide – electrode (anodic current) (Figure 1-8), finding that at a low biomass density, the reduction of ferricyanide by the cyanobacteria was kinetically limited, but at a higher biomass density, the reduction of ferricyanide was mass transport limited.

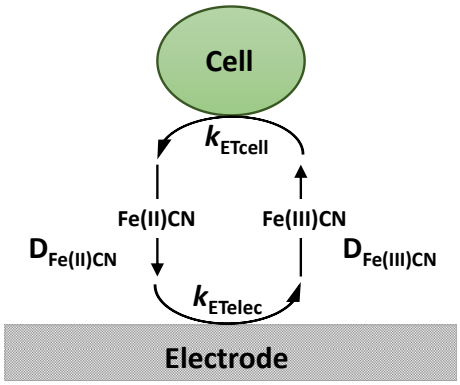

Figure 1-8. Schematics of mechanism to measure ferricyanide (Fe(III)CN) reduction by cyanobacteria. Ferrocyanide (Fe(II)CN) is re-oxidised in the electrode. At low cell densities, Fe(III)CN reduction is kinetically limited by k_{ETcell}, while at high cell densities, Fe(III)CN reduction is diffusion limited by $D_{Fe(III)CN}$. Adapted from Thorne *et al.*[52]

When biofilms are studied, the processes involved in the catalysis of electroactive microorganisms represent a more complex system (Figure 1-9). In this case the mass transport of the organic feed (if any) towards the electrode surface where the biofilm is settled could be the limiting factor. However, well stirred bioelectrochemical systems still show lower than expected currents, therefore there is a metabolic kinetic component limiting the process. Furthermore, within a biofilm not only the monolayer of microorganisms on the electrode surface acts as the electron donor, but also the relay of electrons from distant microorganisms occurs.[39]

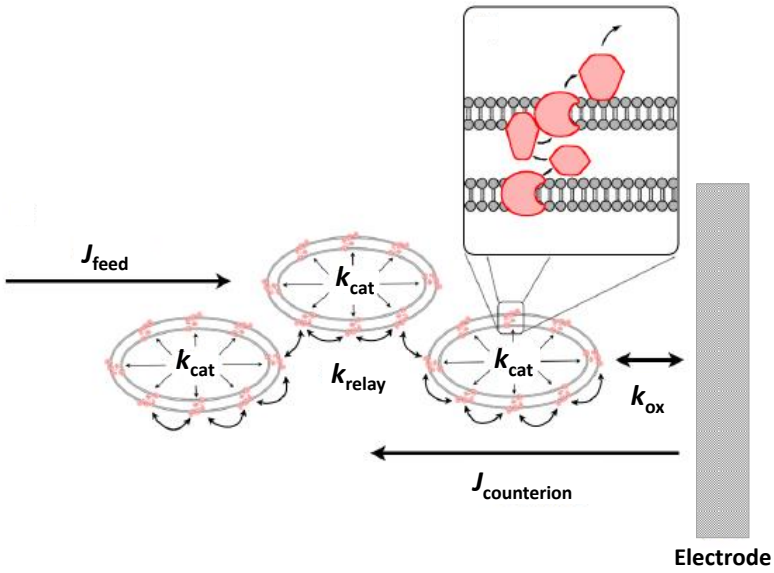

Figure 1-9. Schematics of processes involved in the redox catalysis of an organic feed (fuel), if any, to generate an electrical current at the electrode. Representing the mass transport and kinetic limitations in an exoelectrogenic biofilm. Taken from LaBelle and Bond.[39]

1.4.3 Cyclic voltammetry

Cyclic voltammetry is one of the simplest ways to determine mechanisms regarding the reduction or oxidation of a redox species taking place at the electrode. The study of the half-reaction is conducted in the working electrode of a three-electrode electrochemical platform, together with a counter electrode and a reference electrode.

Cyclic voltammetry consists in the screening of the working electrode by sweeping the applied potential linearly in time, forward and backward between two potential values (Equation 1-9). An initial potential E_1 is swept to reach a vertex potential E_2, then sweep back to reach a vertex potential E_3, which is generally equal to E_1. The potential changes at a fixed rate known as the scan rate v.

$$a)\ E(t) = E_1 + vt$$

$$b)\ E(t) = E_2 - vt$$

$$\{E_1 \leq E \leq E_2\}$$

Equation 1-9. Applied potential as a function of time with scan rate *v* subject to a minimum and maximum potential for cyclic voltammetry measurements with a) forward scan and b) back scan.

Figure 1-10 shows a generic cyclic voltammogram of a reversible redox reaction. Typically, the initial potential E_1 is such that reactions are not favourable, then if overpotentials are positive, the oxidation reaction occurs. In reversible systems, the rapid electrode kinetics implies that the currents are mass transport limited. Initially there is an abundance of reactant and the raise in current is Nernstian driven, as currents continue to increase (larger overpotentials), the diffusion layer also increases and the depletion of reactants in the electrode surface becomes significant, then currents reach a peak (i_p^a). The current drop observed in the following more positive overpotentials reveals the diffusion limitation, where the anodic current is restricted by the flux of fresh reactant reaching the electrode. When sweep back, the system is pushed to the reverse process, applying negative overpotentials and thus, inducing the reduction of the oxidised species, which initially are abundant in the proximity of the electrode due to the preceding forward scan. In a reversible system, the reverse current shows the same behaviour, with a Nernstian current raise, a peak cathodic current (i_p^c), and a diffusional controlled current drop. The area under the voltammogram of the reverse peak current is equal but opposite to that of the forward scan, with the ratio of the peak current (i_p^a/ i_p^c) equal to one. The position of peak potentials (E_p: potential at peak current) is independent of the scan rate for reversible systems, with a separation of 59/*n* mV (at standard conditions).

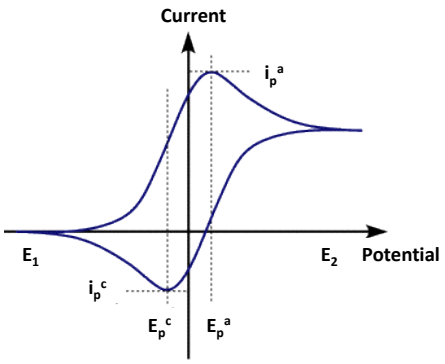

Figure 1-10. Cyclic voltammogram of a reversible redox system, showing peak currents and corresponding peak potentials.[50]

Peak currents of both, reversible and irreversible systems, are directly proportional to the concentration of reactants and to the scan rate. The effect of the scan rate can be understood by inspecting Fick's first law, which dictates that current is proportional to the concentration gradient of reactant at the vicinity of the electrode surface and inversely proportional to the diffusion layer thickness. At fast scan rates, there is less time for the reaction to proceed at a given overpotential, thus a thinner diffusion layer is built up, leaving larger availability of reactant for the successive higher overpotentials. Figure 1-11 shows the voltammogram of a reversible system at increasing scan rates. In irreversible systems, E_p^a shifts to more positive potential at faster scan rates.

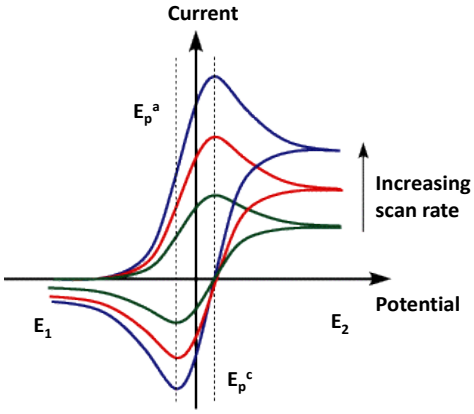

Figure 1-11. Cyclic voltammetry at increasing scan rates of a reversible redox system.[50]

In irreversible systems, the peak potential separation is larger than for reversible systems, basically because of poor kinetics (large activation energy). The shape of the voltammograms is therefore different (Figure 1-12). Reversibility of redox systems refers to the electrode kinetic rates respect to mass transport, and it is not difficult to find systems with kinetic rate constants between reversible and irreversible systems. These systems are known as quasi-reversible. In Figure 1-12, it is observed that the peak potentials shift with decreasing rate constants alongside lower peak currents for the same scan rate.

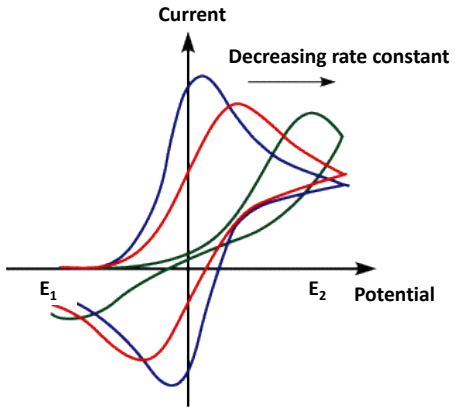

Figure 1-12. Cyclic voltammogram for reversible (blue), quasi-reversible (red) and irreversible (green) reactions at the same scan rate.[50]

A special case in cyclic voltammetry is that of redox couples immobilised on the electrode surface. In the case of immobilised redox species, there is limited reactant abundance. The voltammogram is driven by the Nernst equation (reversible system) or electrode kinetics (irreversible system). In an ideal reversible system, a peak current is reached symmetrically in the forward and back scan and the peak potential separation is zero (Figure 1-13).[53,54]

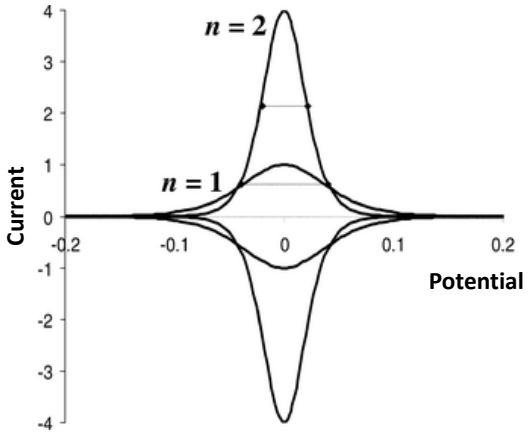

Figure 1-13. Ideal cyclic voltammogram for redox couple immobilised on the electrode undergoing reversible reaction, with *n* denoting number of electron transferred in a given reaction. Taken from Armstrong *et al.*[53]

Cyclic voltammetry is a simple method to study an electrochemical reaction occurring at the electrode surface. However, one of the limitations of the technique is related to background capacitive currents, higher with increasing scan rates, accompanying the measurements, which in some systems could

mean that small signals are lost. Pulse wave voltammetry techniques are an alternative to enhance the faradaic signals.[49] Alternatively, the first derivative of the voltammogram can be obtained to distinguish redox signals.[39,54] As capacitive currents are constant at a fixed scan rate, the first derivative shows the midpoint potentials (when concentration of oxidised species equals reduced species), which can approximate the standard potential characteristic of a redox couple.[39]

1.4.4 Potential step chronoamperometry

Chronoamperometry consists in the sudden change in potential from one value to another (potential step), the latter is held constant in time, while measuring anodic (or cathodic) currents as a function of time (Figure 1-14). In general, the potential is chosen positive or negative enough to push the system to complete reactant consumption (opposite process thermodynamically unfavourable).[50,51]

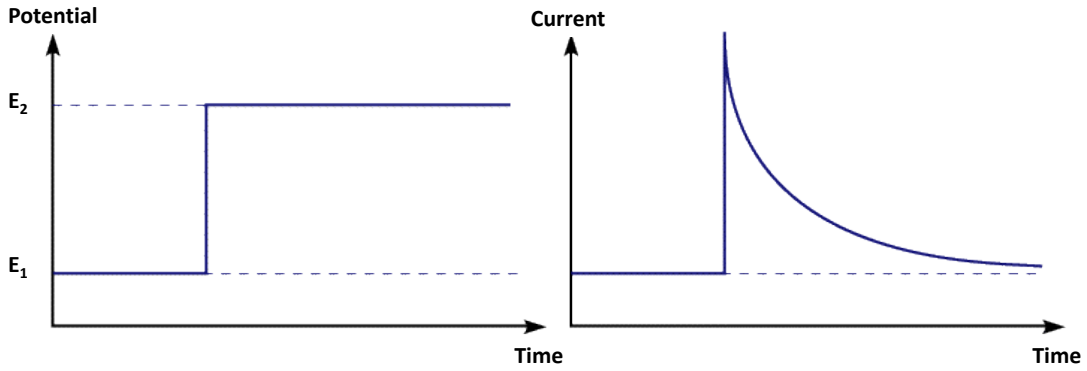

Figure 1-14. Potential step chronoamperometry, potential and current profile as a function of time.[50]

Immediately after the potential step, from no net current at E_1, a large increase in current is observed, caused by a high rate of reaction alongside the great availability of reactant at the electrode surface.

As the reaction proceeds at the electrode surface the concentration of reactant becomes lower, generating a concentration gradient known as the diffusion layer. The latter gets thicker in time, with the concentration of the reactant changing in a linear manner at the proximity of the electrode surface (Figure 1-15). A thicker diffusion layer means that fresh reactant from the bulk solution faces a longer trajectory to reach the electrode surface. Currents drop because the diffusion layer grows rapidly, following a diffusion controlled dynamic.

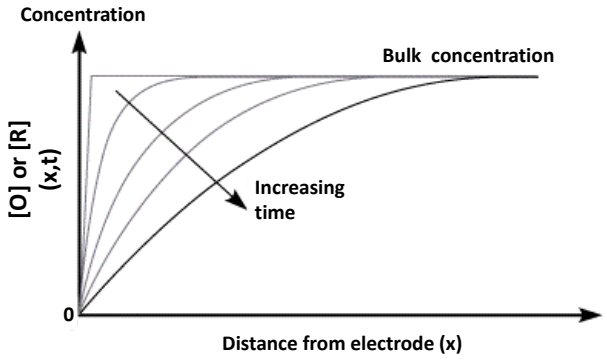

Figure 1-15. The growth of the diffusion layer thickness in time.[50]

In the long term, the profile of reactant concentration between the electrode surface and the bulk solution can be considered linear, with the diffusion layer thickness relating to the net current as shown in Equation 1-10.

$$\frac{i}{nFA} = D_o \frac{[O]_{bulk} - [O]_o}{\delta_o}$$

Equation 1-10. Relationship of the diffusion layer thickness δ_o to the current.

In a well stirred system, fresh reactant is brought to the electrode surface, therefore larger currents are observed and a thinner diffusion layer is established. The maximum current achievable is limited by the rate at which reactants reach the interface and the concentration of reactant at the electrode surface becomes virtually zero. Consequently, the limiting current reached in a well stirred diffusion controlled process is given only by the concentration of reactant at the bulk solution, and the diffusion layer thickness can be estimated using Equation 1-10.[51]

Fick's second law predicts the local changes in concentration as a function of time (Equation 1-11).

$$\frac{\partial C_o(x,t)}{\partial t} = D_o \left(\frac{\partial^2 C_o(x,t)}{\partial x^2} \right)$$

Equation 1-11. Fick's second law of local changes in the concentration of diffusional species as a function of time.

The Cottrell equation (Equation 1-12) derives from integrating Fick's second law (for planar boundary conditions) and describes the current profile as a function of time. The diffusion coefficient can be measured by plotting *i* vs $t^{-1/2}$. If the reaction is diffusion controlled, then a linear relationship is obtained, although instrumental limitations as well as experimental limitations can affect the initial measurements.[51]

$$|i| = \frac{nFAD_o^{1/2}[O]_{bulk}}{\pi^{1/2}t^{1/2}}$$

Equation 1-12. Cottrell equation.

If the system is left for long enough under an oxidising potential, anodic currents will decay tangentially to zero, as there is no fresh supply of reactant. If the system is well stirred, the system approaches a steady-state value (Figure 1-16) characterised by the thickness of the diffusion layer.[51]

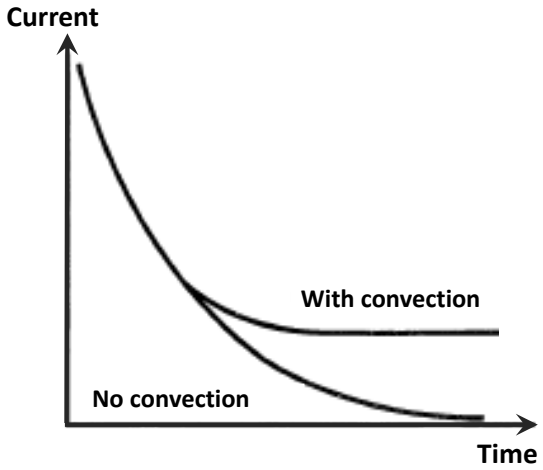

Figure 1-16. Current – time transient for a potential step to a stationary electrode (no convection) and to an electrode in stirred solution (with convection).[51]

By applying a step potential, a profile of discharge is obtained, likewise, by applying a second step to drive the reverse reaction, the system is recharged and a similar plot is obtained. The latter is known as double step potential chronoamperometry.

1.4.5 Electrochemical characterisation of microorganisms

Cyclic voltammetry has been preferably used to characterise the electrochemical activity of microorganisms over an electrode.[39,54] To quantify the kinetics of the electroactive bioelectrodes, rigorous experimental setups are necessary in order to normalise measurements,[39] which are not always practical in laboratory conditions. However, cyclic voltammetry is still a useful tool to study extracellular electron transfer, obtaining thermodynamics information as well as qualitative information on the nature of the electron-transfer process, including: midpoint potential of redox species, reversibility of redox species and dependency with scan rate, influence of mass transfer, among other.[54]

Cyclic voltammetry of most studies on biofilms are carried out at slow scan rates (1 – 10 mV s^{-1}). This is important for two reasons: capacitive currents are proportional to the scan rate and in non-dense biofilms or biofilms with low exoelectrogenic capacity, faraday current signals could be lost at high scan rates,[54] and to allow all proteins involved to be oxidised and reduced many times, known as turnover condition.[39,54]

Turnover conditions require continuous feeding of the organic substrate (electron donor) to the biofilm. By eliminating the diffusion limitation of the organic feed with good agitation, currents are Nernst-driven (current increases) and enzymatically limited (current plateaus), the latter is established due to enzymatic kinetics (V_{max}) of intracellular oxidation reactions or cell-electrode charge transfer rates. Back currents follow the same trajectory as the forward current, because the reactant is not depleted but continuously replenished. Sigmoidal waveforms are observed in the exoelectrogen *G. sulfurreducens*.[55] In some cases a completely flat current is not seen, but currents keep increasing slowly, suggesting that direct electron transfer occurs at slow rates and against a large overpotential, therefore V_{max} is not reached. This has been the case in voltammetry studies of biofilms of *S. oneidensis* in turnover conditions at scan rate of 1 mV s^{-1}.[35,56] If scan rates are high relative to diffusion rates, which can occur by applying a scan rate of 10 mV s^{-1} despite agitation, a peak current will be observed in the forward sweep, with the current dropping in a more or less proportional way to $t^{-1/2}$ due to the electrode donor being consumed/depleted.[57]

In non-turnover conditions, previous to voltammetry measurements, biofilms are starved from the electron donor, inducing a single oxidation or reduction event by each redox centre at the outer surface of the microorganism. In this case, the redox centres in the biofilm act as immobilised redox species. Non-turnover conditions enable the identification of marked current peaks which are not always distinguished due to the presence of more than one redox complex on the cell surface or the

presence of large amounts of soluble redox mediators.[39] Non-turnover conditions have demonstrated many redox peaks in the exoelectrogen *G. sufurreducens*.[58]

In non-turnover conditions, a cathodic current is also developed in the reverse sweep, which is not seen in turnover conditions where there is a flow of electrons maintaining cytochromes in the reduced state, but in non-turnover conditions cytochromes stay oxidised and are able to accept electrons from the electrode. Different to ideal absorbed redox compounds, peak currents of absorbed proteins in the forward and backward sweep commonly are offset 30 – 60 mV due to conformational changes, film heterogeneity or overpontetials required to reach buried redox centers.[39,59]

Biofilms acting as electron acceptors can be associated to cell to cell interactions which are necessary to transfer electrons long distance (relay).[39,55] Turnover cyclic voltammetry of thin and thick biofilms of *G. sulfurreducens* proved that for thick biofilms the magnitude of the current is considerably larger implying cell to cell electron transfer, however only in thin biofilms were all cytochromes oxidised in the forward sweep, indicating that at long distance there are limitations on the relay of electrons through the biofilm.[40]

Harnisch and Freguia[54] published a useful summary of cyclic voltammetry outputs for the exoelectrogen *G. sulfurreducens* (Figure 1-17), showing the different waveforms obtained for turnover and non-turnover conditions at different scan rates or conditions of growth. The first derivative of turnover voltammogram is also shown. It can be seen that a biofilm is a complex redox system with many redox active regions. It is also shown that at high scan rates, capacitive currents significantly increase making it difficult to distinguish redox active regions.

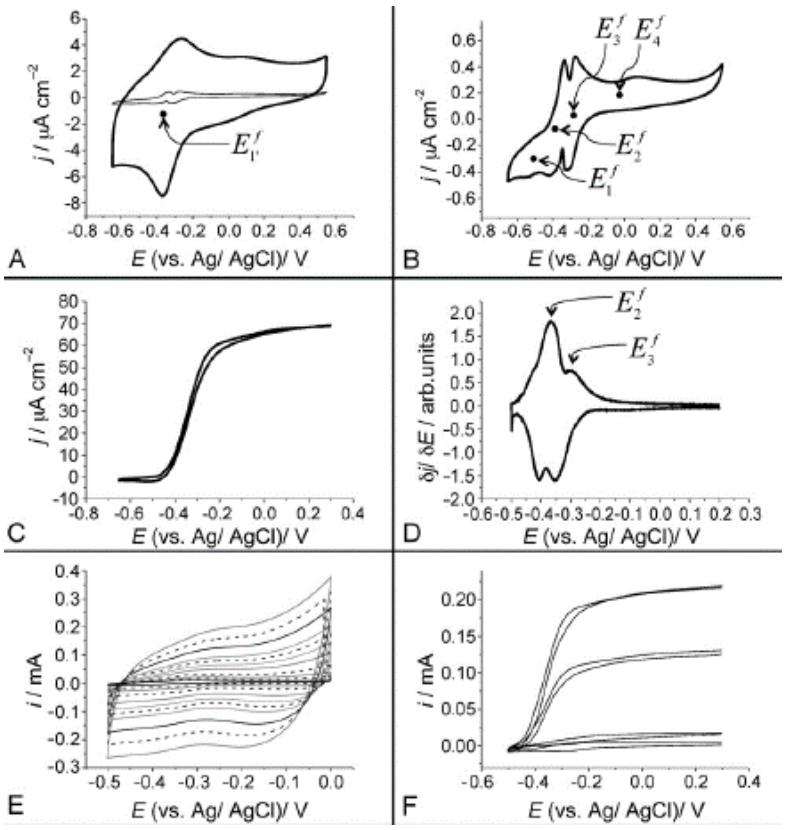

Figure 1-17. Example cyclic voltammetry measurements of *Geobacter sulfurreducens* biofilms as presented by Harnisch and Freguia.[54] A) Non-turnover condition using scan rates of 1 mV s^{-1} and 50 mV s^{-1} (bold). B) Non-turnover condition using scan rates of 1 mV s^{-1}. C) Turnover condition using scan rates of 1 mV s^{-1}. D) First derivative of C). E) Non-turnover condition with increasing scan rate form 1 mV s^{-1} and 100 mV s^{-1}. F) Turnover condition at different states of bioelectrocatalytic activity.

1.5 Microbial bioelectrochemical cells for bioelectricity generation

A microbial bioelectrochemical cell is a type of galvanic electrochemical cell, meaning that the oxidation (anode) and reduction (cathode) half-reactions are thermodynamically favourable to occur spontaneously at the electrodes interfaces, and a flow of electrons is established from anode to cathode (bioelectricity), with an equivalent flow of ions in the electrolyte.

In microbial bioelectrochemical cells, microorganisms can be the electron donor (bioanode), the electron acceptor (biocathode), or both. Typically, microorganisms have been used as electron donors in the anode, while air cathodes have been implemented (Figure 1-18). Oxygen (in air) has a high electrochemical potential and is freely available. The use of an ion exchange membrane to isolate anode and cathode is optional.

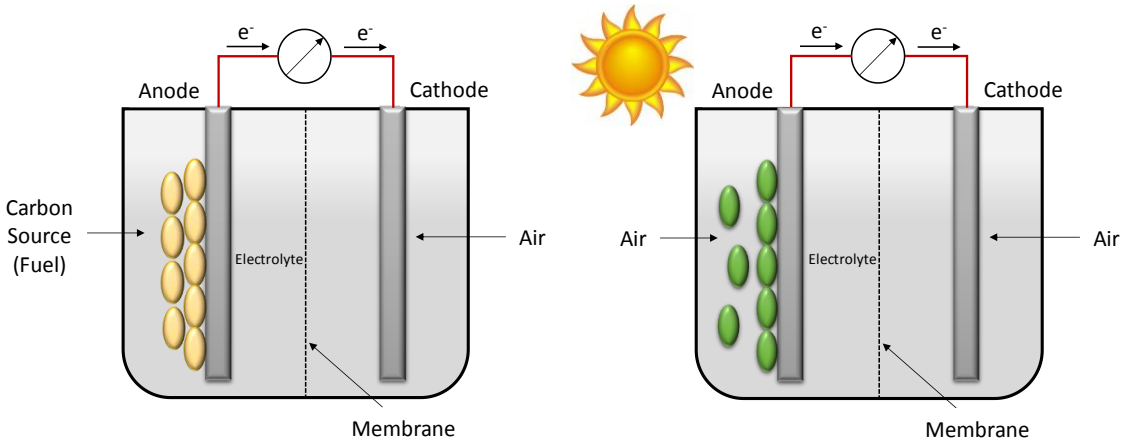

Figure 1-18. Schematic of bioelectrochemical cells showing a bioanode and an air cathode. Left: Microbial fuel cell. Right: Biophotovoltaics. A membrane is optional.

Depending on the energy input of the bioelectrochemical cell, three distinctive groups exist, microbial fuel cells (MFC), photo-microbial fuel cells (photo-MFC) and biophotovoltaics (BPV). Any electrochemical cell, chemical, enzymatic or microbial, is governed by the same principles.

1.5.1 Electrochemical cell theory

The flow of electrons is a response to the electromotive force (E_{mf}) in the electrochemical cell, defined as the difference between the cathodic electrochemical potential and the anodic electrochemical potential. Thermodynamically, the force driving the useful work (W) that the electrical current can produce, which equals the negative Gibbs free energy of the system (Equation 1-13).

$$W = E_{mf} Q = -\Delta G$$

Equation 1-13. Thermodynamic work, useful energy available in an electrochemical cell.

Where *Q* corresponds to the amount of charge transferred in the reaction (coulombs C) and equals to the product between the moles of electrons exchanged (*n*) and the Faraday's constant (F = 9.64853 × 10^4 C mol^{-1}). Equation 1-14 shows the theoretical electromotive force of an electrochemical cell.

$$E_{mf} = -\frac{\Delta G}{nF}$$

Equation 1-14. Electromotive force of the electrochemical cell.

The electromotive force can be calculated from the thermodynamic values at standard conditions (E^{o}_{mf}), corresponding to the difference of the standard potentials of the cathodic and anodic half reactions (as described in Section 1.4.1). The same than for half reactions, in non-standard conditions the electromotive force is given by the Nernst equation (Equation 1-15).

$$E_{mf} = E^{0}_{mf} - \frac{RT}{nF}\ln(\pi)$$

Equation 1-15. Nernst equation for the electromotive force of an electrochemical cell. *R* is the gases constant, *T* is the temperature and π is product concentration over reactant concentration.

The standard potentials, and thus the electromotive force derived from it, provide a thermodynamic theoretical maximum potential, but there are many factors decreasing the electrochemical cell potential. The electrochemical cell is a physical entity with associated energy losses. Furthermore, in biological systems very little information exists, and in many cases the redox activity detected in microorganisms is due to unidentified redox active complexes/compounds. Therefore, empirical characterisation of an electrochemical cell is a common way to evaluate them.

The electrochemical cell is a voltage source, as such it can be represented in an electrical circuit (Figure 1-19). When the voltage source is connected to an external load an electrical current is established (Equation 1-16). There is a voltage loss due to the work generated in the circuit, and the voltage of the cell is given by the current and the resistance in the circuit as given by Ohm's law (Equation 1-17). Part of the energy is lost in internal electrical movement (R_s), and part of the energy powers the external load (R_L). To reduce internal losses, voltage sources are fabricated with appropriated conductive materials. While in an electrochemical cell there are other elements imposing additional resistivity, the electrolyte and the electrochemical reactions occurring at the electrodes surface are two major electrical components.

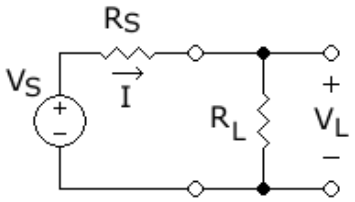

Figure 1-19. Electrical representation of an operational electrochemical cell.

$$i = \frac{V}{R_s + R_L}$$

Equation 1-16. Electrical current in a circuit powered by a source with internal resistance R_s, connected to an external load with internal resistance R_L.

$$V = iR$$

Equation 1-17. Ohm's Law. Voltage difference across a conductor with resistance R with electrical current *i*.

1.5.2 Electrochemical cell characterisation

In an electrochemical cell language, the voltage of the source, which is the voltage difference at zero current, is denominated the open circuit potential (OCP) and the source resistance is denominated the internal resistance (R_{int}). Equation 1-18 describes the general equation derived from the electric circuit and governing the operation of the electrochemical cell, where V_{cell} is voltage drop and *i* is electrical current.

$$V_{cell} = OCP - i * R_{int}$$

Equation 1-18. Electrochemical cell voltage. V_{cell}: voltage drop, OCP: open circuit potential, *i*: electrical current and R_{int}: internal resistance.

To obtain higher power output (P_{out}), higher OCP values alongside with lower R_{int} values are needed (Equation 1-19).

$$P_{out} = i * V = i^2 R_L$$

Equation 1-19. Ohm's Law. Power output.

In a general way, the performance of a microbial bioelectrochemical cell is described by the OCP, R_{int} and the maximum power generated (P_{max}).[12,60] It is a common practice to normalise electrical current and power over anode area. The size of the electrode is also relevant, because higher densities can be achieved with smaller electrode surface.[61]

1.5.2.1 Polarisation curve

In order to identify and characterise the electrochemical parameters of an electrochemical cell, experimental polarisation curves are obtained (Figure 1-20).[49]

A polarisation curve represents the voltage as a function of current. It can be recorded for the anode, the cathode or the whole cell, using a potentiostat or by varying the external load using discrete resistor values and measuring the voltage drop across them, then the current is calculated using Ohm's law (Equation 1-17). The internal resistance of the electrochemical cell is equal to the slope of the polarisation curve in the linear segment (ohmic losses dominance).

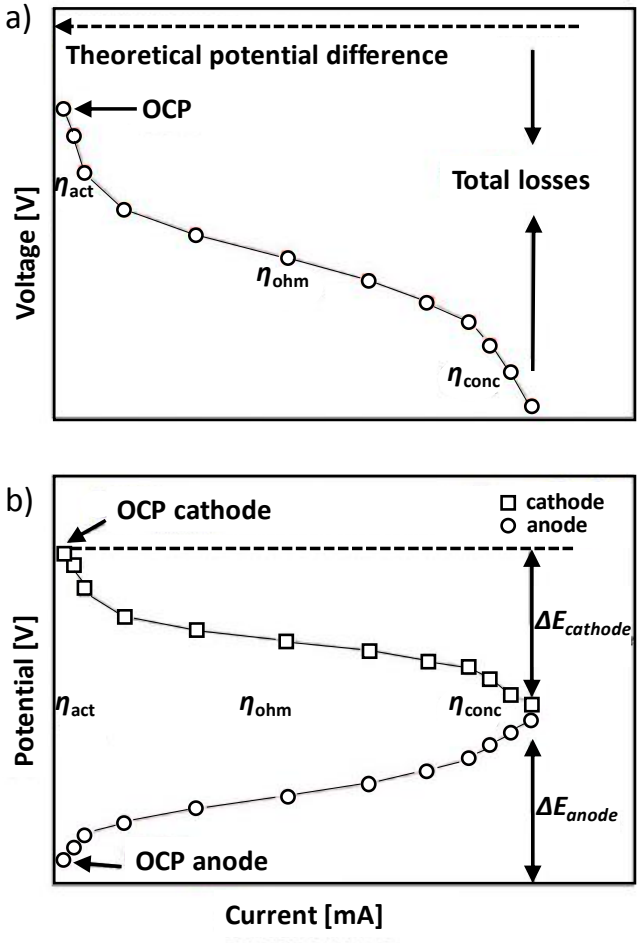

Figure 1-20. a) Current – Voltage polarisation curve for electrochemical cells. b) Separate polarisation for anode and cathode electrodes against a reference electrode. Adapted from Zhao *et al*.[49]

At zero current, there is an overpotential loss associated to internal currents in the electrodes (entropy) and to redox species crossover. Consequently, the OCP of a bioelectrochemical cell is always lower than the predicted initial electromotive force.[12,49] Likewise, the voltage of the cell is lower than the theoretical potential difference as defined by the Nernst equation at changing reactants/products concentrations due to various irreversible potential losses (overpotentials).

In Figure 1-20, it is observed that the polarisation curve of an electrochemical cell has different regions, including an activation overpotential loss (η_{act}), an ohmic overpotential loss (η_{ohm}) and a mass transport overpotential loss (η_{conc}). As currents increase, overpotential losses tend to increase.

Activation losses (η_{act}) are caused by charge transfer resistance related to the activation energy barrier that the system has to overcome for the reaction to proceed. Activation loss is highly non-linear.[12,49]

Ohmic losses (η_{ohm}) are caused by resistances in the electrodes and electrical connections, as well as in the flow of ions through the electrolyte. Specifically, ohmic losses depend on the conductivity and size of the electrodes, the conductivity of the electrolyte and the distance between electrodes, also the conductivity of the membrane separating anode and cathode if there is one.[12,49]

Mass transport or concentration losses (η_{conc}) are mainly caused by the change of concentration of the reactants at the surface of the electrodes, as products appear in the surface, the diffusion of reactants from bulk solution and of products out to bulk solution is necessary to maintain higher potentials. At higher current the rate of diffusion becomes limiting, and the ratio of reduced to oxidised species at the anode surface decreases which causes the anode potential to rise, therefore concentration losses increase abruptly. Agitation reduces concentration losses.[12]

In biofilms there are metabolic losses, or in simple words , there is a potential loss due to energy utilisation in the microbe cell.[12,62] Furthermore, at high current the rate of electron transfer might be higher than metabolic rates, diminishing the number of reduced redox centres in the outer surface of the biofilm, thus increasing concentration losses. In biofilms, the electrical contact between the microorganisms and the electrode also contributes to ohmic losses.[49,62]

1.5.2.2 Power curve

In addition to the polarisation curve, power curves are obtained to represent the power dissipated as a function of the current (Figure 1-21). The power curve is deduced from the polarisation curve applying Ohm's law (Equation 1-19). A power curve starts from zero (at OCP no current is produced), increases as a function of current to a point of maximum power, beyond decreases with increasing currents and becomes zero again (short-circuit condition). As dictated by the maximum power transfer theorem (also known as Jabobi's Law),[63] to obtain maximum power dissipated in the external load, the resistance of the external load must be equal to the internal resistance of the electrochemical cell. At a higher external resistance, the total circuit resistance is high and the power magnitude is lowered, while at a lower external resistance most of the power is dissipated in the electrochemical cell, thus the power dissipated in the load is lowered. Therefore, from the power curve there is another way of determining the internal resistance of the electrochemical cell, which can be approximated to the external load at the highest recorded power.

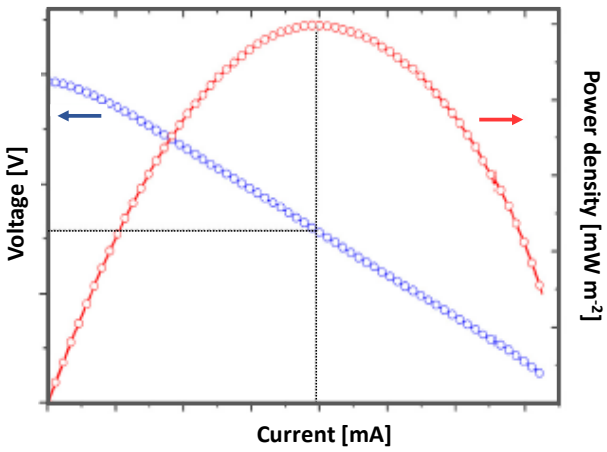

Figure 1-21. Power curve following the polarisation curve of an electrochemical cell. Taken from Thomas *et al.*[64]

1.5.2.3 Overshooting phenomenon

In microbial electrochemical cells, it has been seen that at high currents an overshoot occurs (current and power drop simultaneously). This current drop is explained as a demand for electrons higher than that the biofilm can supply. It happens when the external loads are changed in a discrete way and the sudden change in electron demand causes that intracellular anolytes are depleted; therefore, currents drop when they are expected to increase. In many cases, the system is recovered and currents increase again, showing the adaptability and robustness of the biofilm.[65]

1.5.3 Microbial fuel cells

Typically a MFC is inoculated with sludge or marine sediments and is operated in anaerobic conditions to eliminate oxygen as an electron acceptor.[12,63,66] The sludge or sediments contain a consortia of microorganisms, and upon exposure to an oxidising potential, the consortia is enriched with exoelectrogenic bacteria.[66] Interestingly, mixed consortia of exoelectrogenic bacteria perform better than pure cultures.[61,67]

Air cathodes are commonly implemented, although other redox systems, for instance ferricyanide/ferrocyanide, have also been used showing higher performance (50 – 80%), but with the requirement of replenishment of the catholyte.[68] The cathode surface area is recommended to be larger than the bioanode surface area. Oh *et al.*[68] showed that relative to anodes and cathodes of the same surface area, changing the cathode to one three times larger increased the performance in 24%,

while a four times smaller cathode decreased the performance in 56%, demonstrating that oxygen reduction is a limiting step.

Apart from the three main parameters defining the electrochemical cell (OCP, R_{int} and P_{max}), in MFCs there are other parameters regarding fuel efficiency utilisation:

- Coulombic efficiency (CE): defined as the ratio of coulombs measured as current and the total theoretical coulombs contained in the fuel (organic substrate).[60]
- Energy Efficiency (EE): defined as the ratio of power produced by a MFC and the theoretical heat energy by combustion of the fuel (organic substrate).[60]

The highest power output reported is for a MFC inoculated with mixed consortia, reaching 6,900 mW m^{-2}, still far from the theoretical estimation of 17 – 19 W m^{-2}. In realistic scenarios 6.9 W m^{-2} is only achievable in ideal conditions of feed and MFC design (cathode area 14 time larger).[69,70]

MFCs reach significantly higher current densities than light driven electrochemical cells. Albeit, the limitation of MFCs is the requirement of fuel to generate power. For this reason the technology finds viable applications mainly in the field of wastewater treatment.[71] Recently, Fan *et al*.[72] designed a MFC platform fed with wastewater showing an important improvement, with a power generation of 4.3 W m^{-2}, 10 times higher than the previous efforts.

1.5.4 Photo-microbial fuel cells

As the need of a fuel imposes a barrier for MFCs, the focus of research has been broadened to photosynthetic microbial fuel cells (photo-MFCs), with sunlight as the energy source and carbon dioxide in air as the carbon source for the microorganism subsistence. Various platforms have been enclosed under the term of photo-MFC. In general, cultures responding to light define the most typical photo-MFC platforms.[73–75] But also, mixotrophic microorganisms and anoxygenic photosynthetic microorganisms constitute platforms which use organics and light as source of energy.[76–78] The concept of photo-MFC is even broader and has been used to describe a MFC with a conventional bioanode and with a photo-biocathode, where photosynthetic microorganisms generate an oxygen rich environment.[79] Finally, the idea of photosynthetically cultured biomass to feed a conventional MFC is also, in a global way, associated to light driven electricity generation.

1.5.4.1 Mixed consortia photo-MFC

Mixed consortia photo-MFCs are based on the synergistic relationship between photosynthetic microorganisms (producers) and heterotrophic bacteria (consumers). This system works with sludge or marine sediments which respond to illumination.[73,74,80] it is not restricted to photosynthetic microorganisms and Plant-MFCs have been developed.[74,81]

Photosynthetic microorganisms extrude organic compounds useful for the metabolism of heterotrophic bacteria,[82] which can be exoelectrogenic bacteria and by oxidising the photosynthetic exudates they catalyse the generation of an extracellular electron flow. This type of platform has also been termed complex-photosynthetic-MFC.[83]

In microbial mixed consortia photo-MFC has been observed that currents increase in the dark, possibly due to adverse effects of oxygen generated during photosynthesis.[73,84]

Power outputs as high as 84 mW m^{-2} and 222 mW m^{-2} have been observed in microbial mixed consortia photo-MFC and Plant-MFC, respectively, however average power outputs are significantly lower, 0.3 mW m^{-2} and 21 mW m^{-2}, respectively.[74]

1.5.4.2 Anoxygenic photo-MFC

Anoxygenic photosynthetic microorganisms, the sulphur green and non-sulphur purple bacteria, have resulted in light driven electricity generation.[77,85,86] Furthermore, the non-sulphur purple bacteria *R. palustris* achieved a relative high power output of 2,720 mW m^{-2}, placing it at the level of the best exoelectrogens. This high power output was obtained independent from light, therefore it could be seen as an indirect participation of photosynthesis.[85] Nonetheless, the same *R. palustris* had shown an increased power upon exposure to higher light intensity.[77]

However, these microorganisms perform anoxygenic photosynthesis and an electron donor for photosynthesis other than H_2O is required, for instance acetate or sulphide, therefore there is still the need to feed a fuel and there is not difference with conventional MFCs.

1.5.4.3 Photo-biocathodes

Oxygen reduction in MFC built with air cathodes is a limiting step. Photo-biocathodes provide a way to enrich the cathodic chamber with oxygen, while running with anaerobic exoelectrogenic bacteria in the anode. Moreover, air cathodes in MFC without expensive catalyst (platinum) have been demonstrated.[79,87,88] The use of such oxygen rich photo-biocathodes in MFCs have shown light positive response, showing up to 3-fold higher power outputs.[79,87,88] The improvement in the performance of MFC built with photo-biocathodes is due to cathodic potential raise and lower cathodic resistance.[79] Furthermore, higher light intensity results in higher oxygen evolution which translates in higher power outputs.[79]

It has also been demonstrated that immobilised oxygenic photosynthetic microorganisms in the cathode results in higher performance due to an enrichment of oxygen in the proximity of the electrode surface.[89]

1.5.4.4 Photo-bioreactor MFC

In this system, the photosynthetic microorganisms are cultivated separately to produce biomass and nutrients and these are then fed as the fuel to a MFC.

Dried powder of the microalgae *Chlorella vulgaris* was fed into a MFC, reaching a relatively high power output of 980 mW m^{-2}.[74] In another example, the dried biomass of the filamentous cyanobacteria *A. maxima* was fed to a MFC obtaining higher power than when fed with acetate or glycerol.[90]

Strik *et al.*[91] developed a system where a photo-bioreactor for algae growth was coupled to a MFC in a continuous process. The latter relied on the excretion of soluble organic matter, algae lyses or hydrogen production in the photo-bioreactor, feeding the MFC and generating a maximum power output of 110 mW m^{-2} (photobioreactor section), but the power generation was only 14 mW m^{-2} on average.

1.5.5 Biophotovoltaics

In the case of fully photosynthetic systems, those without heterotrophic bacteria, the name of biophotovoltaics (BPV) has been given, as photosynthetic activity directly generates electricity.[14] However, currents in the dark are also observed.[14,92]

BPV devices represent a self-driven system for renewable clean energy generation. Despite lower power outputs than those obtained in MFCs or photo-MFCs, BPV sustainability greatly surpasses other systems, therefore in recent years increasing attention has been given to BPV research within the scientific community.[46,93]

BPVs are based on oxygenic photosynthetic microorganisms, with water as the initial electron donor (fuel). In mediatorless BPVs currents are also detected, meaning that photosynthetic microorganisms hold direct electron transfer capacity.[14,94] Power outputs as high as 100 mW m^{-2} were reported in a micro-size BPV.[95]

As mentioned before, in BPV systems the energy input is light and the fuel is water, therefore the coulombic and energy efficiency as defined previously do not apply. These parameters in BPV devices are redefined in terms of light and photosynthetic activity energy conversion.

- Coulombic efficiency (CE): defined as the ratio of coulombs measured as current and the total coulombs from split molecules of water measured as O_2 production rate (photosynthesis rate).[14]
- Energy Efficiency (EE): defined as the ratio of power produced by a BPV device and the energy irradiated by the light source over the anode surface area.[96] The energy efficiency as defined would depend on the type of light source used in an experimental setup. Photosynthesis pigments can absorb a fraction of light spectrum and therefore the efficiency calculated will be affected by the light source. To overcome this situation some studies on BPV devices have used filtered light,[14] or LED light.[47,97]

A theoretical maximum power output range of 700 – 7700 mW m^{-2} was calculated for cyanobacteria based BPV by McCormick *et al*.[83] corresponding to a 0.7 – 2.9% of the initial power input. This calculation was based on several assumptions regarding light intensity, absorption efficiency, metabolic losses, and device overpotential losses. Two scenarios of cellular activity were analysed, 3% of electrons entering the photosynthetic electron transport chain is essential for cellular upkeep, and a more conservative 33%. By doing so, it implies that these numbers will be achievable if cyanobacteria readily transfer the other fraction of electrons extracellularly to an electrode, which requires an active route of export. The latter has not been defined in the case of cyanobacteria and its identification remains critical for the technology development. Higher exoelectrogenic capacity in photosynthetic platforms could be achieved as the following:

- Screening for photosynthetic microorganisms with a natural higher exoelectrogenic capacity.[14,98] This search should consider the environment on which microorganisms live.

- Genetically modification of photosynthetic microorganisms introducing exoelectrogenic pathways or deleting electron sinks.[47,93,99] This approach is being explored, although a better understanding of the metabolic pathways redirecting electrons to the cell surface is required.
- Conditioning photosynthetic growth (environmental pressure) in order to positively upregulate their own exoelectrogenic capacity.[100] Finding conditions enhancing extracellular electron transport rates in wild-type strains is paramount to target open field application.

1.6 Biophotovoltaics operational conditions

An important element in the BPV performance is the photosynthetic culture/biofilm activity as the electron donor. The operational conditions of the platform, which depend on the selected microorganism(s), will determine its biocatalytic capacity. Therefore, it is a central point to find conditions which enhance the exoelectrogenic activity of photosynthetic microorganisms, as well as minimise energy losses in the electrochemical cell.

1.6.1 Light

Various studies have found that electricity generation occurs under illumination and increases with higher light intensities.[101–104] However, some examples in the literature have used photosynthetic microorganisms to drive an electrical current exclusively in darkness, using illumination as a recharge stage.[105] Moreover, Fu *et al.*[94] found that in a bioelectrochemical platform using the cyanobacterium *Spirulina platensis,* currents rapidly dropped by transitioning from darkness to illumination, while currents were maintained in the dark. In another work, Fu *et al.*[106] observed that OCPs were higher in the dark, and gradually decreased with an increasing light intensity. While the authors failed to argue on an explanation, their electrochemical cell consisted of a mediatorless single chamber device with two platinum electrodes (anode hosting the biofilm and cathode), thus in the light during photosynthesis the anode was enriched with oxygen, very likely causing the overpotential loss. Same electrodes material should be avoided in a BPV device using an air cathode.

Photosynthetic microorganisms absorb defined wavelength ranges. McCormick *at el.*[14] showed that under different light wavelengths the variations of photosynthetic rates and maximum power generation in a mediatorless BPV device were comparable. Red light induced the highest photosynthetic rates and the highest power in the cyanobacterium *Synechococcus sp.* WH5701, while

rates were lowered in green and blue light. While the microalgae *Chlorella vulgaris* showed high rates in red and blue light, but low in green light.

In a ferricyanide mediated BPV platform studied by Bombelli *et al.*[13], light intensity did not show a great influence, while at low light intensities there was an increase in power generation, the increments were not significant. In general, it was seen that the maximum power output was independent of the light intensity, although the authors also showed that the time to reach peak power was longer at low light intensities. Therefore, even though there was an independency from photosynthesis, it allowed a rapid generation of intracellular reducing power, but ultimately the "bottleneck" is at electron export level.

1.6.2 Temperature

Biomass growth has an optimal temperature and a maximum temperature the cells can stand, therefore the temperature that a BPV can be operated is restricted by the chosen microorganism(s). Fu *et al.*[94] studied the effect of temperature in a BPV device inoculated with the cyanobacterium *Spirulina platensis* (in dark), at 20, 30 and 40 °C, finding a clear increase in power at higher temperatures.

However, the operation of BPV platforms require minimal energy inputs, therefore most studies are carried out between 20 to 30 °C.[13,14,47,107]

1.6.3 Cultural pH

Just as with temperature, microorganisms grow optimally at given pH values, also within a range. Many cyanobacterial species are alkaliphiles, with optimal pH between 7.5 and 9.0, and rarely below pH 5.5.[108]

Fu *et al.*[94] studied the effect of pH in BPV devices inoculated with cyanobacterium *Spirulina platensis* (in dark), measuring power output at pH 5.5, 8.3 and 9.9. No great difference was seen between pH 8.3 and pH 9.9. The same for OCP values. At pH 5.5, OCP values were around 1.8-fold higher, consequently power output was also higher. The increase in OCP was very likely due to the higher oxygen reduction potential (cathode), but also increased pH was suggested to reduce R_{int} allowing higher power. In any case, the result showed that the cell performance improved in acidic conditions.

1.6.4 Media conductivity

The electrolyte in the reactor is also given by the chosen microorganism(s). It corresponds to the cultivating medium. In the selection of the microorganism, freshwater and marine species, both cyanobacteria and microalgae, have been studied.[14] The conductivity of the media is very low in aqueous solutions compared to seawater, thus the R_{int} of the electrochemical cell can change dramatically from one system to the other. For instance, Bombelli *et al.*[14] worked with four different photosynthetic microorganisms in a mediatorless BPV, with R_{int} resistances of 22 kΩ 333 kΩ for freshwater species, and 3 kΩ for marine species. However, most of the studies in BPV platforms have utilised freshwater species, possibly due to more data available for model freshwater photosynthetic microorganisms.

Interestingly, McCormick *et al.*[100] used media modification by increasing salinity in culturing the freshwater cyanobacterium *Synechocysis sp.* PCC6803. High salt (0.25 M NaCl) caused higher exoelectrogenic reduction of ferricyanide, but an understanding on the induction of higher exoelectrogenesis in high salinity was not presented.[100] Nonetheless, this demonstrated that exoelectrogenic capacity can be enhanced by environmental factors. Moreover, the increase in salinity guarantees lower R_{int} in a bioelectrochemical cell.

1.6.5 Mediator concentration

Plasma membrane impermeable redox mediators provide a more efficient system in extracellular charge transfer. Ferricyanide/ferrocyanide are impermeable to the plasma membrane with a redox potential of approximately 230 mV vs Ag/AgCl,[109] constituting in an ideal redox mediator for this purpose.

Bombelli *et al.*[13] studied the effect of the concentration of ferricyanide on power output, finding that power increased with increasing concentration of ferricyanide (0.5 mM to 35 mM) to reach a maximum and then dropped at higher concentrations (35 mM to 50 mM). Only at 50 mM an inhibitory effect was seen over oxygen evolution (photosynthesis). The same tendency happened in the dark, but the highest power was obtained at 15 mM. Higher concentration of the artificial redox mediator increases reduction rates to a limit because exoelectrogenic activity should reach maximum rates. At higher concentrations, power output dropped because the half-cell potential was lowered due to a higher ferricyanide to ferrocyanide ratio, as given by the Nernst equation (Equation 1-4).

Thorne *et al.*[110] found that in cultures of the microalgae *Chlorella vulgaris* there was a loss in the effective concentration of the mediator, up to 14% of ferrocyanide was missing, due to trapping in the cell surface. The latter reduces the efficiency of the bioelectrochemical cell, particularly if the addition of mediator is at low concentration, a counterproductive occurrence in mediated platforms.

High concentration of mediator can have toxic effects long term, due to membrane polarisation and diffusion to the intracellular compartment, where it can accumulate and interfere in many metabolic reactions. For the same reason, typically 1 mM ferricyanide is added to BPV platforms.[47,48,111]

1.6.6 Nutrients

The availability of nutrients is important for cell viability. The lack of nutrients, or starvation, induces a series of responses by the cell to cope in stressful conditions until nutrients are replenished. For instance, nitrate starvation induces the production of algal lipids, a valuable source for biofuel generation.[112]

In various microalgae and plant roots, iron starvation has resulted in increased ferricyanide reduction capacity, due to the overexpression of ferric reductases in the plasma membrane (assimilatory reduction).[113–115] For instance, *Chlamydomonas reinhardtii* showed 10-fold increase in ferricyanide reduction rates.[116] Nonetheless, this metabolic activity has not been exploited in BPV platforms, possibly due to the low endurance that photosynthetic microorganisms have to grow in iron deprivation.

1.6.7 CO_2

The carbon dioxide effect over biomass production through photosynthesis has been studied broadly, particularly for applications on CO_2 sequestration in photoreactors.[117,118] However, within BPV platforms, it has been argued that CO_2 is the main competitor for electrons and that levels of CO_2 should be maintained low. As proposed by Bradley *et al.*,[45] CO_2 fixation should be inhibited or uncoupled from photolysis of water to increase exoelectrogenic rates.

Good aeration to supply with CO_2 is still necessary, otherwise cell viability will be lost. Furthermore, there are a few examples of microalgae and plant roots grown in high CO_2 (20% CO_2 in microalgae, 0.08% CO_2 in plant), showing higher extracellular ferric reductase activity.[119,120]

1.6.8 Biomass

Increasing biomass increases the abundance of the biocatalyst, thus higher currents can be sustained. Fu *et al.*[106] showed that higher biomass loaded in the cell increased OCP values in a mediatorless system, in light and darkness. OCP values reached a maximum at a given biofilm density above which decreased. Fu *et al.*[106] study is interesting because it shows that biomass density is not only important to ensure electron availability, but the biofilm thickness and electrode coverage also has an impact in the performance of the electrochemical cell. However, OCP values dropped after an optimal biomass density, which was independent of light. It can be speculated that further layers in the biofilm cannot transfer electrons, but still interact with the inner layers, changing the interaction within the biofilm, thus reducing OCP. Similarly, it was demonstrated that in thick biofilms of *G. sulfurreducens* the upper layers remain reduced.[40]

In a ferricyanide mediated BPV platform, increasing biomass concentration was shown to be linear to peak power output.[13] Although, the authors correctly argued that the linearity will be lost at very dense cultures, because higher cell density will cause adverse effects on light penetration and ferricyanide diffusion.

1.7 Exoelectrogenesis in oxygenic photosynthetic microorganisms: the case of cyanobacteria

Oxygenic photosynthetic microorganisms presenting exoelectrogenic activity are not a rare exception, several have been reported to generate current in BPV devices. For instance, the cyanobacteria *Synechococcus sp.*, *Spirulina platensis* and *Synechocystis sp.*, and the microalgae *Chlorella vulgaris* and *Chlamydomonas reinhardtii*, are among the photosynthetic microorganisms found to have an exoelectrogenic response.[14,48,94] However, cyanobacteria and microalgae are not adapted to export electrons as part of major metabolic pathways.

The utilisation of cyanobacteria in biotechnological applications is particularly preferred due to their lower energy requirements and simpler physiology.[8] They are a good compromise between a simple electron transfer route, from water to electrode, and the level of biological organisation to sustain their own growth and maintenance.[45] Cyanobacteria have three distinctive biological membranes (Figure 1-22), the thylakoid membrane, fostering photosynthetic and respiratory complexes; the plasma membrane or cellular membrane, containing respiratory complexes and various transporter

proteins and enzymes; and the outer membrane, a final semipermeable envelope containing protein and channels (porins).

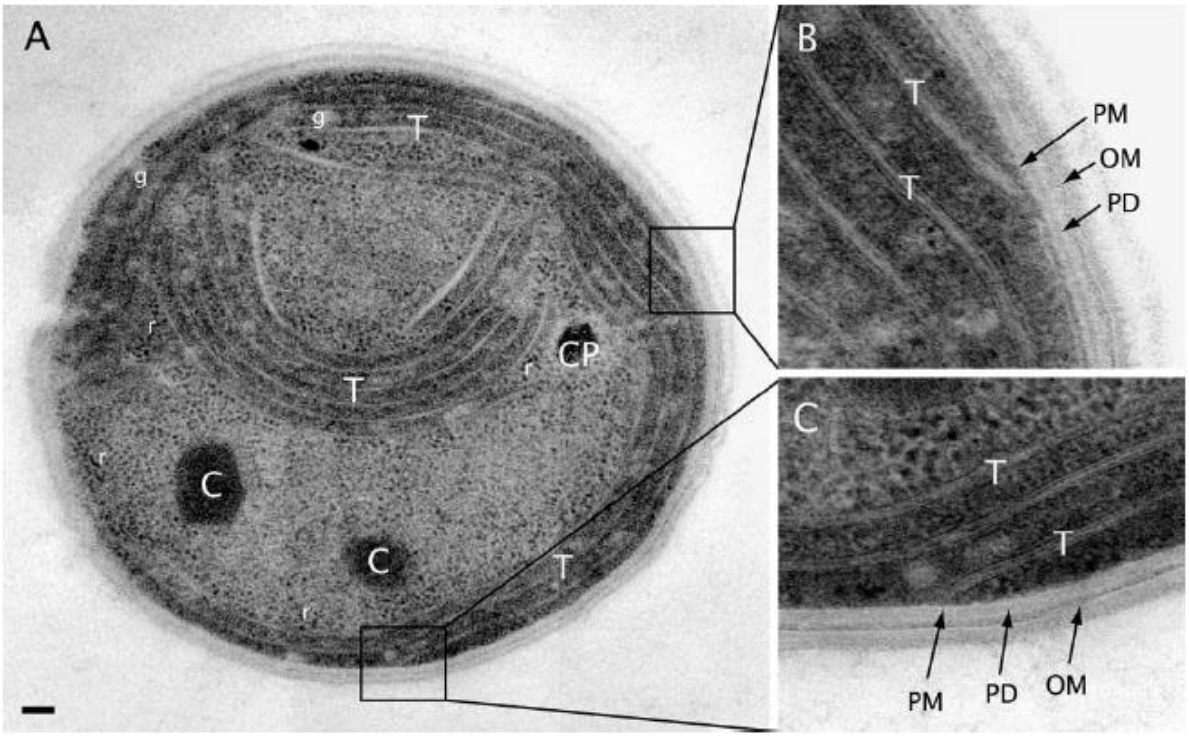

Figure 1-22. Electron micrograph of a thin section of the cyanobacterium *Synechocystis* PCC6803. B and C are enlargement of the corresponding boxed areas in A, showing proximity of thylakoid membrane to the plasma membrane. T: thylakoid membrane, PM: plasma membrane, PD: peptidoglycan layer, OM: outer membrane, C: carboxysomes (subcellular structure for CO_2 fixation), CP: cyanophyn granule (nitrogen and carbon storage), g: glycogen granule, r: ribosomes. Bar: 100 nm. Taken from Liberton *et al.*[121]

The maximum possible photo-current generation in cyanobacteria was estimated as 1 pA $cell^{-1}$, considering that the typical photosynthetic oxygen evolution rates are in the order of 500 $\mu molO_2$ mg_{Chl}^{-1} h^{-1}.[45] However, water splitting and extracellular electron transport would have to be exclusively coordinated. In a real scenario, low exoelectrogenic capacity and limited understanding of the metabolic pathways involved in cyanobacteria exoelectrogenesis have restricted the development of photo-bioelectricity generation by cyanobacteria, and microalgae have received renewed attention.[48,111]

Nonetheless, due to inherent cyanobacteria advantages, they still represent an active line of research.[83,93] As cyanobacteria are prokaryotes, many cyanobacteria have their genomes fully annotated, therefore genetic modifications are more accessible, providing a platform which can be engineered to a desire product, for instance, *in vivo* generation of electricity.[47,99]

Many studies have shown that photosynthesis is the main driver of the exoelectrogenic activity observed, as typically currents increase in the presence of light, while photosynthesis inhibitors diminish the response. Studies with different photosynthesis inhibitors suggest that electrons exit the photosynthetic electron chain at the end of the light reactions, thus available as reducing power (NADPH).[13,45] Furthermore, a bioelectrochemical cell inoculated with a mutant of *Synechocystis* lacking PSII showed hindered currents when compared with the wild-type, indicating that PSII is necessary for extracellular current generation.[107] Nonetheless, currents in the dark are also recorded, implying alternative sources of reducing power within the cell (NADH) as a result of the metabolism of carbohydrates.[13,45]

The flux of electrons generated in the light reaction is mainly directed to CO_2 fixation, while the oxidation of carbohydrates is directed to respiration with oxygen as the final electron acceptor, or to synthesis of biomolecules. The detected exoelectrogenic activity corresponds to a minimal fraction of the electron being metabolised, about 0.3% (from photosynthesis) in wild-type *Synechocystis sp.* PCC6803.[47] Therefore, to find a point of electron export and metabolic pathway providing reducing power is paramount to make use of cyanobacteria photo-biocatalysis capability.

So far, different strategies have been explored to intercept cyanobacteria photosynthetic electrons in an electrode (Figure 1-23), by using membrane soluble redox mediators (no exoelectrogenesis needed), by using membrane impermeable redox mediators and by direct electron transfer, while NAD(P)H appears to be the electron donor for the exoelectrogenic activity,[13,45] with photosynthesis being a direct contributor of reducing power towards the extracellular electron transport process.

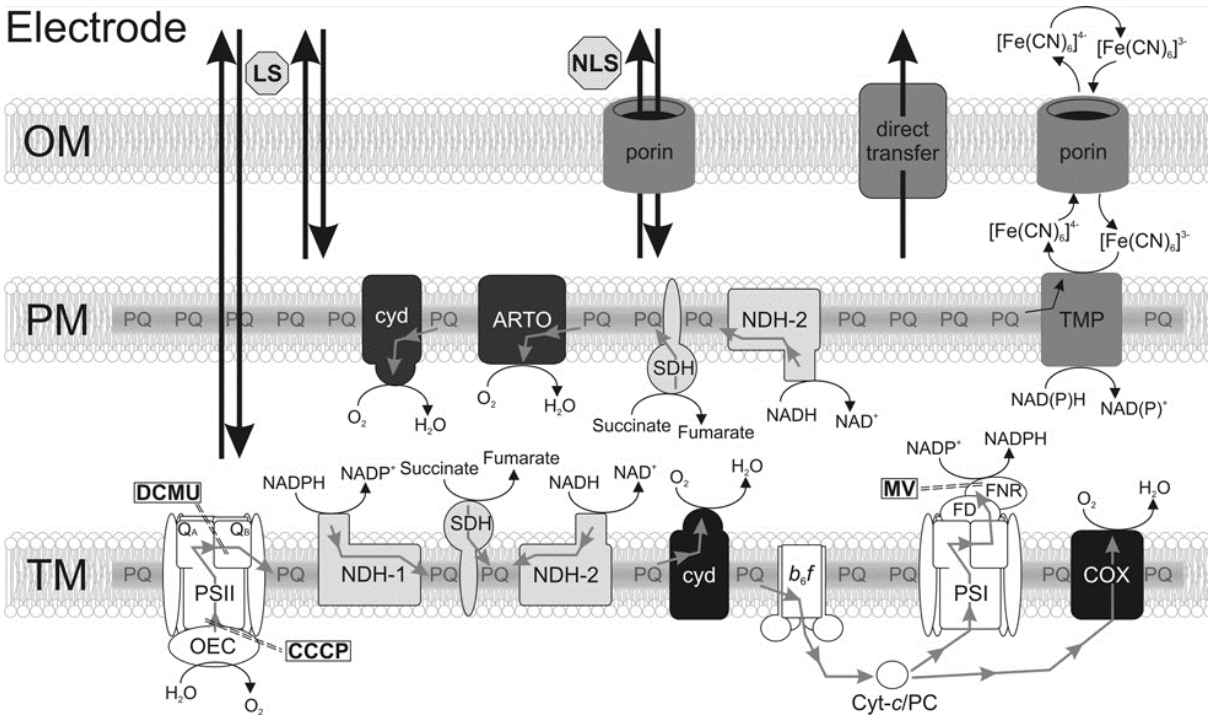

Figure 1-23. Electron transport within cyanobacteria and to an electrode. LS: lipid soluble. NLS: non-lipid soluble. TMP: unknown transmembrane protein. DCMU, CCCP and MV are electron transport inhibitors. Taken from Bradly *et al.*[45]

In cyanobacteria, also in microalgae, currents are considerably higher in artificially mediated platforms, typically plasma membrane impermeable ferricyanide. Therefore, many studies on BPV devices carry on using impermeable redox mediators.[48,111] Furthermore, ferricyanide provides a colorimetric method to measure exoelectrogenesis. Ferricyanide can be measured spectrophotometrically at 420 nm, while ferrocyanide has negligible absorbance at 420 nm, meaning that conversion can be measured. Many studies have used this method to determine the extracellular reduction capacity in cyanobacteria and microalgae.[47,99,113]

Photosynthesis is at the centre of the exoelectrogenic capacity of cyanobacteria, therefore understanding the photosynthetic process is essential to improve extracellular electron transfer rates.

1.8 Oxygenic photosynthesis in cyanobacteria

Cyanobacteria have been around for long time, the oldest fossils suggest their occurrence on Earth being 3.5 Gyr ago.[122] Their success is based in their capacity to perform oxygenic photosynthesis.

Oxygenic photosynthetic organisms sustain their growth mainly on light (energy), H_2O (electron donor) and CO_2 (carbon source and final electron acceptor), all very abundant on the earth surface. However, H_2O is a very stable molecule and to be oxidised a large amount of energy is required. Furthermore, CO_2 requires a strong reductant, such as NADPH, and a large amount of ATP. Oxygenic photosynthesis utilises two electron excitation steps and a series of electron carriers to overcome the energy requirement to deliver electrons to $NADP^+$ (Figure 1-24). Cyanobacteria were the first to carry out oxygenic photosynthesis thanks to the appearance of the two chlorophyll containing protein complexes cooperatively transferring electrons from water to $NADP^+$, photosystems PSII and PSI, localised in the thylakoid membrane.

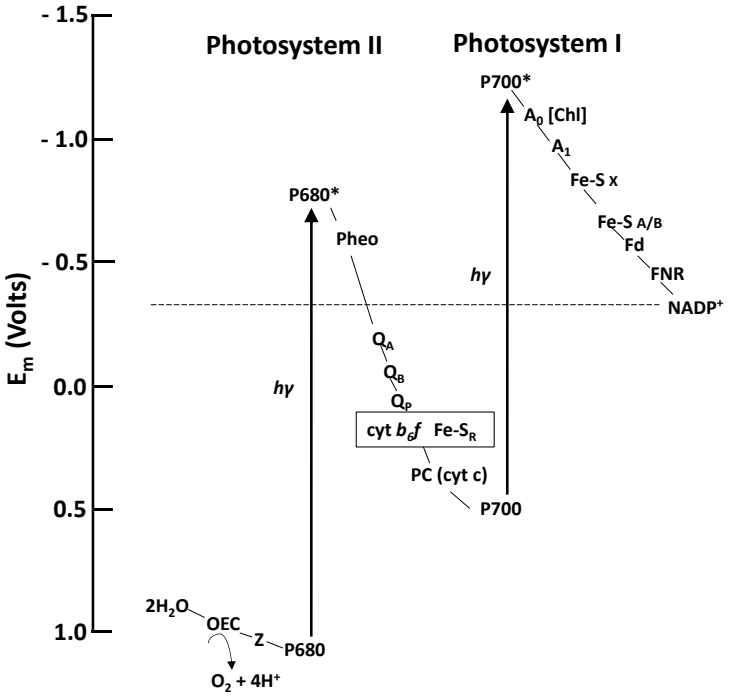

Figure 1-24. Z-scheme of oxygenic photosynthesis based on chl*a* absorption in two photosystems PSII and PSI. E_m corresponds to midpoint potentials. Adapted from Mielke *et al.*[51]

PSII (Figure 1-25) is the reaction centre conducting the light-induced charge separation which allow the catalysis of water oxidation (water splitting) with the concomitant reduction of plastoquinones (lipid soluble redox active co-factors). PSII is formed by more than 20 subunits. All redox active co-factors reside in two photo-chemical active proteins denominated D_1 and D_2. Closely associated to D_1 and D_2 there are two chlorophyll (Chl*a*) binding antenna proteins, denominated CP43 and CP47. Also in the protein complex there is the extrinsic bound protein of the oxygen-evolving complex (OEC).[123,124]

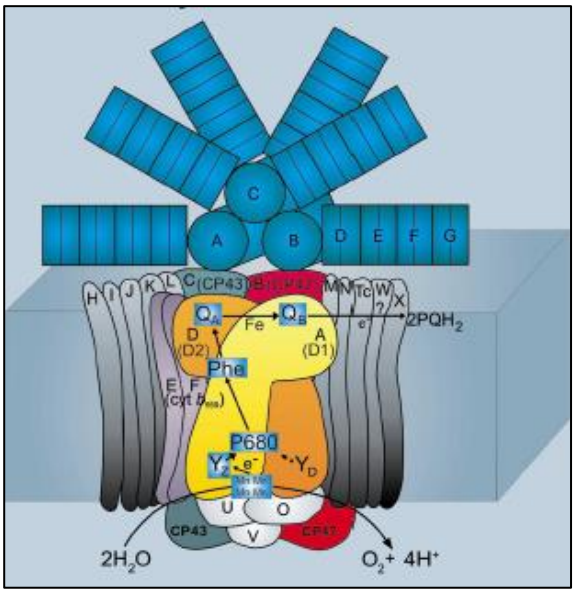

Figure 1-25. Photosysthem II (PSII). Showing light harvesting antenna (PBS) and electron carrier reactions. Taken from Hankamer *et al.*[123]

The primary electron donor is P680 (Chl*a* molecule), which absorbs light energy. An electron is excited (P680*) and transferred to pheophytin (Phe), the primary electron acceptor, which in turn reduces a bound plastoquinone Q_A, and the reduction of another plastoquinone Q_B follows. Q_A is a one-electron acceptor, firmly bound in Q_A binding pocket. Differently, Q_B is a two-electron acceptor and it is released from it binding site once it receives two electrons from Q_A and two protons from the cytoplasm. On the other side, $P680^+$ (chlorophyll cation radical), oxidises a tyrosine residue Y_Z (redox active amino acid), which in turn is reduced by a manganese ion, the latter forms part of a four-manganese cluster. This metal centre is the active site of water oxidation. When the cluster accumulates four oxidising equivalents, two molecules of water are oxidised generating oxygen (O_2) and four protons.[123,124]

Light, the energy input for the reaction centres, is harvested by pigment-protein antenna systems. In cyanobacteria, the antenna systems are known as phycobilisome (PBS), rod-like arrays of phycobiliproteins bound to the PSII core reaction centre by linker proteins. The light energy absorbed in the periphery of the PBS is transferred to the reaction centre by radiationless excitation energy transfer (Figure 1-26), therefore energy must be transferred rapidly to avoid energy losses (~120 picoseconds). PBS transfers excitation energy to PSII and to a less extent to PSI. Under low light intensity, photosynthetic organisms increase their antenna content.[124]

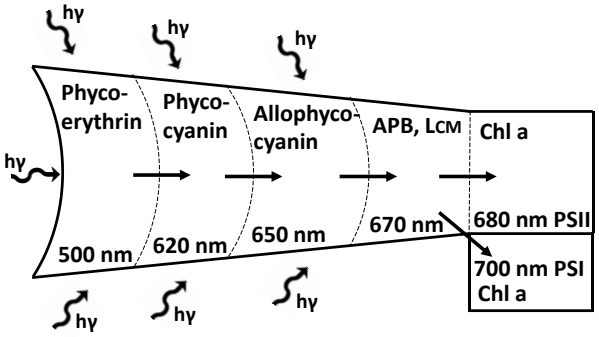

Figure 1-26. Energy flow in phycobilisome (PBS) in cyanobacteria. Radiationless excitation energy transfer from short-wavelength to long wavelength-absorbing pigment-protein complexes. Composition of PBS varies widely among cyanobacteria.[124]

The protonated Q_B joins the free pool of plastoquinones (PQ) in the thylakoid membrane, in its reduced form PQH_2 (plastoquinol). In cyanobacteria there are respiratory complexes in the thylakoid membrane and they can also feed electrons to the plastoquinone pool, as illustrated in Figure 1-23.[45,125,126]

PSII photo-catalysis generates a weak reductant (PQH_2). The plastoquinol-cytochrome c_{553}/plastocyanin oxidoreductase (Cyt b_6f complex), a third protein complex in the thylakoid membrane, catalyses the rate limiting quinol oxidation, transferring electrons from PQH_2 in the membrane to a soluble electron carrier, plastocyanin or cytochrome c_{553} (c_{553} in copper limiting conditions), found in the intrathylakoidal space (lumen), and translocating the two protons to the lumen. A proton gradient is created which is used by ATPases in the thylakoid membrane to synthesise ATP (photophosphorylation).

A second photo-catalysis occurs when PSI oxidases the soluble plastocyanin (or cytochrome c_{553}), with the concomitant generation of a strong reductant to obtained NADPH. PSI is formed by 11 subunits. Two central subunits PsaA and PsaB, form two interlocked semicircles enclosing redox active co-factors. Most of chlorophyll antenna are bound to PsaA/B, with its N-terminal resembling to CP43 and CP47 in PSII. While the C-terminal is structurally similar to D_1 and D_2, but it is different in that they coordinate 12 (PsaA) and 13 (PsaB) Chl*a* molecules of the antenna, thus PsaA/B C-terminal cannot be considered as a pure reaction centre domain. Peripheral subunits also bind redox active co-factors and participate in electron transfer with soluble electron carriers.[127]

In PSI, the primary electron donor is P700 (Chl*a* dimer), and the primary electron acceptor is A_0 (Chl*a* monomer). A_0 rapidly reduces the bound phylloquinone (A_1), stabilising the separated charge.

Electrons are then transferred to F_X, an iron-sulphur cluster [4Fe – 4S], and then to other iron-sulphur clusters F_A and F_B. The latter are exposed to the cytoplasmic side, where the soluble electron carrier ferredoxin is reduced (flavodoxin replaces ferredoxin in iron deprivation). The ferredoxin:$NADP^+$ oxidoreductase (FNR) catalyses the electron transfer from ferredoxin to $NADP^+$.[124,127] Alternative oxidoreductases within the metabolism of cyanobacteria can also catalyse electron transfer from reduced ferredoxin to other electron sinks within the cell.[125]

Reduced ferredoxin is used as described in what is known as non-cyclic electron transport to generate NADPH (and other metabolites), or alternately, ferredoxin can return electrons to the thylakoid membrane in cyclic electron transport around PSI, by reducing the PQ pool instead. The catalysis of Cyt b_6f transfers the electrons to plastocyanin with proton gradient creation, thus ATP synthesis results from the process, while plastocyanin is oxidised by PSI to re-enter the cycle.[124] Additional ATP generated in cyclic electron transport is used in CO_2 fixation and other metabolic reactions which require energy, for instance pumping of bicarbonate (HCO_3^-) and other nutrients.

Light quantity and quality (including darkness), inorganic carbon concentration (CO_2, HCO_3^-), and nutrient availability, imply conditions with higher or lower energy requirements, resulting in the alteration of the proportion of non-cyclic versus cyclic electron transport in the photosynthetic chain.[124,128] There are two recognised mechanisms that cells use as a response to the change in energy demand. The first mechanism provides a rapid adjustment of the photosynthetic apparatus from State 1 to State 2, by a redistribution of light harvesting antenna between the two photosystems, called “state transition”. This takes seconds to minutes, therefore is referred to as a short-term adaptation.[124] State 1 is induced by oxidation of the intersystem electron carriers, related to excess excitation of PSI as compared with PSII. State 2 is induced by reduction of intersystem electron carriers, by excess excitation of PSII, but also by dark respiratory pathways in the thylakoid membrane.[128] The second mechanism consists in the adjustment of the photosynthetic apparatus by changing the stoichiometry between PSI and PSII (Table 1-2). It is also a relatively rapid response, however it depends on the synthesis of new proteins and thylakoids, and it takes hours to days to be fully adapted, therefore it is referred to as long-term adaptation.[124] It is believed that the short-term adaptation of the photosynthetic apparatus induces further long-term adaptation (Figure 1-27).[124]

Strain	Condition	PSI:PSII
***Synechococcus sp.* PCC6301**	Fluorescent light (PSII light)	2.5
	Far-red light (PS I light)	1.0
	3.0% CO_2	2.5
	0.2% CO_2	4.2
***Synechocystis sp.* PCC6714**	Weak white light	2.9
	Strong white light	1.3
	Dark, heterotrophic	2.3

Table 1-2. Photosystems relative abundance PSI/PSII in cyanobacteria depending in the environmental conditions.[124]

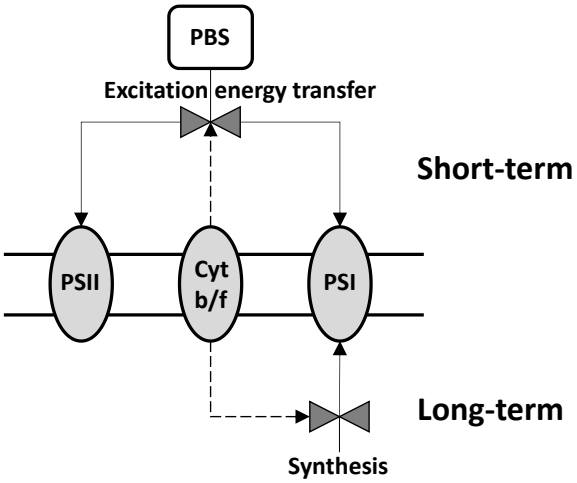

Figure 1-27. A model for short-term and long-term adaptation mechanisms for adjustment of the thylakoid system.[124]

The homeostatic regulation of the photosystems allows the cells to perform high light conversion efficiency in changing environments. The PSI:PSII molar ratio can be estimated by oxidation-reduction difference absorption spectra P700 (for PSI) and Cyt *b*-559 (for PSII) in extracted thylakoid membrane.[129] Alternatively, low temperature (77K) fluorescence spectra of intact photosynthetic cells provides an estimation of the PSI:PSII stoichiometry.[49] The latter method has also been associated to the short-term adaptation (State 1 – State 2 transition), as it has been observed that the fluorescence spectra is altered rapidly in some extreme changing conditions (only 1 hour).[130]

The photosynthetic process is completed only when CO_2 is fixated, however, excess light energy is continuously harvested in the photosystems, as CO_2 fixation rates and consequently regeneration of $NADP^+$, are limited. Photo-inhibition (photosystem damage) can occur in very high light, if excited PSII is not rapidly oxidised, because of the generation of reactive oxygen species (ROS).[126,131] Photosynthetic microorganisms have evolved mechanisms to protect themselves from high light, dissipating energy that is not needed. Carotenoids associated in the PBS, which function as photo-

receptors, also protect both photosystems by thermal energy dissipation, thus reducing the amount of energy being transferred to chlorophyll molecules, likewise carotenoids are known to prevent formation or directly quench singlet oxygen.[131] The interlink between photosynthesis and respiration in the thylakoid membrane also confer a protective mechanism, by acting as alternative electron sink.[126] The utilisation of reducing power in exoelectrogenesis could alleviate the system when exposed to high light intensities. However, a route of redirection of reducing power to the extracellular ambient is not a strategy described in the protection of photosystems.

The photosynthetic apparatus is highly dependent on iron as co-factor.[132,133] Iron starvation induces the increment in iron uptake machinery, which can be through extracellular reductive mechanisms.[134–136] The latter is a type of exoelectrogenic activity, but it is not well identified in cyanobacteria.

The effect of CO_2 partial pressure on the photosynthetic process is also relevant. As shown in Table 1-2, the PSI/PSII ratio is lower at higher CO_2 concentration, implying higher non-cyclic electron transport in the photosynthetic process, therefore higher generation of NADPH and consequently CO_2 fixation. NADPH is the alleged substrate for extracellular electron transport (Figure 1-23), therefore increasing its intracellular generation could positively impact exoelectrogenesis in cyanobacteria.

1.9 Aims and propose systems

The aim of this thesis is the development of photosynthetic – exoelectrogenic cultures and biofilms, utilising cyanobacteria as the photo-biocatalyst in BPV platforms.

The development in the design of BPV devices has non-biological aspects. The selection of electrode materials, the selection of the cell configuration and the selection of membrane (optional) are of great significance to construct an efficient platform. Inexpensive materials are proposed in order to deliver a sustainable cost effective design.

The selected photosynthetic strain is the model cyanobacterium *Synechococcus elongatus* PCC7942, formerly known as *Anacystis nidulans* R2, (PCC7942 hereafter). PCC7942 has been broadly studied in biotechnological applications, including its genetic modification to harbour an outer membrane cytochrome to exploit extracellular electron transfer. The experimental designs proposed in this thesis aim to provide a system using wild-type PCC7942 which is sustainable and can be integrated with other photo-bioprocesses, especially regarding bioenergy and CO_2 mitigation.

In this thesis, electrochemical cell devices were constructed to evaluate the performance of PCC7942 as the electron donor. Different BPV designs were implemented as a strategy to improve the efficiency of the electrochemical cell. Other exoelectrogenic microorganisms were tested in the same platforms with the aim of providing a comprehensive assessment, particularly MFCs inoculated with *Shewanella oneidensis* were used to provide a better assessment of the different platforms. Additionally, the reduction of ferricyanide (soluble redox mediator) was measured to quantify the exoelectrogenic capacity of photosynthetic cultures, with the aim of dismissing the complexity of mediatorless extracellular electron transfer.

Cyanobacteria are poor exoelectrogens, however it is possible to find conditions enhancing their exoelectrogenic capacity. The strategies proposed in this thesis to increase exoelectrogenesis in PCC7942 are growth in iron limitation and growth under CO_2 enrichment. These conditions have been associated to extracellular electron transfer in microalgae and plants. In this thesis, the two environmental conditions are investigated in PCC7942.

PCC7942 has been a model for the study of iron starvation in cyanobacteria. The changes in the photosynthetic electron chain is well characterised. The transcripts profile of PCC7942 grown in iron limitation is published. Particularly, PCC7942 has iron-deficiency-induced proteins, including an oxidoreductase, which are thought to function in an iron acquisition system.

PCC7942 has been studied under CO_2 enrichment and found to be capable of growing in an extremely high CO_2 content, up to 40%. The highest growth rate has been correlated to 5% CO_2. The transcripts profile of PCC7942 grown in high CO_2 compared to air has also been reported.

The information available for PCC7942 regarding iron metabolism and growth under CO_2 enrichment placed it a promising candidate for the proposed strategies.

Finally, the electrochemical characterisation of PCC7942 it is demonstrated, using analytic electrochemical techniques. A protocol to apply electrochemical techniques in the development of BPV devices is proposed.

1.10 Thesis layout

In Chapter 2 is presented a detailed description of the protocols, materials and fabricated devices used in the experimental procedures carried out for the work expounded in this thesis.

The evaluation of the performance of PCC7942 as an electron donor is presented in Chapter 3. A benchmark study comprised of two stages is reported, consisting of a systematic assessment of PCC7942 performance in mediatorless BPV devices and in its capacity of extracellular reduction of ferricyanide. Firstly, PCC7942 was evaluated in a comprehensive comparative study against the performance of the exoelectrogenic bacterium *S. oneidensis* MR-1, which was utilised to establish the efficiency of different electrochemical cell designs. The second stage consists in the comparison against other photosynthetic cultures, including the microalgae *C. vulgaris* CCAP 211/52 and cultures of PCC7942 containing heterotrophic bacteria.

Chapter 4 explores iron limited growth as a strategy to improve the exoelectrogenic capacity of photosynthetic microorganisms, particularly using PCC7942. Ferricyanide reduction rates by the photosynthetic cultures were obtained to quantify the exoelectrogenic response. The favourable pH for the extracellular reaction to occur was also established. Mechanistic aspects involved in iron limited PCC7942 exoelectrogenesis are explored and analysed according to published data. Enhanced power generation in a ferricyanide mediated and in mediatorless BPV devices was demonstrated.

In Chapter 5, another strategy to further improve PCC7942 exoelectrogenic capacity was explored. Iron limited cultures were exposed to high and extremely high CO_2 concentrations in order to establish the effect of CO_2 enrichment over PCC7942 exoelectrogenic capacity. A synergistic effect between enriched CO_2 and iron limitation is established. The effect of CO_2 on the cultural pH was also analysed in terms of the favourable pH for biomass growth and for exoelectrogenesis. Power generation in a ferricyanide mediated BPV device under extremely high CO_2 concentration was demonstrated.

An analytical approach to study PCC7942 biofilms in mediatorless platforms is presented in Chapter 6. Conventional electrochemical techniques, cyclic voltammetry and double step potential chronoamperometry, were applied. A protocol developing platforms for applying electrochemical techniques is proposed to screen for exoelectrogenic cyanobacteria and/or suitable anode materials. The iron-deficiency-induced exoelectrogenic capacity of PCC7942 was demonstrated in such platforms.

Finally, general conclusions are presented in Chapter 7 and future work recommendations are discussed in Chapter 8.

Chapter 2 Materials and Methods

2.1 Introduction

The following chapter presents a description of the protocols and techniques applied in the experimental work conducted for the development of this thesis. The materials and designs utilised in the execution of the experimental work are also described.

2.2 Culture cultivation

The microorganism strains used in this thesis are *Synechococcus elongatus* PCC7942, *Chlorella vulgaris* CCAP 211/52, *Synechocystis sp.* PCC6803 and *Shewanella oneidensis* MR-1. *Synechococcus elongatus* PCC7942 was the main strain studied throughout this thesis.

2.2.1 *Synechococcus elongatus* PCC7942

Synechococcus elongatus PCC7942 (formerly known as *Anacystis nidulans* R2) was obtained from the Pasteur Culture Collection. PCC7942 is a freshwater cyanobacterium, it was grown in BG11 (Blue-Green medium) for freshwater algae and protozoa. BG11 was prepared using nine stock solutions and autoclaved. Table 2-1 describes stock solutions composition and the BG11 recipe. PCC7942 stocks were kept in BG11 agar plates and in liquid culture at room temperature (approximately 20 °C), in a 12 hour light/dark cycle illuminated with white light fluorescent tubes, with an intensity of 50 µmol m^{-2} s^{-1}, and shaking speed of 120 rpm in air.

	Stock solution [g l^{-1}]	Concentration per litre of BG11
$NaNO_3$	15	100 ml
K_2HPO_4	4.0	10 ml
$MgSO_4 \cdot 7H_2O$	7.5	10 ml
$CaCl_2 \cdot 2H_2O$	3.6	10 ml
Citric acid	0.6	10 ml
Ammonium ferric citrate	0.6	10 ml
Na_2EDTA	0.1	10 ml
Na_2CO_3	2.0	10 ml
Trace metal solution:		
H_3BO_3	2.86	1 ml
$MnCl_2 \cdot 4H_2O$	1.81	
$ZnSO_4 \cdot 7H_2O$	0.22	
$Na_2MoO_4 \cdot 2H_2O$	0.39	
$CuSO_4 \cdot 5H_2O$	0.08	
$Co(NO_3)_2 \cdot 6H_2O$	0.05	
pH adjusted to 7.1 with 1 M NaOH or 1 M HCl before autoclaving. For solid BG11, add 15.0 g per litre of Bacteriological Agar.		

Table 2-1. BG11 (Blue-Green medium) composition. Recipe was followed as recommended by the Culture Collection of Algae and Protozoa. All reagent were laboratory grade or ACS grade chemicals.

For the study of growth in buffered media, BG11 was amended with HEPES-NaOH (Sigma Aldrich) at a concentration of 10 mM or 20 mM and the pH adjusted to 7.0 or 8.0 respectively.

2.2.2 *Chlorella vulgaris* CCAP 211/52

Chlorella vulgaris CCAP 211/52 was obtained from the Culture Collection of Algae and Protozoa. *C. vulgaris* CCAP 211/52 is a freshwater microalgae, it was grown in 3N-BBM+V (Bold Basal Medium modified with 3-fold nitrogen and vitamins). 3N-BBM+V was prepared using nine stock solutions and autoclaved. Table 2-2 describes stock solutions composition and the 3N-BBM+V recipe. *C. vulgaris* stocks were kept in 3N-BBM+V agar plates and in liquid culture at room temperature (approximately 20 °C), in a 12 hour light/dark cycle illuminated with white light fluorescent tubes, with an intensity of 50 µmol m^{-2} s^{-1}, and shaking speed of 120 rpm in air.

	Stock solution [g l^{-1}]	Concentration per litre of 3N-BBM+V
$NaNO_3$	25.0	30 ml
$CaCl_2 \cdot 2H_2O$	2.5	10 ml
$MgSO_4 \cdot 7H_2O$	7.5	10 ml
$K_2HPO_4 \cdot 3H_2O$	7.5	10 ml
KH_2PO_4	17.5	10 ml
NaCl	2.5	10 ml
Trace metal solution:		
Na_2EDTA	0.750	6.0 ml
$FeCl_3 \cdot 6H_2O$	0.097	
$MnCl_2 \cdot 4H_2O$	0.041	
$ZnCl_2$	0.005	
$CoCl_2 \cdot 6H_2O$	0.002	
$Na_2MoO_4 \cdot 2H_2O$	0.004	
Vitamin B_1		
Thiaminhydrochloride	1.2	1 ml
Vitamin B_{12}		
Cyanocobalamin	0.01	1 ml
For solid 3N-BBM+V, add 15.0 g per litre of Bacteriological Agar.		

Table 2-2. 3N-BBM+V (Bold Basal Medium modified with 3-fold nitrogen and vitamins) composition. Recipe was followed as recommended by the Culture Collection of Algae and Protozoa. All reagent were laboratory grade or ACS grade chemicals.

2.2.3 *Synechocystis sp.* PCC6803

Synechocystis sp. PCC6803 was a kind donation from Professor Christ Howe laboratory, Biochemistry Department, University of Cambridge. PCC6803 is a freshwater cyanobacterium, it was grown in BG11 (Table 2-1). PCC6803 stocks were kept in BG11 agar plates and in liquid culture at room temperature (approximately 20 °C), in a 12 hour light/dark cycle illuminated with white light fluorescent tubes, with an intensity of 50 µmol m^{-2} s^{-1}, and shaking speed of 120 rpm in air.

2.2.4 *Shewanella oneidensis* MR-1

Shewanella oneidensis MR-1 (formerly known as *Shewanella putrefaciens* MR-1) was obtained from Leibniz Institute DSMZ-German Collection of Microorganisms and Cell Cultures. MR-1 is an anaerobic facultative proteobacteria, it was grown in Tryptic Soy (Soybean-Casein Digest Medium), which composition is described in Table 2-3. Tryptic Soy was prepared from a pre-mixed powder (Sigma Aldrich) and autoclaved. *S. oneidensis* stocks were kept in Tryptic Soy agar plates at 4 °C.

	Concentration [g l^{-1}]
Tryptone	17.0
Soytone	3.0
Dextrose	2.5
NaCl	5.0
K_2HPO_4	2.5
For solid Tryptic Soy, add 15.0 g per litre of Bacteriological Agar.	

Table 2-3. Tryptic Soy (Soybean-Casein Digest Medium) composition. Medium was used as recommended by the Leibniz Institute DSMZ-German Collection of Microorganisms and Cell Cultures.

2.2.5 Axenicity test

Cultures were routinely checked to ensure that axenic conditions were kept by plating in Tryptic Soy agar (Table 2-3). Plates were wrapped in aluminium foil and incubated at 30±1 °C for four days to check absence of other bacterial growth.

2.2.6 Growth characterisation

Cultures were studied in triplicate unless otherwise stated. Cultures were placed in an incubator set at 30±1 °C and shaking speed of 120 rpm in air unless otherwise stated, in a 12 hour light/dark cycle illuminated with white light fluorescent tubes with an intensity of 90 µmol m^{-2} s^{-1}.

2.2.6.1 Biomass and chlorophyll content

Biomass was measured as optical density (OD) at 750nm (OD_{750}) for photosynthetic microorganisms: *S. elongatus* PCC7942, *Synechocystis sp.* PCC6803 and *C. vulgaris* CCAP 211/52; and at 600 nm (OD_{600}) for *S. oneidensis* MR-1. OD was measured with a Thermo Scientific Evolution 201 UV-Visible spectrophotometer. The blank for the spectrophotometry measurement was supernatant collected from rapid centrifugation (18,000xg).

Chlorophyll extraction was carried out with culture aliquots of 1 ml, in Eppendorf tubes of 1.5ml. Aliquots were centrifuged at 18,000xg for 1 minute, 0.9 ml of the supernatants were removed and pellets were dissolved in the remaining 0.1 ml. A volume of 0.9 ml of 99.9% methanol (Sigma Aldrich) was added to each tube, which were left for at least 15 min in the dark before rapid centrifugation, the supernatant was transferred to spectrophotometer-cuvettes, and the absorbance was measured at 665nm to determine Chl*a* concentration in cyanobacteria PCC7942 and PCC6803; an extinction

coefficient of 12.9447 µg ml^{-1} was used for calculations.[137] The molecular weight of Chl*a* equal to 893.51 g mol^{-1} was used to transform chlorophyll biomass units when necessary. For the microalgae *C. vulgaris*, chlorophyll extraction was conducted as described and absorbance was measured at 652nm and 665nm, with extinction coefficients for Chl*a* equal to -0.80962 and 16.5169 respectively; and for Chl*b* equal to 27.4405 and -12.1688 respectively.[137]

2.2.6.2 *S. elongatus* PCC7942 biomass calibration curve

A biomass calibration curve was constructed for PCC7942. From a culture of PCC7942, six equal aliquots of 9.5 ml were added to centrifuge tubes (15 ml), which had been previously dried on oven and weighted. Aliquots were centrifuged at 4,0000xg for 10 minutes. Pellets were washed twice with isotonic solution consisting of 0.5 M ammonium bicarbonate (Sigma Aldrich). Tubes plus pellets were then placed in an oven set at 105 °C for 1 hour, and afterwards let to cool down inside a desiccator. Once cooled down, tubes plus pellets were weighted. The biomass was calculated by subtracting the tube mass. From the same cultures, seven dilutions were prepared, each dilution in four replicates. OD_{750} was measured. Figure 2-1 shows the curve biomass versus OD_{750}. An extinction coefficient at 750nm of 3.5329 mg^{-1} ml cm^{-1} was determined.

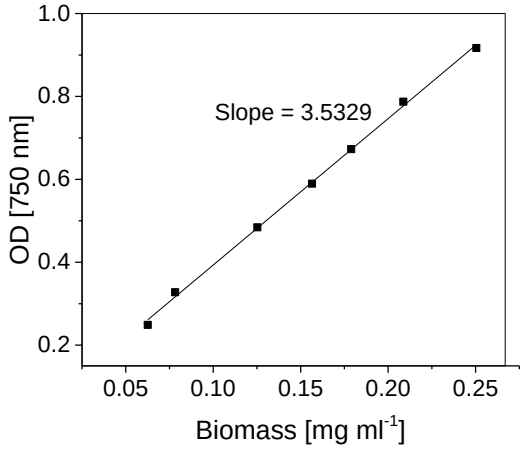

Figure 2-1. Biomass calibration curve for PCC7942 optical density at 750 nm.

2.2.6.3 pH and DO measurements

pH measurements were determined using the pH-meter Hanna Instrument® HI-2211 in samples in the light and after 3 hours of darkness. Dissolved oxygen (DO) measurements were determined using the DO-meter Hanna Instrument® HI-2040 edge® in samples in the light and after 3 hours of darkness.

2.2.6.4 Photosynthesis and respiration rates

Photosynthesis rates were estimated by continuously monitoring oxygen evolution in light and darkness with the DO-meter Hanna Instrument® HI-2040 edge®. Samples of 25 ml were adapted in the dark previously to record the measurements of the light oxygen evolution for 15 minutes, and immediately after, dark oxygen evolution for 15 minutes. Data was recorded with the log function of the DO-meter in intervals of 30 seconds. Gross photosynthesis was calculated as the addition of net photosynthesis (light oxygen evolution) and respiration (dark oxygen evolution).

2.3 Iron limitation study

Chapter 4, Chapter 5 and Chapter 6 present experimental work using photosynthetic microorganisms grown in iron limited conditions.

Media for experiments was prepared with Millipore® ultrapure water (polished water 18.2 MΩcm at 25 °C). In the preparation of iron limited media, ammonium ferric citrate in BG11 (Table 2-1) was replaced by ammonium citrate in a stoichiometric proportion and ferric chloride was omitted in 3N-BBM+V (Table 2-2). Iron traces in chemical reagents implied that traces of iron were still introduced.

All glassware and devices were acid washed to remove solids and in that way to minimise iron presence. Measuring cylinder and beaker for media preparation, bottles for media stock storage, Erlenmeyer flasks for culturing and electrochemical devices were left overnight filled with 1 M nitric acid, then rinsed with Millipore® ultrapure water.

Iron limited cultures were inoculated with biomass from stock cultures at initial OD_{750} equal to 0.5. Inoculum was centrifuged at 4,000xg for 10 minutes, followed by two washing steps using fresh media to remove iron impregnating the pellet. Cultures were incubated at 30±1 °C and 120 rpm in air unless otherwise stated.

2.4 CO_2 enrichment and cultural pH regulation

To provide a CO_2 enriched atmosphere, cultures were grown in Erlenmeyer flasks with two port caps. Filter units (0.2 µm PTFE) were attached to the ports to keep sterile conditions (Figure 2-2). 20% CO_2 in air or 5%CO_2 in air was supplied from a gas cylinder (Air-liquids) at 10 ml min^{-1}.

Figure 2-2. Photography of PCC7942 cultures grown under CO_2 enrichment, showing in and out connections.

To control the cultural pH in the 20%CO_2 system, two variations of BG11 were prepared, buffered with 10 mM or 20 mM of HEPES-NaOH (Sigma Aldrich) and initial pH adjusted to 7.0 and to 8.0 respectively. pH was not buffered in the 5%CO_2 system.

2.5 Electrochemical device fabrication and operation

Two galvanic electrochemical cell designs were fabricated for electricity generation. Additionally, a three electrodes electrochemical system was fabricated for conducting electrochemical measurements.

2.5.1 Single chamber device

The single chamber consisted of an electrochemical cell with 18 mm diameter active electrode area. No membrane was used. The anodic electrode was indium tin oxide (ITO)-coated glass (1 mm thick, Sigma Aldrich) and the cathodic electrode was platinum coated carbon paper (3 mg of Pt per m^2, Alfa Aesar). The cathode was pierced with a small hole in the middle to allow access to the inner cell chamber. Titanium strips were used to electrically connect to both, anode and cathode. The titanium strips were crimped to electrical wires, connection points were wrapped with polytetrafluoroethylene (PTFE) tape. Two polydimethyl siloxane (PDMS, Sylgardl) ring gaskets of 50 +/- 10 mm thickness were used to seal and create the cell chamber. Two acrylic frames were used to house all the cell components together as shown in Figure 2-3. No membranes were used. Devices were sterilised by autoclaving. Once inoculated, devices were sealed with a breathable, antibacterial and semi-transparent adhesive film (Opsite Flexfix) in order to maintain sterile conditions and reduce evaporation. The single chamber device was used in the experimental procedure presented in Chapter 3 (mediatorless) and in Chapter 4 (ferricyanide mediated).

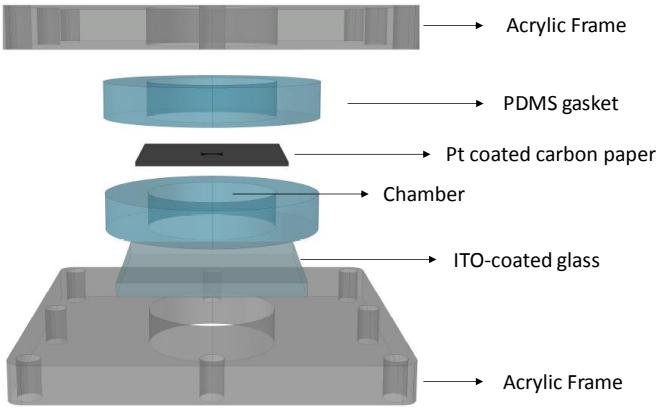

Figure 2-3. Schematics of single chamber electrochemical cell.

2.5.2 Membrane electrode assembly device

The membrane electrode assembly (MEA) device consisted of an electrochemical cell with 18 mm diameter active electrode area. The MEA was assembled with a cathode consisting of platinum coated carbon paper (3 mg of Pt per m^2, Alfa Aesar), with a membrane consisting of Nafion® (Sigma Aldrich) membrane (proton exchange membrane), or alternatively two layers of nitrocellulose membrane (Amersham™Protran™, 0.2 µm pore size), two layers of membrane are necessary to fully avoid short-circuits within the pores, and with an anode consisting of carbon paper (Toray) or carbon felt (Alfa

Aesar), 0.190 mm and 1.59 mm thickness respectively. When using Nafion®, the cathode and the membrane were hot pressed with the catalyst (platinum) facing the membrane. Titanium strips were used to electrically connect each electrode. The titanium strips were crimped to electrical wires, connection points were wrapped with polytetrafluoroethylene (PTFE) tape. Two acrylic frames were used to house the assembly together using 2 ± 1 mm polydimethyl siloxane (PDMS) ring gaskets. An acrylic cylinder of length 50±3 mm was solvent welded to the top frame to make the anodic chamber. In the upper side of the cylinder a 4±1 mm hole covered with nitrocellulose membrane (0.2 µm pore size) was placed for ventilation. Figure 2-4 shows a schematic of the MEA-BPV device. Devices were sterilised by autoclaving. Once inoculated, devices were sealed with a breathable, antibacterial and semi-transparent adhesive film (Opsite Flexifix) in order to maintain sterile conditions and reduce evaporation. The MEA device was used in the experimental procedure presented in Chapter 3 (mediatorless) and in Chapter 6 (mediatorless).

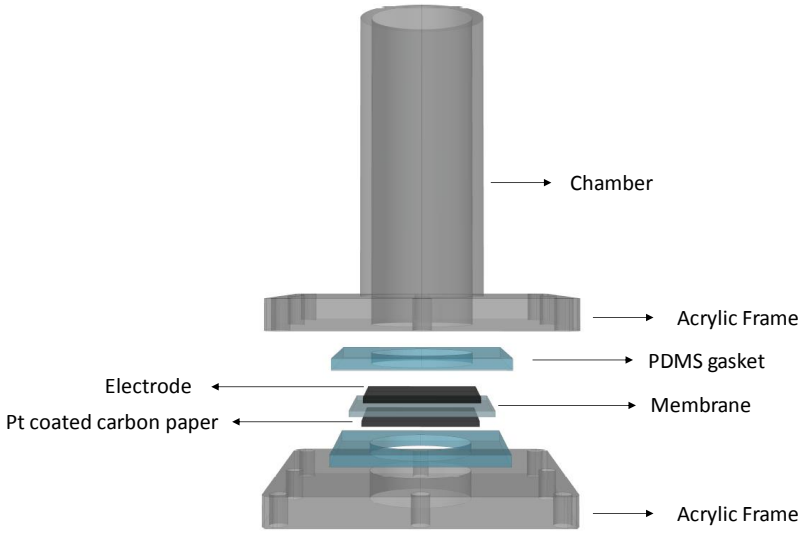

Figure 2-4. Schematics of membrane electrode assembly (MEA) electrochemical cell.

A variation of the described MEA device consisted in an electrochemical cell with connections for tubing inlet/outlet in an enclosed anodic chamber (Figure 2-5). MEA was fabricated as described using nitrocellulose as the membrane and the bottom PDMS gasket was not perforated, therefore the cathode was not open to the atmosphere. MEAs were placed in between a rigid frame and a lateral flanged arm in a Duran® bottle (250 ml). The lateral arm had a volume of 5 ml, with internal diameter of 18 mm. The bottle cap to feed CO_2 enriched air had two ports with hose sockets. Filter units (PTFE, 0.22 µm pore size) were attached to the ports to keep sterile conditions. An alternative cap consisted

of a vented cap, using nitrocellulose membrane (0.22 µm pore size), for normal atmospheric composition. This MEA device was used in the experimental procedure presented in Chapter 5 (ferricyanide mediated).

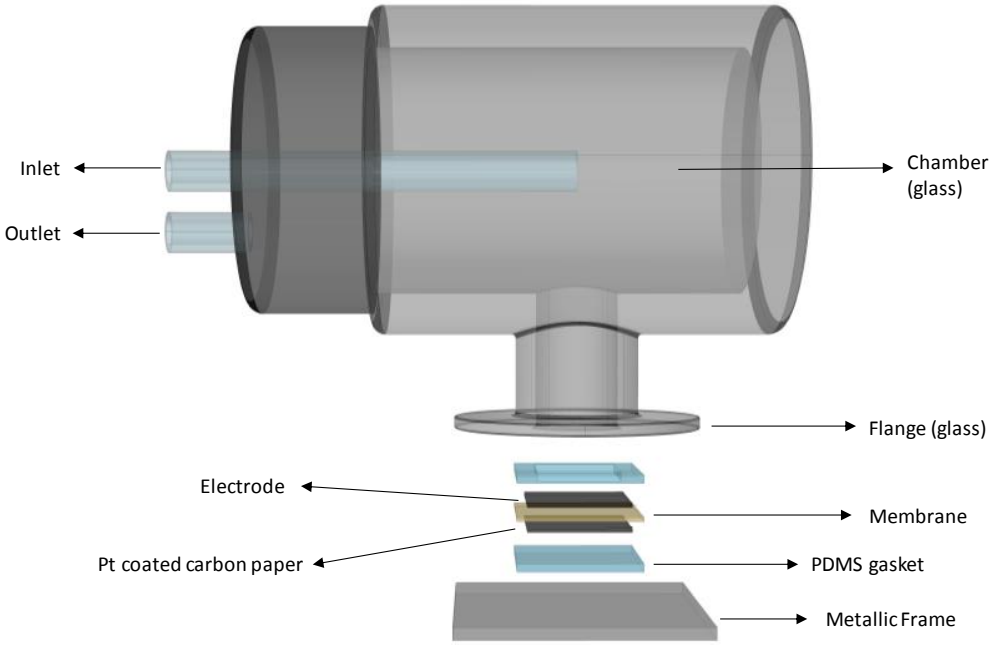

Figure 2-5. Schematics of membrane electrode assembly (MEA) electrochemical cell with inlet/outlet for CO_2 enrichment.

2.5.3 Surface functionalisation of carbon materials

Carbon paper and carbon felt electrodes were treated with oxygen plasma (plasma treated PT). Oxygen plasma was applied with a power of 50 W and a frequency of 40 kHz for 30 seconds. In order to assess wettability of the carbon materials, both non-treated and plasma treated, contact angle was measured with a Drop Shape Analyser (Kruss DSA100) integrated with the software DSA.

2.5.4 Electrochemical cell operation and characterisation

Electrochemical cells were operated inside an incubator set at 30±1 °C. When using photosynthetic microorganisms, a 12 hour light/dark cycle was followed. For all single chamber devices, light was supplied with a light box with light intensity of 70 µmol m^{-2} s^{-1}. For all MEA devices, light was supplied with white light fluorescent tubes in a top panel with light intensity of 90 µmol m^{-2} s^{-1}. Devices were

connected to a PicoLog® ADC-24 high resolution data logger (Pico Technology), passing through an op-amp (operational amplifier) box and continuously monitored with the PicoLog Recorded Software. Data was recorded every 2 minutes. A total of 16 channels were available for simultaneous recording. Polarisation curves were constructed by connecting the devices to external loads (resistors), which were chosen depending on the device type. Resistors were changed once currents had stabilised. Current and power were calculated by applying Ohm's law.

In BPV devices operated under CO_2 enriched atmosphere, 20%CO_2 was supplied from the gas cylinder (Air-liquids) at 5 ml min^{-1}. For the air control, this was circulated by the fan in the incubator.

If specified, cathodic and anodic potentials were measured at the end of experiments using a Ag/AgCl reference electrode (RE, MF-2052 RE-5B Basi®) and a digital multimeter (UNI-T UT60E).

2.5.5 Three electrode electrochemical system and measurements

The thee electrode electrochemical system consisted of a working electrode (WE) fixed at the bottom of a cylindrical chamber of 50 mm internal diameter and with a well of 18 mm diameter (Figure 2-6). The WE had an 18 mm diameter active electrode area. A titanium strip was placed as electrical contact for the WE. The counter electrode (CE) was 99.9% platinum mesh (Alfa Aesar) and an Ag/AgCl reference electrode (RE, MF-2052 RE-5B Basi®) was used. The latter were introduced in the chamber just on the day of measurements. The chamber assembled with the WE was sterilised by autoclaving. To keep sterile conditions, good ventilation and illumination, the cylinder top was covered with a piece of transparent PET and a vented area using nitrocellulose paper (0.2 µm pore size), which was sealed with antibacterial tape.

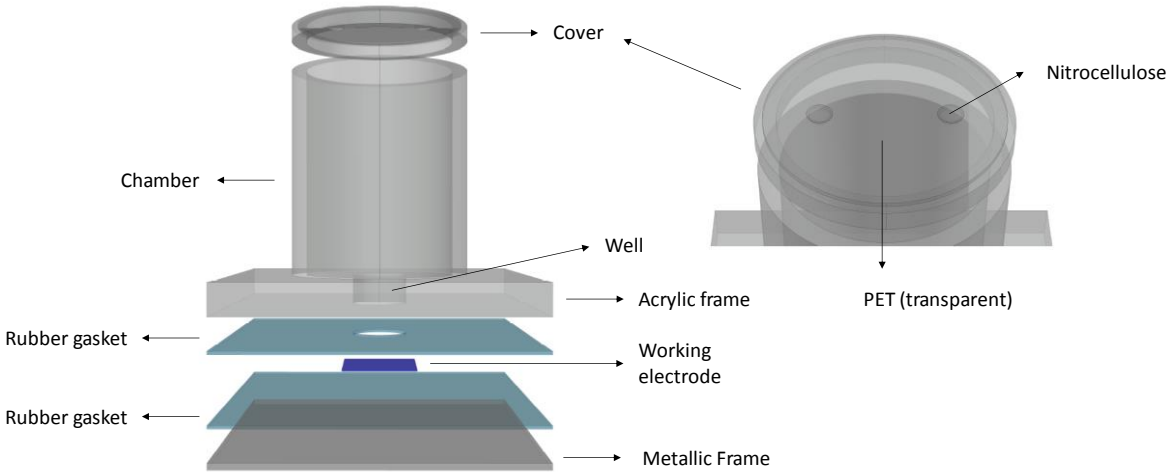

Figure 2-6. Schematics of device holding the working electrode.

Electrochemical measurements, cyclic voltammetry and potential step chronoamperometry, were conducted in an incubator at 30±1 °C under aerated conditions. For measurements under illumination, light intensity was 90 µmol s^{-1} m^{-2}. Electrochemical measurements were conducted using a PalmSens MultiEmStat^3 four-channel potentiostat, integrated with the MultiTrace software, or alternatively, using a Methohm Autolab µAutolab single-channel potentiostat, integrated with the NOVA software.

2.6 The ferricyanide assay

The ferricyanide assay was used to quantify the exoelectrogenic activity of photosynthetic cultures, and it was conducted in different conditions. The assay is based on the electrochemical conversion of ferricyanide ($Fe(CN)_6^{-3}$) to ferrocyanide ($Fe(CN)_6^{-4}$) by redox complexes in the plasma membrane and possibly in the outer membrane of microorganisms (Figure 2-7). Ferricyanide has a peak absorbance at 420 nm, while ferrocyanide has negligible absorbance at 420 nm. An extinction coefficient at 420 nm of 1.052 mM^{-1} cm^{-1} was obtained in the construction of a calibration curve (Figure 2-8). The calibration curve was constructed with six dilutions of potassium ferricyanide. Each dilution was prepared in triplicate. Absorbance was measured with a Thermo Scientific Evolution 201 UV-Visible spectrophotometer. The depletion of ferricyanide in time enables to measure ferricyanide reduction (FeCN-R) rates.

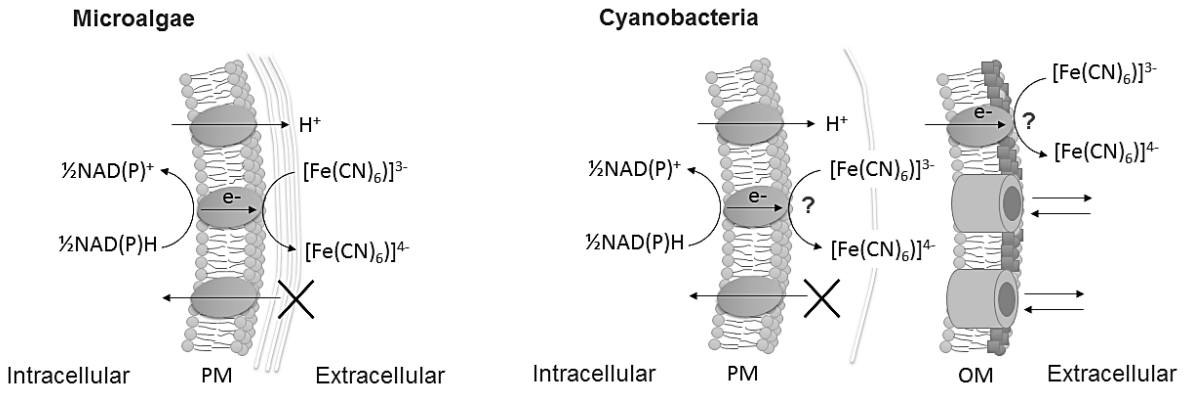

Figure 2-7. Ferricyanide reacting at cell extracellular surface of photosynthetic microorganisms. In microalgae only a plasma membrane exists, and ferric reductases and NADPH oxidases are known plasma membrane oxidoreductases. In cyanobacteria, a plasma membrane and an outer membrane exist, the points of reaction have not been identified. NADPH and NADH are the intracellular metabolites which are believed to be the substrate for the reaction.[45]

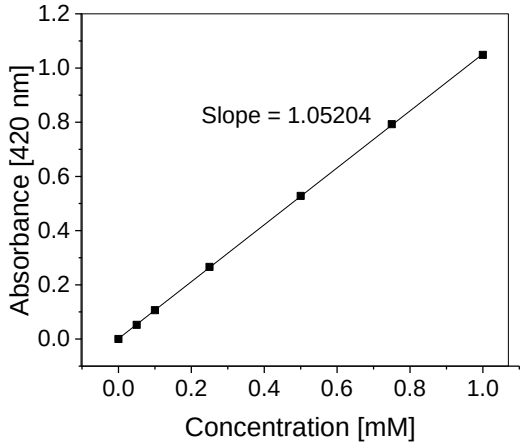

Figure 2-8. Ferricyanide calibration curve. Absorbance at 420 nm.

The assay was conducted in 6 ml culture samples with a biomass density at OD_{750} equal to 2. Samples were obtained by centrifugation at 4,000xg for 10 min and resuspension of the pellets in the appropriate volume of modified BG11 (Table 2-1), which lacked ammonium iron citrate, citric acid and EDTA (BG11(-)x3 hereafter), in order to avoid iron and redox active compounds. For *C. vulgaris* samples, 3N-BBM+V lacking ferric chloride was used.

To conduct the ferricyanide assay at different pH, BG11(-)x3 was amended with HEPES-NaOH (Sigma Aldrich) at a concentration of 10 mM and the pH was adjusted at pH 7.0, pH 7.8 or pH 6.2.

Alternatively, sodium bicarbonate (Sigma Aldrich) at a concentration of 0.1 M was added to maintain alkaline pH (pH 9.5).

Samples at OD_{750} equal to 2 were transferred to 50 ml narrow mouth Erlenmeyer flasks. The assay was conducted at 30±1 °C and 120 rpm, under illumination. The light intensity was 90 µmol m^{-2} s^{-1}. For measurements in the dark, cultures were transferred to vented flasks, wrapped in aluminium foil and incubated for at least 3 hours before centrifugation and resuspension. Erlenmeyer flask were also wrapped in aluminium foil to conduct the assay in darkness.

The 6 ml culture samples were left to acclimatise for at least one hour before proceeding to add ferricyanide. Potassium ferricyanide (Sigma Aldrich) was added to each sample from a stock solution (100 mM), to reach a concentration in the sample of approximately 1 mM. Aliquots of 1 ml were withdrawn with 1 ml syringes and filtered using filter units (PTFE, 0.45 µm pore size, Sartorius Minisart). Aliquots were taken at 0, 10, 30 and 120 minutes. The filtrate was received in a spectrophotometry-cuvette, and analysed for ferricyanide concentration spectrophotometrically at 420nm. Ferricyanide reduction rates were calculated by linear regression.

For samples grown under CO_2 enrichment, the ferricyanide assay in the light was conducted under the corresponding 20%CO_2 or 5%CO_2 atmosphere, unless otherwise stated. While conducting the ferricyanide assay, Erlenmeyer flasks were closed with rubber sealing stoppers the inlet and outlet of gas was through long thin needles. Samples were withdrawn with a long-thin needle, except for the first and last sample.

The FeCN-R rates are expressed in three equivalent units, regarding comparison to other photosynthetic microorganisms published data in FeCN-R rates. To compare with microalgae, FeCN-R rates were normalised over micrograms of chlorophyll, while to compare with cyanobacteria, FeCN-R rates were normalised over nanomoles of chlorophyll. Finally, within cultures of PCC7942 grown in different conditions (Chapter 5), chlorophyll content varied, therefore FeCN-R rates were normalised over milligrams of biomass.

2.7 Photosynthesis inhibition

To test exoelectrogenesis under illumination in the absence of photosynthesis, the photosynthesis inhibitor DCMU (3-(3,4-Dichlorophenyl)-1,1-dimethylurea, Sigma Aldrich) was used. DCMU interrupts

the photosynthetic electron chain as it binds the plastoquinone Q_B site in PSII (as shown in Chapter 1 Figure 1-25).

Stock solution of DCMU was prepared on 95% ethanol (Alfa Aesar) at a concentration of 9 mM. A volume of 10 µl of DCMU solution was added to the 6 ml culture samples, to reach a final DCMU concentration of 15 µM. DCMU was added 50 minutes before proceeding with the ferricyanide assay (Section 2.6). In parallel, non-inhibited samples were analysed in the light and in the dark. A volume of 10 µM of 95% ethanol was added to these samples.

2.8 pH evolution

pH evolution in culture samples (30 ml), upon addition of 1 mM ferricyanide, was measured using a pH electrode connected to the Picolog® DrDAQ data logger (Pico Technology) continuously monitored with the PicoLog Recorder Software. Data was recorded every 30 seconds. Measurements were conducted at 30 °C and 120 rpm in air.

2.9 Superoxide detection methods

XTT (2,3-Bis(2-methoxy-4-nitro-5-sulfophenyl)-2H-tetrazolium-5-carboxanilide inner salt, Sigma Aldrich) was used to detect superoxide iron by colorimetry. Formazan (derived from XTT reduction) has a peak absorption at 470 nm with an extinction coefficient of 21,600 $M^{-1}cm^{-1}$.[138]

XTT was added to the 6 ml culture samples, with the same characteristics than those prepared for the ferricyanide assay (Section 2.6), to reach a final concentration of 150 µM. Aliquots of 1 ml were withdrawn with 1 ml syringes and filtered using filter units (PTFE, 0.45 µm pore size). Aliquots were taken at 0, 10, 30 and 120 minutes. The filtrate was received in a spectrophotometry-cuvette, and analysed for formazan concentration spectrophotometrically at 470nm. Absorbance was measured with a Thermo Scientific Evolution 201 UV-Visible spectrophotometer.

Alternatively, the ferricyanide assay (Section 2.6) in the presence of Superoxide Dismutase (SOD bovine, Sigma Aldrich) were conducted. SOD solution was prepared in 10 mM PBS buffer (Sigma Aldrich) at a concentration of 1.5 mg ml^{-1} equivalent to 4,400 unit ml^{-1}. A volume of 90 µl of SOD solution was added to the 6 ml culture samples to reach a final concentration of 60 unit ml^{-1}. SOD was added 10 minutes before proceeding with the ferricyanide assay.

2.10 Cryo-immobilisation freeze drying and SEM imaging of biofilms

To prepare biofilms forming on electrode materials, 1.5 ml of culture of PCC7942 OD_{750} equal to 0.75 were inoculated in a tube of 10 mm diameter with the electrode flat at the bottom and left to settle down at room temperature (approximately 20 °C). After 8 days, the substrates were collected and washed thrice with cold water to remove non-attached cells.

Adherent cells on the substrates were quench frozen, by plunging, cell face first into melting ethane cooled in liquid nitrogen. They were freeze dried in a Quorum/Emitech K775X apparatus. After freeze drying the substrates were attached to SEM stubs with silver DAG. The dry substrates were coated with 16nm of iridium in a Quorum/Emitech K575X sputter coater. They were viewed in a FEI Verios 460L operated at 2 kV and 50pA.

2.11 Confocal microscopy

Images of PCC7942 were obtained with Leica SP5 confocal microscope. The cell size was estimated.

2.12 Separation and enrichment of outer membrane from PCC7942

This work was conducted in collaboration with Prof B. Norling and Dr L. Zhang from the School of Biological Sciences, Nanyang Technological University, Singapore.

Six independent cultures of PCC7942 in iron limited and iron sufficient conditions were prepared, each with initial OD_{750} equal to 0.5. Three cultures per condition were then mixed to increase the total biomass per sample, centrifuged at 4,000xg and wash with 20 mM PBS buffer. Pellets were stored at -80 °C and then sent in dry ice to Singapore.

The membranes of PCC7942 were enriched in outer membranes by sucrose density centrifugation as the first step followed by aqueous two-phase partitioning as the second step.[139] These techniques were mainly executed by Dr L. Zhang during a visit to Prof B. Norling Lab.

Cell breakage was conducted with glass beads (0.17 – 0.18 mm Glasperlen, Sartorius) in 1.5 ml of PBS buffer (pH 7.8, 20 mM) containing protease inhibitor. To break the cell, the mix was vortexed for 2 minutes and rested in ice for two minutes, repeating five times. 2 ml of buffer was added to wash and solubilised the sample. Glass beads were left to settle down and the supernatant containing the

sample was centrifuge at 2,000xg and 4 °C for 10 minutes to separate remaining glass beads and unbroken cells. The collected supernatant was centrifuged at 244,717xg and 4 °C for 50 minutes. The pellet was homogenised with small amount of PBS buffer (pH 7.8, 20 mM) weighted and centrifuged, then sucrose 42% was added 7.2 times the weight.

The pellet (membranes) was then separated by sucrose gradient, with 5 ml at 60% → 60 ml 50% → 5 ml sample (42%) → 5 ml 38% → 6 ml 35%, 6 ml 30%, and balanced weight with 10% sucrose. The gradient was centrifuged at high speed. The fractions of thylakoid, plasma and outer membrane were then collected and diluted in buffer, then centrifuged at high speed during 1 ½ hour to obtained membrane enriched fractions.

To further enrich the membrane fractions, two phase fractioning was conducted. The method consisted in mixing the samples with two polymers, 5.8% (w/w) Dextran T-500 and 6.2% (w/w) polyethylene glycol, leaving to rest in ice for 30 minutes. The mix samples were then centrifuged at low speed for 5 minutes to separate the two phases. The upper and bottom phases were washed with the other respective polymer. The process was repeated three times. The final samples were centrifuged at high speed to recover the enriched membrane fractions. Protein quantification of each sample was determined using the mini-Peterson method.[140]

2.13 Mass Spectrometry (Proteomics)

PCC7942 membrane fraction enriched in outer membrane was used in the proteomic study. The latter was executed by the Cambridge Centre for Proteomics (CPP), Department of Biochemistry, University of Cambridge.

TMT labeing for MS (6 plex) was carried out according to the company's protocol (ThermoScientific). Briefly, two samples (two conditions) and two replicates were reduced, alkylated and digested with tryspin overnight before being labelled with 4 TMT tags. The tagged peptides from the 4 solutions were then combined and analysed by LC-MS/MS.

All LC-MS/MS experiments were performed using a Dionex Ultimate 3000 RSLC nanoUPLC (Thermo Fisher Scientific Inc, Waltham, MA, USA) system and a QExactive Orbitrap mass spectrometer (Thermo Fisher Scientific Inc, Waltham, MA, USA). Separation of peptides was performed by reverse-phase chromatography at a flow rate of 300 nL/min. Solvent A was 0.1% formic acid in water and B was 0.1% formic acid in 80% acetonitrile and 20% water. The total run time was 2 hours (including wash and re-

equilibration using a gradient of 2-40% B over 100 minutes. The LC eluant was sprayed into the mass spectrometer by means of an Easy-spray source (Thermo Fisher Scientific Inc.). All m/z values of eluting ions were measured in an Orbitrap mass analyser and data dependent scans (Top 20) were employed to automatically isolate and generate fragment ions by higher energy collisional dissociation (HCD) in the quadrupole mass analyser. Measurement of the resulting fragment ions was performed in the Orbitrap analyser. Peptide ions with charge states of between 2+ and 5+ were selected for fragmentation.

Proteome Discoverer v2.1 (Thermo Fisher Scientific) and Mascot (Matrix Science) v2.6 were used to process raw data files. Data was aligned with the UniProt cyanobacteria database (942563 sequences; 274357650 residues), in addition to using the common repository of adventitious proteins (cRAP) v1.0. Protein identification allowed a tolerance of ± 25 ppm and ± 0.8 Da along with permission of up to 2 missed tryptic cleavages. Quantification is achieved by calculating the sum of centroided reporter ions within a ± 2 millimass unit (mmu) window around the expected m/z for each of the four TMT reporter ions.

Chapter 3 Evaluation of various microbial electrochemical systems to benchmark the exoelectrogenic performance of the cyanobacterium *Synechococcus elongatus* PCC7942

3.1 Introduction

The generation of electricity catalysed by whole microbes relies not only on their exoelectrogenic capacity, but also on the efficiency of the electrochemical cell fostering them.

In this chapter, the evaluation of the exoelectrogenic capacity of the model cyanobacterium *Synechococcus elongatus* PCC7942 (PCC7942 hereafter) is presented as a benchmark study, consisting of understanding the performance of PCC7942 as an exoelectrogen through a comparative analysis against other systems, to then improve the platform or identify aspects needing improvement.

Several designs for bioelectrochemical cells have been proposed for both MFCs and BPVs. Some studies have used a given platform to screen various microorganisms,[14,141] while other have used one strain to study different platforms.[142] However, a cross comparison between MFCs and BPVs is not found in the literature. The latter implies the lack of a comprehensive analysis on the factors favouring or limiting the two different bioelectrochemical platforms, besides testing a device design with exoelectrogenic bacteria sets a more robust approach.

The power obtained in a bioelectrochemical cell is the result of many parameters and not only of exoelectrogenic activity, therefore power output only gives partial information on a microorganism exoelectrogenic capacity. The latter is critical in photosynthetic microorganisms whose exoelectrogenic capacity is not well characterised.

The benchmark study presented in this chapter was designed to provide a systematic and comprehensive analysis of the exoelectrogenic capacity of PCC7942, as well as of the performance of BPV platforms. The study has two stages:

- First, the design of mediatorless BPV platforms fostering PCC7942 is assessed in relation to the performance of the same platforms fostering the exoelectrogen *S. oneidensis* MR-1.

- Second, the exoelectrogenic capacity of PCC7942 is assessed in relation to other photosynthetic cultures, including the microalgae *Chlorella vulgaris* CCAP 211/52 and co-cultures of PCC7942 (bacteria present). The exoelectrogenesis capacity is evaluated using ferricyanide reduction (ferricyanide assay) and mediatorless platforms.

The aim of this chapter is to understand the advantages and limitations of utilising cyanobacteria for photo-bioelectricity generation, setting a baseline for the next chapters, where novel sustainable strategies to enhance exoelectrogenic capacity of PCC7942 will be presented.

3.1.1 *Synechococcus elongatus* PCC7942 as a source of bioelectricity

PCC7942 is a model of obligate photoautotroph cyanobacterium (not able of heterotrophic metabolism). In bioelectrochemical systems, PCC7942 was one of the first cyanobacteria to be employed for photo-bioelectricity generation. However, this first study was conducted using a redox mediator permeable to the plasma membrane, therefore shuttling electrons from the intracellular compartment. This approach was independent of PCC7942 exoelectrogenic capacity and disruptive to the cell viability.[28]

Only recently Sekar *et al.*[99] demonstrated that PCC7942 is able to reduce ferricyanide (plasma membrane impermeable) and to generate electricity in the absence of mediators in chronoamperometry experiments. More interestingly, Sekar *et al.*[99] evaluated a genetically modified PCC7942 harbouring the outer membrane cytochrome OmcS, which increased both ferricyanide reduction rates (2-fold) and mediatorless electrical current generation (9-fold), although current generation was measured only for a short period of 8 minutes.

OmcS is a six-heme cytochrome from the metal reducing exoelectrogenic bacteria *Geobacter sulfurreducens*. It is localised in the extracellular side of the outer membrane and it is involved in ferric oxide reduction.[143] The incorporation of OmcS in the outer membrane of PCC7942 proved that redox active complexes reside in the periplasm of wild-type PCC7942, which can supply electrons to the outer membrane. Not only opening avenues to use synthetic biology to engineer mediatorless platforms, which is considered the way forward to improve the technology,[93] but also encouraging the investigation to find conditions that enhance the export of the available electrons.

Electricity generation in long operation experiments has not been reported for PCC7942.

3.1.2 Shewanella oneidensis MR-1: a model exoelectrogenic bacteria

Shewanella oneidensis MR-1 (formerly known as *Shewanella putrefaciens* MR-1, *S. oneidensis* hereafter) is a well-studied exoelectrogenic microorganism. The highest power generated in a MFC by *S. oneidensis* is 3,000 mW m^{-2}, among the highest for axenic exoelectrogenic bacteria.[29]

S. oneidensis is an anaerobic facultative gram-negative bacterium. The capacity of *S. oneidensis* to reduce extracellular compounds derives from the respiratory electron chain coupled to the cell surface, with redox protein complexes spanning from the plasma membrane to the outer membrane. Two decaheme c-cytochromes (MtrC and OmcA) on the extracellular side of the outer membrane have been confirmed to directly transfer electrons to an electrode. Besides, *S. oneidensis* secretes soluble electron shuttles such as riboflavin, which was detected to accelerate electron transfer. Baron *et a*l.[56] determined that riboflavins have a redox midpoint potential at -400 mV vs Ag/AgCl, with starting potential (lowest potential showing anodic currents) at -450 mV vs Ag/AgCl, while MtrC and OmcA showed a broad electroactive region with a redox midpoint potential at -200 mV vs Ag/AgCl and starting potential at -400 mV vs Ag/AgCl, confirmed by mutants with deletion of MtrC/OmcA showing strongly inhibited electrochemical activity. In another study, Roy *et al.*[144] found that the electrochemical redox region associated to MtrC/OmcA was at less negative potentials, with starting potential at -100 mV vs Ag/AgCl, which was also confirmed by mutants lacking the two cytochromes.[144] The difference in the potentials reported for MtrC/OmcA might be related to the electrode material, while Baron *et a*l.[56] used a graphite carbon working electrode, Roy *et al.*[144] used a gold working electrode; in both studies *S. oneidensis* was fed with lactate.

Riboflavin is preferentially excreted in anaerobic conditions and it has been accounted as the main contributor in anaerobic electrode respiration by *S. oneidensis*.[144,145] However, riboflavin concentration in cultures/biofilms grown anaerobically is not always detectable in electrochemical studies.[56,144] Furthermore, riboflavin secretion has also been detected in carbon limiting conditions in aerobic and micro-aerobic environments. Therefore, the function of riboflavin has been proposed as a redox sensing metabolite upon changing environments.[144]

MFCs are usually operated in anaerobic conditions, although many configurations in aerobic systems have been proposed in favour to eliminate the proton exchange membrane. Rosenbaum *et al.*[11] found that in aerobic conditions, *S. oneidensis* produced enhanced power outputs, which were explained as the result of higher biomass activity. Furthermore, the exposure of *S. oneidensis* to oxygen promotes the utilisation of a variety of organic compounds as fuels for electricity generation, with higher power in anaerobic or aerobic conditions depending on the fuel fed to the MFC. For instance, glucose is not

utilised in anaerobic conditions, but in aerobic conditions it serves as a fuel in a MFC, although in the long term currents are inhibited in favour of aerobic respiration.[146,147]

3.1.3 Exoelectrogenesis of photosynthetic microorganisms and mediatorless BPV devices

A mediatorless BPV relies on three main factors: the exoelectrogenic capacity of the photosynthetic microorganism, the electrochemical interaction between the biofilm with the electrode and the design of the electrochemical cell.

The cell surface of cyanobacteria (gram-negative bacteria) and of microalgae are different, therefore the interaction with an electrode differs accordingly. Figure 3-1 depicts the structure of the cell envelope in cyanobacteria and microalgae. The cell envelope in cyanobacteria involves the plasma membrane (PM), followed by a periplasmic space (PS) and finally a semipermeable outer membrane (OM). The outer membrane has protein channels (porins) which selectively transport nutrients and metabolites in and out of the cell. There is also an external layer associated to the outer membrane, the S-layer. It is formed by polysaccharides and glycoproteins covering the cell envelope, being a final protective and selective coat, which also participates in cell adhesion and recognition.[148] In microalgae, only the plasma membrane exists covered and protected by the cell wall, a dense extracellular matrix consisting of polysaccharides and glycoproteins.[149]

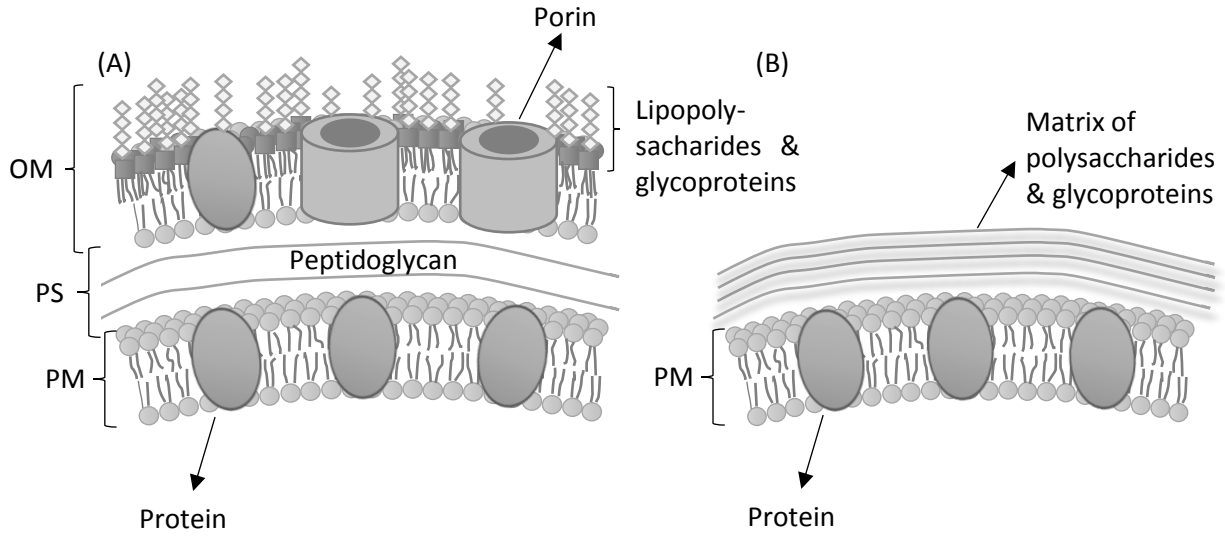

Figure 3-1. Schematics of cell envelope of (A) cyanobacteria (gram-negative) and (B) microalgae.[148,149] OM: outer membrane, PM: plasma membrane, PS: periplasmic space and Porin: protein channel.

In microalgae, there is vertical electron movement through the plasma membrane due to the activity of ferric reductases and NADPH oxidases, both with an oxidoreductase function.[150] In cyanobacteria, less knowledge has been gained. As described in Chapter 1 – Section 1.7, exoelectrogenesis in cyanobacteria is photosynthesis driven, however electron export pathways through the cell envelope have not been identified. The complexity of the cell envelope dictates that mediatorless platforms are less efficient than platforms using soluble redox mediators, like ferricyanide, which can readily access the plasma membrane.

The selection of the anode material becomes very important in a mediatorless system, due to the direct electrochemical interaction with the cell envelope. The latter will determine the magnitude of the electrochemical cell OCP and activation overpotential losses, while the conductivity of the electrode will impact ohmic losses.

To obtain higher power output, higher OCP values alongside with lower R_{int} values are needed (Chapter 1 – Section 1.5.1). These parameters depend on many other factors, including the chosen cathode, the electrolyte resistivity and the membrane resistivity (if any). Improving these factors will increase OCP values or decrease R_{int}, or ideally, both simultaneously.

The cell design chosen in BPV studies varies. In general, it can be divided into single chamber devices or two-chamber devices, but the cell configuration also varies, mainly due to the utilisation of membranes. Membranes are used in order to isolate the anodic and cathodic reaction, otherwise reactive species crossover causes polarisation loses, which can be critical in some cases, but if this effect is minimal the membrane can be disregarded.

Indium tin oxide (ITO)-coated on glass or on polyethylene terephthalate (PET) in the anode have been broadly used in BPV devices with a variety of cyanobacteria and microalgae, in mediated as well as mediatorless BPVs, typically in combination with platinum coated carbon paper in the cathode, with and without the use of a membrane.[14,48,98,101] The advantage of transparent electrodes implies that light intensity over the anode, where a photosynthetic biofilm is formed, is maximised. ITO-coated electrodes also present the advantage of being hydrophilic. Bombelli *et al.*[142] analysed a series of anode materials including ITO-coated PET, stainless steel, glass coated with a conductive polymer and carbon paper, as part of a mediatorless platform inoculated with the freshwater filamentous cyanobacterium *Pseudanabaena limnetica*. The study found that higher power outputs were correlated with higher hydrophilicity and surface roughness.

Other anode materials have been studied in BPVs. Reduced graphene oxide (RGO)-coated glass was found to have a higher OCP value than ITO-coated glass when using the freshwater microalgae

Chlorella sp. UMACC313 in a mediatorless system.[92] Lin *et al.*[105] used gold mesh anodes and graphite carbon cloth cathodes in a platform inoculated with the freshwater cyanobacterium *Spirulina platensis*, operated in the dark. Carbon nanotubes fixed on carbon paper (CNT/CP) have been tested as anode material inoculated with the freshwater cyanobacterium *Nostoc sp.*, in combination with an enzymatic (Laccase/CNT/CP) cathode.[151] Recently, the development of engineered materials have received attention in the development of BPV platforms, with one interesting study using nanocomposites electrodes and the marine cyanobacterium *Synechococcus sp.* BDU140432, achieving relatively high OCP values.[152] Power generation in these platforms can differ largely not only due to different OCP values but also because of different R_{int} values. Different cell configurations, electrode size and the use of freshwater or marine species, do not allow a comprehensive comparison of the exoelectrogenesis and direct electron transfer capacity of the microorganisms analysed.

The size of the electrochemical cell is another important factor. As relatively low OCP values are obtained in BPVs (<700 mV), current densities can be increased by reducing the electrode area. Micro-size MFCs have been demonstrated for exoelectrogenic bacteria,[153] as well as for photosynthetic microorganisms.[95,154] Bombelli *et al.*[95] obtained relatively high power density (100 mW/m^2) in a micro-size BPV using solidified molten InBiSn as the anode material inoculated with the freshwater cyanobacterium *Synechococystis sp.* PCC6803, but the platform presented a high R_{int} (2.2 MΩ) despite the addition of NaCl (0.25 M) to the aqueous medium. High R_{int} is a setback of micro-size cells.[155]

To improve energy recovery in BPV devices, it is imperative to improve the electrochemical cell performance. However, for the technology to move forward the assembly cost must be minimal as it is in the core of microbial catalysis to provide inexpensive platforms. Inexpensive materials should be sought, which at the same time are suitable for a reactor design allowing direct illumination of the biofilm for continuous operation. Furthermore, the use of wild-type strains should be considered as part of an accessible design, enabled to operate in open field applications without the restriction of a contained environment which conveys extra costs.

3.1.4 Membrane electrode assembly and carbon electrodes

A membrane electrode assembly (MEA) is a type of electrochemical cell consisting of a sandwich of three layers: anodic electrode, membrane and cathodic electrode (Figure 3-2). Porous electrode materials are required for reactants to diffuse, and an ion exchange membrane, typically a proton exchange membrane (PEM) is used,[156] but filter paper has also been used.[96] This assembly reduces the distance for the electrolyte to diffuse (membrane thickness), reducing R_{int}, while the membrane

physically separates electrodes preventing a short circuit. MEA assemblies are broadly used in fuel cells, including MFC and photo-MFC.[73,96]

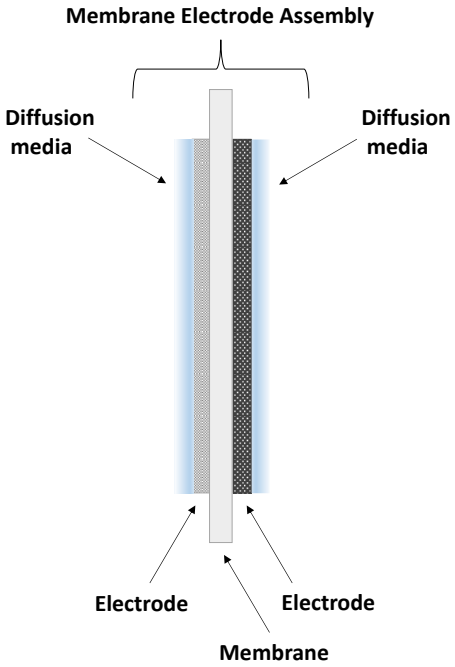

Figure 3-2. Schematics of an membrane electrode assembly (MEA).[81]

Carbon fibres are ideal for the MEA arrangement, due to their high porosity, high conductivity, biocompatibility and reduced cost.[12,157] However, carbon materials are of a hydrophobic nature which hinders their wettability and electrochemical reactivity.[158] Different techniques have been applied to improve the interaction of the carbon electrode with the electrolyte solution, by adding hydrophilic functional groups on the surface of carbon, typically oxygen groups. Treatments can be chemical with strong oxidants, for instance nitric acid and peroxide (so called wet methods), which are time length-dependent.[159] Alternatively, treatment can be heat annealing (400 °C) in the presence of air.[160] However, the most effective methods are still those based on plasma treatment (gas ionisation), where the excited molecules and radicals generated during plasma discharge attack C=C bonds, enabling the introduction of functional groups on the surface without affecting the properties of the bulk material.[159]

Plasma treatment of carbon electrodes (anode) in MFC has shown improvement in biofilm formation of anode respiring bacteria alongside higher electrical current generation.[161,162]

3.1.5 Objectives and proposed systems

The main objective in this chapter is to evaluate the exoelectrogenic capacity of the cyanobacterium *Synechococcus elongatus* PCC7942. A benchmark study was designed to provide a comprehensive and systematic analysis.

In the first stage, the performance of PCC7942 in a mediatorless BPV device is presented and compared to the performance of the device when inoculated with *S. oneidensis* (MFC). By doing so, assessing the performance of the device with a good exoelectrogen and providing a comprehensive comparison of BPVs and MFCs. An initial assessment of *S. oneidensis* biofilms was conducted to establish its electrochemical characterisation in the conditions studied. In an iterative process, different device designs were tested, seeking a suitable design for continuous operation and considering that in BPV platforms inexpensive materials are needed. The design and evaluation of the BPVs and MFCs was carried out to provide insight to device performance and biocompatibility, also considering the cost associated to the platform.

In the second stage, the exoelectrogenic capacity of PCC7942 is presented and compared to other photosynthetic cultures, including the microalgae *C. vulgaris* CCAP 211/52 and co-cultures of PCC7942 (bacteria present). The cultures were tested in their capacity to reduce ferricyanide, this assay provides a direct measurement of the exoelectrogenic capacity without the complexity of the electrochemical device or the complexity of the cell envelope. Ferricyanide is utilised as a redox mediator in electrochemical cells, thus higher rates of reduction can be extrapolated to a better performance in a mediated BPV platform. The cultures were also tested in their capacity to generate power in light driven mediatorless platforms. The evaluation of the photosynthetic cultures/biofilms was carried out according to their ferricyanide reduction capacity and performance in a mediatorless device.

3.2 The exoelectrogenic performance of PCC7942 in mediatorless BPVs in comparison to MFCs fostering the exoelectrongen *S. oneidensis*

In this section, the performance of PCC7942 biofilms in mediatorless BPV platforms is presented. The exoelectrogenic bacteria *S. oneidensis* MR-1 (*S. oneidensis* hereafter) was used as a reference to evaluate a given platform. Both microorganisms are gram-negative bacteria, but with *S. oneidensis* capable of constitutive extracellular electron transfer.

3.2.1 *S. oneidensis* electrochemical characterisation

S. oneidensis was grown as described in Chapter 2 – Section 2.2.4. To evaluate the effect of the operational conditions chosen over the exoelectrogenic capacity of *S. oneidensis*, cyclic voltammetry was conducted as described in Chapter 2 – Section 2.5.5, on biofilms grown in carbon felt (left to settle for 24 hours). Measurements were conducted in aerobic conditions.

Figure 3-3 presents the voltammetry obtained showing two electroactive regions, one with midpoint potential at -0.4 V vs Ag/AgCl (riboflavins) and starting potential at -0.45 V vs Ag/AgCl, the second at 0.0 V vs Ag/AgCl with starting potential at -0.2 V vs Ag/AgCl. In the case of riboflavins, the midpoint potential is the same than that reported by Baron *et al.*[56] for *S. oneidensis* biofilms in anaerobic conditions fed with lactate. The second region appears to be related to cytochromes activity. While the potential was higher than that reported by Baron *et al.*[56] for biofilms on graphite carbon, it was the same as that reported by Roy *et al.*[144] for biofilms grown on gold electrodes.

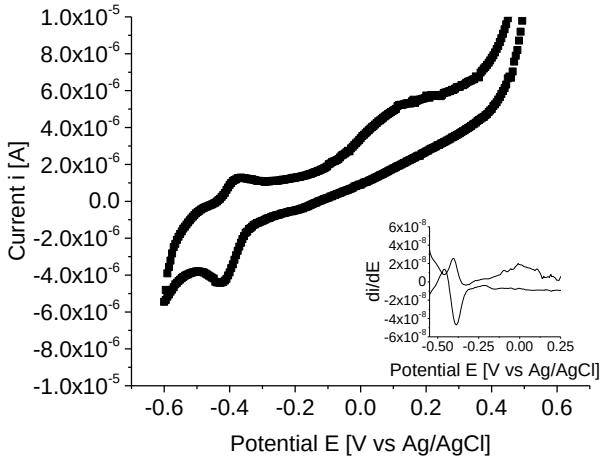

Figure 3-3. Cyclic voltammetry of biofilm of *S. oneidensis* on carbon felt at scan rate of 1 mV s^{-1} in aerobic conditions at 30 °C and fed with tryptic soy broth. The biofilm was left to settle down during 24 hours before conducting measurement. Inset: first derivative.

Diffusion limitation was observed in the voltammetry. Back sweep cathodic currents were observed at the region of riboflavin activity, with a pronounced peak indicating diffusion limitation. Besides, the cathodic current indicates that after riboflavin reacted in the forward sweep, it was not re-reduced by the biofilm nor diffused to the bulk solution.

In cyanobacteria, natural redox mediators have not been described and in the absence of artificial redox shuttles, direct electron transfer has been hypothesised.[14,45] Nonetheless, the diffusion limitation seen for riboflavin suggests that other ions in the electrolyte, including protons, also will face diffusion limitation, which will affect the performance of both MFCs and BPVs.

3.2.2 Mediatorless platforms fostering PCC7942 and *S. oneidensis*: reactor design, membrane and anode material selection

The selection of the electrode material and electrode arrangement, besides the selection of a membrane if necessary, are important in the design of an electrochemical platform. In this section, the construction of a BPV platform utilising PCC7942 is presented and evaluated in respect to the performance of the exoelectrogen *S. oneidensis*.

3.2.2.1 Single chamber device

Conventionally, ITO-coated glass (transparent electrode) has been used as anode material in single chamber BPV platforms.[14,48,98,101] Therefore, it was chosen as the first electrode to evaluate PCC7942. ITO-coated glass fostering PCC7942 showed a dense biofilm formation (Figure 3-4).

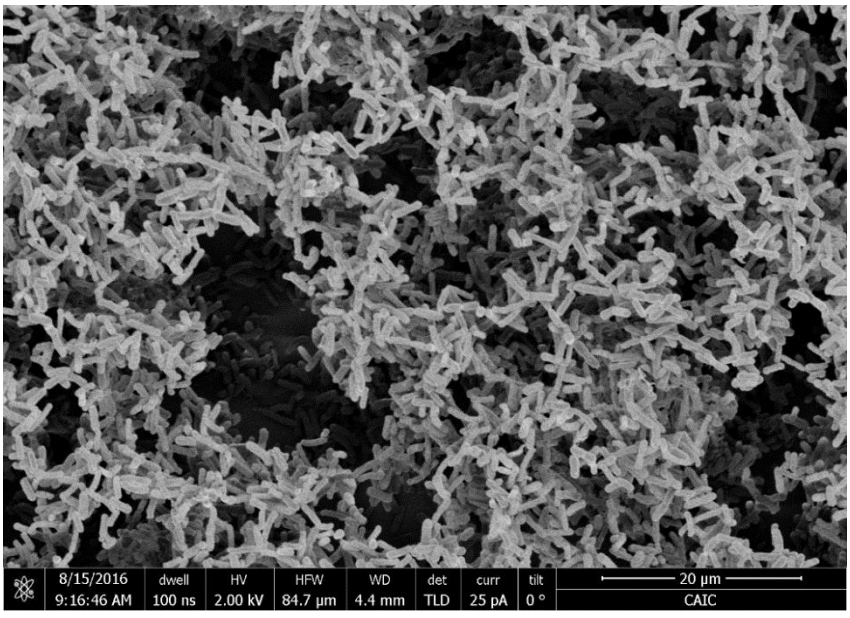

Figure 3-4. SEM images of PCC7942 biofilm on ITO-coated glass. Image obtained as described in Chapter 2 – Section 2.10.

To use ITO-coated glass, single chamber devices were constructed and operated as described in Chapter 2 – Section 2.5.1 and 2.5.4 and pictured in Figure 3-5. This device was used as the control in the study. A volume of 1 ml (OD_{750} 3) was inoculated in the single chamber BPV. PCC7942 biofilms were left to settle down for four days before conducting a polarisation curve. A volume of 1 ml *S. oneidensis* cultures (OD_{600} 1) was inoculated in the single chamber MFC. *S. oneidensis* biofilms were left to settle down for one day before conducting a polarisation curve.

Figure 3-5. Photography of single chamber device, left: top view and right: bottom view.

Figure 3-6 shows the polarisation and power curves for PCC7942 and *S. oneidensis* in the single chamber device and the parameters obtained are summarised in Table 3-1.

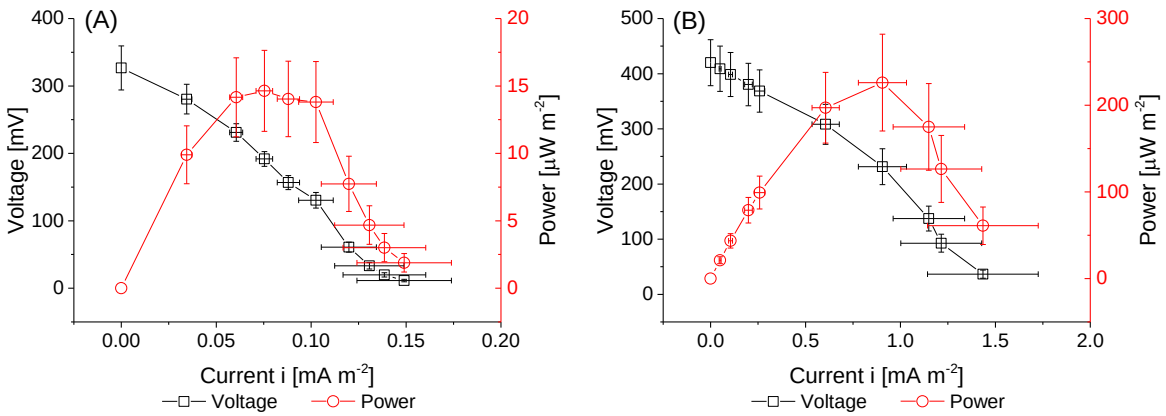

Figure 3-6. Polarisation (black) and power curve (red) obtained from biofilms on ITO-coated glass (anode) in a single chamber device with an air cathode inoculated with (A) PCC7942 (BPV) and (B) *S. oneidensis* (MFC). In (A) the following resistors were used: 32 MΩ, 15 MΩ, 10 MΩ, 7 MΩ, 5 MΩ, 2 MΩ, 1 MΩ, 560 kΩ and 300 kΩ. In (B) the following resistors were used: 32 MΩ, 15 MΩ, 7 MΩ, 5 MΩ, 2 MΩ, 1 MΩ, 470 kΩ, 300 kΩ and 100 kΩ. BPV n=4 ±1SE; MFC n=4 ±1SE.

Single chamber	BPV Blank	BPV PCC7942	MFC Blank	MFC *S. oneidensis* MR-1
OCP [mV]	240.5±15.2	326.8±32.6	148.8±43.3	420.0±41.8
P_{out} [µW m^{-2}]	0.18±0.03	15.4±1.7	5.3±3.9	229.9±54.9
R_{int} [MΩ]	N.D.*	10.9±3.0	16.6±6.7	0.92±1.2
pH (light)	7.0	10.2	7.3	7.3

Table 3-1. Parameters obtained from the polarisation of PCC7942 and of *S. oneidensis* biofilms on ITO-coated glass anodes in a single chamber device with an air cathode. Blanks corresponds to abiotic experiments (media). pH is that of media and cultures. P_{out} corresponds to the highest power measured. R_{int} was estimated from the slope of the linear segment of the polarisation curve. *Not determined due to non-linear polarisation. BPV Blank n=2 ±1SE; BPV n=4 ±1SE; MFC Blank n=4 ±1SE; MFC n=4 ±1SE.

OCP values were higher in MFCs (420.0±41.8 mV) than in BPVs (326.8±32.6 mV). Expectedly, higher power was achieved by MFCs, with 15.4±1.7 µW m^{-2} and 229.9±54.9 µW m^{-2} for BPVs and MFCs respectively. High R_{int} in the electrochemical cells was found, particularly in BPV devices (10.9±3.0 MΩ). The latter is partly due to the significant distance between electrodes (approximately 0.5 cm), but also to the poor conductivity of the media (BG11, 2.5 mS).[14]

The small volume of the single chamber device (approximately 1 ml), impeded to assess the device in long term studies, but increasing the volume of the chamber implies to increase the distance between electrodes (for a fixed electrode area), which would increase R_{int}.

The pH of the cultures inoculated in the devices was also different. PCC7942 alkalinise the media because of photosynthetic activity, as CO_2 fixation induces the influx of bicarbonate ions (C_i intake) accompanied by the efflux of hydroxide ions.[163] pH affects the air cathode performance, while oxygen evolution due to the photosynthetic activity enriches the chamber with oxygen. In the MFC chamber, *S. oneidensis* consuming oxygen reduces oxygen concentration.

The high R_{int} seen in BPVs, but also in the MFCs, implies that more efficient devices can be constructed.

3.2.2.2 Nafion®– MEA device

In order to reduce ohmic losses a membrane electrode assembly (MEA) device was constructed and operated as described in Chapter 2 – Section 2.5.2 and 2.5.4. In this study, the utilisation of carbon fibres in the anode is addressed. Carbon felt and carbon paper were used. MEA devices were inoculated with 5 ml of PCC7942 (OD_{750} 3) or 5 ml of *S. oneidensis* (OD_{600} 1). Devices were characterised after four days and one day respectively.

The membrane commonly used in MEAs, particularly in hydrogen fuel cells but also MFCs and BPVs, is Nafion®, a proton exchange membrane.[156] Nafion® allows mainly diffusion of protons, implying that oxygen generated by the photosynthetic biofilm is not available in the cathode, in constrant to the single chamber device where the cathode benefits from *in situ* photosynthetic oxygen generation (photo-biocathode).

An initial study with Nafion® as the separating membrane in a MEA-BPV, using carbon felt as anode material, showed a light positive response in the OCP obtained. However, values were significant only for one device out of six (Figure 3-7 (A)). Nafion® is an acidic membrane which caused the cultures to reach acidic pH (around 2.5 – 3.0), consequently microorganisms were inactivated with only one BPV device remaining green (Figure 3-7 (B)), that was with possible active cyanobacteria. Remarkably, the BPV device showing a green culture was that reading a significant OCP value. In the case of *S. oneidensis* cultures exposed to Nafion®, the acidity of the membrane was partially buffered and pH of the cultures went down to slightly acidic pH (around 4.5 – 5.0).

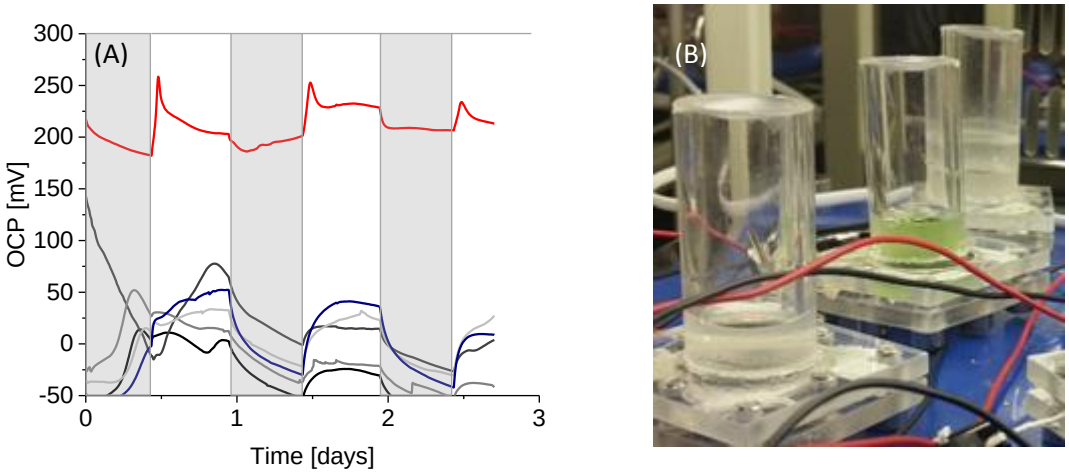

Figure 3-7. (A) OCP profile in a 12 hour light/dark cycle of six Nafion-MEA BPV devices showing only one device reading significant values (red curve). (B) Photograph of the active device (red curve) showing a green culture against devices with inactive cyanobacteria.

A polarisation curve (Figure 3-8 (A)) of the active device resulted in a maximum power output of 151.1 µW m^{-2} with R_{int} of 148.5 kΩ. MEA devices inoculated with *S. oneidensis* (Figure 3-8 (A)) showed a relatively good performance with a maximum power around 6.9±1.6 mW m^{-2} and R_{int} of 29.2±2.9 kΩ, which is similar to some values reported for micro-size MFC fostering *S. oneidensis*.[164,165] Table 3-2 summarises the parameters obtained from the characterisation of MEA devices.

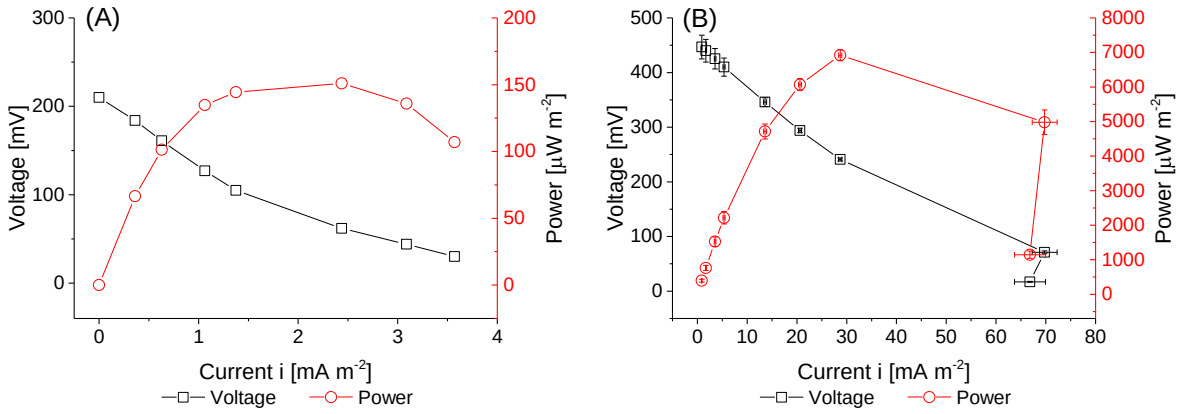

Figure 3-8. Polarisation (black) and power curve (red) obtained from biofilms on carbon felt (anode) in a Nafion®-MEA device with an air cathode inoculated with (A) PCC7942 and (B) *S. oneidensis*. In (A) the following resistors were used: 2 MΩ, 1 MΩ, 470 kΩ, 300 kΩ, 100 kΩ, 56 kΩ and 33 kΩ. In (B) the following resistors were used: 2 MΩ, 1 MΩ, 470 kΩ, 300 kΩ, 100 kΩ, 56 kΩ, 33 kΩ, 4 kΩ and 1 kΩ. BPV n=1; MFC n=4 ±1SE.

Nafion®-MEA	**BPV Blank**	**BPV PCC7942**	**MFC Blank**	**MFC *S. oneidensis***
OCP [mV]	-38±14	210	271.0±31.8	453.3±22.9
P_{out} [µW m^{-2}]	-	151.1	422.3±121.5	6920.1±157.8
R_{int} [kΩ]	-	148.5	175.1±58.6	29.2±2.9
pH	-	2.5 – 3.0	-	4.5 – 5.0

Table 3-2. Parameters obtained from the polarisation of PCC7942 and *S. oneidensis* biofilms on carbon felt (anode) in a Nafion®-MEA device with an air cathode. Blanks correspond to abiotic experiments (media). P_{out} corresponds to the highest power recorded. R_{int} was estimated from the slope of the linear segment of the polarisation curve. Blank BPV n=3±1SE; BPV n=1; Blank MFC n=4±1SE, MFC n=4±1SE.

Acidic pH is positive to the performance of the membrane/cathode, however it hinders cellular activity including inhibited secretion of riboflavins, therefore power has been reported to be lower at acidic pH than at neutral pH.[166] Nonetheless, similar OCP values were obtained in the single chamber MFCs and the Nafion®-MEA-MFCs. The latter with lower R_{int} resulted in 30-fold higher power output generated by the *S. oneidensis* biofilms.

The OCP value in the Nafion®-MEA-BPV was around 100 mV lower than that of the single chamber BPVs despite the lower pH (higher cathode potential), demonstrating that low pH causes adverse effects in the photo-biocatalysis by PCC7942. However, the lower R_{int} of the Nafion®-MEA-BPV resulted in 10-fold higher power output than that generated in the single chamber device.

pH is a relevant parameter in the performance of a MFC/BPV and to provide a cultural pH suitable for the microorganisms is necessary, but the use of Nafion® will demand addition of buffers implying an additional cost, alternatively a non-acidic membrane could be used.

3.2.2.3 Nitrocellulose – MEA device

The MEA was redesigned, replacing Nafion® with a nitrocellulose membrane (0.2 µm porous size). The latter does not affect the pH of the cultures, therefore all BPV devices could be active. Furthermore, the membrane chosen is still very porous and hydrophilic providing a physical separation for the anode and cathode as well as for the microbes but not for the electrolyte and gases. Carbon felt and carbon paper were analysed as anode materials. Due to the number of platforms evaluated in this section, the MFCs and BPVs are presented separately.

3.2.2.3.1 Nitrocellulose-MEA-MFC

MFCs fabricated with nitrocellulose-MEAs presented lower performances than devices with Nafion®-MEAs. Figure 3-9 shows the polarisation and power curves obtained for the nitrocellulose-MEA-MFCs. The parameters obtained from the polarisation are summarised in Table 3-3. Power outputs by *S. oneidensis* in nitrocellulose-MEA-MFCs were 10 times lower than Nafion®-MEA-MFCs (Table 3-2), with 619.4±63.5 µW m^{-2} and 720.9±60.6 µW m^{-2} for carbon felt and carbon paper MEAs respectively. OCP values were similar in all the MFC designs.

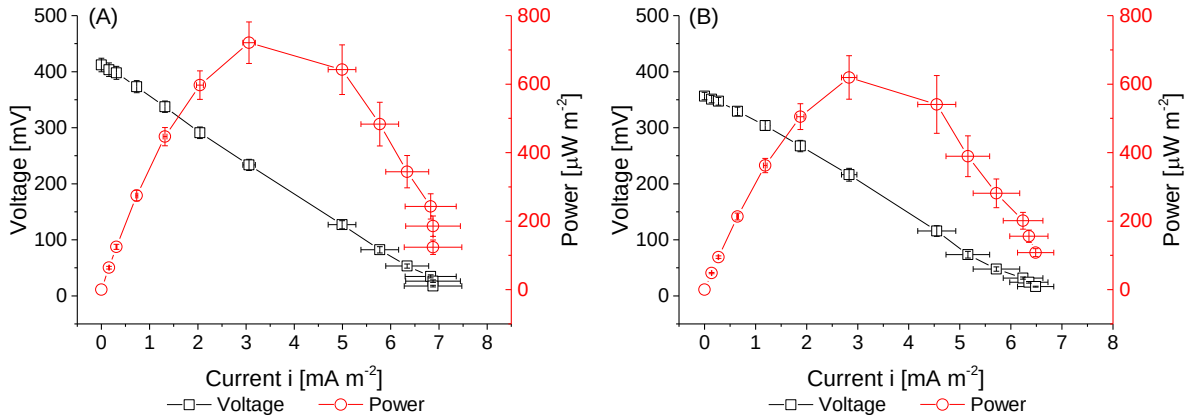

Figure 3-9. Polarisation (black) and power curve (red) obtained from biofilms of *S. oneidensis* on (A) carbon felt and (B) carbon paper (anodes) in a nitrocellulose-MEA MFC device with an air cathode. In (A) and (B) the following resistors were used: 10 MΩ, 5 MΩ, 2 MΩ, 1 MΩ, 560 kΩ, 300 kΩ, 100 kΩ, 56 kΩ, 33 kΩ, 20 kΩ, 15 kΩ and 10 kΩ. MFCs n=4 ±1SE.

Nitrocellulose-MEA	Blank CF	Carbon Felt	Blank CP	Carbon Paper
OCP [mV]	196.3±15.4	356.5±6.50	134.8±5.0	412.0±12.1
P_{out} [µW m^{-2}]	31.2±5.8	619.4±63.5	7.8±0.5	720.9±60.6
R_{int} [kΩ]	1372.9±146.3	220.3±24.6	2716.0±46.7	187.0±8.8

Table 3-3. Parameters obtained from the polarisation of *S. oneidensis* biofilms on carbon felt and carbon paper (anodes) in a nitrocellulose-MEA device with an air cathode. Blanks corresponds to abiotic experiments (media). P_{out} corresponds to the highest power recorded. R_{int} was estimated from the slope of the linear segment of the polarisation curve. Blanks and MFCs n=4 ±1SE.

An important difference between Nafion®-MEAs and nitrocellulose-MEAs was that the latter resulted in higher R_{int}. In the assemblies with Nafion®, the cathode is embedded in the membrane providing intimate contact between the catalyst and the acidic membrane, enhancing cathode reactivity and/or minimising cathodic ohmic losses.

3.2.2.3.2 Nitrocellulose-MEA-BPV

The hydrophobicity of carbon materials represents a limiting factor when using aqueous electrolyte, which can be critical for biofilms with a low exoelectrogenic capacity. To overcome the hydrophobicity of carbon materials, oxygen plasma treatment was used to increase the wettability of the surface. The hydrophobicity was determined as described in Chapter 2 – Section 2.5.3. Table 3-4 shows the contact angles of bare carbon and plasma treated carbon. It can be seen that the plasma treated carbon materials were hydrophilic, with full adsorption of water.

Material	Bare carbon	Plasma treated carbon
Carbon Felt	160.0±1.5	0
Carbon Paper	140.9±2.1	0

Table 3-4. Contact angle of carbon felt and carbon paper, n=3 ±1SE.

The biofilm formation on all carbon materials, including plasma treated materials, was similar (Figure 3-10). Figure 3-11 shows a photograph of the set of nitrocellulose-MEA-BPVs.

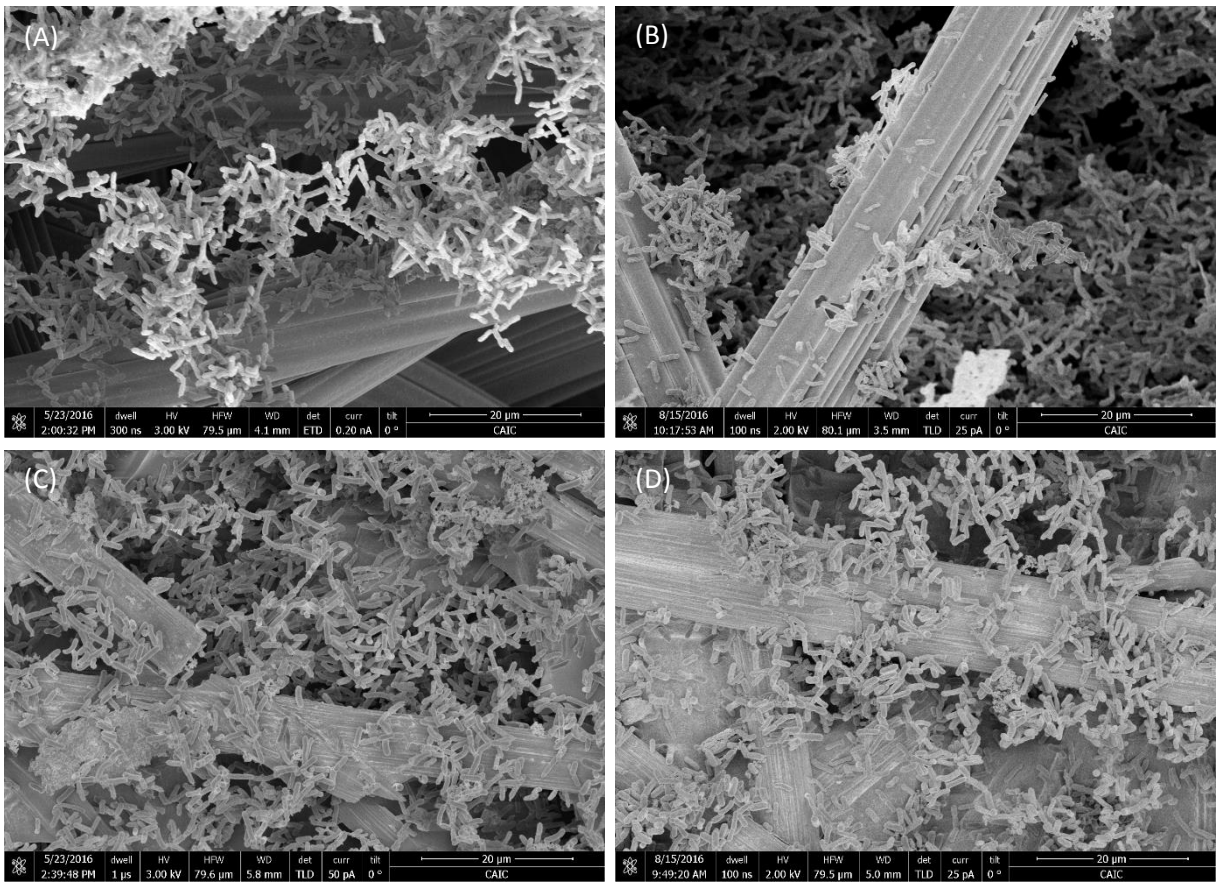

Figure 3-10. SEM images of PCC7942 biofilms on (A) carbon felt, (B) plasma treated carbon felt, (C) carbon paper and (D) plasma treated carbon paper. Images obtained as described in Chapter 2 – Section 2.10.

Figure 3-11. Photograph of nitrocellulose-MEA-BPV devices inoculated with PCC7942 (Day 1).

The characterisation of the nitrocellulose-MEA-BPVs is presented in Figure 3-12 and Table 3-5 summarises the parameters obtained. OCP values were similar to those of the single chamber BPV devices (Table 3-1) and higher than the one active Nafion®-MEA-BPV (Table 3-2). Carbon paper (non-treated) MEA-BPVs had lower R_{int} than the single chamber BPV, but the power obtained for the latter was as high. This demonstrates how ITO-coated glass performance is better as an anode material for PCC7942 biofilms, due to lower activation losses as observed when comparing the respective polarisation curves (Figure 3-6 (A) and Figure 3-12).

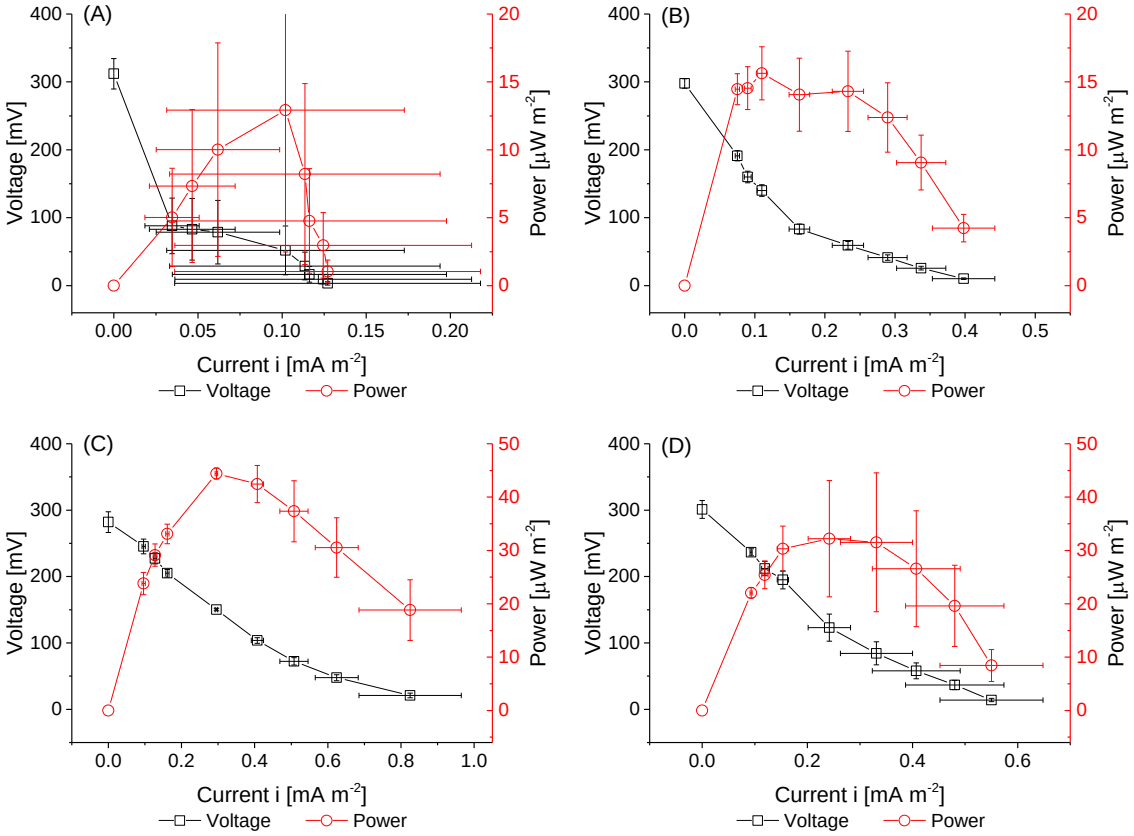

Figure 3-12. Day 4. Polarisation (black) and power curve (red) of biofilms of PCC7942 on (A) carbon felt, (B) carbon paper, (C) carbon felt plasma treated and (D) carbon paper plasma treated (anodes) in a nitrocellulose-MEA-BPV device with an air cathode. The following resistors were used: 10 MΩ, 7 MΩ, 5 MΩ, 2 MΩ, 1 MΩ, 560 kΩ, 300 kΩ and 100 kΩ. CF NT n=3 ±1SE; CP NT n=4 ±1SE; CF PT n=3 ±1SE; CP PT n=3 ±1SE.

	Blank CF	Carbon Felt	Blank CP	Carbon Paper
		Non-treated		
OCP [mV]	175.0±23.5	312.0±22.5	100.8±66.1	298±7
P_{out} [µW m^{-2}]	3.1±0.6	13.2±10.3	0.09±0.04	16.3±2.5
R_{int} [MΩ]	N.D.*	N.D.*	N.D.*	5.0±0.9
		Plasma treated		
OCP [mV]	224±6.4	282±16	175±5.5	301±14
P_{out} [µW m^{-2}]	59.8±4.9	46.2±2.1	15.6±0.9	38.1±10.4
R_{int} [MΩ]	0.8±0.1	1.7±0.3	1.2±0.2	3.1±0.8

Table 3-5. Parameters obtained (Day 4) from the polarisation of PCC7942 biofilms on carbon felt and carbon paper in nitrocellulose-MEA-BPV devices with an air cathode. Blanks correspond to abiotic experiments (media). P_{out} corresponds to the highest power recorded. R_{int} was estimated from the slope of the linear segment of the polarisation curve. Blank CF-NT, n=3 ±1SE; Blank CP-NT n=3 ±1SE; BPV CF-NT n=3 ±1SE; BPV CP-NT n=4 ±1SE; Blank CF-PT n=3 ±1SE; Blank CP-PT n=3 ±1SE; BPV CF-PT n=3 ±1SE; BPV CP-PT n=3 ±1SE.

The large error bar in the polarisation of carbon felt MEA-BPVs are due to one device out of three giving higher values, the other two only showed large drops in voltage as soon as connected to external loads. The one device showing a better polarisation, resulted in a power output of 38.5 µW m^{-2} and R_{int} of approximately 2.5 MΩ, which are better parameters than those obtained for carbon paper MEA-BPVs. The limitation of carbon felt to perform is its high hydrophobicity (Table 3-4) together with the thickness of the fibre (1.59 mm), carbon paper is also highly hydrophobic but thinner (0.190 mm). These conditions impeded the electrolyte to impregnate the fibre, resulting in an extremely high R_{int}.

The R_{int} of MEAs assembled with plasma treated carbon materials were lower for both carbon felt and carbon paper. Furthermore, the R_{int} of blanks for the MEA-BPVs assembled with plasma treated carbon materials were similar to the blanks of the MEA-MFCs, indicating a better comparative platform. Expectedly, the lower R_{int} in the plasma treated MEAs translated in higher power outputs. However, the blanks in the plasma treated carbon felt MEAs showed higher power than those in the inoculated carbon felt MEA-BPVs.

Blanks were operated at neutral pH, which aided the cathodic reaction. However, despite the lower pH in the blanks, OCP values were not higher than in the BPV devices, indicating that in the latter the higher OCP values were a result of biological activity. The pH of the blanks was not buffered at alkaline pH because addition of buffers changes the blank composition.

Blanks of carbon paper MEAs delivered lower power, with a clear influence of PCC7942 in the performance of the BPV device. From the blanks characterisation, it is observed that carbon felt is a more reactive electrode than carbon paper, this was also seen in the blanks of MFCs (Table 3-3).

Another improvement seen as a result of the plasma treatment was that activation losses were lower, demonstrating a gain in reactivity due to the more hydrophilic electrode surface.

To further analyse MEA performance, devices were left under load (connected to a resistor). The external load was chosen according to the highest power recorded. Power outputs in a 12 hour light/dark cycle is observed in Figure 3-13 and Figure 3-14. A clear light/dark pattern was seen in the BPV devices, suggesting light dependence, thus photosynthetic activity driving the system. The light/dark pattern was not seen in the blanks and although plasma treated carbon felt MEA-Blanks kept high power outputs, on average the MEA-BPVs fostering PCC7942 became higher (in the light).

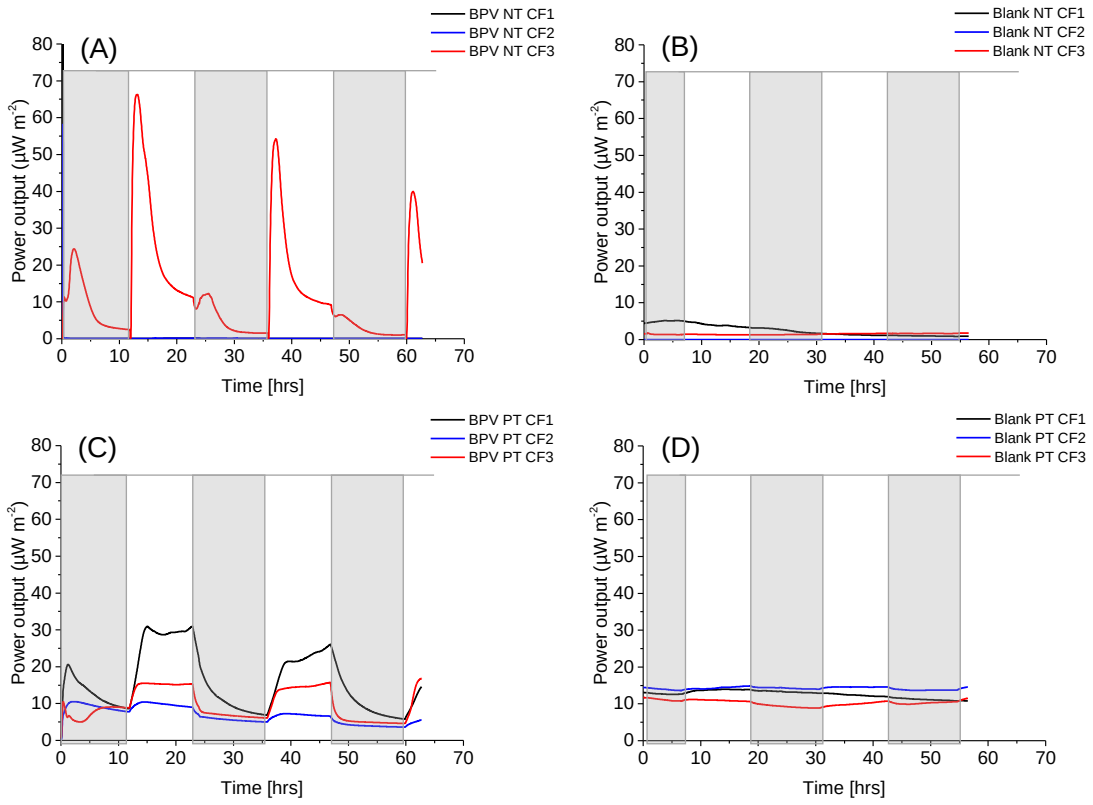

Figure 3-13. Power output profile in a 12 hour light/dark cycle for MEA-BPV (and Blanks) devices fostering PCC7942 on carbon felt in the anode assembled with nitrocellulose and an air cathode. (A) non-treated carbon felt MEA-BPV (NT CF); (B) non-treated carbon felt MEA-Blank (NT CF); (C) plasma treated carbon felt MEA-BPV (PT CF), (D) plasma treated carbon felt MEA-Blank (PT CF).

As mentioned, the MEA-BPV holding carbon felt presented one operative device. This device, showed a large increase in power upon illumination, reaching the highest power recorded within the nitrocellulose-MEA-BPVs, but then decreased rapidly. The latter indicates that as photosynthesis was

activated currents increased, but the hydrophobicity of the electrode impeded the diffusion of electrolyte and as protons got depleted in the cathode, currents dropped.

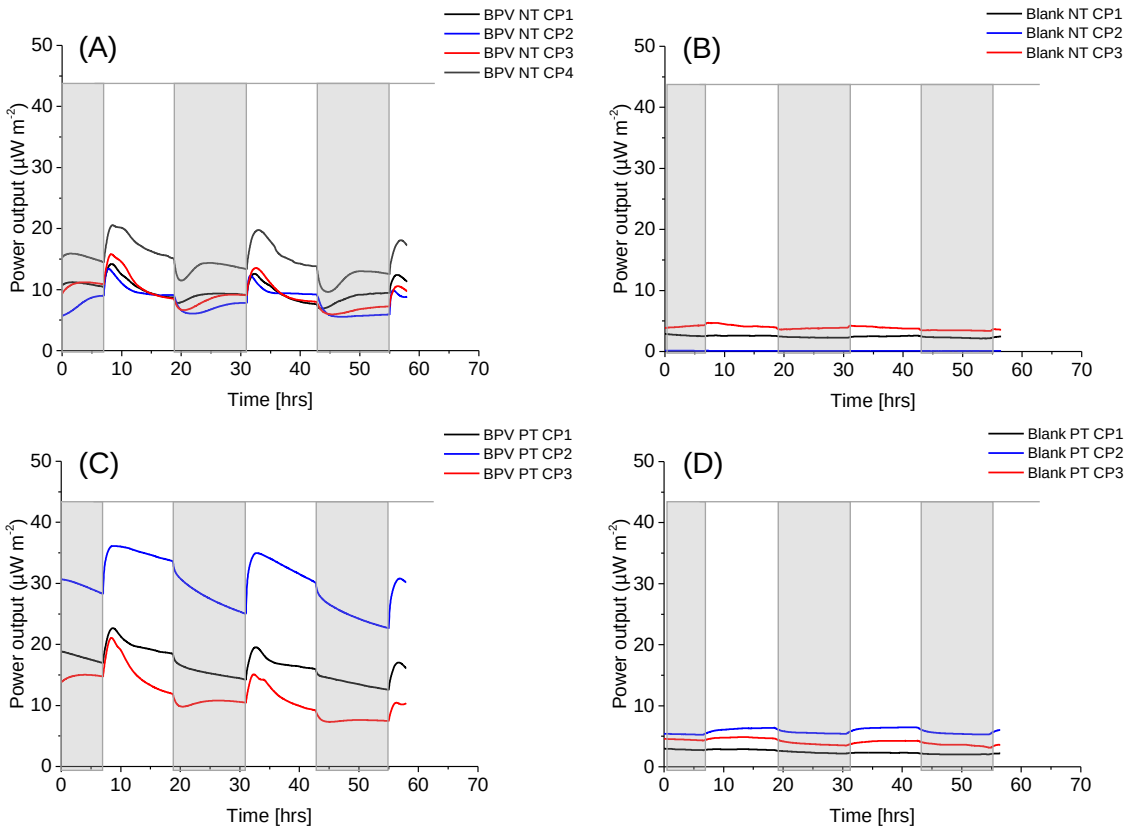

Figure 3-14. Power output profile in a 12 hour light/dark cycle for MEA-BPV (and Blanks) devices fostering PCC7942 on carbon paper in the anode assembled with nitrocellulose and an air cathode. (A) non-treated carbon paper MEA-BPV (NT CP); (B) non-treated carbon paper MEA-Blank (NT CP); (C) plasma treated carbon paper MEA-BPV (PT CP), (D) plasma treated carbon paper MEA-Blank (PT CP).

After MEA-BPVs were left under load, new polarisation curves were conducted after six days (ten days after inoculation). Polarisation and power curves are presented in Figure 3-15 and the parameters obtained are summarised in Table 3-6. Better reproducibility in the carbon felt MEAs was found, at the same time an improvement in R_{int} was seen in both carbon felt and carbon paper MEAs. The activation losses in the nitrocellulose-MEA-BPVs assembled with non-treated carbon materials were lower than at Day 4, indicating that incubation for a longer time enabled the carbon electrodes to reach a higher level of electrolyte impregnation. However, despite lower R_{int}, power outputs were not higher than at Day 4 because there was a drop in OCP values.

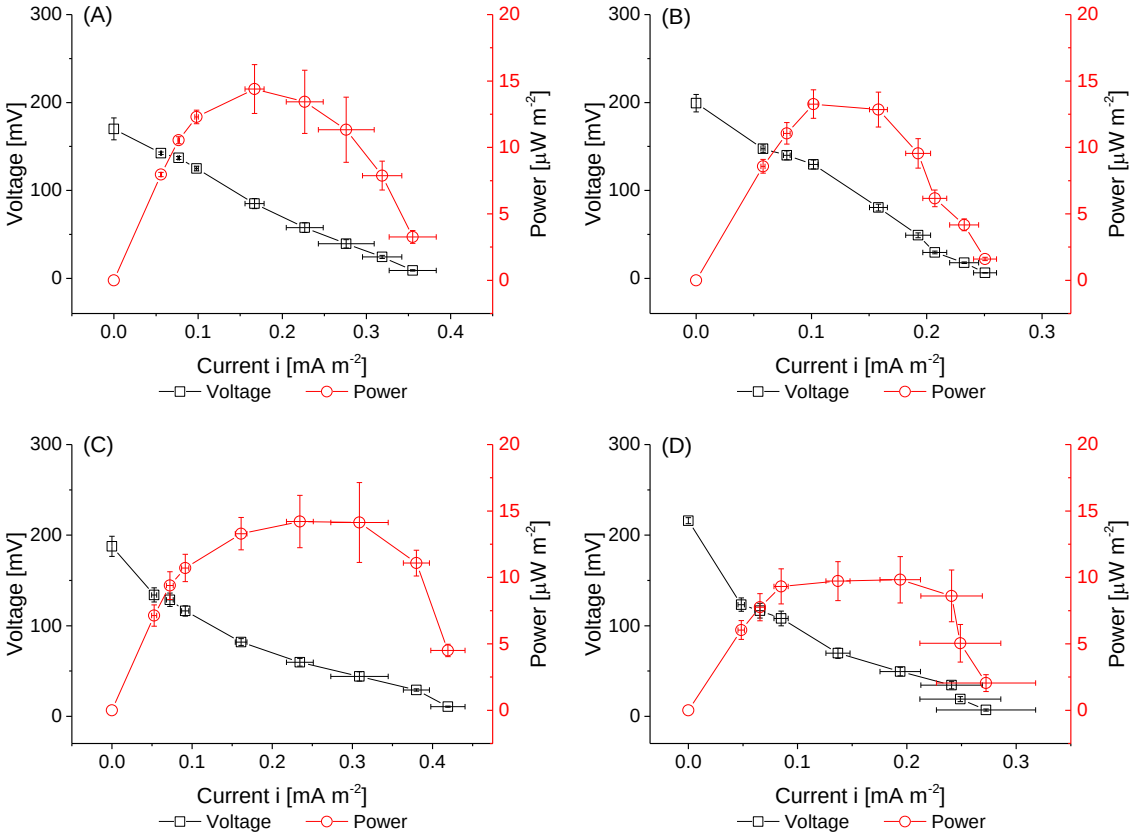

Figure 3-15. Day 10. Polarisation (black) and power curve (red) of biofilms of PCC7942 on (A) carbon felt, (B) carbon paper, (C) carbon felt plasma treated and (D) carbon paper plasma treated (anodes) in a Nitrocellulose-MEA-BPV device with an air cathode. The following resistors were used: 10 MΩ, 7 MΩ, 5 MΩ, 2 MΩ, 1 MΩ, 560 kΩ, 300 kΩ and 100 kΩ. CF-NT n=3 ±1SE; CP-NT n=4 ±1SE; CF-PT n=3 ±1SE; CP-PT n=3 ±1SE.

	Carbon Felt	**Carbon Paper**	**Carbon Felt Plasma Treated**	**Carbon Paper Plasma Treated**
OCP [mV]	170.0±12.0	199.0±9.8	188±11	216±3.3
P_{out} [µW m^{-2}]	14.8±1.5	13.4±1.2	15.6±1.9	10.4±2.6
R_{int} [MΩ]	2.3±0.5	2.8±0.2	1.3±0.5	1.8±0.4

Table 3-6. Parameters obtained at Day 10 (after six days under load) from the polarisation of PCC7942 biofilms on carbon felt and carbon paper in nitrocellulose-MEA-BPV devices with an air cathode. Blanks correspond to abiotic experiments (media). P_{out} corresponds to the highest power recorded. R_{int} was estimated from the slope of the linear segment of the polarisation curve. CF-NT n=3 ±1SE; CP-NT n=4 ±1SE; CF-PT n=3 ±1SE; CP-PT n=3 ±1SE.

Furthermore, power outputs from devices assembled with plasma treated anodes were not higher than non-treated ones (Day 10). The latter occurred even though non-treated MEAs, holding both carbon felt and carbon paper, had higher R_{int} than their respective treated condition (Table 3-6). The polarisation curves from nitrocellulose-MEA-BPVs holding plasma treated anodes (Day 10), for both

carbon felt and carbon paper, demonstrated greater activation losses than non-treated MEAs, changing the tendency seen at Day 4 and explaining the resulting power outputs.

In the MEA assemblies a substantial amount of biomass got trapped at the bottom of the electrode experiencing continuous darkness, promoted by the hydrophilicity gained by the electrodes if these were plasma treated. The latter implies a counterproductive aspect of the MEA assemblies as the effective useful biomass is lower than that initially fed to the device. Trapped biomass in the darker side of the anode was not observed only for non-treated carbon felt.

3.2.2.3.3 Anodic and cathodic potential of MEAs fostering PCC7942 and *S. oneidensis*

Figure 3-16 shows the anodic and cathodic potential for nitrocellulose-MEA-BPV devices, in the light and after 3 – 4 hours of darkness, and the associated pH in the device chamber (Day 11). Anodic and cathodic potentials were not recorded throughout the study and only at the end, in favour of maintaining the sterile environment in the electrochemical cell. Anodic potentials in the dark were more positive, although no large differences were seen.

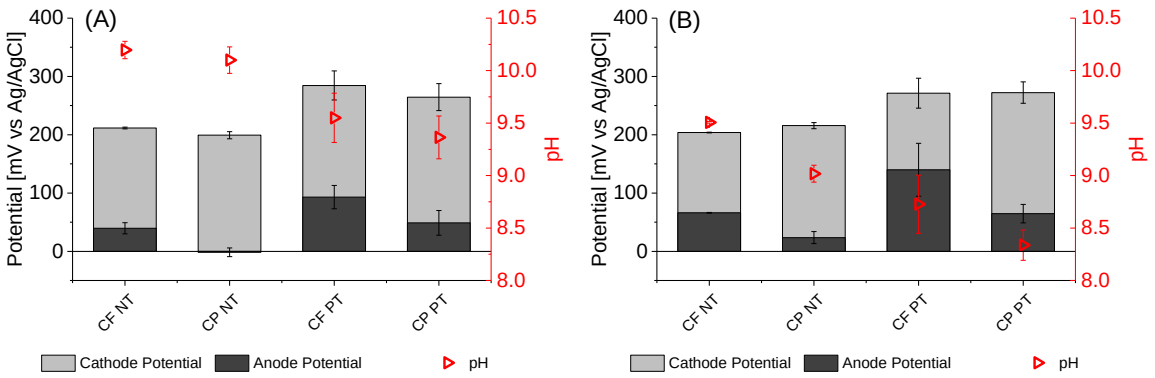

Figure 3-16. Day 11. Anodic and cathodic potential obtained from nitrocellulose-MEA-BPV devices fostering PCC7942 biofilms on carbon felt (CF) and carbon paper (CP) anodes, non-treated (NT) and plasma treated (PT), and an air cathode, (A) in the light phase and (B) in the dark phase. pH of the anodic chamber is shown in the right axis. Potentials in the dark were recorded after 3 – 4 hours in dark conditioning. CF-NT n=3 ±1SE; CP-NT n=4 ±1SE; CF-PT n=3 ±1SE; CP-PT n=3 ±1SE.

Carbon paper (non-treated) presented the lowest anodic potential (-1.7 ± 7.4 mV vs Ag/AgCl), indicating that it is a better material in terms of anode performance than carbon felt. However, R_{int} in

the carbon paper MEA-BPVs were higher, therefore the overall device performance was not better than carbon felt MEA-BPVs.

In Figure 3-16 it is observed that the anodic potential in the plasma treated electrodes was more positive in both carbon felt and carbon paper. At the same time, the pH of the anodic chamber was slightly less alkaline.

In the course of this investigation it was found that a strategy commonly used in electrochemical cells to improve wettability and reactivity of carbon materials did not confer a long term improvement in the electrochemical reactivity for this particular biological system (PCC7942). Furthermore, the drop in pH could be evidence of lower photosynthetic activity. Nevertheless, lower R_{int} showed promising results in short term MEA-BPV operation, therefore other types of surface treatment to increase carbon wettability should be sought.

The potential of anodes fostering *S. oneidensis* (MFCs) and the air cathodes were measured after five days under load. Figure 3-17 shows the anodic and cathodic potential of nitrocellulose-MEA-MFC devices. The OCP dropped in respect to the initial value (Table 3-3) for carbon felt MEAs but not for carbon paper MEAs, mainly caused by a lower cathode potential. At the same time, alkalinisation of the anodic chamber was seen in carbon felt MEA-MFCs but not in carbon paper MEA-MFCs, indicating that proton consumption in the cathode of carbon felt MEA-MFCs was unbalanced in relation to proton generation in the biofilm. The latter is possibly due to carbon felt having a higher specific surface area, causing that the cathode area to become a limiting factor, in the long term causing alkalinisation and lowering cathode potential.

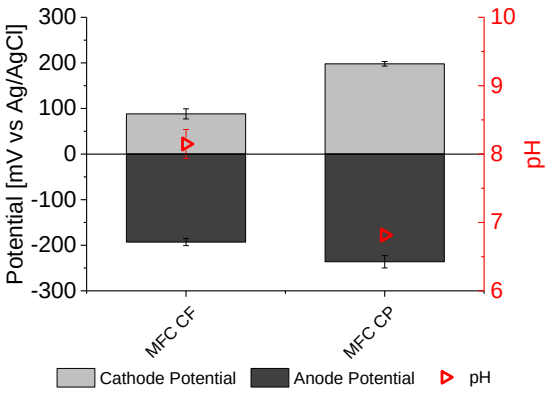

Figure 3-17. Anodic and cathodic potential at Day 6 (after 5 days under load) obtained from MEA-MFC devices fostering *S. oneidensis* biofilms on carbon felt and carbon paper assembled with nitrocellulose and an air cathode. pH of the anodic chamber is shown in the right axis. MFC CF-NT n=4 ±1SE; MFC CP-NT n=4 ±1SE.

The anodic potential in the MFCs (around -200 mV vs Ag/AgCl) was in accordance with the cytochromes redox potential (Section 3.2.1 Figure 3-3). Riboflavin has a lower redox potential; therefore, riboflavin contribution was not significant, possibly due to low concentration in the aerobic conditions.

The cathodic potentials in MFCs were similar and even lower than those seen in BPVs, despite the lower pH in MFCs. The reduced concentration of oxygen around the cathode in the MFCs caused by bacterial consumption of oxygen impacted the cathode potential. In this case, photosynthetic biofilms showed an advantage because they provide an oxygen enriched environment.

3.2.3 Benchmark outcomes

Through the iteration in the electrochemical cell design, the performance of PCC7942 in mediatorless BPV platforms was improved, although long-term operation was a setback. As expected, the comparison with *S. oneidensis* (MFC) demonstrated that PCC7942 extracellular electrochemical reactivity is privative, however there is a large limitation in the performance of the device tested related to non-biological factors. The aqueous electrolyte and inhibition in acidic pH are external factors which lower the performance of BPVs. The best electrochemical platform fabricated was not suitable for PCC7942 because of excessive acidity, however pH could be buffered to solve the compatibility issue.

As mentioned, bioelectrochemical devices ought to have a reduce cost. Appendix A contains the price of the different materials. While a techno-economic analysis is needed for a complete assessment, the cost of fabrication of the devices presented in this chapter (lab scale models) is related to the anode material and to the membrane. Carbon materials convey a significant diminution in the cost of the anode, while nitrocellulose paper is significantly less expensive than Nafion®.

Table 3-7 summarises the outcomes of the first stage of the benchmark.

	Single chamber device (ITO-coated glass anode)	Nafion®-MEA device (carbon felt anode)	Nitrocellulose-MEA device (carbon felt and carbon paper anodes)
Device performance	Control	Large improvement.	Minor improvement if carbon materials are treated. No improvement in the long term.
Biocompatibility	Yes	No for PCC7942 biofilms. Buffers could be used.	Yes
Materials	Control	Anode material is less expensive, but the membrane is an additional cost.	Anode material and membrane are less expensive.

Table 3-7. Benchmark outcome summary for the development of BPV devices fostering PCC7942.

3.3 Exoelectrogenic capacity of PCC7942 in comparison to other photosynthetic systems

To compare the exoelectrogenic capacity of PCC7942 against other photosynthetic cultures, the ferricyanide assay was conducted. The latter provides a method to measure the exoelectrogenic activity of a photosynthetic culture avoiding the complexity of an electrochemical cell and of the cell envelope of a given microorganism. Additionally, MEA-BPVs were used to evaluate power generation in a mediatorless platform.

3.3.1 Selection of photosynthetic systems

In this study, the microalgae Chlorella vulgaris CCPA 211/52 was chosen to compare the performance of PCC7942 against a microalgae strain. *Chlorella* strains have been investigated in previous BPV studies.[14,92]

Photo-MFCs are platforms using heterotrophic bacteria, but with light as the source of energy because of the presence of photosynthetic organisms. If no additional substrates are fed to the device, the system is driven entirely by light. While working with photosynthetic axenic cultures (cultures with a single microorganism) it is likely to introduce bacterial contaminants, which are airborne bacteria colonising the cultures and consequently generating a non-axenic culture or co-culture. These bacteria grow favourably in PCC7942 cultures without modification of the media. Because all microorganisms interact with their surroundings in many ways, it is expected that extracellular electrochemical interactions are present to some extent in all bacteria. Two unspecified co-cultures were analysed.

One consisting of two bacteria and PCC7942 (co-culture A hereafter). The second co-culture consists of one bacterium, different to those in co-culture A, and PCC7942 (co-culture B hereafter).

3.3.2 Ferricyanide reduction capacity by PCC7942, co-cultures of PCC7942 and the microalgae *C. vulgaris* CCAP 211/52

The ferricyanide assay was conducted for all photosynthetic cultures as described in Chapter 2 – Section 2.6, after two, five and eight days of culturing. Cultures were prepared with initial optical density OD_{750} of 0.5.

Figure 3-18 shows the FeCN-R rates obtained from the different photosynthetic systems. The capacity of PCC7942 to reduce ferricyanide was measured in the traditional alkaline environment. It was found to be minimal compared with the other systems. Furthermore, in the dark PCC7942 FeCN-R rates tended to negligible values.

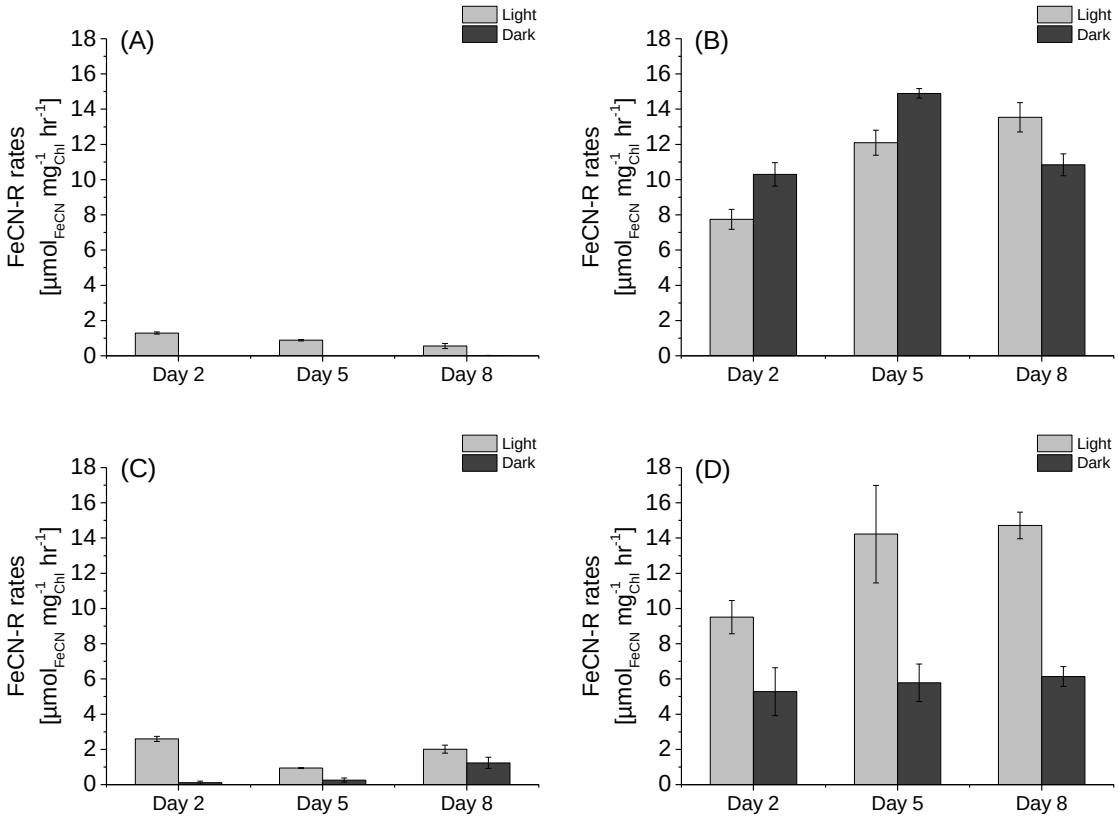

Figure 3-18. Ferricyanide reduction rates (FeCN-R) by photosynthetic cultures. (A) PCC7942, (B) *C. vulgaris*, (C) co-culture A and (D) co-culture B. FeCN-R rates n=3 ±1SE.

FeCN-R rates obtained from *C. vulgaris* were about 14 times higher than those from PCC7942. This is a significant difference, demonstrating that microalgae *C. vulgaris* has a constitutive exoelectrogenic capacity. The highest rate recorded for PCC7942 FeCN-R was 1.3 µmol mg_{Chl}^{-1} hr^{-1} (Day 2), two times lower than that reported by Sekar *et al.*[99] for wild-type PCC7942 in light (2.4 µmol mg_{Chl}^{-1} hr^{-1}). However, it is still in the same order of magnitude and within experimental errors.

Co-culture A showed a similar response in FeCN-R rates to that of axenic cultures, although rates in the light were approximately 2-fold higher. Co-culture B had a significant enhanced capacity in reducing ferricyanide, approximately 14-fold in the light, demonstrating that the presence of a single bacteria conferred to the co-culture a redox catalytic capacity. The latter means that even though PCC7942 is not a constitutive exoelectrogenic cyanobacterium, it can drive an exoelectrogenic response by fostering the growth of more exoelectrogenic bacteria. The presence of bacteria conferred to the photosynthetic co-culture a clear exoelectrogenic capacity in the dark. However, it is still seen that exoelectrogenic rates of the co-cultures were higher in the light than in the dark. Rates in the dark of co-culture A were low but tended to increase with time. In contrast, rates in the dark of co-culture B were significantly high relative to axenic cultures.

In *C. vulgaris* cultures, rates in the dark were in the same order of magnitude than those in the light. This independence from the light implies that, similarly to exoelectrogenic bacteria, intracellular reducing power reacting in the cell surface derives from the metabolism of an organic compound (downstream CO_2 fixation). NADPH generated in the oxidative pentose phosphate pathway and NADH generated in the respiratory pathway are light independent substrates which could be driving the exoelectrogenic activity in *C. vulgaris*.[116]

Ferricyanide reduction capacity in microalgae has been associated to plasma membrane ferric reductases and NADPH oxidases.[48,116] The annotation of ferric reductases and NADPH oxidases in *C. vulgaris* has not been described, but ferric reduction capacity associated to iron uptake was reported.[167] In *Chlorella kelerri*, a microalgae of the same genus, ferric reductase activity has also been measured.[114] By conducting the ferricyanide assay in PCC7942 and *C. vulgaris* CCAP 211/52, representing cyanobacteria and microalgae, it is clear that microalgae have greater exoelectrogenic capacity. Ferricyanide can access the plasma membrane with relative ease, in both cyanobacteria and microalgae. In a mediatorless system a direct interaction with an extracellular solid substrate is necessary, thus the exoelectrogenic response in the absence of a soluble electron shuttle needs a separate analysis.

In the next sub-sections, *C. vulgaris* (BPV) and co-cultures (photo-MFC) are evaluated in their capacity to generate electricity in a mediatorless platform.

3.3.3 Mediatorless BPV devices fostering the microalgae *C. vulgaris* CCAP 211/52

Mediatorless MEA-BPVs assembled with plasma treated carbon paper and nitrocellulose as the membrane, were used to study *C. vulgaris* in its ability to interact directly with an electrode. Figure 3-19 shows polarisation and power curves for Day 4 and Day 10. It was found that the more exoelectrogenic *C. vulgaris* did not perform better in a mediatorless BPV platform when compared with PCC7942. Table 3-8 summarises the parameters for both microorganisms (on plasma treated carbon paper).

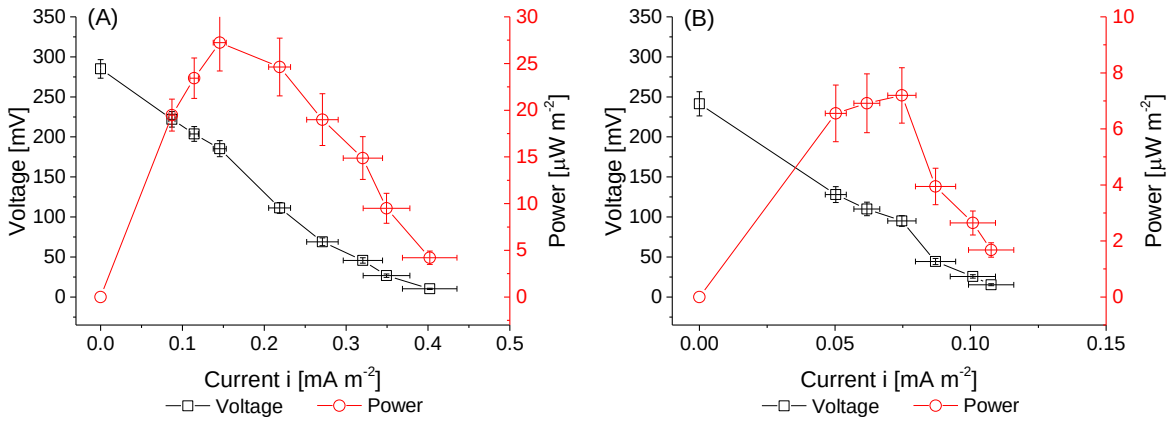

Figure 3-19. Polarisation (black) and power curve (red) (A) at Day 4 (fresh biofilm) and (B) at Day 10 (after six days under load) obtained from MEA-BPV devices fostering *C. vulgaris* biofilms on plasma treated carbon paper in the anode assembled with nitrocellulose and an air cathode. In (A) the following resistors were used: 10 MΩ, 7 MΩ, 5 MΩ, 2 MΩ, 1 MΩ, 560 kΩ, 300 kΩ, and 100 kΩ. In (B) the following resistors were used: 10 MΩ, 7 MΩ, 5 MΩ, 2 MΩ, 1 MΩ and 560 kΩ. BPVs n=3 ±1SE.

MEA-BPV	***C. vulgaris* (Day 4)**	***C. vulgaris* (Day 10)**	**PCC7942 (Day 4)**	**PCC7942 (Day 10)**
OCP [mV]	285.0±11.6	241.3±15.1	301.0±14.0	216±3.3
P_{out} [µW m^{-2}]	27.2±3.0	7.2±1.0	38.1±10.4	10.4±2.6
R_{int} [MΩ]	3.2±0.2	5.3±0.3	3.1±0.8	1.8±0.4
pH (light, Day 11)	-	6.73±0.04	-	9.4±0.2

Table 3-8. Parameters obtained from the polarisation of MEA-BPV devices at Day 4 (fresh biofilms) and at Day 10 (after six days under load) fostering *C. vulgaris* biofilms or PCC7942 biofilms on plasma treated carbon paper in the anode assembled with nitrocellulose and an air cathode. P_{out} corresponds to the highest power recorded. R_{int} was estimated from the slope of the linear segment of the polarisation curve. *C. vulgaris* BPV CP-PT n=3 ±1SE; PCC7942 BPV CP-PT n=3 ±1SE.

At Day 4, a similar OCP (285.0±11.6 mV) and the same R_{int} (3.2±0.2 MΩ) than the values obtained for PCC7942 (301.0±14.0 mV and 3.1±0.8 MΩ) resulted in similar power output. However, differently to PCC7942 MEAs, the R_{int} of *C. vulgaris* MEAs became higher at Day 10 (5.3±0.3 MΩ), while the drop in OCP was not as significant as for PCC7942. This indicates that in MEAs fostering *C. vulgaris* there was a hindered electrochemical interaction between the biofilm and the electrode, increasing ohmic losses associated to electron transfer. Figure 3-20 shows the SEM image of a biofilm of *C. vulgaris* on carbon paper, exhibiting an evidently less dense biofilm than those of PCC7942 (Figure 3-10), thus demonstrating loose attachment.

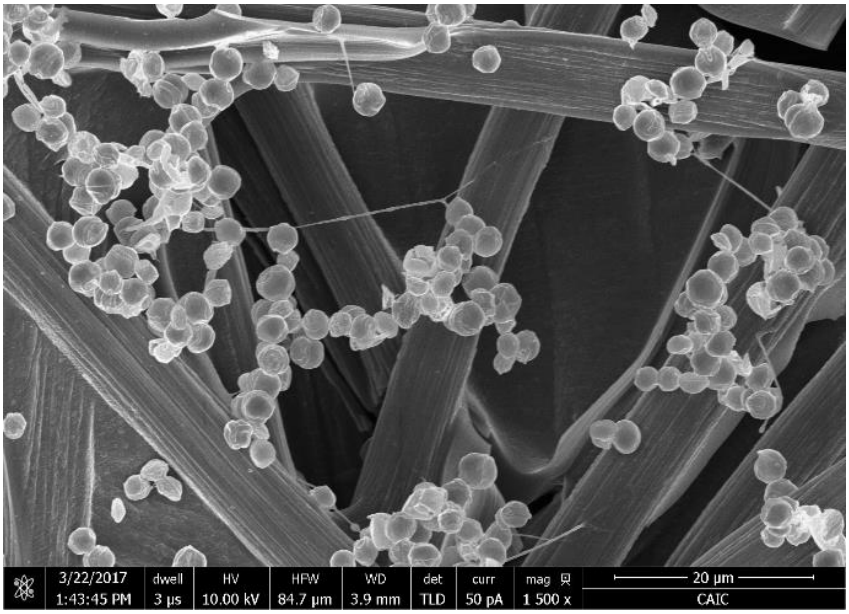

Figure 3-20. SEM image of a biofilm of *C. vulgaris* on carbon paper. Image obtained as described in Chapter 2 – Section 2.10.

MEA-BPVs fostering *C. vulgaris* did not show a significant activation loss, with a polarisation curve tending to a linear curve, which was seen at both Day 4 and Day 10 (Figure 3-19). The reactivity of *C. vulgaris* biofilms is consistent with a more exoelectrogenic microorganism, indicating that there is an electroactive mechanism in the plasma membrane ready to react, but as discussed, possibly ohmic losses due to cell wall insulation hindered *C. vulgaris* photo-biocatalysis.

The light/dark pattern of currents by *C. vulgaris* showed a positive light response (Figure 3-21), although the increase in currents upon illumination was smaller than those seen in PCC7942 (Figure 3-14), correlating to the similar ferricyanide reduction capacity in the light and in the dark. Likewise, power generation (currents) reported in previous studies using *C. vulgaris* biofilms in mediatorless

platforms were lower in the dark than in the light, but always showing relatively high dark performance.[14,92]

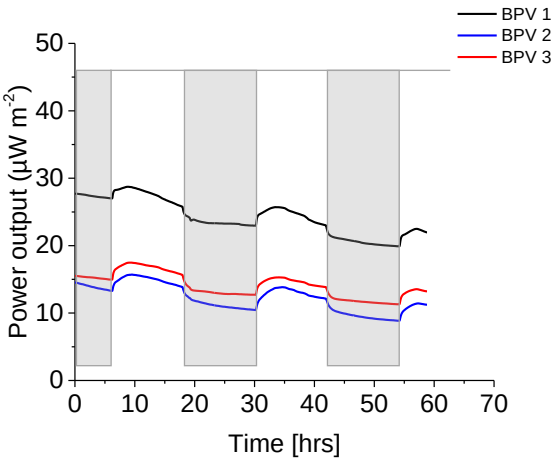

Figure 3-21. Power output profile in a 12 hour light/dark cycle for nitrocellulose-MEA-BPV devices fostering *C. vulgaris* on plasma treated carbon paper in the anode and an air cathode.

3.3.4 Mediatorless photo-MFC fostering co-cultures of PCC7942

To investigate the capability of the co-cultures to generate electricity in mediatorless systems, MEA-photo-MFCs assembled with carbon paper (non-treated), nitrocellulose membrane and an air cathode. In Figure 3-22, bacteria in PCC7942 co-cultures are observed.

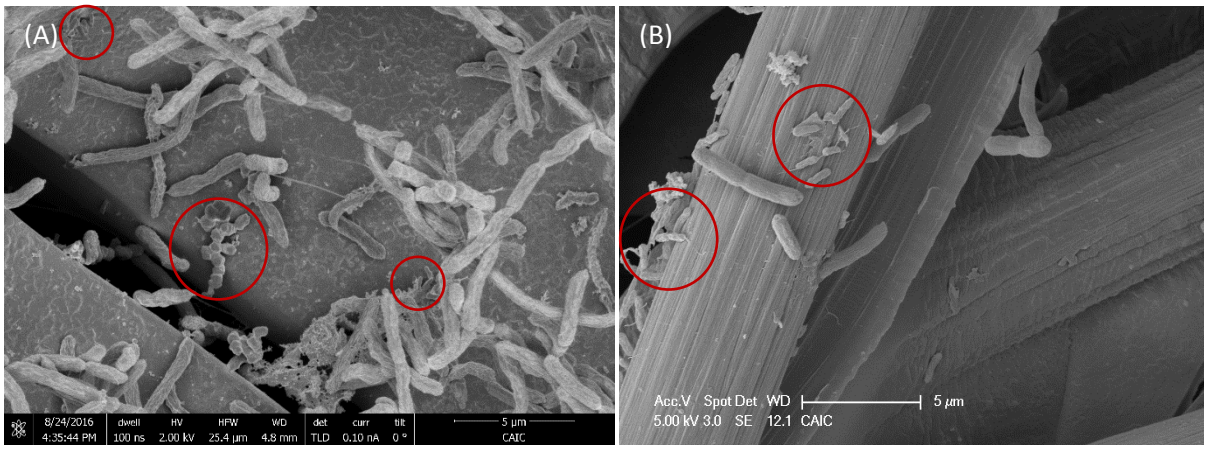

Figure 3-22. SEM images of co-cultures of PCC7942. (A) co-culture A and (B) co-culture B. Red circles outline bacteria presence. Images obtained as described in Chapter 2 – Section 2.10.

Figure 3-23 presents the polarisation and power curve for both MEA-photo-MFCs fostering co-culture A and B. Table 3-9 summarises the parameters determined for each system as well as for axenic PCC7942. Non-treated carbon paper was chosen because in the long term the treatment was ineffective in MEAs inoculated with PCC7942, also present in the co-cultures.

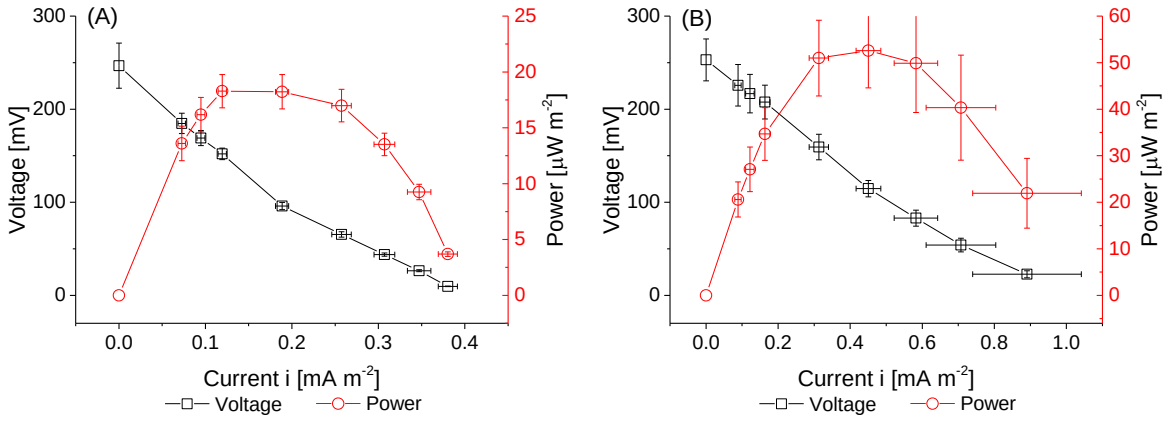

Figure 3-23. Polarisation (black) and power curve (red) obtained from MEA-photo-MFC devices fostering (A) co-culture A and (B) co-culture B biofilms on bare carbon paper in the anode assembled with nitrocellulose and an air cathode. In (A) and (B) the following resistors were used: 10 MΩ, 7 MΩ, 5 MΩ, 2 MΩ, 1 MΩ, 560 kΩ, 300 kΩ, and 100 kΩ. Co-culture A n=3 ±1SE; co-culture B n=3 ±1SE.

MEA-photo-MFC	Co-culture A	Co-culture B	PCC7942 (Day 4)
OCP [mV]	246.8±24.3	253.0±22.5	298±7.0
P_{out} [µW m^{-2}]	18.3±1.4	58.6±11.2	16.3±2.5
R_{int} [MΩ]	~2.0*	1.1±0.3	5.0±0.9

Table 3-9. Parameters obtained from the polarisation of MEA-photo-MFC devices at Day 4 (fresh biofilms) fostering co-culture A and co-culture B biofilms or PCC7942 biofilms on bare carbon paper in the anode assembled with nitrocellulose and an air cathode. P_{out} corresponds to the highest power recorded. R_{int} were estimated from the slope of the linear segment of the polarisation curve. *Not determined due to non-linear polarisation, however the highest power was recorded at 2 MΩ. Co-culture A photo-MFC n=4 ±1SE; co-culture B photo-MFC n=3 ±1SE; PCC7942 BPV n=4 ±1SE.

Results obtained for the mediatorless photo-MFC platforms demonstrated the same pattern than that of the ferricyanide assay. Biofilms from co-culture A showed a similar electrocatalytic response to that of axenic PCC7942, while biofilms formed from co-culture B could generate 3.6-fold higher power outputs, correlating to a higher exoelectrogenic capacity. Furthermore, polarisation curves reveal that MEAs fostering co-culture B showed no significant activation losses, demonstrating good electrochemical reactivity; while a first region of activation loss controlled both MEAs fostering axenic PCC7942 and co-culture A.

MEAs inoculated with co-culture B showed a lower R_{int} (1.1±0.3 MΩ), while co-culture A MEAs also were lower than the axenic biofilms (~2 MΩ). The values are still higher if compared to MFCs because of poor electrolyte conductivity, carbon paper hydrophobicity and possibly to a poor electrochemical interaction between the biofilm and the electrode. Nonetheless, R_{int} in photo-MFC inoculated with co-culture B was lower than R_{int} from all the previous BPV devices, even those with plasma treated carbon materials. This result demonstrates that the high R_{int} in these platforms has an important component related to the resistivity of electron transfer within the biofilm and the electrode. Furthermore, FeCN-R rates of co-culture B were similar to that obtained for *C. vulgaris*, but co-culture B biofilms produced higher power output, demonstrating that the bacterium in co-culture B had a better electrochemical interaction with the electrode.

The capability of direct power generation with time in a 12 hour light/dark cycle is presented in Figure 3-24. Co-culture A shows similarities to axenic cultures in the early response to an external load, with a positive light response. However, by the second period there was a difference in the initial response, instead of dropping, power outputs in the dark increased very rapidly only to then drop steeply. While in the light, power first dropped and then increased. The light/dark pattern from co-culture A shows an overlapping between the response of the axenic culture and the heterotrophic bacteria, as changes in pH and oxygen availability could alter exoelectrogenic activity of the heterotrophic bacteria within the biofilm.[73,84] A negative light response was clear for co-culture B, with power increasing in the dark and showing independence from photosynthetic activity. Higher power in the dark became more noticeable with time, twice as much the power initially recorded. The negative light response in photo-MFC has been reported and correlated to photosynthetic oxygen evolution inhibiting the exoelectrogenic bacteria.[73,84]

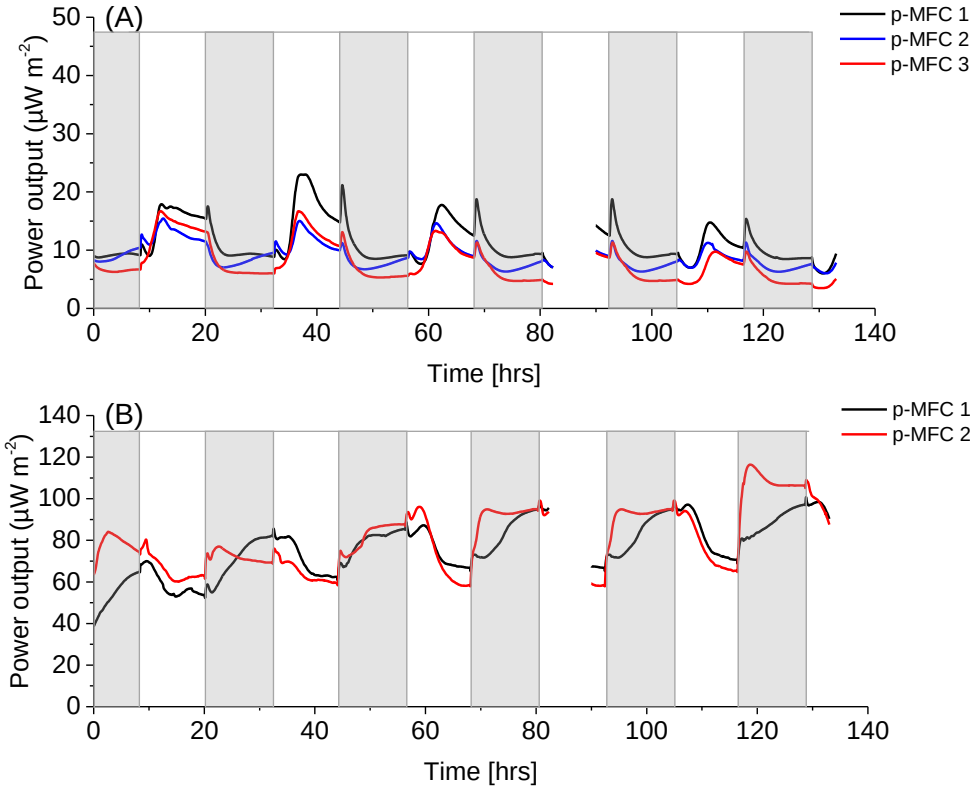

Figure 3-24. Power output profile in a 12 hour light/dark cycle for MEA-photo-MFC devices fostering PCC7942 co-cultures on carbon paper in the anode assembled with nitrocellulose and an air cathode. (A) co-culture A and (B) co-culture B. Recording was stopped and started again (gap).

This study has demonstrated that sterile conditions are necessary in order to truly evaluate the exoelectrogenic capacity of a given cyanobacterium, in mediatorless but particularly in mediated platforms. Some reports show poor care in maintaining sterile conditions.

As seen in Figure 3-24, depending on the length in light after a period of darkness or in dark after illumination, mediatorless devices could be wrongly found to have a light positive response. Therefore, if a given BPV is not continuously monitored, the presence of bacteria could be neglected. Nonetheless, in the systems studied, differences in power outputs and R_{int} were not large and the resulting performance could be affected by the cellular activity of the inoculated culture, the effective biomass density settled on the electrode, the aeration, to name a few. Therefore, the light/dark pattern is the main feature to verify the axenicity condition. Albeit, in field application non-sterile conditions occur and growth of bacterial species will be present and it will be beneficial for power generation.

The strategy of combining photosynthetic systems with heterotrophic bacteria as mixed consortia has been explored in photo-MFCs.[75,96] An attempt on constructing a co-culture of wild-type PCC7942 and *S. oneidensis* was not successful. Recently a co-culture with the cyanobacterium *Synechocystis sp.* PCC6803 and *S. oneidensis* was reported to increase current density seventy times in a micro-size photo-MFC platform, when compared to the same platform inoculated only with cyanobacteria.[168]

In this study, without selecting a specific heterotrophic bacterium, a 14-fold increase in light driven exoelectrogenesis and 3.6-fold increase in power generation were obtained. As previously described, Sekar *et al.*[99] genetically modified PCC7942 achieving a 2-fold increase in FeCN-R rates (in the light) and 9-fold increase in current generation (8 minutes measurement) in a mediatorless system. By comparing Sekar *et al.*[99] work involving the transformation of PCC7942 with the outer membrane cytochrome OmcS and co-culture B, it is demonstrated that in cyanobacteria the low exoelectrogenic activity is not limited only by the final point of electron export, but is also due to a low intracellular redirection of electrons to the extracellular side. To genetically modify cyanobacteria with a complete exoelectrogenic pathway is a challenging task, which has been made possible with *E. coli* harbouring the extracellular respiratory pathway cymA – MtrCAB from *S. oneidensis*, but it took over a decade of research and engineering to achieve a strain capable of expressing the entire extracellular respiratory pathway with its native functions.[93] Mixed consortia of photosynthetic and heterotrophic bacteria are abundant in nature, but constructed co-cultures in laboratory conditions are less successful to thrive. PCC7942 has been engineered to secrete sugars in order to sustain heterotrophic bacterial growth in constructed co-cultures,[169,170] offering a possible alternative for photo-MFC applications. In any case, restrictions are imposed in using genetically modified microorganisms in open field applications.

3.3.5 Benchmark outcomes

The evaluation of PCC7942 as an exoelectrogen has shown that there is a hindered extracellular electron transfer in comparison to other photosynthetic cultures. Although the reduction of ferricyanide does not necessarily translate into higher performance in mediatorless platform. Ferricyanide accesses the membranes in the cell envelope with ease (Figure 2-7), therefore it is a good indication of the first step in the generation of an electrical current in BPV devices. The biological limitation of PCC7942 as an exoelectrogen is an essential aspect to overcome. Strategies to enhance exoelectrogenesis in wild-type cyanobacteria are imperative. Table 3-10 summarises the outcomes of the second stage of the benchmark.

	Axenic PCC7942	*Chlorella vulgaris*	Co-cultures of PCC7942
Ferricyanide reduction rates	Control	Large improvement.	Large improvement.
Mediatorless device performance	Control	No difference	Higher than axenic devices.
Long term performance	OCP value decreases.	R_{int} increases.	Power output increases.

Table 3-10. Benchmark outcomes from the comparison of PCC7942 exoelectrogenic capacity against other photosynthetic systems.

3.4 Conclusions

In this chapter, to understand the exoelectrogenic capacity of PCC7942 (wild-type) within a physical and biological context, a multi-platform study was constructed in order to compare PCC7942 performance against other exoelectrogenic systems, including a well known exoelectrogen and other photosynthetic cultures. The development of more efficient bioelectrochemical cells, fabricated with inexpensive materials, was also targeted as a strategy to improve the sustainability of photo-bioelectricity generation.

The exoelectrogenic capacity of PCC7942 to generate photo-bioelectricity was evaluated in a benchmark study, evaluating the ability to interact electrochemically with three electrodes: ITO-coated glass, carbon felt and carbon paper; and two electrode arrangements: single chamber (ITO-coated glass) and MEA (carbon materials). Expectedly, BPVs fostering PCC7942 were greatly outperformed by MFCs inoculated with *S. oneidensis* in all platforms, despite a non-optimal operation of the MFCs. Nonetheless, PCC7942 showed the ability to perform in mediatorless platforms.

Acidity in the electrolyte (media) has major repercussions in the performance of the electrochemical cell. While it is positive for the cathodic reaction, it inactivates alkaliphile cyanobacteria. MEAs assembled with Nafion® were counterproductive for BPVs due to excessive acidification. However, it was proven that Nafion® reduced the R_{int} of MEAs, delivering a more efficient electrochemical cell. Alternatively, the non-acidic membrane nitrocellulose was used in MEAs. These platforms presented lower efficiency but were compatible with cyanobacterial biofilms.

Improving wettability of carbon materials by adding oxygen groups proved to work in reducing R_{int}, but in the long term treated electrodes were outperformed. Non-treated carbon materials are better anode for PCC7942, but imposes higher R_{int}. Although, in the long term R_{int} tended to decrease.

The microalgae *C. vulgaris* is a better candidate as exoelectrogen than PCC7942, which is primordial for power generation, although to exploit *C. vulgaris* mediators are needed.

Co-cultures of photosynthetic microorganisms and heterotrophic bacteria serve as a strategy to improve photo-bioelectricity generation. However, although power outputs were higher for co-cultures, these values were still minimal in comparison to MFCs (*S. oneidensis* MR-1) fed with rich organic media. In a co-culture, the photosynthetic microorganism represents the limiting factor as bacteria rely entirely in the extrusion of useful organic compounds, which is limited. Co-cultures occur naturally, therefore in field applications it is almost certain that bacteria will be present. The latter is beneficial as demonstrated in this study. However, for the success in the development of photo-bioelectricity, the photosynthetic microorganism should become the main electron donor as it is the densest within the culture. Genetic engineering has been used to improve PCC7942 exoelectrogenesis and also increase extrusion of organic compounds, however there are restriction in using genetic modified microorganisms in field applications, challenging investigative lines to enhance the exoelectrogenic activity in wild-type cyanobacteria.

Chapter 4 Exoelectrogenic capacity of *Synechococcus elongatus* PCC7942 under iron limited growth

4.1 Introduction

Strategies to increase the exoelectrogenic capacity of photosynthetic microorganisms are needed in order to further develop photo-bioelectricity generation as a viable technology. Synthetic biology has been used to increase extracellular electron export in cyanobacteria, including the transformation of PCC7942 with the outer membrane cytochrome OmcS.[99] However, improvement is still minor in relation to other exoelectrogenic systems, including photosynthetic microalgae (Figure 3-18). Further genetic transformations imply technical challenges.[93]

Iron limited growth and neutral pH have a positive effect on extracellular ferric reductase activity in microalgae and plants (a type of exoelectrogenesis), but it has not been described in cyanobacteria.

In this chapter, the study on the effect of iron limitation and pH over the exoelectrogenic activity of photosynthetic microorganisms is presented, with especial emphasis in an iron-deficiency-induced novel exoelectrogenic capacity found in *Synechococcus elongatus* PCC7942.

4.1.1 Iron requirements and bioavailability

Photosynthetic organisms have particularly high requirements of iron due to their extra photosynthetic machinery, with 22-23 iron atoms required for a completely functional photosynthetic apparatus (Table 4-1).[132,133] Furthermore, complexes and soluble carriers do not exist in the 1:1 molar ratio, therefore a minimal functional photosynthetic apparatus has an even greater iron requirement.[124]

Function associated to photosynthesis	Protein/Protein complex	Number of Fe atoms
Photosynthesis electron chain	PSII	2 – 3
	PSI	12
	Cytochrome b_6f	5
	Cytochrome c_6*	1
	Ferredoxin	2
Oxidative stress protection	Catalase	4
	Fe superoxide dismutase	1
	Ascorbate peroxidase	1
Cyclic electron transport	NAD(P)H/PQ oxidoreductase	8 – 18

Table 4-1. Iron content per protein or protein complex in the photosynthetic apparatus or associated to photosynthetic activity. *Cytochrome C_6 in many cyanobacteria and green microalgae can be alternated by copper-containing plastocyanin, while higher plants only have plastocyanin. Table adapted from Raven *et al.* (1999).[133]

Iron requirements are higher in cyanobacteria than those in eukaryotic microalgae.[171] The greater demand for iron in cyanobacteria is a genotypic trait related to a higher PSI/PSII ratio in the thylakoids, which can also change phenotypically in response to environmental changes,[133] as it was described in Table 1-2. Table 4-2 shows examples of PSI/PSII ratio in cyanobacteria and in microalgae grown in normal conditions.

	PSI/PSII (Fluorescence /77K Ratio)	Ref.
Cyanobacteria		
***Synechococcus elongatus* PCC7942**	1.3 – 1.5	172,173
Anabaena variabilis M3	2.6	172
Anabaena variabilis ATCC29413	2.4	172
Eukaryotic algae		
Chlorococcum littorale	0.6 – 0.8	130,174
Stichococcus bacillaris	0.8	174
Chlorella sp. UK001	1.5	130

Table 4-2. PSI/PSII ratio for various cyanobacteria and microalgae (eukaryotic) species. Growth conditions regarding air, light quantity and quality might change in the different referenced studies.

Iron is the fourth most abundant element in the earth crust, accounting for more than 4% of the total mass, existing mainly as iron oxide (Fe_2O_3).[175,176] Iron has three stable oxidation states: (0), (+2) and (+3), as elemental iron, ferrous and ferric respectively. In the system Fe-H_2O, iron is present mainly in a precipitated solid state (Figure 4-1). At pH of natural waters, ranging from pH 5 to pH 9.5, ferrous ions are soluble; but at the potential of aerated water (generally 0.35-0.5 V vs SHE),[177] ferrous is oxidised to insoluble ferric hydroxide ($Fe(OH)_3$). Ferric ions are soluble only at very acidic pH. The insolubility of iron complexes implies that iron bioavailability is restricted.

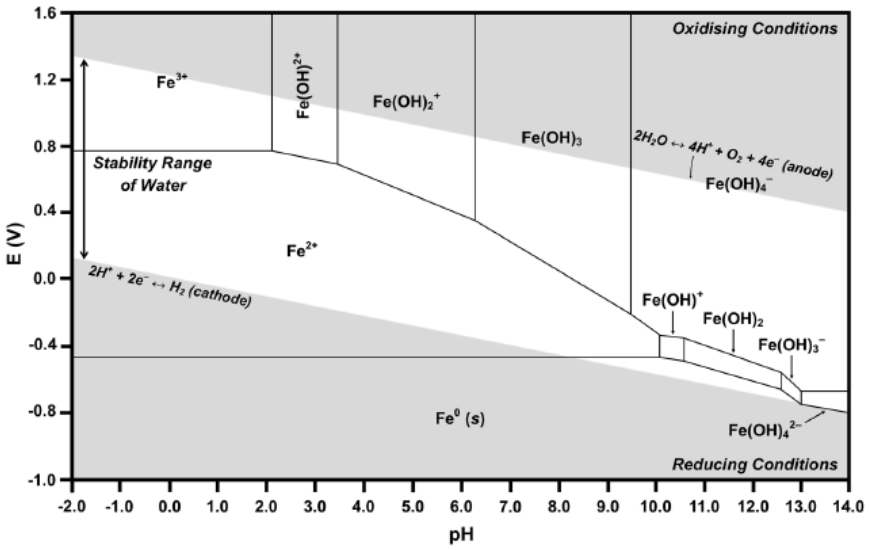

Figure 4-1. Pourbaix diagram for Fe-H_2O. Taken from Channei *et al.* 2017.[178]

4.1.2 Strategies for iron uptake in photosynthetic organisms

As a result of the low bioavailability of iron, photosynthetic organisms have evolved different responses to face the frequent exposure to iron scarcity. Two distinctive mechanisms have been identified in cellular iron assimilation (Figure 4-2), defined as Strategy I and Strategy II.

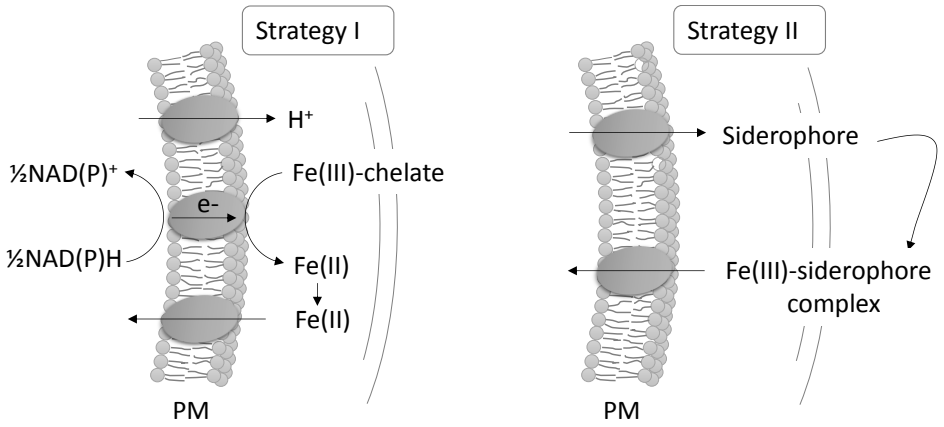

Figure 4-2. Iron uptake strategies in microalgae and cyanobacteria in the cell surface. Only in the case of cyanobacteria an outer membrane encapsulates the cell (gram-negative bacteria). Strategy I consists of a reduction in exogenous chelated ferric with the subsequent uptake of the more soluble ferrous. Proton extrusion commonly accompanies the reduction. Strategy II consists of a secretion in endogenous siderophore compounds, which chelates insoluble ferric with the subsequent uptake of the ferric-siderophore complex. Some microorganisms utilise both, strategy I and II. Strategy I involves the extracellular reduction of ferric, therefore it is a type of exoelectrogenic capacity.

As a strategy for iron uptake (Strategy I), ferric reductases (FREs) with a conserved transmembrane ferric reductase domain (FRD superfamily) are found in the plasma membrane of some eukaryotes (mammalian cells, yeast, algae and plants) and some bacteria.[150] FREs catalyse electron transfer from cytosolic NADPH to extracellular ferric, reducing it to the more soluble ferrous (Equation 4-1), which is then readily transported through high affinity ferrous transporters. Iron starvation upregulates the expression of FRE triggering higher ferric reductase activity and a higher iron uptake capacity.[113,114,179] The activity of FRE usually is accompanied by the secretion of protons and small compounds which are siderophores or natural redox mediators.[180]

$$NADPH + 2Fe^{+3} \xrightarrow{FRE} 2Fe^{+2} + H^{+}$$

Equation 4-1. Plasma membrane ferric reductase activity.

For many plant species, it has been reported that the optimal pH of ferric reductases in the plasma membrane is slightly acidic with values as low as pH 5.5.[181] Furthermore, ferric reductases are strongly inhibited in soils with high pH.[180] Likewise, ferric reductases in the algae *C. reinhardtii* have been reported to be optimal at pH 6.8 – 7.0,[182] and to acidify the media after reacting.[116]

Strategy II consists of siderophore secretion for ferric chelation, followed by the uptake of the soluble Fe(III)-siderophore complex trough specific ferric transporters in the plasma membrane (Figure 4-2). Iron starvation induces production of siderophores.[183–185]

Photosynthetic microorganisms might use Strategy I, Strategy II, or both. However, proteins with the conserved ferric reductase domain have not been annotated for cyanobacteria.[150] Therefore, traditionally the strategy accepted for iron uptake in cyanobacteria is Strategy II.

Many cyanobacteria do not produce siderophores, therefore reductive mechanisms are being investigated.[186] Evidence of a reductive iron uptake pathway has been described for several cyanobacteria, suggesting that a reductive mechanism could be common, functioning alone or in coordination with siderophore secretion (Figure 4-2).[134–136] Insight into a reductive iron acquisition mechanism described for the model cyanobacterium *Synechocystis sp.* PCC6803 revealed ferric reduction due to the action of the Alternate Respiratory Terminal Oxidase (ARTO) in the plasma membrane with the subsequent uptake of ferrous through a ferrous transporter (feoB).[186–188]

4.1.3 Extracellular O_2^- generation in photosynthetic microorganism and iron uptake

NADPH oxidases (NOX) in the plasma membrane are found in mammalian cells, plants, fungi and algae.[150] NOX catalyse electron transfer from cytosolic NADPH to reduce oxygen (O_2) generating short life extracellular superoxide (O_2^-), the primary reactive oxygen species (ROS), which then can react further to generate other ROS.

ROSs are generated as a by-product of aerobic metabolism causing oxidative stress. However, ROSs generated by NOX in the plasma membrane are associated to biological functions, participating in immunity, cell signalling, morphogenesis and development.[150]

NOX and FRE are homologous and belong to the same FRD superfamily with a reductase conserved domain.[150] Their common structural organisation is linked to a similar catalytic action, consisting in vertical electron transfer through the plasma membrane (Equation 4-2). NOX are not overexpressed under iron starvation.[189,190] Nonetheless, superoxide photo-reduces ferric ions (Equation 4-3) and its extracellular generation by microorganisms will contribute to iron solubilisation.[191]

$$NADPH + 2O_2 \xrightarrow{NOX} 2O_2^- + H^+$$

Equation 4-2. Plasma membrane NADPH oxidase activity.

$$O_2^- + Fe^{3+} \xrightarrow{Light} Fe^{2+} + O_2$$

Equation 4-3. Photo-reduction of ferric by superoxide.

With exception of one cyanobacterial strain (*Acaryochlorys marina* MBIC 11017), NOXs have not been annotated in cyanobacteria.[150] Nonetheless, generation of extracellular O_2^- by cyanobacteria has been accounted responsible for ferric reduction, as the superoxide dismutase enzyme inhibits the extracellular reaction.[192,193] Particularly, Manabu Fujil *et al.*[193] studied the cyanobacterium *Microcystis aeruginosa*, showing that ferric reduction rates by O_2^- were increased under the stress of iron limitation.

4.1.4 Iron starvation in PCC7942

PCC7942 has been broadly studied in iron starvation as a model cyanobacterium for the understanding of cyanobacteria iron homeostasis and metabolic changes when facing iron scarcity. PCC7942 particularly is a cyanobacterium with great endurance to iron starvation.[194]

Iron is a co-factor in many ROS-detoxifying enzymes (catalases, peroxidases and SOD), thus inevitably iron starvation leads to severe oxidative stress.[195] Furthermore, in PCC7942 there is a close relationship between iron homeostasis and oxidative stress, with major iron-deficiency-induced proteins also being induced by oxidative stress within minutes.[196] Therefore, the generation of intracellular ROS during iron starvation has been suggested to trigger the upregulation of iron-deficiency-induced proteins.

Nodop *et al.*[197] reported the transcript profiling of iron starved PCC7942. Changes in photosynthetic and respiratory transcripts were found. Additionally, the expression of iron regulated proteins, IsiABC and IdiABC, enables the adaptation of the photosynthetic electron transfer chain for PCC7942 to endure iron starvation.[195–199] The rapid adaptation of PCC7942 to iron starvation consists in the replacement of ferrodoxin (1 Fe) by flavodoxin (IsiB), the formation of a supercomplex antenna around PSI known as IsiA complex, and the protection of the electron acceptor side of PSII against oxidative damage by a protein denominated IdiA.[195]

PSI has a high iron demand (12 Fe) and consequently the amount of functional PSI decreases.[194] The PSI/PSII fluorescence ratio decreases accordingly and the photochemical efficiency of PSII is also reduced.[173] Lower photosynthetic linear electron flow, higher photosynthetic cyclic electron flow and increased respiratory activity in iron starved PCC7942 have been measured.[195]

Ivanov *et al.*[194] reported that despite the major changes in the photosynthetic machinery, PCC7942 is able to sustain relatively high photosynthetic rates in iron limited conditions. This is because of the capacity to partially uncouple PSII and PSI, with PSI cyclic electron transport generating ATP and with PSII photo-reducing $NADP^+$. NADPH is then available for CO_2 fixation and biomass growth is sustained. However, contrarily to other studies, Ivanov *et al.*[194] found that in iron starved PCC7942 cellular respiration rates were 50% lower than those in iron sufficient conditions. Respiratory changes in iron starved PCC7942 might vary according to the length of time it is exposed to iron starvation. In the long term, chlorophyll content and biomass growth will decline.[173] Furthermore, Sherman and Sherman[200] reported that even though after a period of iron deprivation doubling times were approximately the same in iron limited and iron sufficient cultures of PCC7942, iron limited cells were only one-half to two-thirds as long, which was detectable at the level of light microscopy.

Apart from changes in the photosynthetic electron chain, iron uptake capacity is upregulated by iron deficiency, with higher hydroxamate-type siderophores secretion and overexpression of ferric transporters.[124,183,197,201]

The proposed reductive mechanism by Kranzler *et al.* for *Synechocystis sp.* PCC6803, involving ARTO and feoB, is not possible in PCC7942.[186–188] Neither ARTO nor feoB homologies are found in PCC7942 genome.

A novel iron acquisition system in PCC7942 was proposed by Nodop *et al.*[197] as an increment in the transcripts of proteins in the cell envelope of iron starved cells was found, including a porin in the outer membrane SomB1, the operon IrpAB, with IrpA, a plasma membrane protein and IrpB, a c-type cytochrome, and ftr1, a high affinity Fe(II) uptake system, all regulated by the same transcriptional factor idiB. The latter indicates that possibly a reductive mechanism under iron starvation is activated.

Homologous proteins to IrpAB are not present in all cyanobacteria genomes.[197] While homologous of frt1 has been identified in other photosynthetic microorganisms in relation to iron uptake. For instance, in *Synechocystis sp.* PCC6803, frt1 was found to be essential for growth in iron starvation.[202] In *C. reinhardtii*, ftr1 was found to be expressed together with a ferrireductase in iron-deficient cells.[189]

4.1.5 Ferricyanide reduction activity in photosynthetic organisms

Ferricyanide reductase activity in photosynthetic organisms has been used to probe plasma membrane redox activity and nutrient acquisition, as well as to shuttle electrons from the cell surface to an electrode.

The reduction of ferricyanide has been well documented for plants and microalgae. In plant roots growing in iron deficient conditions, ferricyanide reductase activity increases, which has been associated to the overexpression of ferric reductases in the plasma membrane (strategy I).[115,181,203] Likewise, in microalgae ferric reductases can reduce ferricyanide, whose activity increases in iron starvation.[113] However, a constitutive ferricyanide reductase activity also exists, detected in plant tissues where ferric reductases are not expressed, whose metabolic function has not been yet determined.[115,181,203] Similarly, ferricyanide reductase activity in diatoms is constitutive and not related to iron uptake and it was found to be high relative to that in plants and microalgae.[204]

Ferricyanide reductase activity in algae and plants is accompanied by acidification of the extracellular media.[116,181,203,205] The vertical transfer of electrons through the plasma membrane causes

depolarization of the membrane, while protons and $NAD(P)^+$ accumulate in the nearby. H^+-ATPases in the plasma membrane then catalyse proton transfer providing charge compensation. K^+ efflux has also been associated to charge compensation.[203]

Cyanobacteria also have the capability to reduce ferricyanide, although ferricyanide reduction rates are considerably lower than those in other photosynthetic organisms (Figure 3-18). Nevertheless, ferricyanide has been successfully used to shuttle electrons from cyanobacteria to an electrode in biosensors and BPV devices.[13,206]

Strategies involving genetic engineering to increase exoelectrogenic capacity in cyanobacteria have been developed for two model cyanobacteria, in *Synechocysistis sp.* PCC6803 and as previously described, in PCC7942. Respiratory terminal oxidase (rto) mutants of *Synechocysistis sp.* PCC6803 were constructed in order to enhance exoelectrogenesis, showing increased ferricyanide reduction rates, in the light and in the dark, with electrons being diverted mainly from respiration.[47] Additionally, *Synechocysistis sp.* PCC6803 was found to increase ferricyanide reduction rates when grown in high salt (0.25 M NaCl), with high salt having a greater effect in rto mutants.[100] In PCC7942, genetic engineering transformation with the outer membrane cytochrome OmcS increased its ability to reduce ferricyanide in relation to the wild-type.[99]

The use of photosynthetic inhibitors has demonstrated direct participation of reducing power (NADPH) from photosynthesis in the extracellular reduction of ferricyanide.[13,204] Ferricyanide reduction in iron limited *Chlamydomonas* cells, but not in iron sufficient cells, showed a 50% inhibition of CO_2 fixation at saturating irradiance and up to 100% at sub-saturating irradiance.[207] NADPH generated in the oxidative pentose phosphate pathway was also found to be the electron donor used in extracellular ferricyanide reduction.[116] Besides, reducing power (NADH) redirected from respiration to ferricyanide has been demonstrated.[47,115,207]

4.1.6 Objectives and proposed systems

Growing evidence on extracellular iron reductive mechanisms in cyanobacteria indicates the possible existence of extracellular electron transfer routes. In microalgae and plants reductive mechanisms exist and are optimal in a range around neutral pH. In cyanobacteria, the optimal pH for reductive mechanisms has not been established.

In this chapter, photosynthetic systems exposed to iron limited growth are presented, with emphasis on PCC7942, with the objective of investigating the effect of iron limitation on cyanobacterial extracellular electron transfer.

Ferricyanide reduction rates (FeCN-R rates) were calculated as a measure of the exoelectrogenic capacity and the cultural pH favouring the reaction was investigated. In order to establish possible metabolic activity associated to exoelectrogenic activity, photosynthesis inhibition, proton extrusion and extracellular superoxide generation were also investigated.

Ferricyanide mediated BPV devices conditioned by iron availability and pH were implemented to demonstrate enhanced photo-bioelectricity generation by PCC7942. The effect of iron limited growth in mediatorless BPV devices was also evaluated.

4.2 PCC7942 exoelectrogenic capacity in iron limited conditions

The exoelectrogenic capacity detected in cyanobacteria is not well understood. In an effort to unveil possible conditions enhancing cyanobacterial exoelectrogenesis, PCC7942 was studied in iron limited conditions.

4.2.1 PCC7942 cultures characterisation in iron limitation

Iron limited cultures were prepared as described in Chapter 2 – Section 2.3. Iron sufficient cultures were also prepared as the control. Cultures were initiated at an initial OD_{750} of 0.5.

PCC7942 iron limited cultures did not exhibit a lower growth rate than that of iron sufficient cultures throughout the two weeks of study (Figure 4-3), besides no effect on the chlorophyll content was observed, suggesting that iron limitation did not slow down the cell viability. Furthermore, oxygen evolution from iron limited cultures was similar to that from iron sufficient cultures in two weeks old samples, with photosynthetic rates and respiration rates resulting no significantly different (Figure 4-3).

Figure 4-3. (A) Growth curve of PCC7942 in iron limited and iron sufficient conditions at 30 °C and 120 rpm, under light intensity of 90 µmol m^{-2} s^{-2} in a 12 hour light/dark cycle. (B) Photosynthetic and respiration rates at Day 14 of cultures of PCC7942 in iron limited and iron sufficient conditions as oxygen evolution in the light (photosynthesis) and in dark immediately after (respiration). (n=3 ±1SE).

PCC7942 is a fast growing cyanobacterium when grown in optimal conditions.[208] In this investigation, culturing conditions are like those encountered in BPV applications, which is a regime of light/dark cycle under atmospheric air. A temperature of 30 °C was chosen as a compromise between room temperature (20 °C) and optimal growth temperature (38 °C). These conditions meant low growth rate, with doubling times of 4 days between days 2 – 8, which was lowered in later days to 6.7 days (Figure 4-3 (A)). Photosynthetic rates and respiration rates, as oxygen evolution, (Figure 4-3 (B)) were accordingly low, with photosynthetic oxygen evolution only 372±21.1 pmol $nmol_{Chl}^{-1}$ min^{-1} versus approximately 5200 pmol $nmol_{Chl}^{-1}$ min^{-1} previously reported for maximum photosynthetic oxygen evolution in PCC7942 at 38 °C (converted from 0.35 $mmolO_2$ mg_{Chl}^{-1} h^{-1}).[194] Nevertheless, BPV platforms ought to operate with minimal energy inputs, impeding to provide better conditions for growth.

Figure 4-4 shows microscope images of iron limited and iron sufficient cultures (15 days old), with no obvious difference in cell size, contrarily to what was seen by Sherman and Sherman,[200] in which cells in iron limited growth were two-third smaller in average. pH and DO measurement also showed similarity (Figure 4-5).

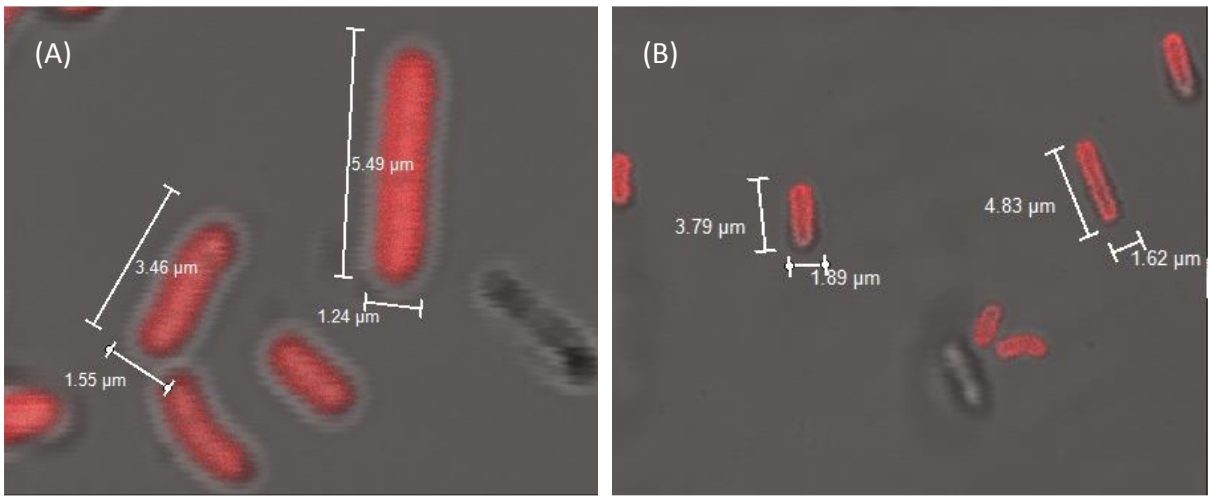

Figure 4-4. Confocal microscope images of (A) iron limited and (B) iron sufficient cells (PCC7942) after 15 days of culturing. Images obtained as described in Chapter 2 – Section 2.11.

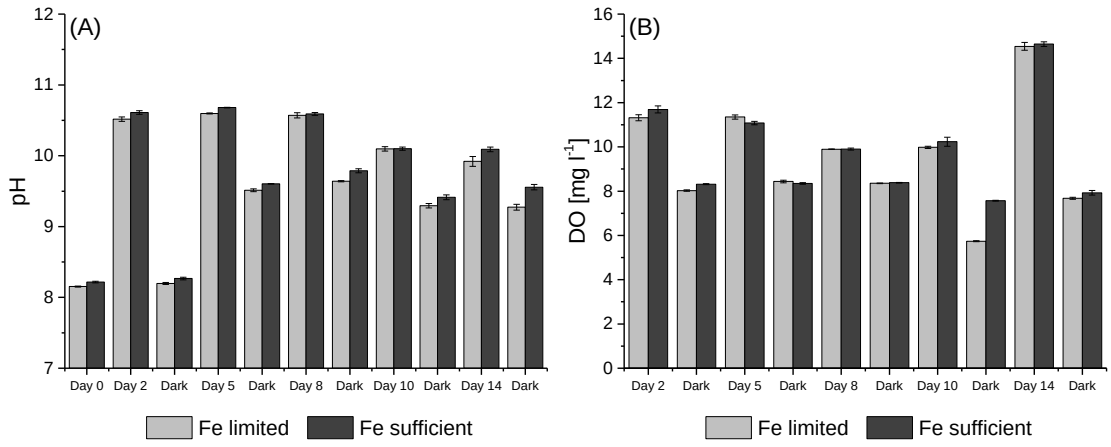

Figure 4-5. pH and dissolved oxygen (DO) in PCC7942 cultures conditioned by iron availability. Biomass density varies according to Figure 4-3.

The endurance of PCC7942 in iron limitation can be the result of the modification of the photosystems as previously reported, especially the overexpressed IsiA can support PSI activity and IdiA can actively protect PSII.[194,195] However, iron limitation for 2-4 days is the time frame for most studies, with cultures showing the symptoms of iron starvation.[194,196,197,209] Cultures in the current study were growing at a slower rate than those in the published studies, which could explain the dissagrement found regarding iron limited culture characterisation, in terms of growth rate, chlorophyll content, cell size and photosynthetic activity.

4.2.2 Ferricyanide reduction capacity: exoelectrogenesis

To investigate possible pathways of extracellular electron transfer in PCC7942 for applications in photo-bioelectricity generation, the relationship between iron limited growth and extracellular reductive capacity was evaluated.

4.2.2.1 PCC7942 exoelectrogenesis under prolonged iron limitation

Iron limited PCC7942 cultures were studied over a period of 14 days. Cultures were prepared with initial OD_{750} at 0.5, as described in Chapter 2 – Section 2.3. At days 2, 5, 8, 11 and 14 samples were collected and analysed for ferricyanide reduction (FeCN-R) rates. A control set of iron sufficient cultures was also studied at days 2 and 14. The ferricyanide assay was conducted in the light and in the dark as described in Chapter 2 – Section 2.6. As seen in Figure 4-6, the FeCN-R rates developed were remarkably different in the two conditions, especially after long exposure to iron starvation. Rates were measured at pH 7.0, because rates were found to be higher around neutral pH (Figure 4-7). Reduction of ferricyanide in BG11(-)x3 and in supernatants, from both iron limited and iron sufficient cultures, were also analysed and no significant reduction capacity was found (Appendix B).

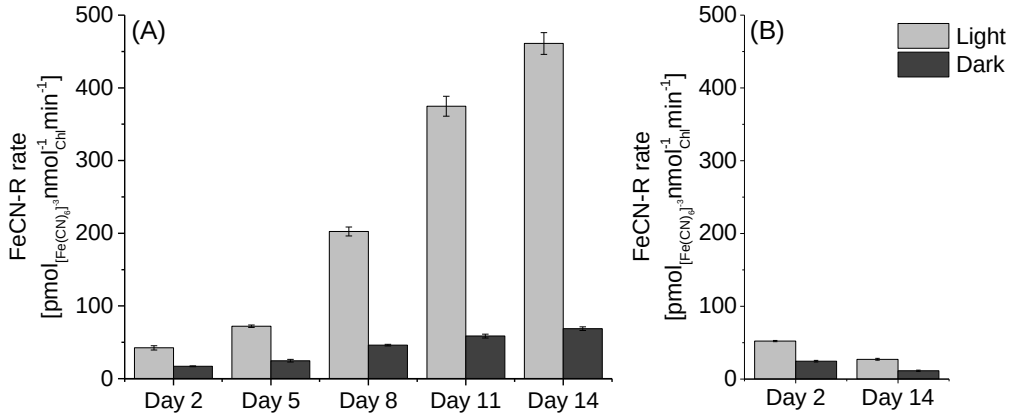

Figure 4-6. Ferricyanide reduction rates of PCC7942 (A) in iron limited conditions and (B) in iron sufficient conditions, for different days of culture growth. FeCN-R rate n=3±1SE.

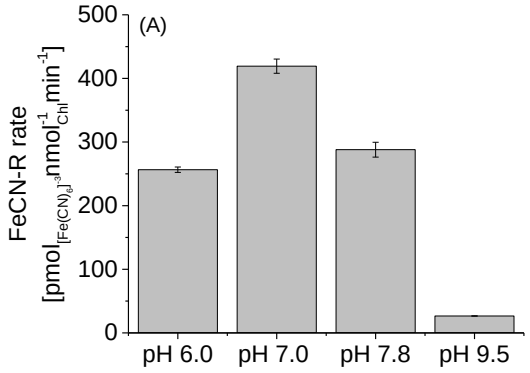

Figure 4-7. Ferricyanide reductase activity of iron limited PCC7942 cultures (14 days old) at different pH. FeCN-R rate n=3±1SE.

The reduction rates of iron limited cultures in light (90µmol m^{-2} s^{-1}) increased with time, from around 45 $pmol_{([Fe(CN)_6]^{3-})}$ $nmol_{Chl}^{-1}$ min^{-1} (Day 2) to 460 $pmol_{([Fe(CN)_6]^{3-})}$ $nmol_{Chl}^{-1}$ min^{-1} (Day 14), a 10-fold increase, and equivalent to a 17-fold increase compared with the rates of iron sufficient cultures (Day 14). However, if compared to the control set, iron sufficient PCC7942 in alkaline media as reported in Figure 3-18, there is an increase of 2.7-fold for iron sufficient cells at neutral pH and 24-fold increase for iron limited cells. The latter shows the influence of neutral pH in the reaction kinetics.

Oppositely, for iron sufficient cultures it was seen that young cultures (Day 2) developed higher FeCN-R rates than old cultures (Day 14), indicating that rates were also affected by the stage of growth, or cellular activity. As seen in Figure 4-3, growth rates tended to decrease in later days.

In the dark, FeCN-R rates were considerably lower than those in the light. However, it is noticeable that iron limited cultures also experimented an increase in dark exoelectrogenesis. After 14 days, iron limited cells developed FeCN-R rates in the dark six times higher than those of iron sufficient cells. Increased rates in the dark represent an important improvement for the development of BPV platforms which will be operated in daylight/night cycles.

The relatively high extracellular electron transport induced by iron limited growth, which has never been seen before in cyanobacteria, is possibly supported by a larger intracellular NAD(P)H pool due to a redox imbalance at cellular level caused by the lack of iron.

Due to the low growth rates experimented by the cultures (Section 4.2.1), showing no diminution in growth rate and chlorophyll content in PCC7942 cultures grown in iron limited conditions, the state of

iron starvation the cultures underwent is not clear. However, the study of protein composition in the outer membrane and the plasma membrane, presented in Appendix C, showed that cells grown in iron limitation overexpressed various proteins related to iron uptake, including irpA in the plasma membrane and SomB1 in the outer membrane, both experimenting a 2-fold increase. As described before in Section 4.1.4, these proteins are part of the set SomB1-IrpAB-ftr1, which were reported to increase under iron starvation and allegedly comprise a reductive iron acquisition system.[197]

IrpA is a plasma membrane protein located on the periplasmic side and IrpB is a c-type cytochrome with two CXXC heme-binding sites; these two proteins could be involved in the redirection of electrons to the cell surface or periplasmic space. While SomB1 (porin) and another more abundant porin (SomA2), which showed the largest overexpression, may lead to changes in the permeability of the outer membrane. The inherent permeability of porins to small hydrophilic molecules suggest that ferricyanide (only 0.2 kDa) should move freely in and out.[210] Therefore, the reaction could be happening in the outer membrane, in the periplasm or/and in the plasma membrane.

The high FeCN-R rates of iron limited PCC7942 found in the current experiments could be indirect evidence of this novel Fe(II) acquisition system. In the case of such reductive mechanism, a 2-fold overexpression is low compared to the increase in FeCN-R rates (17-fold increase within neutral pH measurements). The latter indicates that the redirection of intracellular reducing power to the extracellular pathway would also have to be upregulated upstream, hence enlarging substrate availability and in that way increasing the rate of reaction.

4.2.2.2 Ferricyanide reduction rates in the presence of photosynthesis inhibitor

To clarify what is the source of the electrons, in an independent study cells from 14 days old cultures were collected and the ferricyanide assay was conducted in three different conditions, light (90µmol $m^{-2} s^{-1}$), light with addition of DCMU (photosynthesis inhibitor) and darkness. Photosynthesis inhibition was conducted as described in Chapter 2 – Section 2.7. In Figure 4-8, it can be observed that for both iron starved cells and iron sufficient cells, light led to higher FeCN-R rates. For iron limited cells, FeCN-R rates exceed 400 $pmol_{([Fe(CN)_6]^{3-})}$ $nmol_{Chl}^{-1}$ min^{-1}. When DCMU was used to inhibit PSII activity, FeCN-R rates were strongly inhibited, demonstrating that in the light most of PCC7942 exoelectrogenesis activity is driven by the reducing power (NADPH) generated by photosynthesis.

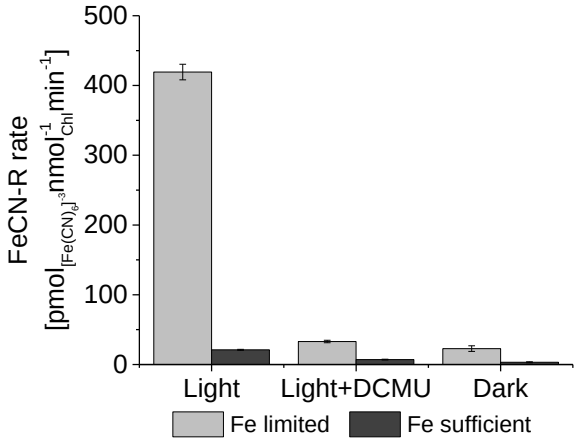

Figure 4-8. Ferricyanide reduction rates of iron limited cultures and iron sufficient cultures of PCC7942, in light, in light plus the photosynthesis inhibitor DCMU and in darkness. FeCN-R rate n=3±1SE.

Interestingly, rates in the presence of DCMU are similar to the rates in the dark, indicating that what drives extracellular reduction in the dark is also actively contributing to FeCN-R activity in the light. The respiratory pathway and the biosynthesis oxidative pentose phosphate pathway are other sources of intracellular reducing power, with generation of NADH and NADPH respectively, which can drive dark or light independent exoelectrogenesis. As was seen in Figure 4-8 iron limitation also induces higher rates in the dark, indicating that a higher reduced pool of NAD(P)H from these two pathways arises under iron limited growth.

The high FeCN-R rates obtained were dependent on photosynthesis as shown by the much lower rate in the presence of DCMU (Figure 4-8), implying that extracellular electron transfer is actively competing with CO_2 fixation. The low exoelectrogenic activity of photosynthetic microorganisms has been discussed and CO_2 fixation accounted as the main competitor for electrons.[45,47] By exposing PCC7942 cultures to iron limitation, exoelectrogenesis can favourably compete for reducing power. Electrons from photosynthesis redirected extracellularly to ferricyanide were reported to be approximately 0.3% in the cyanobacterium *Synechocysistis sp.* PCC6803 (wild-type).[47] In iron limited PCC7942, the estimated redirection of reducing power from photosynthesis to ferricyanide was up to 28%, and around 1% for the iron sufficient cells (Equation 4-4). These percentages are an estimation based on the average photosynthetic oxygen evolution (Figure 4-3 (B)), determined for PCC7942 at Day 14, and after subtraction of FeCN-R rates in the dark. It should be noted that these percentages were achieved at neutral pH, which proved to favour higher rates.

$$2\boldsymbol{H_2O} \xrightarrow{\boldsymbol{Light}} 4\boldsymbol{H^+} + \boldsymbol{O_2} + 4\boldsymbol{e^-} \xrightarrow{2\boldsymbol{NADP^+};\, 2\boldsymbol{H^+}} 2\boldsymbol{NADPH} \begin{array}{l} \downarrow \\ \text{1\%} \\ \downarrow \\ \text{28\%} \end{array} \xrightarrow{\boldsymbol{CO_2}} \frac{1}{6}\boldsymbol{C_6H_{12}O_6}$$

$$4[\boldsymbol{Fe}(\boldsymbol{CN})_6]^{3-} \rightarrow 4[\boldsymbol{Fe}(\boldsymbol{CN})_6]^{4-}$$

Equation 4-4. Photo-biocatalysis in electron transfer from water to extracellular ferricyanide by PCC7942. Iron limited cells present an enhanced redirection of electrons (red arrow) over iron sufficient cells (black arrow) at neutral pH. Estimated percentages are calculated after subtraction of rates in the dark. Ferrocyanide can be reoxidised in the anode of an electrochemical cell for generation of photo-bioelectricity.

4.2.2.3 Effect of pH and acidification in relation to PCC7942 exoelectrogenesis

As mentioned before, it was found that neutral pH is the best condition for higher FeCN-R rates (Figure 4-7). The neutral pH is normally not favourable for cyanobacterial growth, therefore it could be working as another stressing condition as at lower pH the availability of HCO_3^- decreases, limiting RuBisCO activity.[211]

Proteins with a ferric reductase domain have not been described for cyanobacteria.[150] However, the pH-dependence of the FeCN-R activity detected in PCC7942 is like that of ferric reductases in plants and algae, with optimal pH of ferric reductases in the plasma membrane with values as low as pH 5.5[181] and inhibited at high pH.[180–182,205,212] Regulated paths which operate optimally at a more acidic pH as a strategy for iron uptake is likely due to the fact that lower pH favours the solubility of ferrous, the product of ferric reductase activity.[177]

Another feature related to ferric reductases and ferricyanide reductases is proton extrusion.[116,181,203,205] However, other cations can be extruded instead.[203] PCC7942 FeCN-R activity showed acidification in an unbuffered media (Figure 4-9). The evolution of pH in unbuffered cultures of PCC7942 exposed to ferricyanide in iron limited and iron sufficient conditions show that in the light and at alkaline pH there was no significant change, as the dark phase initiated, pH dropped in both conditions due to absence of photosynthetic activity. In the subsequent illumination stage, the conditions of neutral pH and photosynthetic activity co-existed for high FeCN-R rates to proceed. It is observed that pH in the iron limited culture steeply decreased, while in the iron sufficient culture pH increased to then slightly decrease and stabilised, still in alkaline values.

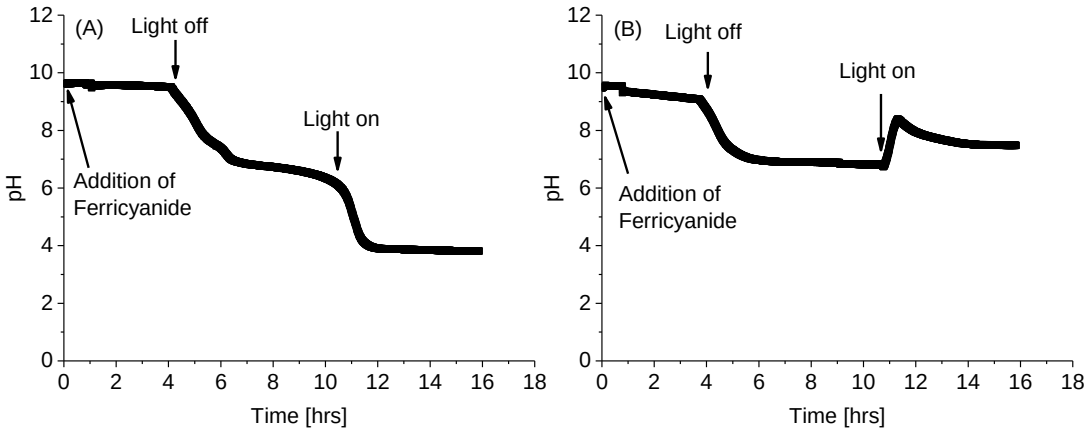

Figure 4-9. pH evolution of PCC7942 cultures in unbuffered media exposed to 1 mM of ferricyanide (A) in iron limitation and (B) in iron sufficiency.

The evolutions of pH for these cultures indicate that parallel to the extracellular reductive reaction, there is extrusion of protons, which results in acidification of the media. Proton extrusion is not caused by the presence of ferricyanide alone, but it is likely related to extracellular electron transport due to polarisation of the plasma membrane and charge compensation. Acidic pH is detrimental for cell activity. Therefore, for long term applications buffers will be necessary.

The conditions found for PCC7942 are also favourable for air cathode performance, due to oxygen reduction potential being higher at lower pH.[213] The acidification of the media (electrolyte) by PCC7942 also can contribute to eliminate, or at least reduce, buffer requirements. However, it is important to mention that intercepting this flow of electrons, for instance to generate electrical current in a BPV platform, could imply that the continuous loss of reducing power might not be sustainable for the viability of PCC7942 in the long term.

4.2.2.4 Ferricyanide reduction rates in the presence of superoxide dismutase

Superoxide (O_2^-) extracellular generation as an endogenous electron shuttle reducing ferric has been documented in cyanobacteria.[192,193] Furthermore, in microalgae and diatoms, extracellular O_2^- generation has been correlated with electricity generation in ferricyanide mediated BPV platforms.[48,111] In order to investigate if the detected FeCN-R capacity of PCC7942 is related to a mechanism involving extracellular superoxide generation, PCC7942 cultures were tested with XTT as described in Chapter 2 – Section 2.9, at pH 7.0 and pH 9.5.

The amount of superoxide detected was minimal (Figure 4-10). However, higher values were achieved by iron limited cultures at both neutral pH and alkaline pH. A higher generation of O_2^- by iron limited cultures can be explained by the cell undergoing oxidative stress, with decreased endogenous metal dependent SOD.[133] Blanks of XTT in BG11(-)x3 were also conducted (Appendix B).

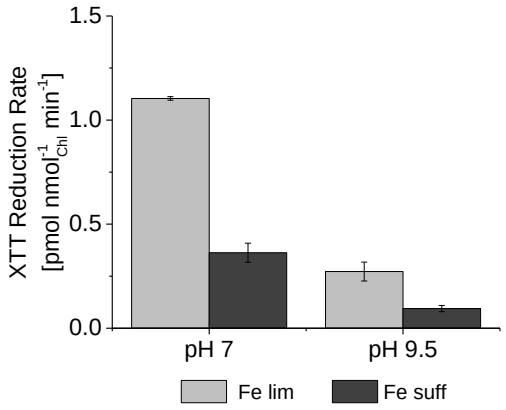

Figure 4-10. XTT reduction rates by iron limited and iron sufficient cultures at neutral and alkaline pH. XTT-R rate n=2±1SE.

In parallel, the ferricyanide assay was conducted in the presence of SOD as described in Chapter 2 – Section 2.9. The pH range of SOD activity is 7.6 – 10.5; therefore, measurements were conducted in buffered media with pH 7.8 and iron limited cultures were used. Figure 4-11 shows that iron limited cultures were not affected in their capacity to reduce ferricyanide in comparison to SOD free cultures, confirming that superoxide ions do not drive the FeCN-R reaction.

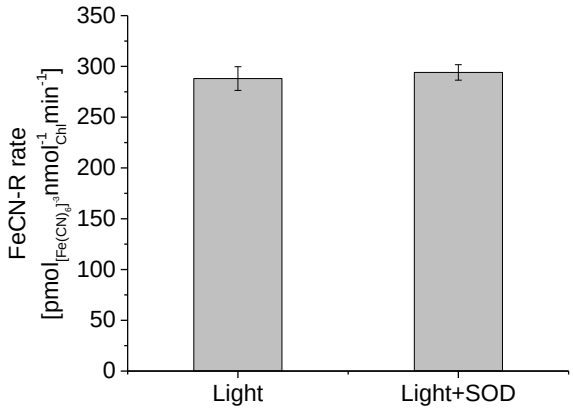

Figure 4-11. Ferricyanide conversion kinetics in time by iron limited cultures at pH 7.8 in the presence of superoxide dismutase SOD. FeCN-R rate n=2±1SE.

4.2.2.5 Comparative analysis of PCC7942 exoelectrogenic capacity

Light driven FeCN-R rates of 460 $pmol_{([Fe(CN)6]^{3-})}$ $nmol_{Chl}^{-1}$ min^{-1} is unprecedented for cyanobacteria (Table 4-3). In *Synechocystis sp.* 6803 deletion of all respiratory terminal oxidases (rto) results in the rate of 45 $pmol_{([Fe(CN)6]^{3-})}nmol_{Chl}^{-1}$ min^{-1}.[47] Therefore, an intracellular redox imbalance due to blockage of terminal oxidases due to lack of iron is unlikely the cause of the high rates obtained in iron limited PCC7942, which achieved rates 10 times higher than those of *Synechocystis sp.* 6803 rto mutants. In high salt, PCC6803 achieved a reduction rate of 50 $pmol_{([Fe(CN)6]^{3-})}nmol_{Chl}^{-1}$ min^{-1}, while rto mutants in high salt achieved the relatively high rate of 135 $pmol_{([Fe(CN)6]^{3-})}nmol_{Chl}^{-1}$ min^{-1},[100] still less than a third of that achieved by the synergistic effect of neutral pH and iron limitation in wild-type PCC7942. FeCN-R rates obtained for iron sufficient PCC7942 at neutral pH, especially with young cultures, are similar to those achieved by *Synechocystis sp.* PCC6803 rto mutant and to the rates induced by high salt in wild-type *Synechocystis sp.* PCC6803. This demonstrates that the effect of neutral pH alone resulted in rates as high as those achieved by other strategies.

Ferricyanide reduction rate in the light						
Ref.	**Microorganism**	**$pmol_{[Fe(CN)6]^{3-}}$ $nmol_{Chl}^{-1}$ min^{-1}**	**$\mu mol_{[Fe(CN)6]^{3-}}$ mg_{Chl}^{-1} h^{-1}**	**Fold change in respect to control**	**Modification/ Conditioning**	**Light Intensity $\mu mol\ m^{-2}\ s^{-1}$**
[47]	*Synechocystis* PCC6803	45		3.2-fold	rto mutant	40 (red)
[100]	*Synechocystis* PCC6803	50		3-fold	High salt	200 (white)
[100]	*Synechocystis* PCC6803	135		8-fold	rto mutant + High salt	200 (white)
[99]	*S.elongatus* PCC7942	35		2-fold	Genetically engineered (OmcS)	80 (white)
[116]	*C.reinhardtii*		130	10-fold	Iron starved	200 (white)
This study	*C.vulgaris*		30.3±0.8	2.2-fold	Iron starved	90 (white)
This study	*Co-culture B**	219.2±11.2		11-fold	Non-axenic	90 (white)
This study	PCC7942	52.3±0.9		2.7-fold	Neutral pH	90 (white)
This study	PCC7942	461±15.0	31±1.0	24-fold	Iron starved + Neutral pH	90 (white)

Table 4-3. Induced ferricyanide reductase activity in photosynthetic microorganisms. Rates are presented in two equivalent units in order to compare with reported values and within microalgae and cyanobacteria. All studies were conducted at 30 °C except *C. reinhardtii* which was conducted at 20 °C. *Co-culture B corresponding to PCC7942 plus a single bacterium as presented and characterised in Chapter 3. The control for FeCN-R rates in PCC7942, including co-culture B, is iron sufficient cultures at alkaline pH.

Respiratory terminal oxidase mutants showed similar rates in the light and in the dark, meaning that in high salt *Synechocystis sp.* PCC6803 rto mutants reached rates in the dark around 130 $pmol_{([Fe(CN)6]^{3-})}nmol_{Chl}^{-1}$ min^{-1}.[100] In the dark, the FeCN-R rates measured for iron limited PCC7942 were

high as well, reaching 70 $pmol_{([Fe(CN)_6]^{3-})}$ $nmol_{Chl}^{-1}$ min^{-1}, also a significant improvement and not far from the previous value reported, but it is in the light where the major contribution was made. The latter shows how the strategies are based in different and parallel approaches. While rto mutants inhibit respiration, diverting reducing power mainly from respiration, iron limitation resulted in diversion of reducing power directly from photosynthesis.

In Chapter 3, high rates were obtained by co-culture B fostering heterotrophic bacteria, which was attributed to an indirect way to redirect electrons from photosynthetic activity. Remarkably, rates developed by iron limited cells doubled the rates of co-culture B, indicating that the bacteria present in the co-culture is not highly exoelectrogenic. However, bacterial density is limited by the productivity of the photosynthetic microorganism. Therefore, as previously stressed, conditions inducing enhanced exoelectrogenic capacity in cyanobacteria is a major improvement in the development of photo-bioelectricity generated by cyanobacteria.

The outer membrane cytochrome OmcS has been proved to reduce Fe(III) oxides,[143] and when it was introduced into PCC7942, it was demonstrated to also reduce ferricyanide. In the PCC7942 strain harbouring the OmcS, FeCN-R rates were improved to 35 $pmol_{([Fe(CN)_6]^{3-})}nmol_{Chl}^{-1}$ min^{-1}, only 2 times higher than the rates for the wild-type.[99] The latter indicates that in addition to the introduced outer membrane c-type cytochrome, in cyanobacteria there is a constitutional mechanism redirecting electrons to the outer membrane, which was available for the cytochrome to react. Under normal conditions, this activity is low, but under stress conditions, such as neutral pH and especially in iron starvation, this reductive mechanism is enhanced. Iron limited PCC7942 (wild-type) achieved rates over 13 times higher than PCC7942 harbouring OmcS (non-stress condition), therefore the sole incorporation of cytochromes in the outer membrane is not sufficient to achieve rates like those in iron limitation.

In relation to FeCN-R activity in microalgae, which are known to possess ferric reductases in the cell surface, higher values have been reported for *C. reinhardtii*.[116] Nonetheless, light intensities and spectrum (colour) differ in the different studies, implying that rates in the light might be not entirely comparable. For instance, *C. reinhardtii* was tested under 200 µmol m^{-2} s^{-1} (white light), more than twice in this study. In order to compare to microalgae in the same conditions, as part of this investigation *C. vulgaris* was evaluated under the same conditions of growth than PCC7942, finding that FeCN-R activity for iron limited cells was similar. More details about the response obtained in *C. vulgaris* under iron limitation is presented later in Section 4.3.

One significant difference in microalgae is the constitutive nature of their extracellular reductase activity, meaning that iron sufficient cells still have a relatively high activity. For instance, for *C. reinhardtii* was reported to be 13.1±1.2 $\mu mol_{([Fe(CN)6]^{3-})}\ mg_{Chl}^{-1}\ h^{-1}$ and for *C. vulgaris* was measured to be 16.0±1.1 $\mu mol_{([Fe(CN)6]^{3-})}\ mg_{Chl}^{-1}\ h^{-1}$, while for PCC7942 iron sufficient cells it was only 1.4±0.1 $\mu mol_{([Fe(CN)6]^{3-})}\ mg_{Chl}^{-1}\ h^{-1}$. This basal reductase capacity in microalgae might not be related only to ferric reductases, but also could be due to plasma membrane NADPH oxidase activity. Nonetheless, PCC7942 presented the highest increase in respect to the control (iron sufficient condition), reaching FeCN-R rates which are comparable to those in microalgae. Iron limited PCC7942 under higher light intensity could prove further improvement.

Recently, PCC7942 has been described as a potential candidate for biodiesel feedstock thanks to its lipid composition, primary fatty acids are C16 – C18, which is suitable for good quality biodiesel.[214] Unsaturated fatty acids in PCC7942, particularly C18:1, have been reported to increase under iron starvation.[209] Therefore, iron starvation could serve as a strategy for an integrated system with biomass growth for biodiesel production coupled to photo-bioelectricity generation.

4.3 The response of other photosynthetic microorganisms to iron starvation

Microalgae are microorganisms which have been characterised in iron starvation studies and iron uptake has been described as an extracellular reductive mechanism.[114,116] As previously discussed, this exoelectrogenic metabolic activity may be related to the generation of electricity in microalgae base BPV platforms.

Exoelectrogenesis by means of FeCN-R rates in *C. vulgaris* is presented in Figure 4-12. As expected, iron limited cultures developed higher reductase activity, which was noticeable after five days of culturing. In terms of growth (Figure 4-13), both conditions present the same rate, although iron limited biomass started declining at Day 8. Chlorophyll content dropped at Day 5 and at Day 8 was considerably lower. A higher chlorophyll content in iron sufficient cultures did not confer higher extracellular reduction rates. *C. vulgaris* endurance to iron starvation is similar to that of other microalgae.[113]

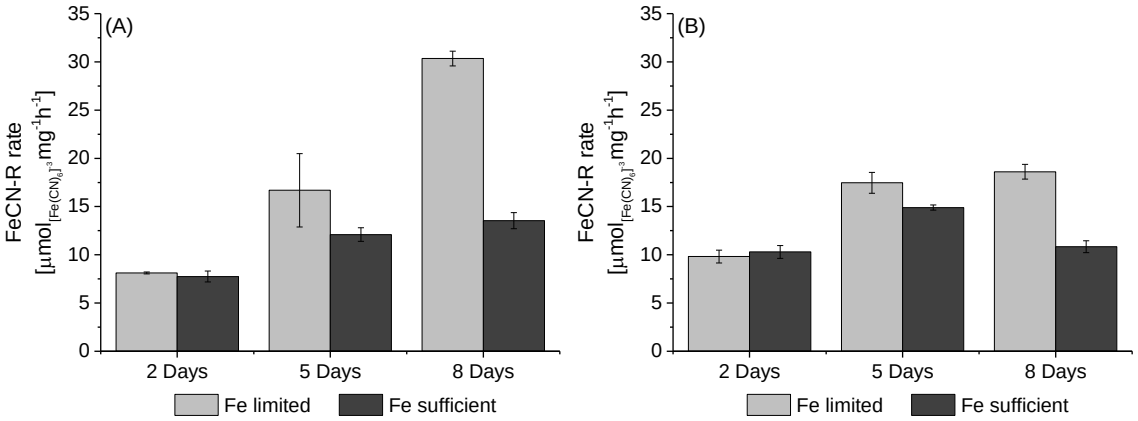

Figure 4-12. Ferricyanide reduction rates of *C. vulgaris* cultures conditioned by iron availability (A) in the light and (B) in darkness. FeCN-R rate n=3±1SE.

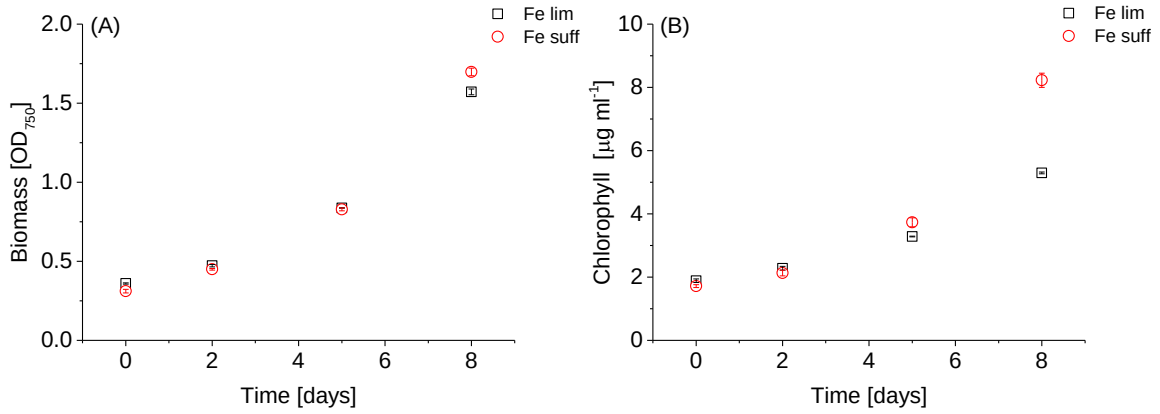

Figure 4-13. (A) Growth curve and (B) chlorophyll content of *C. vulgaris* cultures in iron sufficient and iron limited condition at 30 °C and 120 rpm, under light intensity of 90 µmol m^{-2} s^{-2} in a 12 hour light/dark cycle. BM and Chl n=3 ±1SE.

FeCN-R activity of iron sufficient *C. vulgaris* in the dark developed the same rates than those in the light, while in iron limitation, rates in the dark were lower than in the light, indicating that photosynthesis is delivering the extra reducing power. Higher ferric reductase rates in the light have been reported for other microalgae.[116]

Cyanobacteria on the contrary are less characterised in terms of their ability to reduce extracellular ferricyanide. PCC7942 has an extracellular reductive mechanism induced by iron deficiency, as shown in this chapter.

Synechocystis sp. PCC6803 was a candidate to study in iron limitation. However, in a preliminary study, it was demonstrated that *Synechocystis sp.* PCC6803 lacks endurance to iron limited conditions (Table 4-4). After just 3 days, biomass growth dropped considerably and even though chlorophyll content was still at a normal level, the pH of the iron limited culture was not alkalinised as normally occurs in iron sufficient cultures, indicating a depressed photosynthetic activity. The detrimental effect of iron deprivation was evident. The investigation of conditioning *Synechocystis sp.* PCC6803 by iron starvation was not pursued.

	Day 0		**Day 3**	
	Fe(+)	Fe(-)	Fe(+)	Fe(-)
Biomass OD_{750}	0.634	0.610	0.945	0.783
Chlorophyll *a* [nmol ml^{-1}]	3.30	3.26	5.22	4.52
pH	7.1	7.1	10.5	7.32

Table 4-4. Short term growth characteristics of *Synechocystis sp.* PCC6803 in iron limited conditions.

Cyanobacteria are an extensive phylum and a common mechanism is unlikely, but screening for other cyanobacteria strains with iron-deficiency-induced exoelectrogenesis, ideally marine cyanobacteria, is a way forward. A thermophilic strain of the species *Synechococcus elongatus* was reported to increase ferric-EDTA reduction rates in iron starvation (3 days), rates were very low if compared to the FeCN-R rates, but there was a 10-fold increment.[135] Therefore, the trait could be common among the species.

Throughout the current study, PCC7942 has proven to be a photosynthetic microorganism with particularly high endurance to iron scarcity.

4.4 Photo-bioelectricity generation by iron limited PCC7942

Higher exoelectrogenic capacity in iron limited PCC7942 translated to higher photo-bioelectricity generation. Ferricyanide mediated BPVs and mediatorless BPVs were studied in order to obtain further insight in the effect of iron starvation in PCC7942 exoelectrogenesis.

4.4.1 Single chamber BPV: ferricyanide mediated

Ferricyanide mediated BPV devices were studied as a first approach on exploiting the enhanced exoelectrogenesis of iron limited PCC7942. Single chamber BPVs, fabricated and operated as

described in Chapter 2 – Sections 2.5.1 and 2.5.4. ITO-coated glass used in the anode of the single chamber devices has been used in different BPV studies using ferricyanide as the mediator, which enables to some extent, to evaluate the performance of PCC7942 against similar systems.

Devices were inoculated with iron limited or iron sufficient cultures (17 days old), each condition buffered at pH 7.0 and non-buffered (alkaline). Figure 4-14 shows the power obtained in ferricyanide mediated BPVs.

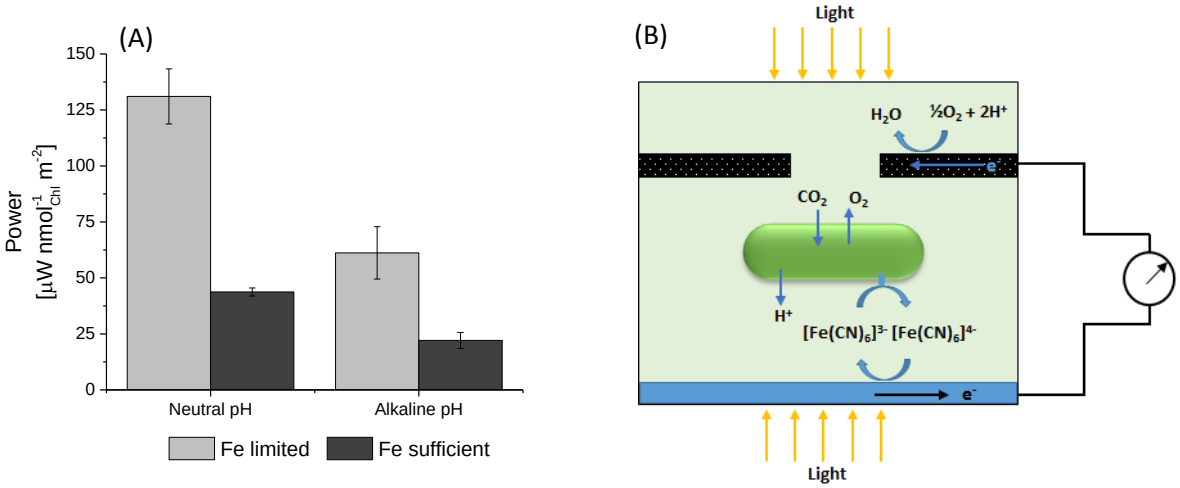

Figure 4-14. (A) Power output obtained in ferricyanide mediated single chamber biophotovoltaics conditioned by iron availability and pH. Initial pH of Fe limited samples at 6.98 and 9.34 and of Fe sufficient samples at 6.94 and 9.50. PCC7942 cultures were resuspended on BG11(-)x3 at OD_{750} equal to 4. A volume of 1.5 ml culture was added to each device. A layer of culture fully covered the cathode. Ferricyanide was added to a concentration of 1 mM. Devices were tested with the following external load: 560 kΩ, 33 kΩ, 10 kΩ, 4.6 kΩ and 1 kΩ. The highest power measured was with 4.6 kΩ. Power n=4 ±1SE. (B) Schematics of electrochemical reactions within the device.

Higher power was generated at a neutral pH for both iron limited and iron sufficient cultures. Moreover, at alkaline pH, iron sufficient cells developed very low currents with the highest power measured of only 22.1±3.6 µW $nmol_{Chl}^{-1}$ m^{-2} compared to 43.7±1.8 µW $nmol_{Chl}^{-1}$ m^{-2}, 2-fold higher, at neutral pH. The latter is a significant improvement in the performance of the system, demonstrating the positive impact of lower pH values on the performance of the BPV device. However, power generated by iron limited cultures was considerably higher, with 131.0±12.3 µW $nmol_{Chl}^{-1}$ m^{-2} at neutral pH and 61.2±11.7 µW $nmol_{Chl}^{-1}$ m^{-2} at alkaline pH. This confirms that iron limitation provides a more exoelectrogenic system which is useful in photo-bioelectricity generation. Overall, providing the right conditions, a 6-fold increase in power generation was achieved.

The ferricyanide assay shows a major improvement which is lessened in the BPV platform. The lack of agitation and lower light intensity could be hindering power generation. Besides, ferrocyanide crossover to the cathode could be inducing overpotential losses. Nonetheless, the power output generated by iron limited PCC7942 in ferricyanide mediated BPV is considerably higher than previous values reported for *Synechocystis* PCC6803 in similar systems (Table 4-5).[13,47] Furthermore, Anderson *et al.*[48] reported electrical current generated by the microalgae *C.reinhardtii* reaching values in the order of 600 µA mg_{Chl}^{-1}, while iron limited PCC7942 reached an electrical current of 522.9±24.4 µA mg_{Chl}^{-1}, demonstrating once again, that the exoelectrogenic capacity gained by PCC7942 is comparable to that of microalgae.

		Bioenergy Generation						
Ref.	**Microorganism**	**nW $nmol_{Chl}^{-1}$**	**µW $nmol_{Chl}^{-1}$ m^{-2}**	**µA mg_{Chl}^{-1}**	**Ferricyanide Concentration**	**Temperature**	**Agitation**	**Light Intensity**
[13]	*Synechocystis* PCC6803	9.28±0.92			5 mM	23°C	No	50 (red) W m^{-2}
[13]	*Synechocystis* PCC6803	16.4±0.6			30 mM	23°C	No	50 (red) W m^{-2}
[47]	*Synechocystis PCC6803*		2.33±0.84		1 mM	21°C	Yes	40 (red) µmol m^{-2} s^{-1}
[48]	*C.reinhardtii*			603	1 mM	21°C	Yes	100 (red) µmol m^{-2} s^{-1}
This study	Iron limited PCC7942	33.3±3.1	131.0±12.3	522.9±24.4	1 mM	30°C	No	70 (white) µmol m^{-2} s^{-1}

Table 4-5. Bioenergy generation for different photosynthetic microorganisms in ferricyanide mediated BPV platforms. Values are presented in different units in order to compare with reported values.

4.4.2 Nitrocellulose-MEA-BPV: mediatorless

The electrochemical measurements presented in Chapter 3 showed that PCC7942 biofilms are able to interact with electrodes without the need of artificial redox mediators. It is important to note that the ferricyanide assay does not distinguish the point of electron export and evidence from electroactive biofilms in mediatorless devices indicate that there is exoelectrogenic activity at outer membrane level.

To further investigate iron limited PCC7942, electricity generation in a mediatorless BPV platform was studied. To allow a long term study of PCC7942 biofilms, the nitrocellulose-MEA-BPV device was used, with carbon felt in the cathode (lower R_{int} in the long term). Devices were fabricated and operated as described in Chapter 2 – Sections 2.5.2 and 2.5.4. Devices were inoculated and left for 14 days before measuring power generation.

Table 4-6 summarised the results from the mediatorless BPVs evaluation. Power output from iron limited biofilms was of the same order in than light (62.0±7.1 µW m^{-2}) and in the dark (68.5±7.4 µW m^{-2}). Iron sufficient biofilms reached an average power of 52.0±0.7 µW m^{-2} in the light and 8.4±3.3 µW m^{-2} in the dark, 1.2-fold lower and 8.1-fold lower respectively. Minimal improvement was observed in the light phase, which is expectable as the system was not operating at neutral/acidic pH and the R_{int} was also higher for the iron limited biofilm.

	Light		**Dark**	
	Fe limited	Fe sufficient	Fe limited	Fe sufficient
OCP [mV]	283.5±1.8	241.0±19.1	*N.M.	*N.M.
R_{int} [MΩ]	2.0±0.2	1.1±0.1	1.3±0.1	1.3±0.1
P_{out} [µW m^{-2}]	62.0±7.1	52.0±0.7	68.5±7.4	8.4±3.3

Table 4-6. Operative values of mediatorless nitrocellulose-MEA-BPV devices fostering PCC7942 biofilms on carbon felt, in iron limitation and iron sufficiency. Devices were operated after two weeks of inoculation. Devices were tested with the following external load: 10 MΩ, 5 MΩ, 2 MΩ, 1 MΩ, 470 kΩ and 330 kΩ. P_{out} corresponds to the highest power measured. R_{int} was estimated from the slope of the linear segment of the polarisation curve. *Not measured. Data n=2±1SE.

In the light, iron limited MEA-BPVs showed higher R_{int}, while in iron sufficient MEA-BPV devices R_{int} were the same than in the light and in the dark. Iron limitation enhances dark exoelectrogenesis in PCC7942, while the lower R_{int} in the dark seen in iron limitation partially explains that dark currents were higher than light driven currents. Besides, pH tends to decrease in the dark phase, which also could contribute to lowering R_{int}. Furthermore, the iron sufficient medium (BG11) contains ferric citrate and ferric-EDTA complexes. Ferric complexes could be acting as mediators, reacting with the alleged redox complexes in the cell outer membrane and ferrous ions would be readily re-oxidised on the anode, interfering in the performance of the iron sufficient biofilm.

Figure 4-15 (A) shows the electrical current sustained by biofilms of PCC7942 for three days. These biofilms were in a non-buffered system (alkaline pH), therefore not optimal for the exoelectrogenic activity of PCC7942. However, buffering the system at neutral pH in the long term impacts cellular activity.

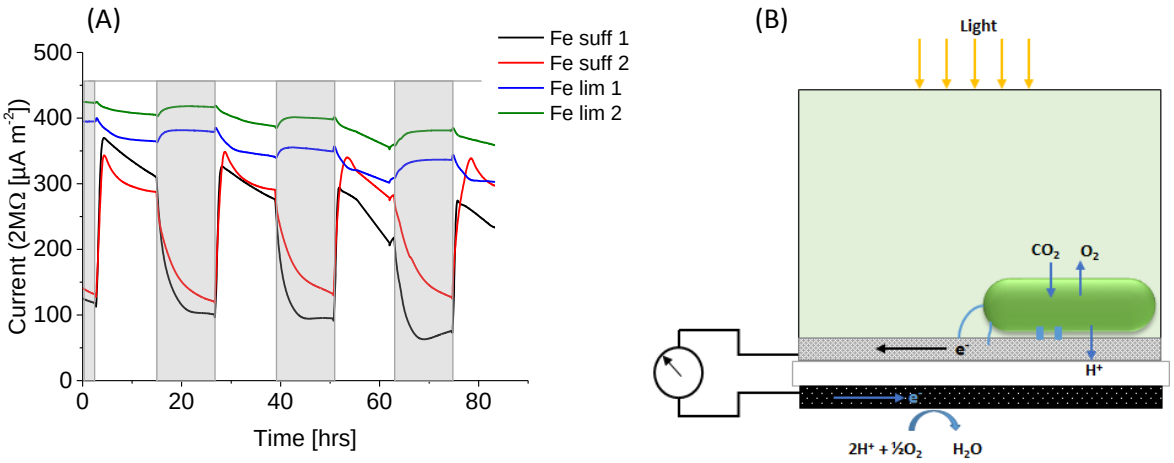

Figure 4-15. (A) Current profile in a 12 hour light/dark cycle for nitrocellulose-MEA-BPV devices fostering iron limited and iron sufficient PCC7942 biofilms on carbon felt in the anode (after 14 days of inoculation). Currents shown are through a 2 MΩ external load. (B) Schematics of electrochemical reactions within the device.

Though the system was not set at a neutral pH, it is clear that iron limited biofilms developed higher currents. Furthermore, it was during the dark phase that the benefit of operating with an iron limited system showed a major improvement, as currents did not drop as they did for iron sufficient biofilms. A positive light pattern was clearly seen in iron sufficient biofilms, the same as in Figure 3-13 and Figure 3-14 (Chapter 3).

The dark current in iron limited biofilms was slightly higher than in the light, opposite to the observation in the ferricyanide assay. The long term current profile indicates that iron limited PCC7942 cells adapted to decrease the redirection of reducing power to the extracellular, which would allow normal photosynthetic activity – CO_2 fixation rates.

Power outputs achieved by mediatorless BPVs are lower than those of mediated BPVs. Nonetheless, mediatorless electricity generation by PCC7942 induced by iron limitation has been demonstrated, indicating the existence of an iron-deficiency-induced reductive mechanism at outer membrane level. However, the analysis of outer membrane proteins presented in Appendix C, does not show proteins with conserved oxidoreductase domain. Further analytical protocols, will be necessary to identify the source of electrons in mediatorless systems.

Many factors can affect the mediatorless BPV performance, biomass density, length of biofilm settlement, electrode material, electrode size, pH, salinity, aeration, light penetration, to name the most important, as it was well established by Bombelli *et al.*[95] The scope of the current study was to

understand the reductive mechanism of PCC7942 in a mediatorless device and iron limited PCC7942 resulted to be a promising photo-biocatalyst, but more efficient BPV platforms will be necessary to obtain higher power outputs.

Iron starvation will eventually cause the cells to lose viability. Figure 4-16 shows the photograph of the inoculated devices after several weeks they were studied. It can be observed that iron limited cultures/biofilms bleached, while the iron sufficient condition remained green, implying cellular activity. To engineer the process in a way that iron limited cultures/biofilms remain active is a future challenge, which will require the study and optimisation of feeding iron at rates that keep the cells in an active exoelectrogenic state.

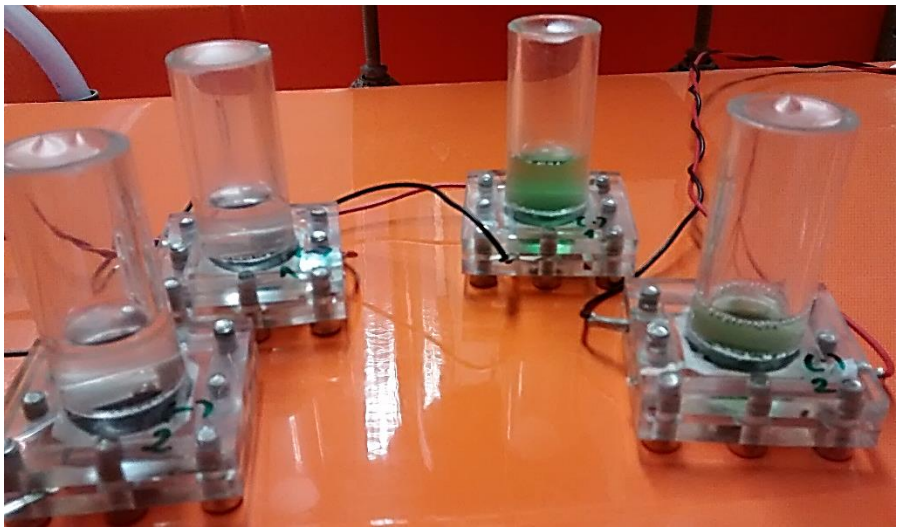

Figure 4-16. Photography of mediatorless MEA devices left for several weeks after characterised. Left: iron limited and Right: iron sufficient.

4.5 Conclusions

The present investigation has demonstrated high exoelectrogenesis capacity in the cyanobacterium *Synechococcus elongatus* PCC7942. Remarkably, PCC7942 grown in iron limited conditions acquires significantly higher reduction capacity of extracellular ferricyanide. Reduction rates are higher in the light and at neutral pH, with redirection of electrons directly from the light reactions of photosynthesis. Nevertheless, in the dark rates are also enhanced compared with the iron sufficient conditions, which is a significant improvement in a light-driven platform. The effect of lacking iron over the photosynthetic machinery and the respiratory oxidases may create a state of intracellular redox imbalance with larger pools of NAD(P)H, which is then available for extracellular reduction, but

mainly an iron-deficiency-induced mechanism is involved in redirecting electrons to extracellular redox species. Extracellular superoxide generation has been previously found to participate in the exoelectrogenic response of some microalgae and cyanobacteria, but this is not the case for PCC7942.

The response observed in the microalgae *C. vulgaris* to iron limited growth confirms what is known about reductive iron uptake mechanisms in microalgae. However, in cyanobacteria there were no reports in iron limitation enhancing their exoelectrogenic activity. By studying the response of the cyanobacterium *Synechocystis sp.* PCC6803 to iron limited conditions, which rapidly showed inhibited growth, it can be concluded that the enhanced exoelectrogenic capacity detected in iron limited PCC7942 is not a common response among cyanobacteria. Hence the lack of reported cases in the academic literature. Possibly the genes for the alternative iron acquisition system SomB1– irpAB – ftr1 together with the endurance of PCC7942 to iron limitation, confer to PCC7942 the desired exoelectrogenic capacity.

Iron limited PCC7942 exoelectrogenesis conveys good properties for the operation of biophotovoltaics in terms of a higher electron availability and in terms of the pH of the system, which positively impacts both the anodic and the cathodic potential. Biophotovoltaics operation conditioned by iron limitation demonstrates a way to externally manipulate the metabolism of cyanobacteria for electricity generation and provides a starting point to further engineer processes using cyanobacteria with constitutive high exoelectrogenic capacity.

Chapter 5 Synergistic effect of CO_2 and iron limitation in the exoelectrogenic capacity of *Synechococcus elongatus* PCC7942

5.1 Introduction

CO_2 neutral processes and CO_2 mitigation are imperative due to the increasing release of CO_2 to the atmosphere by human activity. Photosynthetic organisms have received special attention as a way to transform CO_2 into biomass.[215] Many biotechnological applications utilise photosynthetic microorganisms to produce a range of valuable products,[9] bioelectricity being one of them, while providing a CO_2 neutral process.

In this chapter, the influence of CO_2 partial pressure (pCO_2), as extremely high (20%CO_2) and high (5%CO_2), in the exoelectrogenic capacity of PCC7942 is presented. As described in Chapter 4, PCC7942 exoelectrogenesis is enhanced in iron limited conditions, therefore the synergy between iron limitation and CO_2 enrichment was studied. Increasing pCO_2 changes the cultural pH, therefore the effect of pH in PCC7942 growth and exoelectrogenic activity was also analysed. BPV operation under 20%CO_2 is demonstrated, proving that the utilisation of extremely high pCO_2 is compatible with photo-bioelectricity generation.

5.1.1 Oxygenic photosynthesis and atmospheric CO_2

Obligatory photosynthetic organisms face the challenge to survive with carbon dioxide (CO_2) as the only source of carbon for the biosynthesis of biomolecules (Equation 5-1). The ancient atmosphere was high in CO_2,[216] however due to the success of oxygenic photosynthetic microorganisms (cyanobacteria), a change in the gas equilibria occurred and the atmosphere composition decreased in CO_2 and increased in O_2 over geological timescales.[217] Oxygenic photosynthetic microorganisms had the evolutionary advantage to utilise water as electron donor in the photosynthetic process, but as a consequence, they had to adapt to live in CO_2 limiting conditions. The oxygen rich atmosphere allowed other types of life to thrive, and life emerged as we know it today.

$$6CO_2 + 6H_2O \xrightarrow{Light} C_6H_{12}O_6 + 6O_2$$

Equation 5-1. General equation of oxygenic photosynthesis for the autotrophic synthesis of carbohydrates (glucose).

Since the industrial revolution in the 1760's, a gradual raise in atmospheric CO_2 is occurring as a result of the release of large amounts of CO_2 from fossil fuels, increasing from approximately 277 ppm in 1750 to 400 ppm in today's atmosphere, with a marked increase in more recent decades (Figure 5-1).[1] This year (2017), the atmospheric CO_2 concentration reading at Mauna Loa Observatory (Hawaii) reached 410 ppm.[218]

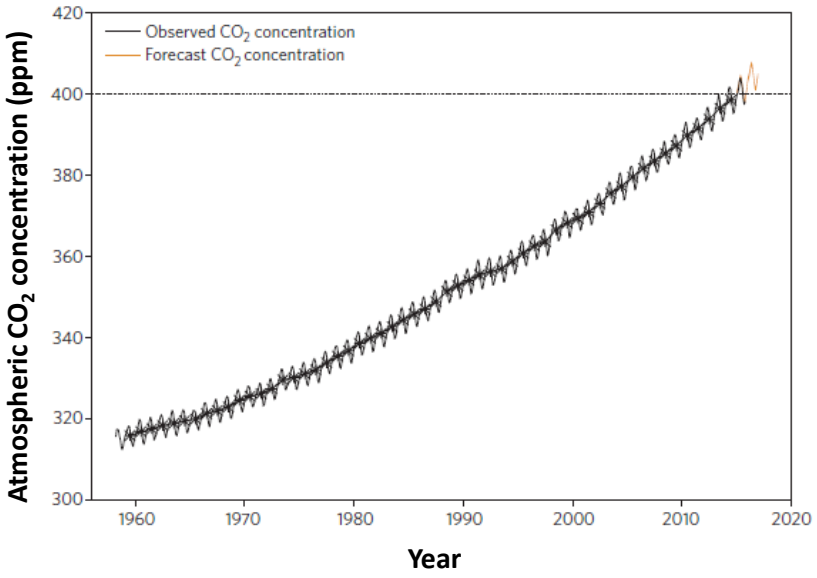

Figure 5-1. Atmospheric CO_2 concentration at Mauna Loa Observatory (Hawaii) over 1957 and 2016. Taken from Betts *et al.*[1] In 2017 atmospheric CO_2 concentration at Mauna Loa hit 410ppm.[218]

It has been demonstrated that a higher CO_2 content in air increases biomass growth in photosynthetic organisms, however this is not accompanied by higher nitrogen assimilation, thus increasing the C:N ratio, resulting in higher starch content and lower protein content.[219–222] The latter effect over plants is particularly negative to crops quality. Furthermore, CO_2 is a greenhouse gas, causing the raise of temperature in the biosphere.[1]

The raise in atmospheric CO_2 has negative consequences in the sustainability of life on earth. Therefore, strategies for mitigation of the industrial release of CO_2 into the atmosphere are

imperative. Cyanobacteria and microalgae do not represent a major food source and they can be cultivated in very high CO_2, constituting a promising platform to sequester CO_2.

5.1.2 Inorganic carbon (C_i) uptake in photosynthetic microorganisms

Photosynthetic organisms are challenged in acquiring CO_2 from the environment. Not only CO_2 levels are low, but also RuBisCo (CO_2 fixation enzymatic complex) exhibits a degree of affinity for O_2 as a substrate (photorespiration). Photorespiration reactions have been related to energy dissipation and photo-protection, also providing some metabolites which are involved in stress protection.[223] Albeit, photorespiration diminishes photosynthesis productivity meaning a waste of carbon and energy for the cell.[223]

Cyanobacteria and microalgae have evolved an effective system to increase CO_2 concentration around RuBisCo, improving photosynthesis efficiency, known as CO_2 concentrating mechanism (CCM). CCM depends on C_i transporters, on carbonic anhydrases (CA) catalysing the reversible transformation of CO_2 and bicarbonate (HCO_3^-) (Equation 5-2) and on an intracellular microenvironment.

$$CO_2 + H_2O \overset{CA}{\leftrightarrow} HCO_3^- + H^+$$

Equation 5-2. Carbonic anhydrase CO_2/HCO_3^- conversion.

C_i active transport can be HCO_3^- uptake and CO_2 uptake and it is dependent on photosynthetic activity. HCO_3^- is preferably accumulated within the cell because CO_2 leaks easily, thus CO_2 is hydrated by periplasmic CA. The HCO_3^- cytosolic pool is then transported to RuBisCo containing organelles where CA increases CO_2 concentration.[224,225] Transcripts of CA mRNA and CA activity are entirely dependent in photosynthesis (light) and environmental CO_2 concentration.[226,227]

In particular, cyanobacteria has an extremely effective CMM mechanism, concentrating CO_2 up to 1000 times around RuBisCo active site achieved in micro-compartments known as carboxysomes, with the catalysis of carboxysomal CA.[224]

5.1.3 Photosynthetic microorganisms grown in high and extremely high pCO_2

In laboratory conditions, microalgae and cyanobacteria can be studied at different pCO_2. In general, air CO_2 levels are defined as low CO_2 or limiting, high CO_2 studies are carried out in the range of 1 – 5% CO_2, while extremely high CO_2 studies are conducted under >20%CO_2.

In cyanobacteria and microalgae, air grown cells show higher quantum requirement of oxygen evolution, and/or a higher PSI/PSII fluorescence ratios, than cells grown in 4.4% – 4.6%CO_2 respectively.[172,228] The latter indicates that in air the photosynthetic electron chain is less efficient, and there is an uneven energy distribution with higher excitation of PSI. Particularly, air grown PCC7942 and other cyanobacteria absorbed 2 – 3 quanta more to produce one molecule of O_2 than high pCO_2 grown cells.[172] Increased PSI excitation allows a higher cyclic electron flow, producing excess energy (ATP), which can be used to support the accumulation of C_i in the cytosol, while in high pCO_2 grown cells accumulation of C_i is not necessary, for the same reason CA activity is higher in low pCO_2 than in high pCO_2 grown cells.[227] Table 5-1 shows the changes in cyanobacterial PSI/PSII ratio in air and in 4.4%CO_2.

	PSI/PSII (Fluorescence 77K Ratio)	
Cyanobacteria	**Air**	**4.4%CO_2**
Synechococcus elongatus PCC7942	1.3	0.9
Anabaena variabilis M3	2.6	1.4
Anabaena variabilis ATCC29413	2.4	1.6

Table 5-1. PSI/PSII ratio for various cyanobacteria species, grown in air and in high pCO_2 (4.4%CO_2).[172]

In extremely high pCO_2 conditions different microalgae strains have shown different responses. There are intolerant strains, tolerant strains after a lag phase, and tolerant strains with no lag phase. Table 5-2 shows the changes in microalgae PSI/PSII ratios in air and in 40%CO_2 after one and eight days. The response of the microalgae *Chlorococcum littorale* (lag phase of 1 – 4 days) showed an initial transition stage showing a sharp increase in PSI/PSII fluorescence ratio, leading to a decreased quantum efficiency of PSII and a highly reduced pool of plastoquinones in the intersystem chain between PSII and PSI, but after many days photosynthetic activity returned to normal levels, although PSI/PSII fluorescence ratio was still slightly higher than in air.[130,174,229] Differently, in the intolerant microalgae *Stichococcus bacillaris,* the plastoquinone pool was gradually reduced but there was no increase in PSI activity, and in the long term photosynthetic activity was inhibited.[174] The microalgae *Chlorella sp.* UK001 grew in 40%CO_2 from air without a lag period.[230] In *Chlorella sp.* UK001 energy distribution in

the photosystems also showed an increase in PSI/PSII fluorescence ratio upon exposure to 40%CO_2 alongside an unaffected quantum efficiency of PSII.[130] Interestingly, in *Chlorella sp.* UK001, and differently to *Stichococcus bacillaris* and *Chlorococcum littorale*, the PSI/PSII fluorescence ratio was higher than 1.0 in air grown cells, meaning a basal higher photosynthetic activity around PSI (cyclic electron flow), which the authors correlated with the rapid adaptation to extremely high pCO_2 (no lag phase).

		PSI/PSII (Fluorescence /77K Ratio)		**Ref.**
Eukaryotic algae	**Air**	**40%CO_2 – Day 1**	**40%CO_2 – Day 8**	
Chlorococcum littorale	0.6 – 0.8	1.2 – 1.5	0.8 – 0.9	[130,174]
Stichococcus bacillaris	0.8	0.9	0.7	[174]
Chlorella sp. UK001	1.5	1.8	2.1	[130]

Table 5-2. PSI/PSII ratio for various microalgae species, grown in air and in extremely high pCO_2 (40%CO_2).

One important factor associated to the extremely high pCO_2 tolerance response was the capacity to maintain a constant pH. Low pH inactivates enzymes in the Calvin-Benson cycle (CO_2 fixation) causing a large pool of NADPH, which in turn causes a highly reduced plastoquinone pool and decreased PSII activity. However, in tolerant strains the increased cyclic electron flux in PSI increases photosynthetic ATP generation which can support H^+-pumping systems to maintain or to restore cytosolic pH.[130,174]

When *Chlorococcum littorale* was transferred from 3 – 5%CO_2 to 40%CO_2, no lag phase was observed, accordingly quantum efficiency of PSII did not decrease.[130,230] In contrast to air grown cells, 5%CO_2 grown cells showed no CA activity. While in the case of *Chlorella sp.* UK001 a much lower CA activity in air grown cells was observed. Therefore CA activity (Equation 5-2) was causing intracellular acidification in the rapid change from air to extremely high CO_2.[230] Nonetheless, after adaptation, Rubisco activity was higher in extremely high pCO_2 than in air.[229]

The regulation of energy distribution between photosystems in response to extremely high pCO_2 is similar to CO_2 limiting conditions (air grown), with a higher PSI activity in respect to moderately high pCO_2 (5%). Extremely high pCO_2 causes intracellular pH stress, while in low pCO_2 accumulation of intracellular C_i is necessary, both processes require photosynthetic energy to maintain pH homeostasis and C_i supply respectively. These examples demonstrate the susceptibility of photosynthesis to CO_2 levels, and high pCO_2 (moderate values 3 – 5%) appear to be the most optimal scenario for photosynthetic growth. Under high light intensity or equivalently diluted cultures, enhanced cyclic electron flows in PSI could be unnecessary.[130]

Energy distribution studies in cyanobacteria under extremely high pCO_2 have not been reported. However, David J. Thomas *et al.*[231] studied several cyanobacteria including PCC7942 in extremely high CO_2, finding that the cyanobacterium *Plectonema boryanum* can grow even in 100%CO_2 atmosphere, while PCC7942 was found to be highly tolerant, growing in atmospheres as high as 40%CO_2 and even at 100%CO_2 cells survived.[231] Differently, *Synechocystis sp.* PCC803 growth was inhibited by extremely high pCO_2.[231]

PCC7942 inorganic carbon (C_i) uptake mechanisms are HCO_3^- uptake and CO_2 uptake supported by cyanobacterial CMM. However, C_i utilisation in photosynthesis is mainly from HCO_3^-, while CO_2 utilisation is significant only at high C_i concentrations, above photosynthesis saturation level.[232] Concentration of HCO_3^- increases at alkaline pH and PCC7942 grows well at alkaline pH.[108]

Metabolic changes in PCC7942 shifted from high pCO_2 to low pCO_2 showed activation of glycolysis, the oxidative pentose phosphate pathway, and glycolate metabolism (product of photorespiration), alongside an increase in transcripts of inorganic carbon transporters.[233] These metabolic and transcriptomes changes show that in low CO_2 not only do they require higher C_i uptake activity, but also cells suffer photorespiration stress and require more energy from the sugar metabolism.

Photo-bioreactors with a high pCO_2 feed have been demonstrated for PCC7942. Within different CO_2 concentrations tested, 5%CO_2 has resulted in the highest biomass growth rates when pH is controlled at 6.8.[234,235]

5.1.4 Biophotovoltaics and pCO_2

Biophotovoltaics have been described as a carbon neutral technology because CO_2 is sequestered from air in the photosynthetic process.[236] CO_2 is the main sink for electrons, this means that reducing power (NADPH) and energy (ATP) generated in the light reactions are largely consumed in CO_2 fixation, therefore reducing power is not constitutively available for extracellular electron transport. Downstream CO_2 fixation, the metabolism of carbohydrates offers a new source of reducing power, mainly the oxidative pentose phosphate pathway (NADPH) and respiration (NADH). However, the latter are also consumed intracellularly.

In early studies of bioelectricity generation, using the lipid soluble electron shuttle HNQ (2-hydroxy-1,4-naphtho-quinone) to intercept directly the metabolic activity of cyanobacteria, it was demonstrated that devices in the light and in the presence of CO_2 (3% v/v in N_2) delivered higher current generation compared to devices under 100%N_2, when using a marine *Synechococcus sp.*

strain,[27] but not when using an *Anabaena variabilis* strain.[26] HNQ can accept electrons from ferredoxin-$NADP^+$ reductase, directly competing with $NADP^+$, and consequently competing with CO_2 fixation. However, CO_2 appeared to have a positive effect in *Synechococcus sp.* which was associated with consumption of endogenous glycogen. Therefore, it was suggested that there could be an indirect participation of CO_2 in the stimulation of glycogen degradation.[27]

Strategies to redirect electrons from the metabolic activity of cyanobacteria to the cell surface are necessary in order utilise externally the solar energy converted into intracellular reducing power. In Chapter 4, it was demonstrated that in PCC7942 iron starvation induces high rates of electrons being redirected from the light reactions to the cell surface when exposed to extracellular ferricyanide, thus actively competing with CO_2 fixation. Inhibition of CO_2 fixation has been suggested as a strategy to achieve higher extracellular electron flow.[45,47] However, the sustainability of the suggested strategy will require a fine balance to not disrupt the normal growth and metabolic activity of cyanobacteria to a point of viability lost.

5.1.5 High pCO_2 in photosynthetic organisms and its relation to iron metabolism

An established correlation between ferric reductase activities in high pCO_2 atmosphere has been demonstrated for some photosynthetic organisms. Takayuki Sasaki *et al.*[237] reported for *Chlorococcum littorale* that the only exposure to 20%CO_2 induced the expression of two proteins related to iron metabolism, one with the ferric reductase domain. Furthermore, Takayuki Sasaki *et al.*[119] showed that *Chlorococcum littorale* exhibited high extracellular ferric reductase activity in iron starvation only when grown in 20%CO_2. The expression and activity of this ferric reductase was diminished if cultures were transferred back to air (CO_2 limiting) or to iron sufficient media.

In another example, the microalgae *Chlamydomonas reinhardtii* was studied in relation to iron uptake while grown in air and in 3%CO_2.[135] It was found that cells grown in high pCO_2 had higher levels of intracellular iron and that iron uptake was through a reductive mechanism (strategy I).

The correlation between CO_2 enrichment and iron metabolism was also established in tomato plants. Chong Wie Jin *et al.*[120] reported that under 0.08%CO_2 and in iron limited medium, higher growth was obtained than in plants grown in atmospheric air and iron limitation. Likewise, iron limited plants in elevated CO_2 presented greater ferric chelate reductase activity, proton secretion, subapical root hair development, and the expression of a series of upregulated proteins, all part of an iron-deficiency-induced response.

These examples demonstrate that extracellular reductive mechanisms can co-exist with high pCO_2 concentrations in some photosynthetic microorganisms, although studies in cyanobacteria are not known. Furthermore, there is a close metabolic relationship between elevated pCO_2 and iron limitation. Particularly, *C. littorale* showed high rates of ferric reduction in extremely high pCO_2 (20%CO_2). Utilisation of streams with very high pCO_2 has great potential in biotechnological applications.

5.1.6 Objectives and proposed systems

In cyanobacterial exoelectrogenesis, electrons redirected to the extracellular interface are a small fraction of the electrons being metabolised. In Chapter 4, it was demonstrated that PCC7942 achieves unprecedented exoelectrogenic activity in iron limited growth and at neutral pH. While it has been suggested that CO_2 fixation should be inhibited to increase exoelectrogenesis, there is little evidence that photosynthetic organisms have increase ferric reductase activity induced by high or extremely high pCO_2. The viability of photosynthetic microorganisms depends on CO_2 assimilation, therefore a more sustainable approach is, instead of inhibiting, to boost CO_2 fixation.

The objective of this chapter is to investigate the effect of CO_2 in the exoelectrogenic capacity of PCC7942 in synergy with iron limitation. PCC7942 cultures were grown in 20% and 5%CO_2, to evaluate the effect of extremely high and high pCO_2. High CO_2 content lowers the cultural pH. Therefore, growth of PCC7942 was conducted in the neutral pH range, suitable for higher FeCN-R rates. The effect of pH over growth and exoelectrogenesis is analysed.

In this chapter, CO_2 enrichment is used as a strategy to enhance FeCN-R rates and to couple extremely high pCO_2 to photo-bioelectricity generation in an integrated framework.

5.2 PCC7942 growth and exoelectrogenesis response under elevated pCO_2

In order to understand the effect of elevated CO_2 partial pressure on the exoelectrogenic capacity in iron limited PCC7942, cultures were grown under elevated pCO_2 and FeCN-R rates were determined as a measure of the exoelectrogenic activity in PCC7942.

Conventionally FeCN-R rates are normalised by chlorophyll content, however within the current study, chlorophyll content of PCC7942 varied in the different growth conditions, therefore rates were normalised over biomass. Rates normalised over chlorophyll are mentioned when appropriate.

5.2.1 PCC7942 under extremely high pCO_2 (20% in air)

Cultures of PCC7942 were studied in 20%CO_2. High pCO_2 causes acidification of the media and buffers were required to control pH. Therefore, air grown cultures in neutral pH were also studied in order to observe the effect of cultures growing at a low pH (not alkaline) over exoelectrogenesis.

5.2.1.1 PCC7942 cultures characterisation in extremely high pCO_2

Iron limited cultures were prepared as described in Chapter 2 – Section 2.3. Cultures were prepared with initial OD_{750} around 0.5. Iron sufficient cultures were also prepared as control. Cultures were grown in 20%CO_2 (in air) as described in Chapter 2 – Section 2.4. For comparison, iron limited cultures grown in air were also studied, growing at alkaline pH and at neutral pH.

Figure 5-2 shows the growth curve and chlorophyll content of PCC7942 cultures in iron limitation grown in air and in 20%CO_2. The pH of the cultures is summarised in Table 5-3. Extremely high pCO_2 caused acidification of the media even though buffered were used.

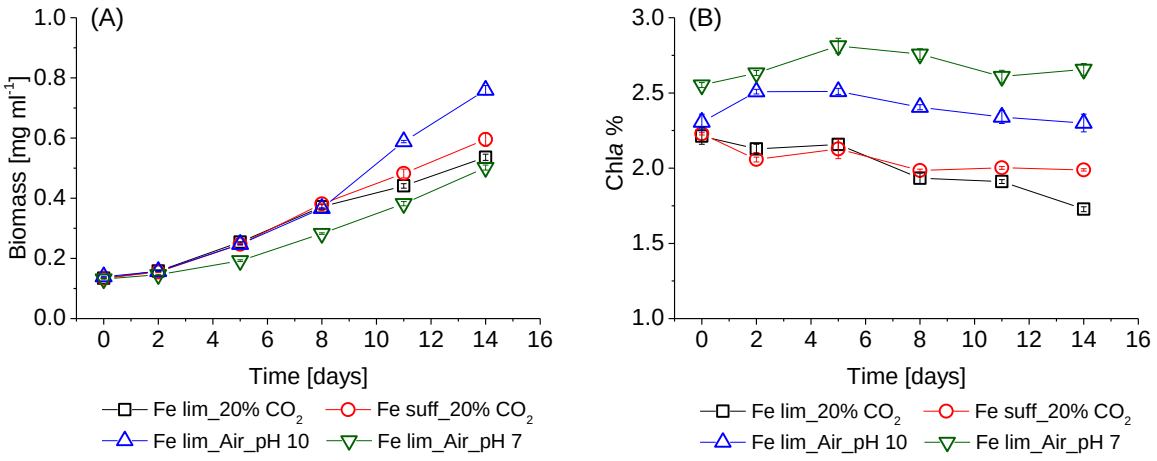

Figure 5-2. (A) Growth curve and (B) Chlorophyll content of PCC7942 cultures grown in air and 20%CO_2, and at alkaline or neutral pH, in iron limited and iron sufficient conditions at 30 °C and 120 rpm, under light intensity of 90 µmol m^{-2} s^{-2} in a 12 hour light/dark cycle. BM and Chl n=3 ±1SE.

	Condition	pH culture (light)	
		Day 2	Day 14
Air Alkaline (not buffered)	Fe lim	10.52±0.03	9.92±0.07
Air Buffered	Fe lim	6.93±0.005	7.31±0.04
20%CO_2 Buffered	Fe lim	6.31±0.04	6.73±0.01
20%CO_2 Buffered	Fe suff	6.26±0.01	6.88±0.02

Table 5-3. pH of PCC7942 cultures grown under air or 20%CO_2 in iron limited and iron sufficient conditions. Cultures were buffered with 10 mM HEPES-NaOH. (n=3; error bars 1SE).

The chlorophyll content dropped under 20%CO_2 pCO_2, which was seen to occur in both, iron sufficient and iron limited cultures. Despite lower chlorophyll content, in the first eight days, growth for 20%CO_2 cultures was at the same rate than iron limited cultures grown in air at alkaline pH (Figure 5-2 (A)), and higher than iron limited cultures grown in air at neutral pH. At high CO_2 levels, the dependence of PCC7942 on HCO_3^- uptake is minimal, and CO_2 uptake contributes in the assimilation of inorganic carbon,[232] therefore despite the low pH in the cultures, growth is supported by the high CO_2 concentration. Furthermore, it was seen that PCC7942 adapted to grow under 20%CO_2 from air without a lag period. However, after eight days, growth rates decreased considerably (Figure 5-2 (A)), which was more accentuated in iron limited cultures, the latter also showed a further drop in chlorophyll content, both normally occurring as a consequence of iron limited growth.[173]

In contrast to 20%CO_2 grown cultures, there was a raise in chlorophyll content for air grown cultures at neutral pH, which was clearly seen in the control (iron sufficient condition), which measured 2.7% chlorophyll content at Day 14, while in the iron limited condition there was an initial increase, but chlorophyll content did not increase further (Figure 5-2). The variations in synthesis of chlorophyll is typical in photosynthetic organisms, as an adaptation to the changes in photosynthetic performance due to environmental factors. Light intensity is inversely proportional to chlorophyll content.[238–240] It also has been seen that lower pH increases chlorophyll content in alkalophilic cyanobacteria.[240] In the current study, the saturating levels of CO_2 showed lower chlorophyll content despite the slightly acidic pH, indicating that high pCO_2 provided good conditions for photosynthetic activity. However, 20%CO_2 is detrimental for growth in later days, possibly due to stress related to other metabolic activities affected by the low pH of the cultural media. It was reported that in microalgae, the stress caused by extremely high pCO_2 in the photosynthetic energy distribution was greater in denser cultures, because light penetration is reduced and cells undergo higher stress.[130] The same could be happening in PCC7942. Nonetheless, confocal images of PCC7942 grown for 14 days in 20%CO_2 showed normal cell size (Figure 5-3).

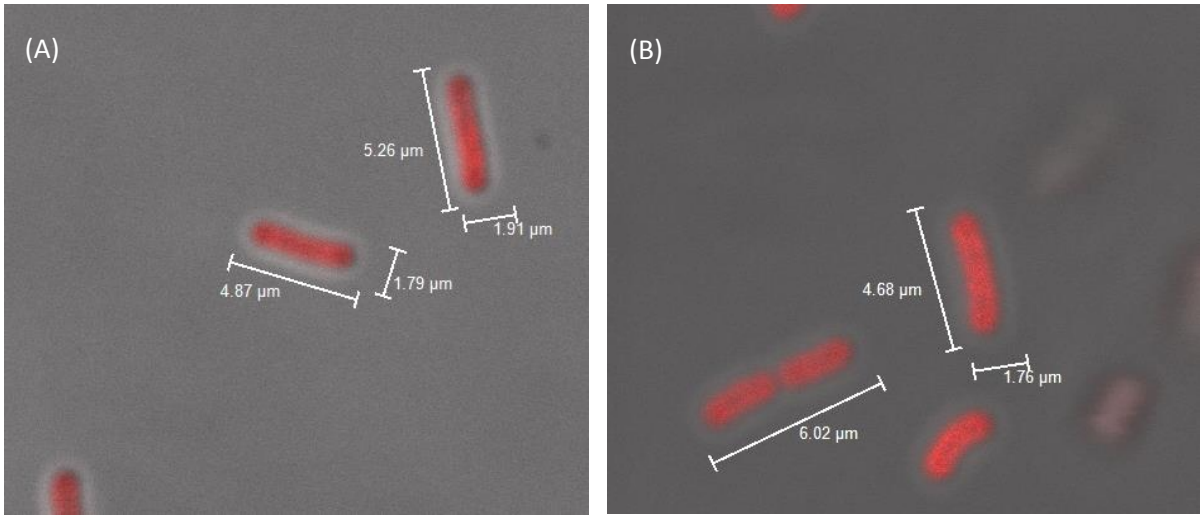

Figure 5-3. Confocal microscope images of (A) iron limited and (B) iron sufficient cells (PCC7942) after 14 days of culturing in 20%CO_2 and slightly acidic pH. Images obtained as described in Chapter 2 – Section 2.11.

5.2.1.2 Ferricyanide reduction capacity: exoelectrogenesis in extremely high pCO_2

The ferricyanide assay was conducted in air or in 20%CO_2 as described in Chapter 2 – Section 2.6.

20%CO_2 in iron limited PCC7942 demonstrated a clear influence of high pCO_2 over the exoelectrogenic capacity of PCC7942. Figure 5-4 shows FeCN-R rates from cultures grown in 20%CO_2: in synergy with iron limitation and in iron sufficiency, likewise from cultures grown in air and iron limitation: at alkaline pH (approximately pH 10.0), and at neutral pH (approximately pH 7.0).

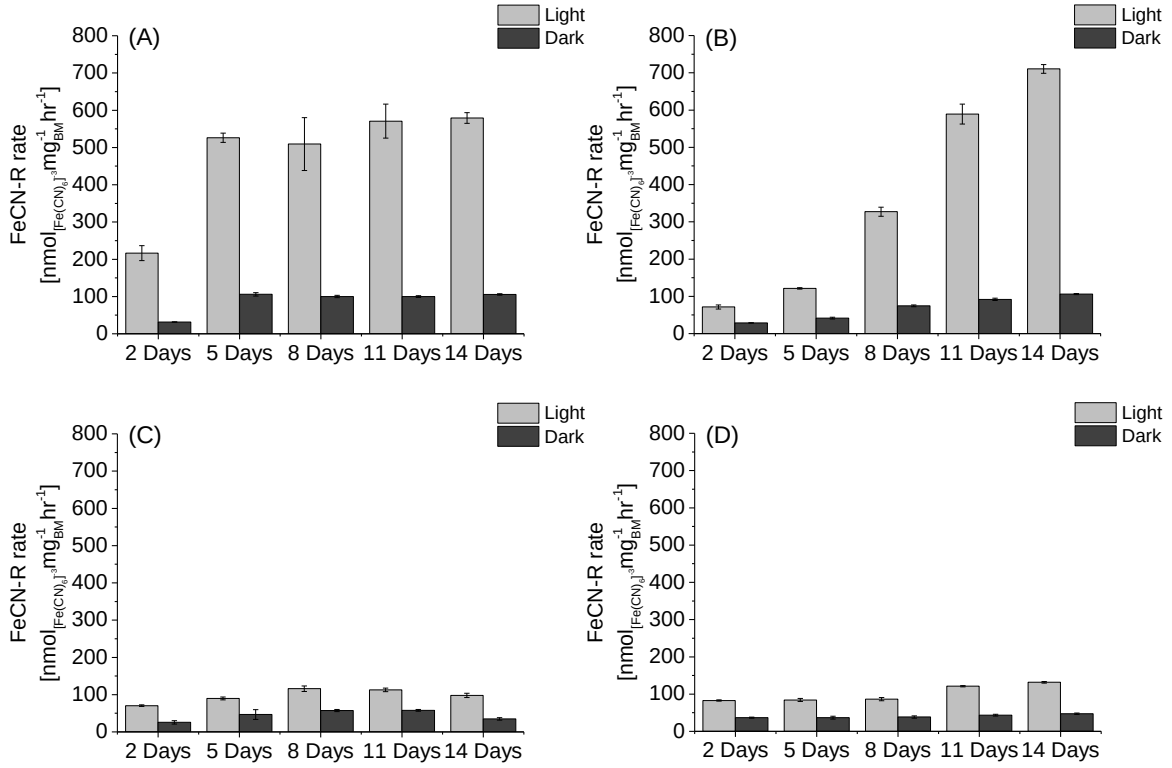

Figure 5-4. Ferricyanide reduction rates obtained from PCC7942 cultures in time, in the light and in the dark, (A) in an iron limited condition under 20%CO_2, (B) in an iron limited condition under air, (C) in an iron sufficient condition under 20%CO_2, and (D) in an iron limited condition under air buffered at neutral pH. FeCN-R rate n=3±1SE.

The major improvement observed for CO_2 enriched cultures was the increment in exoelectrogenic activity at early stages of growth, or shorter time of iron starvation. After only 2 days iron limited cultures in 20%CO_2 developed higher FeCN-R rates than the control (iron sufficiency) and measured rates were higher from Day 5 onwards, while FeCN-R rates for air grown iron limited PCC7942 increased gradually, as shown in Chapter 4, no significant improvement was detected after 2 days compared to the control (iron sufficiency). Only after 11 days it was observed that rates in air grown cultures were similar to those achieved by iron limited 20%CO_2 grown cultures. Figure 5-4 (B) and (D) demonstrate that neither 20%CO_2 in iron sufficiency nor growth at lower pH (neutral in air) caused high FeCN-R.

The rapid increase in exoelectrogenic activity in 20%CO_2 grown iron limited PCC7942 was accompanied by a lower chlorophyll content (Figure 5-2 (B)). Air grown PCC7942 (alkaline growth pH 10) developed a gradual increment in exoelectrogenic capacity, but it reached the highest FeCN-R rates (Day 14), alongside a higher growth rate and a higher chlorophyll content at that point (Figure 5-2). The latter could explain the higher FeCN-R rates once the extracellular reductive mechanism was activated. Nonetheless, if normalised over chlorophyll, the highest value was reached in iron limited PCC7942 under 20%CO_2, with 499.8±14.3 pmol $nmol_{Chl}^{-1}$ min^{-1} against 461.0±15.0 pmol $nmol_{Chl}^{-1}$ min^{-1} for air grown cells. While it is true that normalisation over biomass provides a more specific value in terms of reactor volume, normalisation over chlorophyll allows comparison with other strains (Table 4-3, Chapter 4).[47,99]

PCC7942 grown in air has a PSI/PSII fluorescence ratio of 1.3 – 1.5,[172,173] a value above 1.0 which shows that there is high photosynthetic activity around PSI, therefore there is a normal enhanced cyclic photosynthetic activity, similarly to the microalgae *Chlorella sp.* UK001,[130] which explains that PCC7942 did not show a lag phase in the adaptation to 20%CO_2. In iron starvation PSI/PSII fluorescence ratio decreases because PSI is highly dependent on iron.[173] While in extremely high pCO_2 there are not reports for PCC7942, in the microalgae *Chlorella sp.* UK001 and *C. littorale* it was observed that the PSI/PSII ratio increases to provide more ATP in cyclic photosynthesis.[130,174] These two opposite effects could explain why PCC7942 cultures under 20%CO_2 had a higher demand for iron, triggering the exoelectrogenic response earlier. The latter also explains why in the long term 20%CO_2 grown cultures reached a lower total biomass due to the combined stressing conditions.

Figure 5-5 shows that in the presence of the photosynthesis inhibitor DCMU, added as described Chapter 2 – Section 2.7, FeCN-R rates in the light were strongly inhibited, demonstrating that under 20%CO_2 exoelectrogenesis was mainly driven by photosynthetic reducing power (NADPH), in the same way as for air grown cultures (Figure 4-8, Chapter 4). Dark exoelectrogenesis is significantly lower, however rates in the dark were also increased under iron starvation. The rapid enhancement of FeCN-R rates in iron limited 20%CO_2 grown cells occurred in the light as well as in the dark (Figure 5-4), in both cases, rates appeared to achieve a maximum from Day 5 onwards.

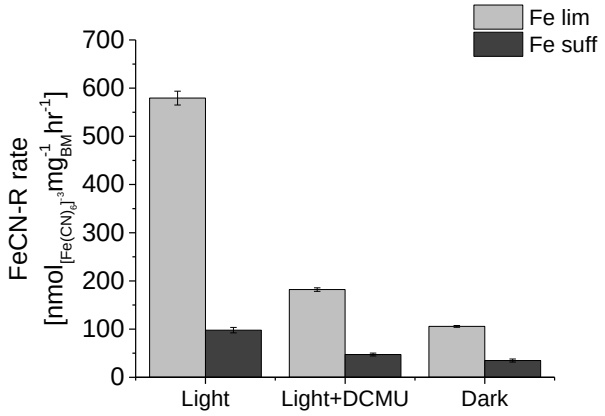

Figure 5-5. Ferricyanide reduction rates obtained from iron limited cultures and iron sufficient cultures of PCC7942 grown under 20%CO_2, in light, in light plus the photosynthesis inhibitor DCMU and in darkness. FeCN-R rate n=3±1SE.

Iron limitation and extremely high pCO_2 have a synergetic effect over the exoelectrogenic capacity of PCC7942. As discussed in Chapter 4, this iron-deficiency-induced exoelectrogenic capacity in PCC7942 is likely related to a reductive iron uptake mechanism. Similarly, the microalgae *C. littorale* presents ferric reductases upregulated by 20%CO_2 and iron deficiency.[119,237] Furthermore, when *C. littorale* was grown in iron limitation under 20%CO_2, high ferric reductase activity was observed after two days, but not for iron limited cultures grown in air, very similar to the results obtained for PCC7942.

It could be argued that buffering the 20%CO_2 system at alkaline pH would provide optimal conditions for growth, however the scope of the current work is to find favourable conditions for enhanced exoelectrogenic capacity, which was found to be higher at neutral pH. Air grown PCC7942 presents a mismatch between favourable pH for growth and the optimal neutral pH for extracellular reduction activity, not suitable for long term development in photo-bioelectricity generation coupled to biomass growth. Buffering air grown PCC7942 to maintain a neutral pH, not only diminished growth rates due to limited C_i assimilation, but also low growth rate reduced iron requirements and exoelectrogenic rates were not enhanced.

5.2.1.3 Exoelectrogenesis in changing atmosphere (short adaptation)

In an independent set of experiments, the effect of extremely high pCO_2 over iron limited PCC7942 was studied in a short adaptation scenario. Samples of iron limited cultures growing in air (alkaline growth) were assayed in 20%CO_2 and samples of iron limited cultures growing in 20%CO_2 were

assayed in air, at neutral pH and slightly acidic pH (approximately pH 6.0). Figure 5-6 demonstrates that CO_2 enrichment did not inhibit the exoelectrogenic activity in air grown cultures, but the pH of the media altered the exoelectrogenic response. Likewise, samples from cultures conditioned under 20%CO_2 did not increase exoelectrogenic activity if transferred to air. Furthermore, oppositely to air grown cultures, 20%CO_2 grown cultures exhibited lower rates at neutral pH. These results show that FeCN-R rates were not affected by sudden changes in the atmospheric composition but they were affected by pH changes, suggesting that the NADPH pool was smaller due to homeostasis imbalance in relation to cultural pH. Recent studies in cyanobacteria pH homeostasis have shown that cultural pH affects the photochemistry of PSII oxygen evolving complex due to pH gradients between the lumen – cytosol – extracellular environments and that high pCO_2 increases PSII activity at the lower pH.[241]

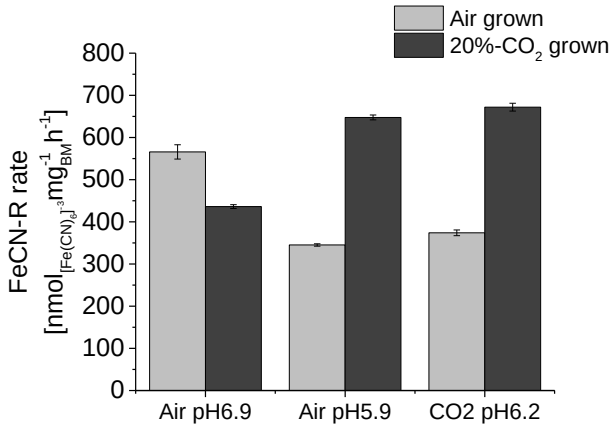

Figure 5-6. Ferricyanide reduction rates in short adaptation experiment obtained from iron limited cultures of PCC7942 grown in air or in 20%CO_2 at different atmosphere composition and cultural pH. FeCN-R rate n=3±1SE.

The optimal pH for ferricyanide reduction differed in cells adapted in air or in 20%CO_2. The optimal pH was not precisely determined, but it is clear that in cultures adapted in 20%CO_2 there is higher ferricyanide reduction rates at a more acidic pH.

5.2.2 PCC7942 under high pCO_2 (5% in air) and extremely high pCO2 (20% in air)

CO_2 enrichment was proved to be an effective strategy to induce higher exoelectrogenic rates in shorter time. However, initial growth rates were not higher than in air-alkaline growth and in the long

term CO_2 fixation appeared to decline compared to air grown cultures. To further investigate the effect of CO_2 over growth alongside exoelectrogenesis in PCC7942, two additional high pCO_2-pH systems were studied. A new set of iron limited cultures grown in 20%CO_2 were tested in a more controlled pH environment (higher concentration of buffer and higher initial pH of the media). Additionally, a set of iron limited cultures grown in 5%CO_2 atmosphere was studied with no buffers added.

5.2.2.1 PCC7942 culture characterisation in iron limitation and high and extremely high pCO_2

Figure 5-7 shows growth and chlorophyll content of these conditions, including iron sufficient cultures for reference, demonstrating that growth, and thus CO_2 fixation, is favourable for those conditions with higher cultural pH (Table 5-4). Particularly, 5%CO_2 established better conditions for growth, the same than in previous studies.[234,235] As no buffers were added in the 5%CO_2 grown cultures, there was an initial acidic condition (pH 6.0). pH was then raised as the cultures grew denser, implying that better growth rates could have been achieved. Nonetheless, to eliminate the cost of adding buffers, and to allow the atmospheric composition to provide the buffering agent, is a major improvement in the design of the process. However, the content of CO_2 in the feed should be controlled to maintain a constant pH. In Figure 5-7 (B) it can be observed that chlorophyll content decreased for iron limited cultures, affected by CO_2 levels but also by the rate of growth, while in iron sufficient conditions chlorophyll content was initially affected by CO_2 levels, but then tended to increase to stabilise around normal values.

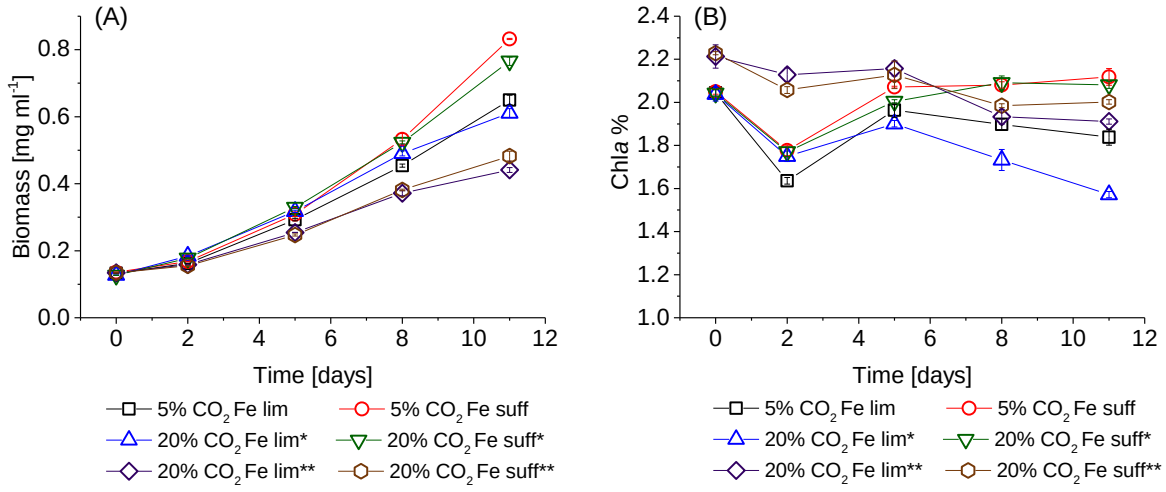

Figure 5-7. (A) Growth curve and (B) Chlorophyll content of PCC7942 cultures grown in 5%CO_2 and 20%CO_2, in iron limited and iron sufficient conditions at 30 °C and 120 rpm, under light intensity of 90 µmol m^{-2} s^{-2} in a 12 hours light/dark cycle. *Buffered 10mM HEPES-NaOH. **Buffered 20mM HEPES-NaOH. BM and Chl n=3 ±1SE.

	Condition	pH culture (light)	
		Day 2	Day 8
5%CO_2 (no buffer)	Fe lim	6.06±0.01	7.21±0.02
5%CO_2 (no buffer)	Fe suff	6.25±0.05	7.51±0.02
20%CO_2 (20 mM buffer)	Fe lim	6.75±0.01	6.84±0.05
20%CO_2 (20 mM buffer)	Fe suff	6.76±0.02	6.90±0.01
20%CO_2 (10 mM buffer)	Fe lim	6.31±0.04	6.59±0.03
20%CO_2 (10 mM buffer)	Fe suff	6.26±0.01	6.66±0.02

Table 5-4. pH of PCC7942 cultures grown under 5%CO_2 or 20%CO_2 in iron limited and iron sufficient conditions. pH n=3±1SE.

5.2.2.2 Ferricyanide reduction rates: exoelectrogenesis in high and extremely high pCO_2

The exoelectrogenic response of the different sets of iron limited cultures under CO_2 enrichment is presented in Figure 5-8, also showing the pH at which cultures where growing and the pH that the FeCN-R assay was conducted. It can be observed that 20%CO_2 provides a system which triggers the exoelectrogenic response in an earlier stage of growth, and that the stronger regulation of pH, implying higher growth rates, favoured higher FeCN-R rates in the early response, with rates at Day 2 2-fold higher than in 20%CO_2 with more acidic cultural pH. The latter is relevant in the design of the process, considering that the conditioning of the cultures should be as short as possible in order to reduce operational costs. However, in 20%CO_2 atmosphere, FeCN-R rates are higher at a more acidic pH than that of the cultural pH. Measurements of FeCN-R rates at pH 6.8 (Figure 5-9) in iron limited cultures grown under 20%CO_2 at pH 6.8, confirmed the findings presented in Figure 5-6, optimal conditions for exoelectrogenesis occurred at a more acidic pH for cultures adapted in a 20% CO_2 atmosphere.

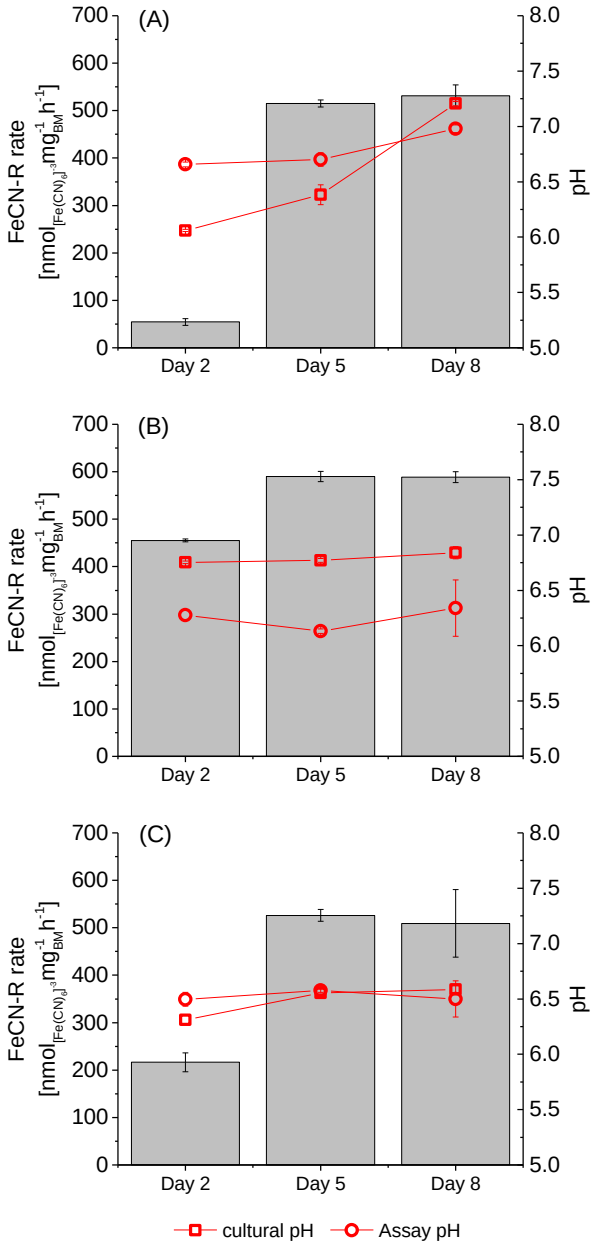

Figure 5-8. Ferricyanide reduction rates obtained from iron limited cultures of PCC7942 grown in (A) 5%CO_2, (B) 20%CO_2 and 20mM HEPES-NaOH, and (C) 20%CO_2 and 10mM HEPES-NaOH. Right axis shows cultural pH and assay pH (at which the ferricyanide reduction reaction was conducted). FeCN-R rate n=3±1SE.

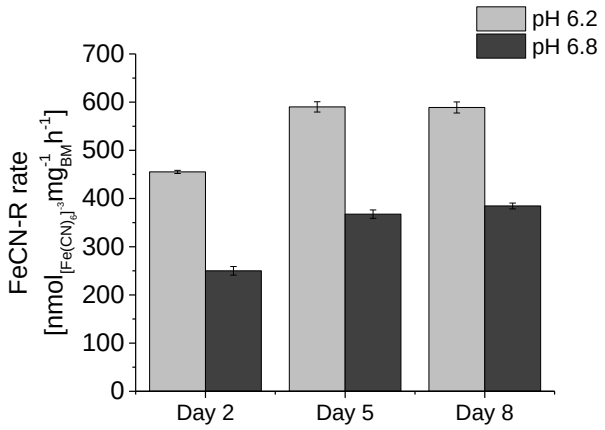

Figure 5-9. Ferricyanide reduction rates at pH 6.2 and pH 6.8 obtained from iron limited cultures of PCC7942 grown 20%CO_2 and 20mM HEPES-NaOH. FeCN-R rate n=3±1SE.

Figure 5-8 shows that 5%CO_2 grown iron limited cultures also presented an enhanced exoelectrogenic response, although at Day 2 there was no improvement, by Day 5 the reduction rates were raised. FeCN-R rates in 5%CO_2 grown samples were measured at neutral pH with rates comparable to those from 20%CO_2 grown samples at pH 6.2. Therefore, 5%CO_2 grown cultures presented a better match between cultural pH (after initial adaptation) and the optimal pH for exoelectrogenesis. In high pCO_2, the photosynthetic energy distribution of PCC7942 was reported to decreased the PSI/PSII fluorescence ratio, changing from 1.3 to 0.9.[172] Therefore, photosynthesis is more efficient and the photosynthetic apparatus is less demanding in terms of iron. However, exoelectrogenesis in cultures under 5%CO_2 were triggered in early stages in comparison with air grown iron limited cultures. In the microalgae *Chlamydomonas reinhardtii* grown in 3%CO_2 there was an increased accumulation of intracellular iron.[135] Similarly, PCC7942 under high pCO_2 (5%) showing quick induction of high FeCN-R rates is very likely related to iron homeostasis. Under high pCO_2 photosynthetic microorganisms can potentially grow faster as seen in Figure 5-7 (A), which would increase the demand for iron, supported by the observed drop in chlorophyll content as seen in Figure 5-7 (B). Therefore, CO_2 inducing ferric uptake, thus exoelectrogenesis, is a competitive adaptation.

The current study has shown different alternatives to utilise high concentrations of CO_2 in synergy to iron limitation, to induce higher exoelectrogenic capacity in PCC7942. A compromise between the outcomes of the study will be necessary in order to maximise the benefit of the response, which will depend on the priorities of a specific process. 5%CO_2 provides good growth rates without the cost of adding buffers (or minimal requirement), alongside high exoelectrogenic activity at neutral pH (same than growth). 20%CO_2 requires buffers and higher exoelectrogenic activity is established at slightly

acidic pH, the latter is detrimental for growth in the long term, but the lower the pH the better for the cathodic reaction in an electrochemical device (BPV). Furthermore, the abundance of high content CO_2 in industrial fumes makes the 20%CO_2 system attractive. PCC7942 has been reported to grow even in 40%CO_2 atmosphere,[231] therefore to combine industrial fumes with PCC7942 cultivation coupled to electricity generation is a viable process.

5.2.3 Exoelectrogenic capacity induced by elevated pCO_2 in iron sufficiency

The exoelectrogenic capacity in iron sufficient PCC7942 under 20%CO_2 was minimal compared to iron limited cultures, demonstrating that the high FeCN-R rates achieved in 20%CO_2 are induced by a synergetic effect between high pCO_2 and iron limitation. However, rates obtained in iron sufficient cultures grown in 20%CO_2 (Figure 5-10) reached 115 nmol mg_{BM}^{-1} hr^{-1} (87 pmol $nmol_{Chl}^{-1}$ min^{-1}), 1.8-fold higher (over biomass), or 2.4-fold higher (over chlorophyll), in respect to iron sufficient cultures grown in air (63 nmol mg_{BM}^{-1} hr^{-1} (36 pmol $nmol_{Chl}^{-1}$ min^{-1}) assayed at neutral pH). The FeCN-R rates obtained from iron sufficient cultures grown in 20%CO_2 represent an improvement. This enhancement is still higher than values achieved through other strategies investigated in order to increase exoelectrogenesis in cyanobacteria (Table 4-3, Chapter 4), 2.5 times higher than PCC7942 genetically engineered and 1.8-fold higher than *Synechocystis sp.* PCC6803 terminal oxidases mutants.[47,99]

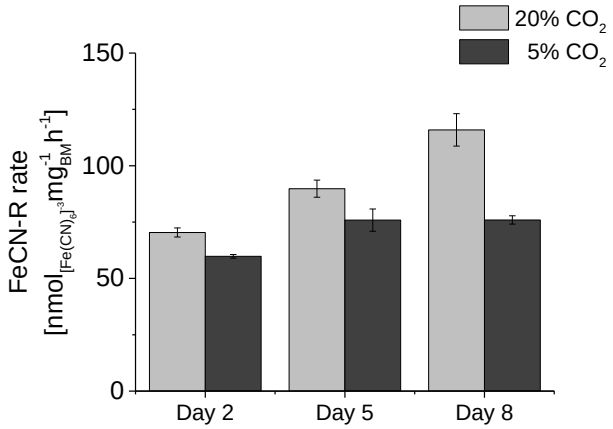

Figure 5-10. Ferricyanide reduction rates obtained from iron sufficient cultures of PCC7942 grown in 5%CO_2 and 20%CO_2. FeCN-R rate n=3±1SE.

In iron sufficient cultures grown in 5%CO_2 FeCN-R rates were 76 nmol mg_{BM}^{-1} hr^{-1} (54 pmol $nmol_{Chl}^{-1}$ min^{-1}), still higher than iron sufficient cultures grown in air. Normalised over chlorophyll there was a 1.5-fold improvement. Both 5% and 20%CO_2 are saturating levels for CO_2 fixation, however extremely high pCO_2 had a greater effect over the exoelectrogenic capacity of PCC7942 (iron sufficient), which correlates to the effect of high or extremely high pCO_2 over the photosynthetic electron chain. Under 5%CO_2 photosynthesis is more efficient with lower iron demand in the photosynthetic apparatus, which explains iron sufficient cultures not developing higher exoelectrogenic capacity. Contrarily, in extremely high pCO_2 the tendency seen for other microalgae is an increased PSI/PSII fluorescence ratio, increasing PSI excitation activity and therefore iron demand.[130,174] As seen in the microalgae *C. littorale*,[119,237] growth in extremely high pCO_2 upregulated the expression of iron-deficiency-induced proteins, thus it is possible that the only exposure of PCC7942 to 20%CO_2 had a similar effect, nonetheless, the same than *C. littorale*, exoelectrogenic rates are enhanced to very high values only in synergy with iron starvation.

While microalgae and cyanobacteria are different organisms, reports about a relationship between iron metabolism and high or extremely high pCO_2 have not been published for cyanobacteria. Therefore, the interrelation between high pCO_2 metabolism and iron upregulated proteins in cyanobacteria will require further investigation in order to fully understand the response. Carbon dioxide is the main sink for photosynthetic NADPH (electrons), thus exoelectrogenesis competes for reducing power, but contrarily to the suggestion that CO_2 fixation should be inhibited to increase extracellular electron transport,[45,47] high pCO_2 did not reduce exoelectrogenesis in PCC7942 cultures. Oppositely, exoelectrogenesis is enhanced, even in iron sufficient conditions. Besides, growth rates (CO_2 fixation) are higher. Nevertheless, the continuous loss of electrons to the extracellular ambient could results in the cells adapting to decrease the extracellular electron flow.

5.3 Photo-bioelectricity generation under extremely high pCO_2 in synergy with iron limitation

As seen in the ferricyanide assay, exoelectrogenesis by iron limited cultures is similar in air grown and 20%CO_2 grown cultures after a period of 11 to 14 days of incubation. The generation of electricity was studied in both atmospheric conditions with iron limited PCC7942 cultures grown in air (Day 15) and in 20%CO_2 (Day 10), in a ferricyanide mediated BPV device. The device was fabricated and operated as described in Chapter 2 – Section 2.5.2 and 2.5.4. An inoculated device is pictured in Figure 5-11.

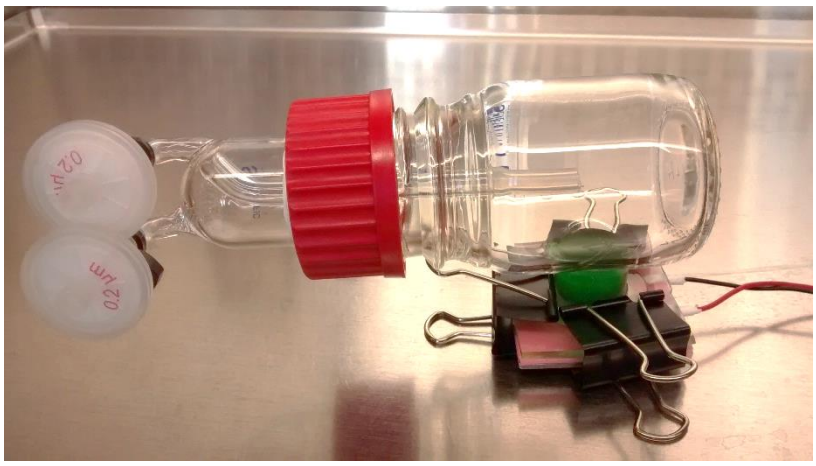

Figure 5-11. Photography of a nitrocellulose-MEA-BPV device for CO_2 enrichment inoculated with iron limited PCC7942.

Figure 5-12 shows that power obtained by the two conditions was also similar, confirming that the operation of BPV platforms under high concentrations of CO_2 is viable. Nonetheless, CO_2 grown samples had lower chlorophyll content, therefore in terms of electrons redirected to ferricyanide, BPVs operated under 20%CO_2 were more efficient.

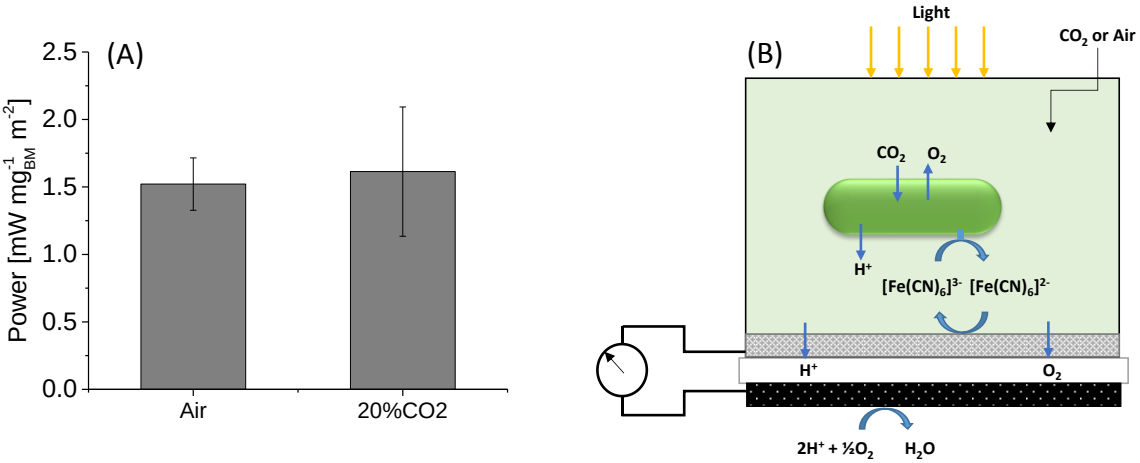

Figure 5-12. (A) Power output obtained in ferricyanide mediated MEA biophotovoltaics conditioned by iron availability and CO_2 partial pressure. PCC7942 cultures were resuspended on BG11 lacking iron at OD_{750} equal to 2. A volume of 4 ml of culture was added to each device. Ferricyanide was added to a concentration of 1 mM. Ferricyanide was added from a 100 mM stock solution filtered sterile. Devices were tested with the following external load: 56 kΩ, 33 kΩ, 20 kΩ, 10 kΩ, 4.6 kΩ, 3 kΩ, 1 kΩ and 0.55 kΩ. The highest power measured was with 3 kΩ. Power n=2±1SE. (B) Schematics of electrochemical reactions within the device.

BPV devices were initially exposed to light for 14 hours, showing a gradual fall in electricity generation (Figure 5-13). Afterwards, devices were exposed to a light/dark cycle (Figure 5-14). BPVs under 20%CO_2 showed a negative light response, while BPVs under air showed a positive light response. The latter is the typical response to light in reported studies (all under air).[13,48] After the initial discharge of the cultures, the difference between light and dark driven currents is small for both conditions, differing from the ferricyanide assay, which suggests that in the long term, exoelectrogenesis is driven mainly by stored energy (downstream CO_2 fixation), and in the light cells rapidly adapt to compete for reducing power, as 20%CO_2 provides a saturating CO_2 condition, CO_2 fixation is boosted. Even though this might be seen as a disadvantage, to allow the photosynthetic microorganisms to assimilate CO_2 is necessary for the long term viability of the system, representing a more sustainable approach. In this way cells were recharged in the light phase, and as seen in Figure 5-14 (A), due to the increase in dark currents, power was kept at higher levels.

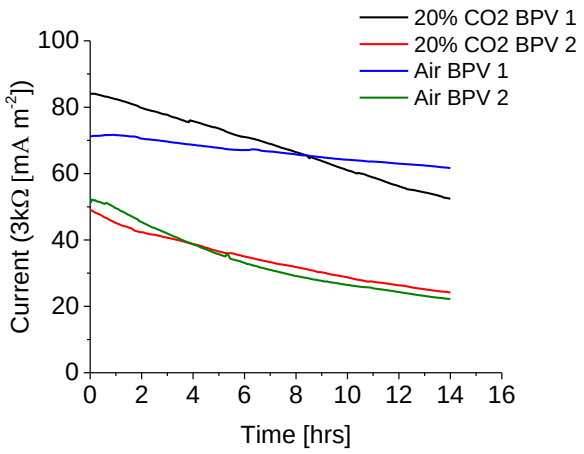

Figure 5-13. Light driven current profile in ferricyanide mediated BPV devices inoculated with iron limited PCC7942 in air and in 20%CO_2. Currents shown are through a 3 kΩ external load.

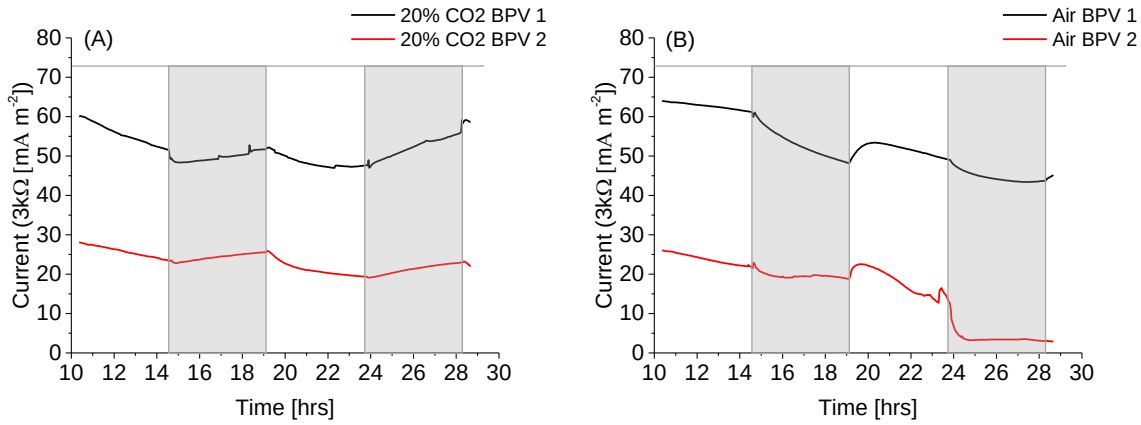

Figure 5-14. Light/dark current profile in BPV devices inoculated with iron limited PCC7942 in (A) 20%CO_2 and (B) air. Currents shown are through a 3 kΩ external load.

The drop in electricity generation in mediated BPV platforms operating with ferricyanide has been seen in previous studies.[48] The amount of reducing power redirected to ferricyanide can be an important fraction of the metabolic reducing power available, thus in the long term, cells might undergo high stressing conditions and viability be reduced. Certainly for air grown cells to shift to neutral pH has an effect in the inorganic carbon supply and photochemistry.[241] Therefore, CO_2 enriched devices are better adapted to operate effectively in the long term. However, further studies are necessary to engineer a process with PCC7942 having a constitutive high exoelectrogenic capacity which can operate in long term applications.

Energy losses due to inefficiencies in the operation of the device also might account for the decrease in currents. For instance, cultures tended to settle down, or aeration of the cathode could have been limited, or pH could be dropping excessively. The electrochemical cell used in this study (Figure 5-12 (B)), used a cathode which was not open to air, but relied in the diffusion of oxygen through the membrane (nitrocellulose paper). Plasma treated carbon paper was used to improve wettability and diffusion of electrolyte to the cathode. Lack of aeration in the cathode reduces cell performance, particularly in the dark when there was no photosynthesis oxygen evolution. Crossover of ferricyanide to the cathode also could be increasing overpotential losses. However, this design offers a practical setup to integrate electrodes in photo-bioreactors. The use of a proton exchange membrane (Nafion®) could be a good alternative as it is highly impermeable to gases, then CO_2 will not escape and oxygen directly from air will be used. However, as seen in Chapter 3, the acidity of Nafion® changes the pH of the cultures, implying extra buffer requirements. Nonetheless, the selection of the membrane it is something which will depend in the convenience of a particular reactor design and application.

5.4 Conclusions

CO_2 enrichment in synergy with iron limitation serves as a strategy to rapidly obtain exoelectrogenic cultures of PCC7942. At the same time, the appropriate pH in the cultures to operate at high extracellular reduction rates coincides with the cultural pH. Within the systems studied, 5%CO_2 enrichment offers enhanced biomass growth and exoelectrogenesis without the need of additional buffers, while 20%CO_2 induces high exoelectrogenic rates rapidly, but buffers are required to overcome excessive acidification of the cultures. The need for CO_2 mitigation from industrial fumes might request operation at higher CO_2 content, in this case 20%CO_2 provides a more suitable system.

Biophotovoltaics have the inherent advantage of minimal energy and feed requirement due to the catalysis of photosynthetic microorganisms with light, water and air being the main drivers of the system. The conditions found in the current investigation do not represent additional costs, oppositely, the lack of soluble iron (bioavailable) is easily achievable and fumes with high content of CO_2 are abundant. The design of more efficient BPV devices allowing good illumination, agitation, gas supply, and low internal resistance is paramount to increase power generation. However, as a proof of concept, it has been demonstrated that it is possible to integrate extremely high pCO_2 streams with exoelectrogenic cyanobacteria to generate electricity.

Finally, it can be concluded that BPV operation under higher CO_2 partial pressure is viable and offer operational advantages. The technology could be integrated with photo-bioprocesses, coupled to industrial fumes for CO_2 mitigation, and simultaneous bioelectricity generation.

Chapter 6 Electrochemical characterisation of PCC7942 biofilms

6.1 Introduction

Mediatorless systems are revisited utilising electrochemical techniques in order to investigate biofilms of PCC7942. The aim of this chapter is to develop protocols for the electrochemical characterisation of PCC7942, which could be applied afterwards to other photosynthetic systems. Biofilms of PCC7942 were investigated using cyclic voltammetry and double step potential chronoamperometry.

Cyclic voltammetry has been traditionally used in biofilm characterisation. However, studies on photosynthetic biofilms are limited. Applying cyclic voltammetry enables the identification of redox active regions within the biofilm.

Double step potential chronoamperometry applied to biofilms is a novel approach presented in this chapter, which seeks to provide an additional, rapid technique to characterise photosynthetic biofilms.

The iron limited condition was used to analyse its higher exoelectrogenic response at the outer membrane level, thus testing the proposed methods.

Mediatorless systems were introduced in Chapter 3 and the effect of iron limitation on PCC7942 was introduced in Chapter 5. To further complement, an introduction regarding electroactive biofilms and electrochemical techniques used in biofilm characterisation is presented, addressing the additional experimental work carried out for this chapter.

6.1.1 Microorganisms electrochemical characterisation

Exoelectrogenic bacteria were first described in MFCs. Characterisation by electrochemical techniques of microbial biofilms followed.[55] Photosynthetic microorganisms were found to possess exoelectrogenic activity in BPV platforms,[14] but the electrochemical characterisation of whole cyanobacterial cell is an area that has been little explored.

For extracellular electron transfer to occur, a path for electrons to flow through the cell envelope is necessary. Therefore, to understand how electrons are exported is an initial step in the study of

mediatorless systems. These pathways are not easily identified, but still, electrochemical techniques can be used to detect their redox activity. Several techniques have been used, however the most utilised is cyclic voltammetry and chronoamperometry.

6.1.1.1 The biochemistry of extracellular electron transfer

Electrons being transferred from the intracellular compartment to the extracellular side are conducted through electron transporter complexes (cytochromes). The electrochemical midpoint potential of some outer membrane cytochromes has been determined (as described in Chapter 3 – Section 3.1.2).

Cytochromes in the outer surface of bacteria correspond to the final step in an electron transfer chain. The latter has been well characterised for *S. oneidensis*. The "state of the art" around *S. oneidensis* exoelectrogenic capacity proposes that electrons are transferred from the PQ pool in the plasma membrane to the tetraheme cytochrome, quinol oxidoreductase CymA, which is located in the periplasm side anchored to the plasma membrane, from there the MtrA/MtrB/MtrC complex transports electrons to the extracellular side. MtrA is a periplasm decaheme cytochrome, MtrB an outer membrane porin, and MtrC an extracellular decaheme cytochrome. In the extracellular side, another decaheme cytochrome OmcA can accept electrons from the MtrABC complex.[242] MtrB has proven to be essential for extracellular electron transfer in *S. oneidensis* despite not being an oxidoreductase, but its function has not been completely understood.[243] Firer-Sherwood *et al*.[244] characterised MtrA structurally to find that MtrA is small enough and has a rod shape to partially penetrate the pore in MtrB, which allows the connection with MtrC, which also have the dimensions to partially fit in MtrB. The model proposed by Firer-Sherwood *et al*.[244] is presented in Figure 6-1. Extracellular anaerobic respiration also occurs in the periplasm of *S. oneidensis*, where a soluble fumarate reductase resides.[245] In the periplasm, soluble organic compounds like fumarate, ferric citrate and nitrate are the final electron acceptors. However, an outer membrane porin upregulated in anaerobic conditions was identified to be necessary for normal growth of *S. oneidensis* if using the mentioned electron acceptors.[246]

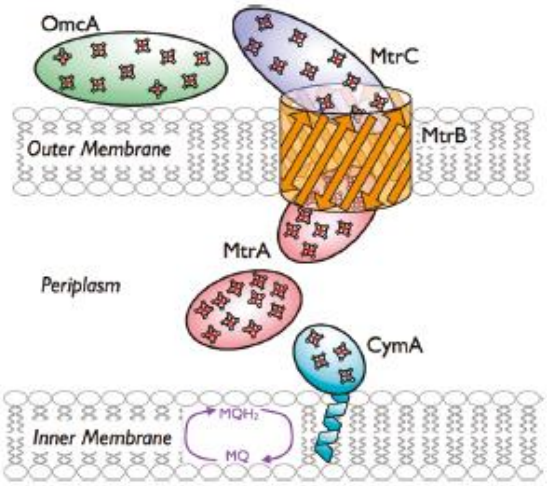

Figure 6-1. Schematic of *S. oneidensis* extracellular electron transport as proposed by Firer-Sherwood *et al*.[244] MtrA is shown in two locations due to its potential dual functionality.

Care should be taken on some misguided studies incorrectly suggesting that cyanobacteria expose the photosynthetic apparatus in the plasma membrane directly to the extracellular, without acknowledging the presence of an outer membrane.[151,247] The current "state of the art" on the biochemistry of cyanobacteria associated to extracellular electron transfer is very limited. There are no reports on the identification of protein complexes involved in direct electron transfer to an electrode.

6.1.1.2 Cyclic voltammetry to characterise biofilms

The electrochemical characterisation of a microorganism is important in order to understand its potential within a MFC or BPV device, which involves both, extracellular electron transfer pathways and biofilm electrode electrochemical reactivity. It is also a way of evaluating the response of a microorganism to different environmental *stimuli* associated to changes in the microbe electrochemical activity. As described in Chapter 1 – Section 1.4.5, cyclic voltammetry has been used in biofilm electrochemical characterisation.

Cyclic voltammetry in turnover conditions (described in Chapter 1 – Section 1.4.5) has been used to simply demonstrate the enzymatic catalysis of exoelectrogenic bacteria in converting an organic substrate to electricity.[55] The magnitude of the response in biofilms of *G. sufurreducens* fed with different concentrations of electron donors was investigated. The limiting current resulted in a rapid

increase at low electron donor concentrations and at high concentrations, the limiting current reached a maximum, emulating a Michaelis-Menten curve.

S. oneidensis was characterised by Wang *et al*.[248] In their work, cyclic voltammetry was conducted in biofilms after hours of being poised at fixed oxidising or reducing potential. As a result of this external *stimuli*, the electrochemical response changed, but also physiological characteristics of the biofilm were altered. An increment in OmcA/MtrC expression was found with the appearance of a cathodic peak when the microorganisms were poised at a high potential (0.04 V vs Ag/AgCl), implying that biofilms became an electron acceptor. While a potential fixed at -0.2 V vs Ag/AgCl was correlated to a reversible electroactive region around -0.4 V vs Ag/AgCl, which corresponds to the redox potential of riboflavin.

Cyclic voltammetry is also useful to screen electrode materials suitable for bioanode development. For instance, carbon materials have been used broadly in MFCs, but a comparative study of biofilms on stainless steel and carbon materials have shown that stainless steel is a promising material with a particular advantage at the more reducing potentials.[249]

The selection of the anodic electrode has become particularly challenging for photo-bioanodes, because the electrochemical activity of photosynthetic microorganisms is limited and not well characterised. Although photo-bioelectricity has been produced using a variety of photosynthetic microorganisms, an electrochemical characterisation of the redox complexes involved in their exoelectrogenic capacity has been elusive. One way to overcome this issue is to work with more effective anode materials. For instance, in a photo-bioanode fostering a bacterial consortia, nanostructured polypyrrole-coated electrode showed an increased voltammetry current profile.[250]

Immobilised redox mediators (osmium and azine redox polymers) on graphite rods used in photo-bioanodes showed increased electrochemical reactivity. The biofilm consisted of cyanobacteria enriched marine sediment, showing slightly higher peak currents in the light than in the dark. In axenic conditions, the voltammetry of the cyanobacterium *Lyptolyngbia sp.* (CYN82) on modified graphite coated with osmium redox polymer showed higher current profile when illuminated, indicating photosynthesis participation.[247] However, the electrochemical profile in these examples still corresponds to that of the immobilised mediator, with cyanobacteria only increasing electron availability.

Recently, Kaushic *et al.*[152] engineered a nanocomposite matrix to use as photo-bioanodes and detected redox active regions in biofilms of a marine *Synechococcus sp.* strain. Although the cyclic

voltammogram of biofilms on bare graphite also showed the redox regions, peak currents were higher in the composite matrix. The redox active regions were -156 mV and +225 mV vs Ag/AgCl.

Cyclic voltammetry is not the only electrochemical method applied to biofilms, but it represents a first step necessary in identifying electrochemical reactive regions. Other methods like electrochemical impedance spectroscopy (EIS) are also being explored to provide a characterisation of the resistivity to charge transfer between a biofilm and an electrode. The electrocatalysis by biofilms typically shows a charge transfer controlled process.[55,57,250]

6.1.1.3 Chronoamperometry to test biofilms

Chronoamperometry is a simple experiment to assess an electroactive biofilm, by applying a fixed potential and recording the current. It can replace a MFC or BPV in the analysis of a given biofilm. However, the applied potential needs to be chosen with care and cyclic voltammetry provides the relevant information to determine useful potential values. For example, Marsili *et al.*[55] grew *G. sulfurreducens* biofilms at a fixed potential of -0.04 V vs Ag/AgCl, 0.2 V higher than the biofilm midpoint potential as defined by cyclic voltammetry. Nonetheless, choosing a potential from experience is also a valid approach.

Positive oxidising potentials as high as 0.4 V vs Ag/AgCl have been chosen to pull electrons out of a photo-active biofilm,[75] possibly because photosynthetic microorganisms have a lower reducing potential (more positive) than in exoelectrogenic bacteria.

Chronoamperometry can also be used to identify current transfer capacity in different conditions. As mentioned in previous chapters, PCC7942 was transformed genetically to harbour the outer membrane cytochrome OmcS (from *G. sulfurreducens*). Current density was measured at 0.1 V vs Ag/AgCl for the wild-type and genetically modified biofilms, with significantly higher current generated by the genetically modified PCC7942.[99]

6.1.2 Objective and proposed systems

The objective of this chapter is to characterise PCC7942 biofilms in mediatorless platforms through analytical studies, with the aim to propose systems which can be used to screen for exoelectrogenic

cyanobacteria and/or for suitable electrode materials. The steps in preparing the photosynthetic biofilm are presented, which are fundamental to obtain an electrochemical response.

Iron limited and iron sufficient biofilms were evaluated in absence of artificial redox mediators, utilising two electrochemical techniques, cyclic voltammetry and double step potential chronoamperometry.

First, cyclic voltammetry was used in order to identify possible redox active regions in the biofilm. ITO-coated glass was chosen as the working electrode. Measurements were conducted in the light and in the dark. Additionally, thick and thin biofilms were characterised. Afterwards, carbon felt and carbon paper were also studied voltammetrically to evaluate the technique with biofilms on the carbon materials proposed in Chapter 3. Finally, a comparison with the exoelectrogen *S. oneidensis* is also presented.

The second proposed method, double step potential chronoamperometry, was used to characterise the reactivity of biofilms of PCC7942 in a rapid measurement. ITO-coated glass was used as the working electrode. Measurements were conducted in the light and in the dark.

6.2 Biofilm preparation for electrochemical studies

The bioelectrochemical device used for the electrochemical studies was fabricated and operated as described in Chapter 2 – Section 2.5.5. When iron limited biofilms were studied, cultures and devices were prepared as described in Chapter 2 – Section 2.3.

The device has a well at the bottom, where the working electrode is set. This well has a small volume (around 4 ml), which was used to inoculate the electrode, using that small volume only. The latter allowed the biofilm to settle down but still being supplied with air and light (Figure 6-2). Devices inoculated with larger volumes formed a biofilm, but no electrochemical activity was detected. The device which is transparent, was sealed to maintain sterile conditions, thus aeration was provided through vents made of nitrocellulose paper (0.2 µm pore size). A dense culture was added (OD_{750} equal to 3) in order to provide abundant biomass and to obtain a thick biofilm. Biofilms were left to settle over 4 days before conducting electrochemical measurements.

Figure 6-2. Photography of bioelectrochemical devices showing PCC7942 biofilms settled on the working electrode (ITO-coated glass) at the bottom of a 4 ml well.

On the day of measurement, the supernatant formed over the biofilm was carefully removed. Biofilms were carefully washed with BG11(-)x3 and then 30 ml of BG11(-)x3 was added to provide enough electrolyte solution to submerge the counter electrode (platinum mesh). Devices were placed in an incubator to maintain 30 ^{o}C (Figure 6-3).

Figure 6-3. Photography of bioelectrochemical devices assembled with the biofilm on the working electrode, the reference electrode (Ag/AgCl) and the counter electrode (platinum mesh). Iron limited and iron sufficient biofilms under illumination incubated at 30 ^{o}C.

Two important points should be noted. First, BG11(-)x3 was not amended with HEPES/NaOH to buffer the system at neutral pH, however the large amount of medium as compared to the biofilm, enabled the system to remain around neutral pH. This was necessary as HEPES/NaOH presented electrochemical reactivity causing the biofilm signal to be lost. Second, buffers are used as the

electrolyte in different reported studies, particularly the PBS buffer is normally used. However, changing the media to PBS did not work in PCC7942 biofilms. Therefore, BG11(-)x3 was chosen in order to maintain similar conditions for the biofilm activity. Although the PBS buffer might work in a different configuration, choosing BG11(-)x3 appeared to be the best option.

6.3 Cyclic voltammetry of PCC7942 biofilms

The electrochemical characterisation of PCC7942 biofilms, in iron limitation and iron sufficiency, was conducted in mediatorless systems. Cyclic voltammetry and double step potential chronoamperometry were applied. As mentioned in previous chapters, the ferricyanide assay is restrictive in informing the point of electron export and can only provide a quantification of electron transfer rates. However, to find electroactive regions in the biofilms is important in order to make more efficient systems. Cyclic voltammetry is a simple technique to identify electroactive regions, but it has been elusive to detect signals in photosynthetic biofilms.

In this section, cyclic voltammetry of PCC7942 biofilms are presented, showing defined electroactive regions. Furthermore, the iron-deficiency-induced higher exoelectrogenic capacity in PCC7942 was clearly detected, associating extracellular measurements with a metabolic state in wild-type cyanobacteria.

6.3.1 Cyclic voltammetry of thick PCC7942 biofilms on ITO-coated glass

In order to study PCC7942 capability of direct electron transfer with an external conductive solid substrate, as well as to establish the region of PCC7942 electrochemical activity, cyclic voltammetry was conducted as described in Chapter 2 – Section 2.5.5, without the assistance of an artificial redox mediator and in a neutral pH environment. ITO-coated glass was previously reported to constitute a good anode material for photosynthetic biofilms,[251] besides, as observed in Chapter 3, PCC7942 biofilms on ITO-glass showed lower activation losses than on carbon materials. Hence, in an initial stage, biofilms of PCC7942 were studied on ITO-coated glass, in darkness and under illumination.

In photosynthetic microorganisms, a non-turnover condition in theory could be achieved by adapting biofilms in the dark. Difficulties on achieving total non-turnover conditions in bacteria can happen, because cells can store sugars and also may downregulate electron transfer proteins.[39] The same occurs with photosynthetic microorganisms, as respiration allows intracellular oxidation independent

of light. The exoelectrogenic activity of PCC7942, at least in fresh samples, is mainly photosynthesis driven, but there is a partial, much lower, participation of dark metabolic pathways.

To study biofilms in the dark, thick biofilms were analysed in order to increase electron availability, adapted to darkness for only 3 – 4 hours, with the aim to reduce intracellular electron pool (absence of photosynthesis), but still allowing possible turnover conditions by an active metabolism (respiration). Slow scan rate was applied (1 mV s^{-1}).

Figure 6-4 shows the voltammetry of iron limited and iron sufficient biofilms on ITO-coated glass in the dark. It is observed that iron limited biofilms developed higher currents.

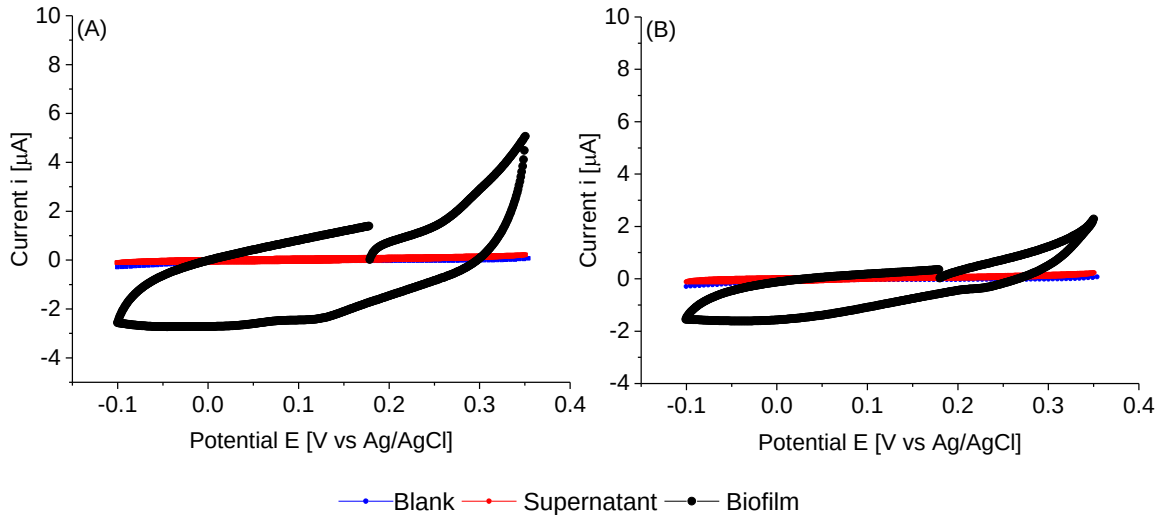

Figure 6-4. Cyclic voltammogram obtained in darkness from PCC7942 biofilms on ITO-coated glass, without artificial redox mediator in (A) iron limitation and (B) iron sufficiency. Measurements conducted in darkness at 30°C (pH 7.30 -7.40). Scan rate 1 mV s^{-1}. Initial potential [OCP – 50 mV] vs Ag/AgCl. Devices were inoculated with the same amount of biomass; however, the density of attached cells might differ.

The potential detected at zero current (OCP vs Ag/AgCl) was around 0.18 V vs Ag/AgCl for both iron limited and iron sufficient biofilms. No plateau current was observed, nor a clear anodic peak, within the potential window studied. In the back sweep, cathodic currents appeared at high positive potentials. All indicating that biofilms adapted in the dark were in a pseudo oxidised state, hence accepting electrons. However, in the back sweep, biofilms were reduced and as potentials were swept forward, anodic currents appeared around 0.0 V vs Ag/AgCl.

Figure 6-5 shows the voltammograms obtained on ITO-coated glass under illumination. In the presence of photosynthesis, biofilms became more reactive and were in a pseudo-reduced state. Higher currents were developed, however currents in the dark were significant.

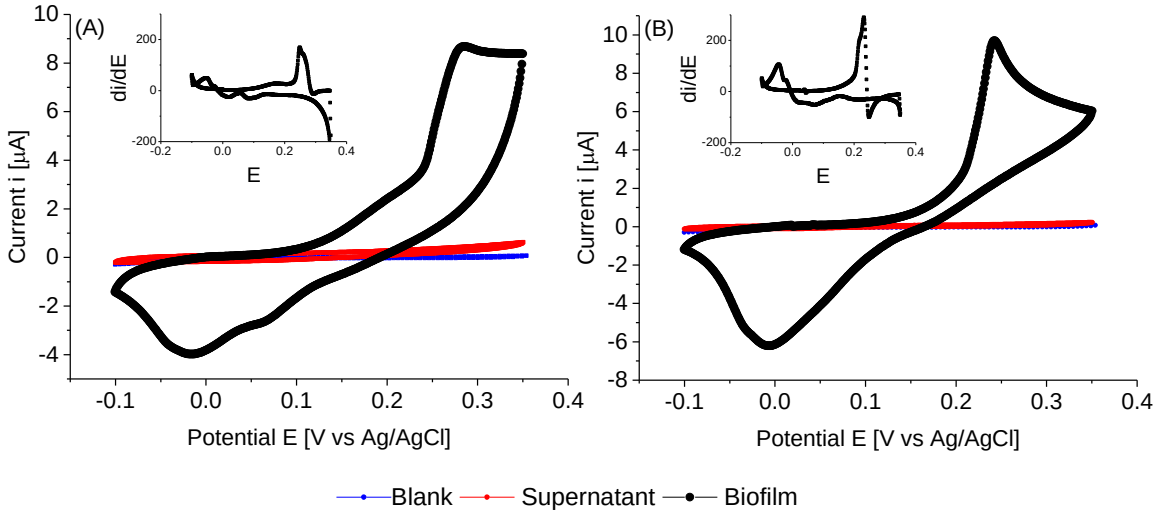

Figure 6-5. Cyclic voltammogram obtained under illumination from PCC7942 biofilms on ITO-coated glass, without artificial redox mediator in (A) iron limitation and (B) iron sufficiency. Measurements conducted in light at 30°C (pH 7.30 -7.40). Scan rate 1 mV s^{-1}. Initial potential [OCP – 50 mV] vs Ag/AgCl. Devices were inoculated with the same amount of biomass; however, the density of attached cells might differ. Insets: first derivative.

Electrochemical activity was detected for both conditions, iron limitation and iron sufficiency, with the iron limited biofilm showing anodic currents at more negative potentials, demonstrating that the higher exoelectrogenic activity in iron limited PCC7942 is, at least partially, independent of a soluble artificial redox mediator. However, waveforms are different to those typically obtained for exoelectrogenic bacteria in turnover conditions,[54,56] therefore it merits further analysis.

The potential measured in zero current (OCP vs Ag/AgCl) was in both cases around 0.0 V vs Ag/AgCl, which coincides with the potential at which anodic currents appeared in the dark after being reduced (Figure 6-4). However, a large activation polarisation loss was seen, especially in the iron sufficient biofilm, implying sluggish kinetics. A large increase in currents developed at higher potentials, with a starting potential around 0.20 V vs Ag/AgCl and a marked midpoint potential around 0.25 V vs Ag/AgCl (Figure 6-5), which in turn coincides with the potential region biofilms adapted in the dark showed the initial OCP value (Figure 6-4). It appears that PCC7942 biofilms present two electroactive regions. Nonetheless, higher reactivity was seen in the potential region around 0.20 - 0.25 V vs Ag/AgCl. Such

high potential implies that in a BPV device the cathodic potential should be very high in order to achieve high current densities, it also explains the low currents against an air cathode at alkaline pH.

Remarkably, iron limited biofilms on ITO-coated glass (Figure 6-5 (A)) were able to sustain currents at higher potentials in a similar fashion to that seen in exoelectrogenic bacteria (sigmoidal-like curve), meaning saturating levels of electron donor and limiting current due to the catalytic rates of enzymatic activity (V_{max}).[39,62] Differently, currents in iron sufficient biofilms on ITO-coated glass (Figure 6-5 (B)) drastically dropped, showing a pronounced peak, in a diffusion-limiting fashion.[39] In the case of biofilms, the availability of electron donor at the electrode is the result of intracellular processes, which for bacteria also depend on the diffusion of an organic substrate. In the case of photosynthetic biofilms, the availability of electron donors is not readily manipulated and it depends on the conditions of photosynthetic growth, mainly light intensity, but an external substrate diffusion step is not present, which eliminates some complexity in the analysis. Therefore, the current drop is likely due to an exhausted biofilm, meaning that electrons are not being replenished at a fast enough rate and indicating metabolic limitation.

The voltammetry of PCC7942 biofilms on ITO-glass supports the idea of a substrate limiting exoelectrogenesis. The proteomic study presented in Appendix C does not show a large overexpression of the alleged reductive iron acquisition system (SomB1-IrpAB-ftr1) and as it was discussed, the high FeCN-R rates in iron limitation would depend on higher intracellular reducing power redirection. The voltammetry of iron limited biofilms shows the continuous supply of electrons, while iron sufficient biofilms showed that electrons were not largely available.

Differently to sigmodal waveforms obtained in exoelectrogenic bacteria, with the back sweep current following the same reverse sigmodal curve,[58] iron limited biofilms showed a marked drop in current at the vertex. However, lower back currents have also been observed in good exoelectrogens.[56] The latter is associated to the reversibility (or irreversibility) of the electrochemical reaction, also depending on the electrode material.

A large cathodic current in the back sweep was detected in illuminated biofilms. In turnover dominated conditions, forward and back scans both generate anodic currents, simply because there is an excess of electron donor.[56,58] However, PCC7942 biofilms showed cathodic currents, indicating that the biofilm remained partially oxidised after the forward scan. Nevertheless, the peak cathodic currents were lower than the peak anodic currents.

The cathodic current in the back sweep exhibited a pronounced peak current for both conditions, featuring an absorbed redox complex behaviour in non-turnover condition (limited number of

oxidised redox centres). This cathodic peak occurred around 0.0 V vs Ag/AgCl, which set its activity in the less positive electroactive region, where lower anodic currents were observed.

Cathodic currents demonstrate that the biofilm can accept electrons. If this intake of electrons in PCC7942 plays a role in natural environments it is a matter still to be investigated, but electron relay between cells within a biofilm is accepted to occur, which implies cells are accepting electrons.[40,58] Figure 6-6 shows PCC7942 biofilm grown over carbon felt fibre with evident *pilus* structures, connecting cells but also attaching cells to the solid surface. The capacity of extracellular electron transfer in bacteria has been associated with electrical conductive nanowires (*pili*), which have been characterised in *S. oneidensis* and in *G. sulfurreducens*.[36,252] Furthermore, in the cyanobacterium *Synechocystis* PCC6803, pilA (a major pilin protein) has been associated to iron uptake from extracellular insoluble ferric oxide, suggesting solubilisation through a reductive mechanism.[136]

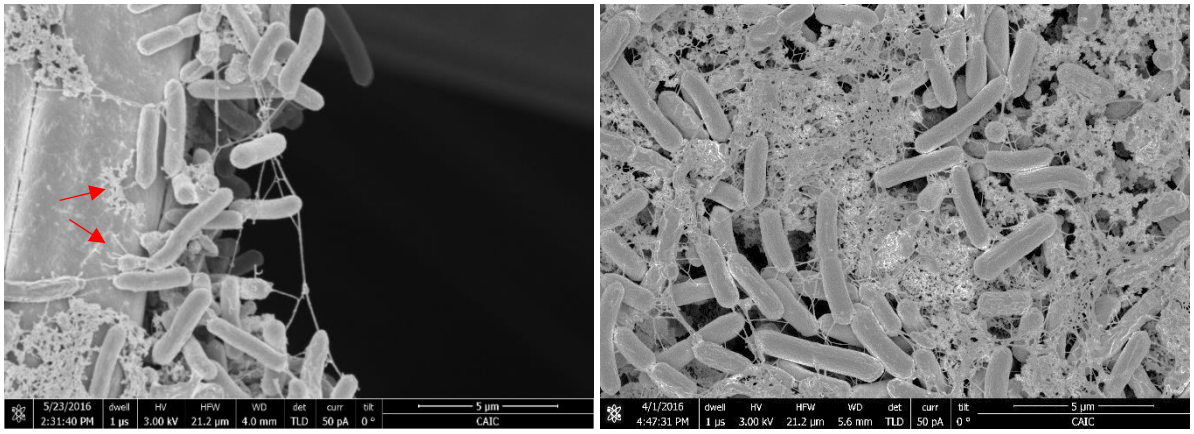

Figure 6-6. SEM images of PCC7942 biofilm on carbon felt showing *pili* structures allowing cell to cell and cell to electrode interactions. Red arrows point out *pili* attached to the solid surface. Biofilms grown in iron sufficient conditions. Images obtained as described in Chapter 2 – Section 2.10.

The difference in the voltammetry results between the two conditions, iron limitation and iron sufficiency, correlates with the results obtained in the ferricyanide assay presented in Chapter 4, under illumination and darkness, therefore it is very likely that the same reductive mechanism(s) induced by iron limitation were involved. Furthermore, because of the difference observed, it is possible to conclude that the signal measured was effectively due to a biological process in the outer surface of PCC7942, indicating that in the outer membrane of PCC7942 the presence of redox active complexes must exist. Extrusion of natural redox mediators can also be part of the response; however cyclic voltammetry of supernatants did not show significant electrochemical reactivity.

6.3.2 Cyclic voltammetry of thin PCC7942 biofilms on ITO-coated glass

The exoelectrogenic rates depend on light intensity. Thick biofilms of PCC7942 imply higher electron availability in terms of number of cells, but at the same time lower photosynthetic rates in the first layers of cells due to shading. A new set of experiments was performed on ITO-coated glass. Biofilms were washed many times to reduce biofilm m thickness. The resulting voltammograms are presented in Figure 6-7. Compared with the first set of thicker biofilms (Figure 6-5), there is a substantial difference in current densities, demonstrating that the thicker biofilms provided a larger electron pool and confirming that relay of electrons in cell to cell interaction occurred.

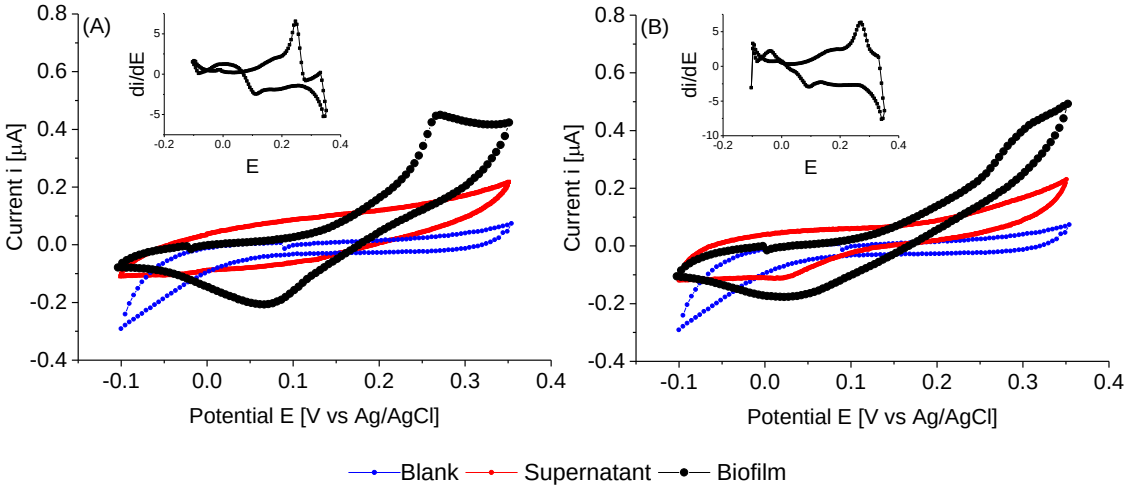

Figure 6-7. Cyclic voltammogram obtained under illumination from thin PCC7942 biofilms on ITO-coated glass, without artificial redox mediator in (A) iron limitation and (B) iron sufficiency. Measurements conducted in light at 30°C (pH 7.30 - 7.40). Scan rate 1 mV s^{-1}. Initial potential [OCP – 50mV] vs Ag/AgCl. Devices were inoculated with the same amount of biomass; however, the density of attached cells might differ. Insets: first derivative.

The waveform of the voltammograms of thin biofilms presented differences as well, particularly different in iron sufficient biofilms. In comparison with thick biofilms, activation polarisation losses were lower and smoother waves were obtained. This is better seen in the first derivative plot (insets Figure 6-7), where higher activity is observed in the region of the first peak in respect to the second peak. Furthermore, the first electroactive region is also observed in the iron sufficient biofilm. It can be concluded that thick biofilms conferred higher resistivity, possibly related to cells reacting in distant layers.

Iron limited thin biofilms (Figure 6-7 (A)) showed a similar waveform to thick biofilms (Figure 6-5 (A)) showing a tendency to plateau currents. In the iron sufficient biofilm, a pronounced peak was not seen, but there is a peak visible on the first derivative (inset). Therefore, it appears that the metabolic limitation was overcome, implying that light penetration had an impact on electron availability. Nonetheless, there was an obvious higher resistivity on iron sufficiency (poor charge transfer) compared with iron limitation. The latter reached V_{max}, while the iron sufficient biofilm required higher overpotentials to drive larger currents.

It is remarkable that iron starvation generated an intracellular electron pool available extracellularly in a saturated-like manner, indicating that the pathway involved was very active in redirecting electrons to the extracellular environment.

6.3.3 Multi-scan cyclic voltammetry of PCC7942 biofilm on ITO-coated glass

In order to assess the stability of the biofilms over applied external potentials, their response was studied over many consecutive scans (constant scan rate). In Figure 6-8 is observed that biofilms under illumination showed a stable behaviour, with currents tending to increase in later scans, therefore showing that biofilms to some extent became more reactive, which was more pronounced in thin biofilms. The latter indicates that an alleged metabolic pathway was affected by the external pressure, or more biomass was involved in the response, the second being supported by the cathodic peak also increasing.

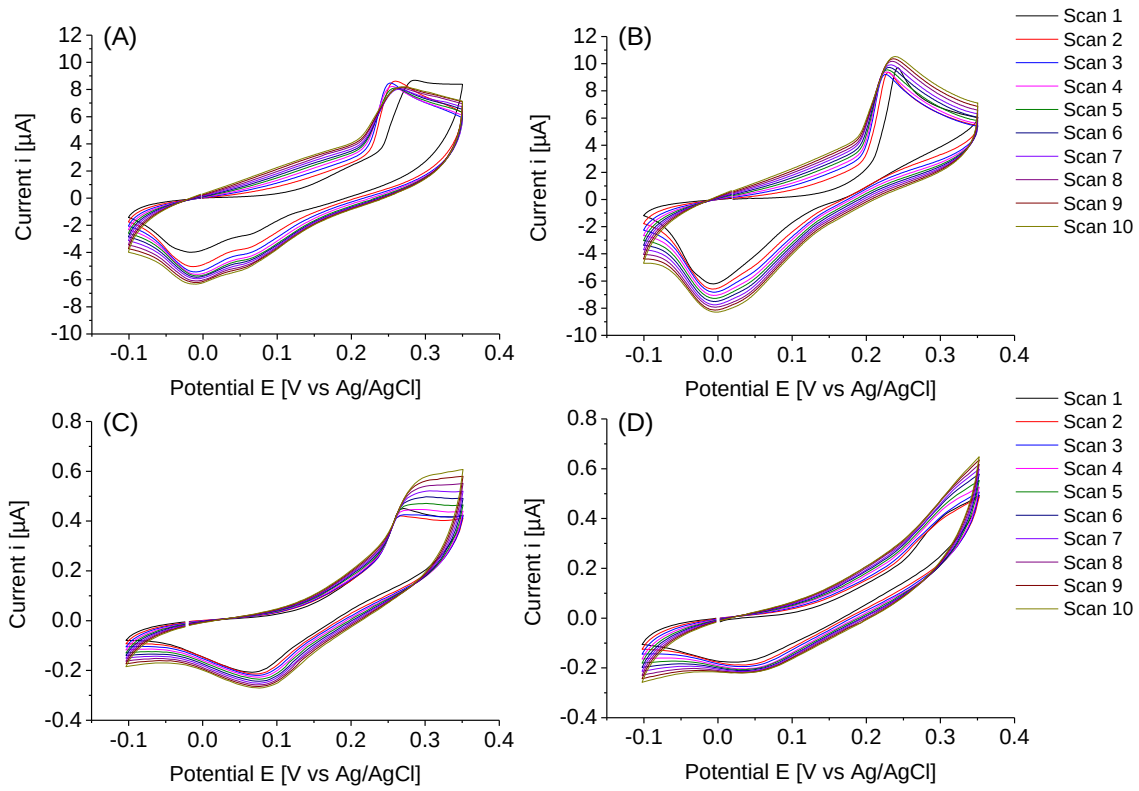

Figure 6-8. Cyclic voltammogram obtained under illumination from thick and thin PCC7942 biofilms on ITO-coated glass, without artificial redox mediator in (A) and (C) iron limitation and (B) and (D) iron sufficiency. (A) and (B) thick biofilms and (C) and (D) thin biofilms. Measurements conducted in light at 30°C (pH 7.30 -7.40). Scan rate 1 mV s^{-1}. Initial potential [OCP – 50 mV] vs Ag/AgCl. Devices were inoculated with the same amount of biomass; however, the density of attached cells might differ, particularly, thick and thin biofilm were intentionally differentiated in terms of biofilm thickness.

In the dark, differently to light driven voltammograms, the signal rapidly decreased in successive scans, thus biofilms lost reactivity after being disturbed (Figure 6-9). The loss of reactivity was particularly rapid in the iron sufficient biofilm. However, the loss of the initial large cathodic current allowed the observation of a cathodic peak at 0.22 V vs Ag/AgCl, which is the same potential region for the second peak in the forward scan seen under illumination, supporting the hypothesis of two distinctive redox active regions.

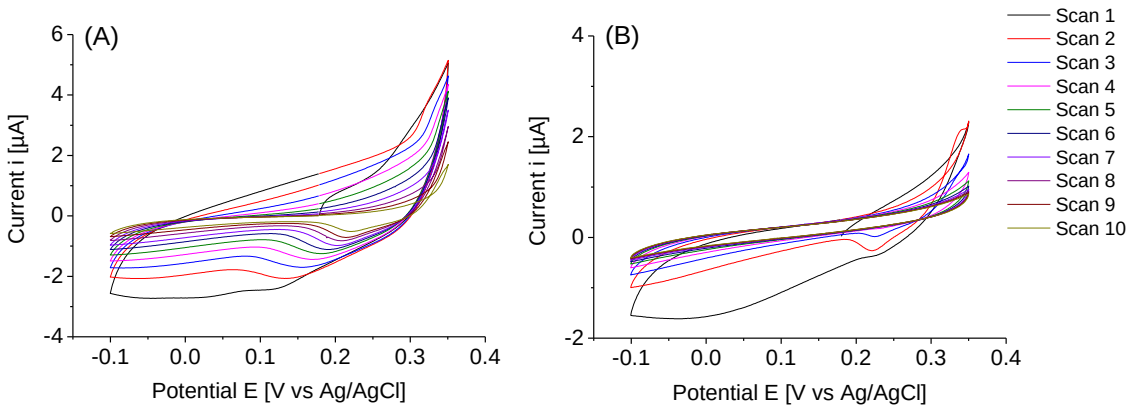

Figure 6-9. Cyclic voltammogram obtained in darkness from thick PCC7942 biofilms on ITO-coated glass, without artificial redox mediator in (A) iron limitation and (B) iron sufficiency. Measurements conducted in light at 30°C (pH 7.30 -7.40). Scan rate 1 mV s^{-1}. Initial potential [OCP – 50 mV] vs Ag/AgCl. Devices were inoculated with the same amount of biomass; however, the density of attached cells might differ. The difference in the axis scale is to enlarge the features in the iron sufficient biofilm.

The cathodic peak at 0.22 V vs Ag/AgCl is best seen in the "scan 2" of the iron sufficient biofilm (Figure 6-4 (B)). It was also observed that as scan number increased for the iron limited biofilm, the same cathodic peak started to become clearer and "scan 10" resembles well the "scan 2" of the iron sufficient condition.

It appears that in the absence of photosynthetic activity, the alleged metabolic pathway redirecting electrons was in an oxidised state and electrons to some extent were internalised by the biofilm and gradually locked due to charge transfer resistivity or irreversibility in intracellular reactions. Therefore, in the successive scans electron availability was lessened. This effect was better seen in iron limited biofilms, after "scan 2" which reduced the biofilm, anodic currents in the forward sweep gradually appeared at more positive potentials and in "scan 10" anodic currents started only at 0.18 V vs Ag/AgCl, the same than the initial zero current potential. This indicates that the alleged redox region at 0.1 V vs Ag/AgCl somehow became inactive.

A redox complex embedded in the cell – electrode interface, with a midpoint potential around 0.22 V vs Ag/AgCl, appears to be present and in the dark, it showed a response similar to that of absorbed redox species (described in Chapter 1 – Section 1.4.3), in the back sweep but not in the forward sweep. A mismatch between forward and backward peak potentials for absorbed proteins is common. It occurs due to high overpotential losses in electron transfer between the buried active site of the complex and the electrode.[39,253]

Higher complexity was found around 0.1 V vs Ag/AgCl, with a possible intake of electrons consumed in intracellular processes, which remains active only under illumination. The results presented indicate that iron starvation induced higher electrochemical reactivity in the cell surface in relation to exoelectrogenesis but also in intake of electrons, possibly due to a common intracellular redox complex.

6.3.4 Cyclic voltammetry of PCC7942 biofilms on carbon materials

Figure 6-10 shows the voltammograms obtained on carbon felt and carbon paper (under illumination). The potential measured in zero current (OCP vs Ag/AgCl) was around 0.0 V vs Ag/AgCl for both carbon felt and carbon felt, as it also was for biofilms on ITO-coated glass (under illumination). However, large activation polarisation losses were seen in iron sufficient biofilms (Figure 6-10 (B) and (D)). Furthermore, the back currents in iron sufficient biofilms were higher than the forward currents, indicating that activation losses were very limiting in the forward sweep. Iron limited biofilms on carbon materials (Figure 6-10 (A) and (C)) showed a more reactive response.

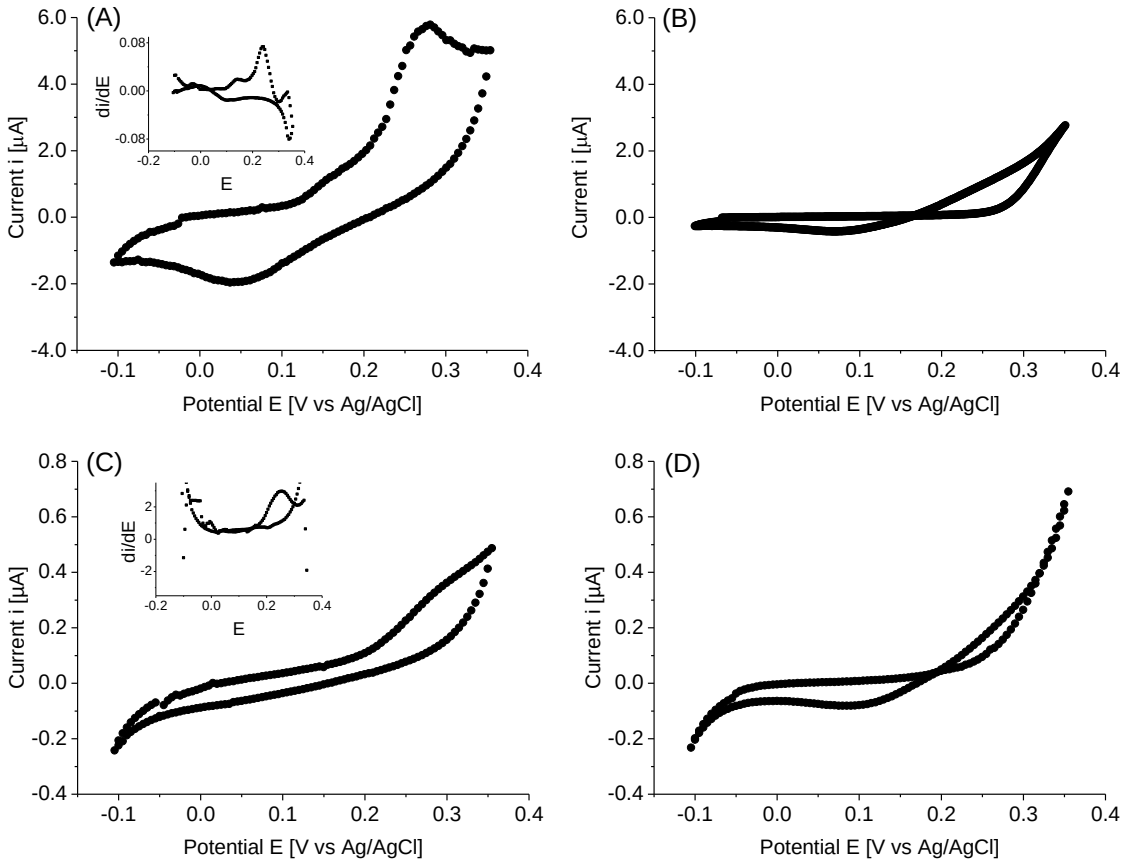

Figure 6-10. Cyclic voltammogram obtained from PCC7942 biofilms on (A) and (B) carbon felt, on (C) and (D) carbon paper, without artificial redox mediator in (A) and (C) iron limitation and (B) and (D) iron sufficiency. Measurements conducted in light at 30°C (pH 7.30 -7.40). Scan rate 1 mV s^{-1}. Initial potential [OCP – 50 mV] vs Ag/AgCl. Devices were inoculated with the same amount of biomass; however, the density of attached cells might differ. Insets: first derivative.

Biofilms on carbon paper showed the lowest reactivity and carbon felt showed lower currents than ITO-coated glass, but a similar waveform of the respective iron limited biofilms. Biomass attachment could not be well controlled, despite the same amount of biomass being inoculated in each experiment, after 4 days biofilm density and the quality of the biofilm attachment could vary. The latter could explain the lower currents.

The lower reactivity of iron limited biofilm on carbon paper (Figure 6-10), in relation to waveform and not current magnitude, implies hindered charge transfer rates. Anodic currents did not plateau, indicating that V_{max} was not reached. Therefore, carbon paper is an inferior choice as anode material for PCC7942, despite setting more negative anodic potentials (as seen in Chapter 3 – Figure 3-16) in iron sufficient conditions.

Iron sufficient biofilms on carbon materials showed significant currents only at high potentials within the potential window, demonstrating that effectively, ITO-coated glass is a better electrode for

bioanodes fostering PCC7942 (if other factors like cell design are not considered). The electrochemistry of iron sufficient biofilms on ITO-glass compared with biofilms on carbon materials explains the results seen in Chapter 3, as BPV devices using ITO-coated glass presented lower activation losses compared with carbon materials. Nevertheless, to screen for electrode materials presenting lower overpotential losses is a future challenge. Cyclic voltammetry using iron limited biofilms was demonstrated to be a useful strategy to increase electron availability, enabling the visualisation of electroactive regions, therefore facilitating the search of materials for photo-bioanode development.

6.3.5 Cyclic voltammetry of iron limited PCC7942 and *Shewanella oneidensis*

In Chapter 3, the voltammetry of *S. oneidensis* was presented to demonstrate that in the conditions tested the presence of the two main reductive mechanisms were active. For comparison purposes, Figure 6-11 shows the voltammetry of iron limited PCC7942 and *S. oneidensis* biofilms on carbon felt, at two scan rates, 1 mV s^{-1} and 10 mV s^{-1}.

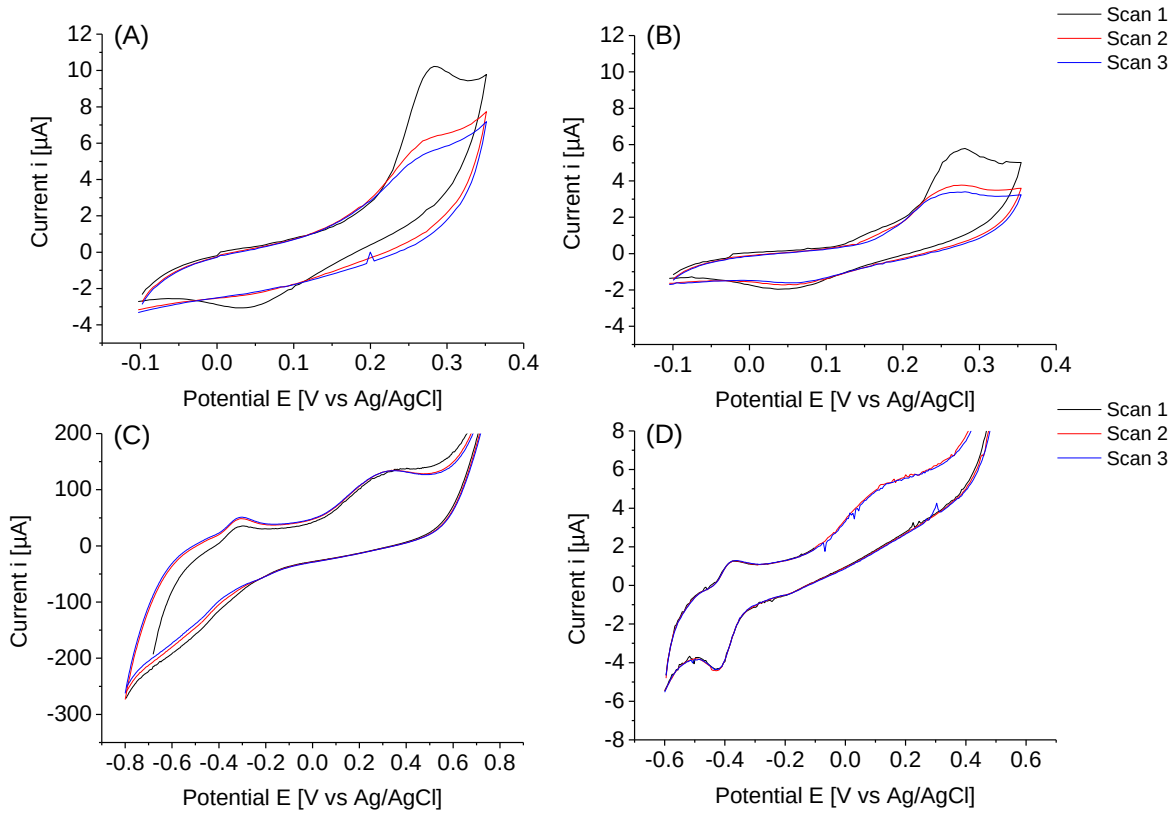

Figure 6-11. Cyclic voltammograms obtained from iron limited PCC7942 biofilms and *S. oneidensis* biofilms on carbon felt, without artificial redox mediator. Scan rate at 10 mV s^{-1} in (A) PCC7942 and (C) *S. oneidensis*. Scan rate at 1 mV s^{-1} in (B) PCC7942 and (D) *S. oneidensis*. Measurements conducted at 30°C (pH 7.30 -7.40) and under light in the case of PCC7942 biofilms. Devices were inoculated with the same amount of biomass; however, the density of attached cells might differ.

The exoelectrogen *S. oneidensis* presented higher current densities and at more negative reducing potentials, demonstrating that a good exoelectrogen not only has a major metabolic pathway (respiration) associated to extracellular electron transfer, but also the reducing potential of the cells is higher (more negative), very likely an adaptation to succeed utilising extracellular electron acceptors (higher driving force).

At 10 mV s^{-1} the voltammetry of PCC7942 showed the same waveform as that at 1 mV s^{-1}. This is remarkable considering that fast scan rates induce larger capacitive currents and signals can get lost in poor exoelectrogenic biofilms,[54] demonstrating that iron limited PCC7942 is potentially a good exoelectrogenic bacteria. Furthermore, the peak current was the same at both 1 and 10 mV s^{-1}. However, the current magnitude in *S. oneidensis* is considerably higher at 10 mV s^{-1} (Figure 6-11 (C)) than at 1 mV s^{-1} (Figure 6-11 (D)), while in PCC7942 it was only doubled, indicating hindered intracellular electron transfer kinetics in the exoelectrogenic pathway, not allowing a complete turnover condition, thus decreasing the total charge availability.[39,54]

Nonetheless, it is not clear how the response correlates with capacitive currents and how these can be affected not only by the scan rate but also by the activity of the biofilm. In the next section, a different technique is introduced, which is based on chronoamperometry, therefore the capacitive effect is not present.

6.4 Double step potential chronoamperometry of PCC7942 biofilms

To further study the electrochemistry of PCC7942 and its capacity to interact with external potentials, as part of this thesis, it is proposed to apply double step potential chronoamperometry. In this section, this technique is demonstrated for biofilms of PCC7942.

Double step potential chronoamperometry allows a rapid characterisation of the discharge and injection of charge into the biofilm, providing further insight into the reversibility of the processes occurring in the system biofilm – electrode and offering a new approach in biofilm electrochemical characterisation.

Iron limited and iron sufficient biofilms were studied. Triplicates of each condition were prepared as described in Section 6.2. In each condition, two biofilms were tested under illumination and one in darkness, with “step 1” at 0.35 vs Ag/AgCl and “step 2” at -0.1 vs Ag/AgCl.

In analysing the current – time curve in Figure 6-12 for iron limited biofilms and in Figure 6-13 for iron sufficient biofilms, the typical response from the reaction $R \rightarrow O+e^-$ can be seen.

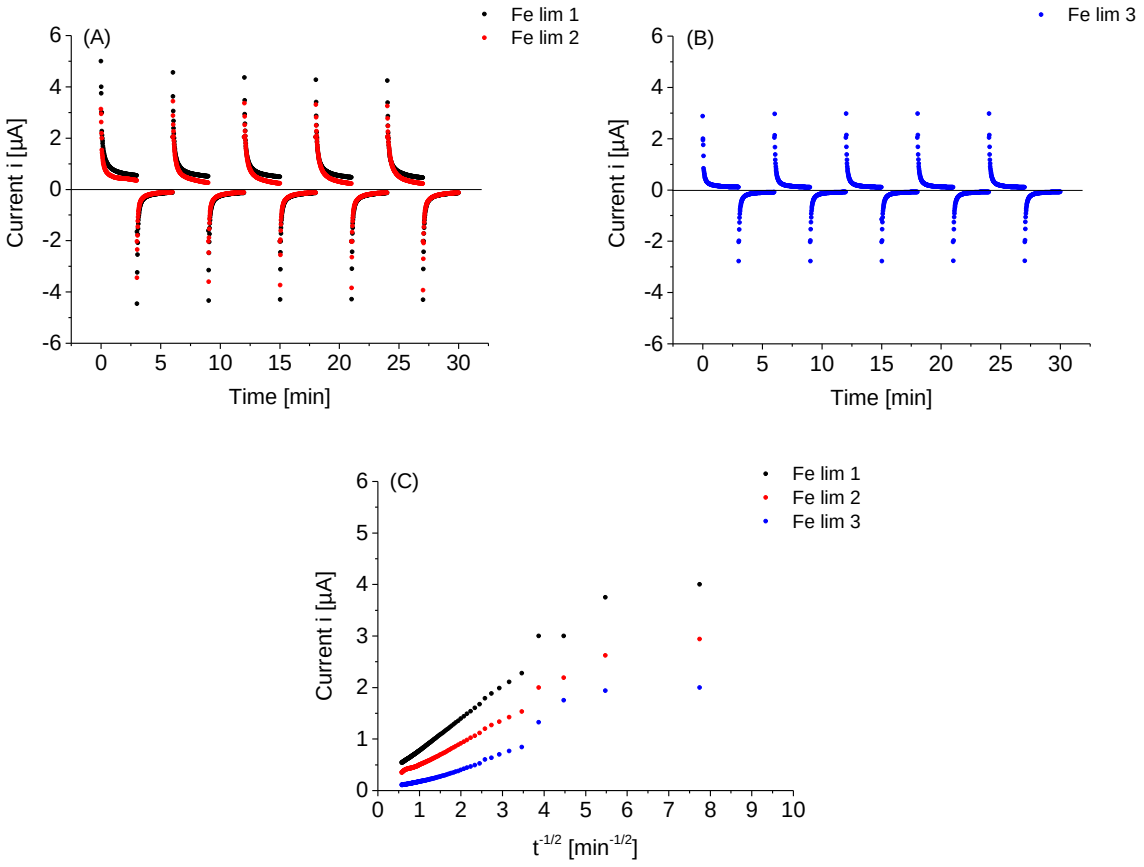

Figure 6-12. Two step potential chronoamperometry obtained from PCC7942 biofilm in iron limitation (A) under illumination and (B) in darkness. (C) Cottrell plot obtained from the chronoamperometry (first cycle). Step 1= 0.35 V and Step 2= -0.1 V vs Ag/AgCl. Measurements conducted in light at 30°C (pH 7.30 -7.40). Devices were inoculated with the same amount of biomass; however, the density of attached cells might differ.

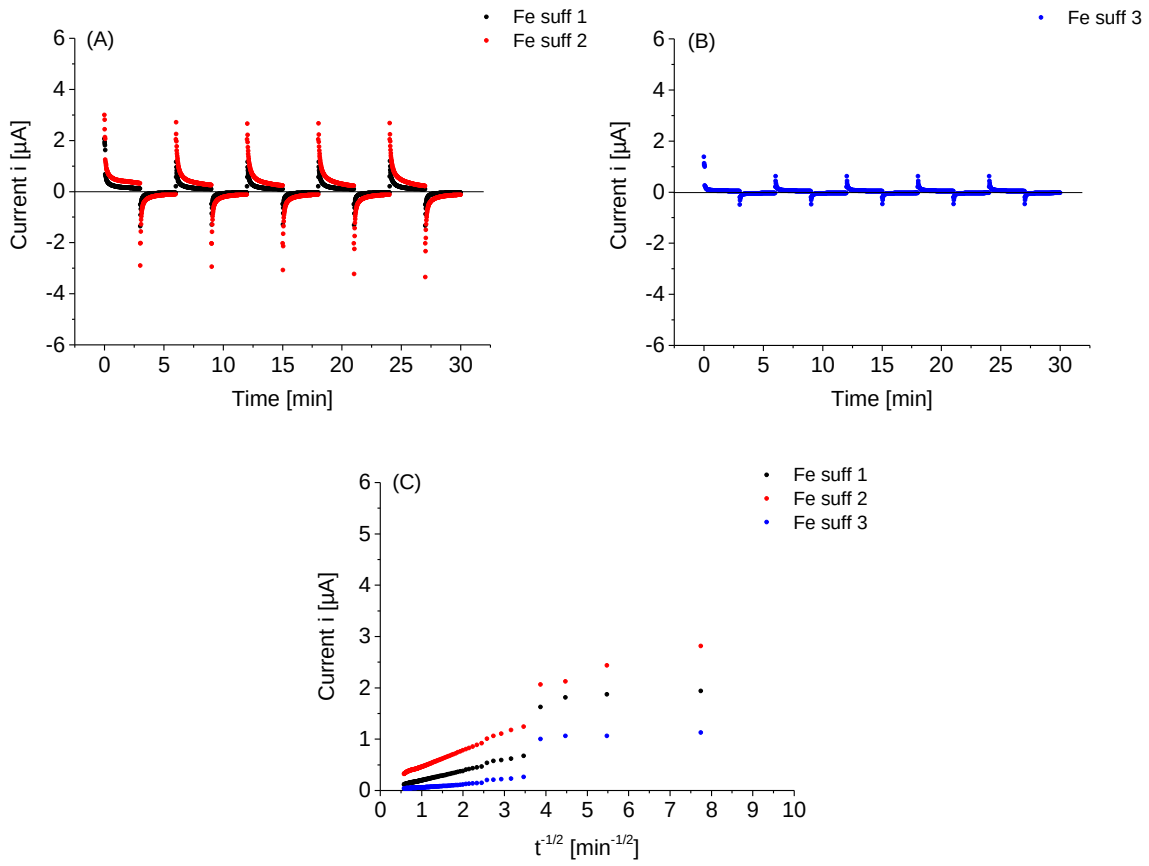

Figure 6-13. Two step potential chronoamperometry obtained from PCC7942 biofilm in iron sufficiency (A) under illumination and (B) in darkness. (C) Cottrell plot obtained from the chronoamperometry (first cycle). Step 1= 0.35 V and Step 2= -0.1 V vs Ag/AgCl. Measurements conducted in light at 30°C (pH 7.30 -7.40). Devices were inoculated with the same amount of biomass; however, the density of attached cells might differ.

Initially, fresh biofilms were reduced and by applying a sudden oxidising potential (step 1) an initial large current is seen, because all redox complexes are instantaneously oxidised. The initial current can be considered proportional to the catalytic rate of redox centres in the cell surface, therefore also to their concentration (assuming a similar electron pool is available). Currents then decreased in a diffusion-limiting-like curve, to some extent proportional to $t^{-1/2}$ (Figure 6-12 (C) and Figure 6-13 (C)) currents did not tend to zero, similarly to the chronoamperometry of soluble redox species in agitated systems (Chapter 1 – Figure 1-16), indicating that under the activity of the exoelectrogenic pathway electrons were continuously supplied. On average, the iron limited biofilm showed 2.2-fold higher peak current in respect to the iron sufficient biofilm, while the average discharging currents stabilised around 0.36 µA, 2.1-fold higher.

In the dark, the initial current was similar to those in the light for the iron limited biofilm, while for the iron sufficient biofilm there was a low initial current which rapidly decreased tending to zero, confirming the previous observation in mediatorless BPV device, the ferricyanide assay and cyclic voltammetry.

"Step 2" showed a negative initial current of the same magnitude to that for "Step 1", demonstrating a similar stoichiometry. Redox centres became oxidised (anodic current) and reduced (cathodic current) in response to the sudden potential change. The recharging current tended to zero as electrons were not consumed intracellularly in the short time measurement. Biofilms were discharged and recharged in successive cycles showing a repeated pattern, demonstrating the reversibility of the reaction(s). This method provides a tool which is rapid, hence avoiding complex processes occurring in the biofilm. One cycle only lasting 6 minutes, although a second cycle should be applied to confirm the response.

As previously mentioned, biomass density in the biofilm could not be finely controlled, therefore a quantitative comparison in relation to the initial currents has a margin of error, but it is an indication of the exoelectrogenic activity of a given biofilm and iron limited biofilms showed larger current. Interestingly, the proteomic study presented in Appendix C showed that iron limitation (16 days) upregulated those proteins potentially related to an exoelectrogenic pathway, IrpA and SomB1, with the overexpression at protein level in the same order of magnitude than the differential currents in the chronoamperometry measurements. The latter should be proportional to the concentration of redox complexes in the biofilm. The identification of redox complexes in the outer membrane of PCC7942 will be necessary to adequately characterise and quantify the electrochemical response observed.

These results are novel in showing that extracellular reductive activity in wild-type cyanobacteria, associated to a specific metabolic condition (iron limitation), was detected using conventional electrochemical techniques.

6.5 Conclusions

In this chapter, an analytic electrochemical approach was taken in order to understand the exoelectrogenic activity observed in mediatorless systems, providing information to develop analytical tools which can serve for the screening of different cyanobacterial strains, as well as for the selection of electrode materials.

Cyclic voltammetry studies, which traditionally have been used to characterise exoelectrogenic bacteria, proved that voltammetry can be used in biofilms of freshwater cyanobacteria. Double step potential was shown for the first time for biofilms of cyanobacteria, showing not only a reactive biofilm as electron donor but also as electron acceptor (same stoichiometry). Nonetheless, the preparation of the biofilm as described in this chapter, involving a good aeration and illumination, is necessary to obtain a healthy reactive biofilm.

The enhanced exoelectrogenic capacity induced by iron limited growth was detected by these techniques in the absence of artificial redox mediators, demonstrating that the more exoelectrogenic systems are distinguished and confirming that the iron-induced higher exoelectrogenic occurs at outer membrane level. Likewise, iron sufficient biofilms in the dark consistently presented very low reactivity, correlating with the results obtained from other techniques. Although, to quantify the response, a way to control biomass density within the biofilm will be necessary.

ITO-coated glass was confirmed through cyclic voltammetry to be a better electrode material than carbon felt and carbon paper, the latter showed large activation overpotential losses when fostering iron sufficient biofilms. An electroactive region around 0.22 V vs Ag/AgCl was found to generate higher currents. Carbon felt and ITO-coated glass was found to have a similar electrochemical profile when reacting with iron limited biofilms, demonstrating that iron limited PCC7942 improved the electrical interaction with carbon felt, a material showing a large activation loss if inoculated with iron sufficient biofilms.

Double step potential measurements showed that in a time slap of 6 minutes, a biofilm can be characterised, provided that the step potentials are defined. Nonetheless, any step potential of interest can be tested.

The findings presented in this chapter represent an important advancement in cyanobacteria based BPV development. To further develop this system, the identification of the proteins involved in the redirection of electrons is primordial to design systems targeting PCC7942 redox complexes in the outer membrane.

Chapter 7 General Conclusions

Photo-bioelectricity generated by cyanobacteria in BPV platforms offers a sustainable technology to recover energy from photo-bioprocesses. However, photo-bioelectricity generation is in early stages of development and advancements in different aspects of the BPV platform are necessary. In this thesis, a detailed study on some of the factors influencing the BPV performance was conducted.

Mediatorless systems are preferred because of sustainability issues, which led to the study of the direct electron transfer between the photosynthetic microorganism and the electrode, but differently to well-known exoelectrogens like *S. oneidensis*, little knowledge exists on how this interaction occurs in cyanobacteria. The work presented in this thesis has corroborated that the cyanobacterium *Synechococcus elongatus* PCC7942, in normal growth conditions, has limited capacity in generating an extracellular electron flow. The latter was seen in mediatorless BPV devices and in ferricyanide reduction (FeCN-R) capacity. The microalgae *C. vulgaris* showed that it was capable of higher FeCN-R rates than PCC7942 and therefore it is a better exoelectrogen, although in a mediatorless BPV device was outperformed by PCC7942. As mediatorless platforms are more sustainable, these results are promising, considering that cyanobacteria are preferred in biotechnological applications. Nonetheless, power output in the BPV devices needs to be improved, which requires higher cyanobacterial exoelectrogenic capacity. Increasing cyanobacteria exoelectrogenic capacity was the main objective of the investigation presented in this thesis.

The exoelectrogenic capacity of PCC7942, as FeCN-R rates, was improved by changing cultural conditions. Iron limited growth greatly enhanced PCC7942 exoelectrogenesis, with 24-fold increase in FeCN-R rates measured at pH 7.0, after fourteen days growing in iron limitation and in alkaline conditions. The FeCN-R rates obtained are unprecedented for cyanobacteria. The influence of the cultural pH in the exoelectrogenic activity proved to be relevant, therefore pH has to be considered in the optimisation of a BPV device inoculated with PCC7942. The latter was demonstrated in a ferricyanide mediated BPV platform (Chapter 4). Lower pH values also have a positive impact in the air cathode potential, therefore the conditions found for higher exoelectrogenic capacity in PCC7942 are better operational parameters for both, anode and cathode. However, neutral pH is not optimal for biomass growth, as it was verified in Chapter 5, PCC7942 growth rate at neutral pH was lowered in air grown cultures.

Remarkably, the performance of iron limited biofilms in mediatorless BPV devices was also improved, indicating that the iron-deficiency-induced exoelectrogenic pathways acts at outer membrane level, with direct electron transfer to a solid substrate (electrode).

The state of iron starvation was seen in the overexpression of the outer membrane proteins and some proteins in the plasma membrane of iron limited grown PCC7942 (in air). This study is presented in Appendix C. Particularly, irpA in the plasma membrane and the porin somB1 were overexpressed (approximately 2-fold). These proteins have been proposed to participate in a novel iron acquisition system involving irpB, a soluble cytochrome, and ftr1, a plasma membrane ferrous transporter. These iron-deficiency-induced proteins could be taking part in the exoelectrogenic pathway. Superoxide generation to reduce ferric, as seen in other cyanobacteria, was proved not to be the mechanism by which PCC7942 reduced ferricyanide.

PCC7942 demonstrated endurance to iron limitation, with growth rates similar to those cultures grown in iron sufficient conditions for the time frame studied. Microalgae *C. vulgaris* showed the symptoms of iron limitation after eight days (in air), while the cyanobacterium *Synechocystis sp.* PCC6803 was not suitable to be studied in iron limitation as growth and photosynthetic activity were severely affected. This comparison establishes that PCC7942 is a good candidate to operate in iron limited conditions, without disregarding that in the long term, iron limitation is detrimental for cellular activity.

In another approach to condition PCC7942, cultures under high (5%) and extremely high (20%) CO_2 partial pressure were studied in Chapter 5. A clear synergetic effect between iron limited growth and CO_2 enriched atmosphere was found, with a rapid enhancement in the exoelectrogenic activity of PCC7942. After only 2 days, FeCN-R rates were significantly higher for iron limited cultures grown under 20%CO_2. The synergetic effect also occurred in iron limited cultures grown under 5%CO_2, although the higher exoelectrogenic rates were triggered earlier under 20%CO_2. The symptoms of iron starvation, biomass growth and chlorophyll content diminution, were rapidly seen in iron limited PCC7942 grown in enriched CO_2. Therefore, it is possible to conclude that the effect of CO_2 enrichment in iron limited PCC7942 was related to a higher iron demand. The latter confirmed that the enhanced exoelectrogenic capacity in iron limited PCC7942 was triggered by the iron starvation state. Besides, iron sufficient cultures grown under CO_2 enrichment also showed higher FeCN-R rates than the iron sufficient cultures grown in air, therefore the sole effect of CO_2 over exoelectrogenesis is positive. Albeit, it is the iron limited condition the state that triggers the exceptionally high rates.

Growth under enriched CO_2 is sustained at relative higher rates in slightly acidic pH (in the range of pH 6.0 to 7.0), with biomass growth being higher under 5%CO_2. Another positive outcome from rising the CO_2 content was that the higher FeCN-R rates, thus exoelectrogenesis, occurred at the same pH values as the pH cultures were growing.

Power generation in a ferricyanide mediated BPV device running under 20%CO_2, inoculated with iron limited PCC7972, performed as well as under air. In the dark, the performance of 20%CO_2 system was better than in air. The latter is an important finding within the BPV research field. It has been suggested that CO_2 fixation should be inhibited to reach higher photosynthesis driven exoelectrogenesis. However, CO_2 has an overall positive effect over the generation of electricity by PCC7942.

The improved exoelectrogenic capacity of PCC7942 grown in iron limitation was well established with ferricyanide as the extracellular electron shuttle, but also in mediatorless platforms iron limited PCC7942 biofilms were able to maintain higher currents. In the long term, it appeared that iron limited exoelectrogenesis tended to the level of dark exoelectrogenic activity. The latter still provides a large improvement in the system, as in a daylight/dark cycle the dark phase comprises around half of the operation time. Nonetheless, to maintain the higher redirection of electrons from photosynthetic activity, as well as to maintain cellular viability, are future challenges which could involve the optimisation of iron feed to the iron starved cultures/biofilms in a controlled way.

The generation of more exoelectrogenic PCC7942 biofilms enabled the electrochemical characterisation of this cyanobacteria, finding two electroactive regions of interest, around 0.10 V and around 0.22 V vs Ag/AgCl. The reversibility of the electrochemical interaction was established, demonstrating that PCC7942 cells are also able to accept electrons from an electrode.

The electrochemical characterisation by conventional techniques is important for the selection and engineering of the photo-bioanode. Iron limited PCC7942 provides a robust cyanobacteria to engineer the photo-bioanode. For instance, although carbon materials showed setbacks in their performances, using iron limited biofilms provided better electrical interaction with carbon felt, which was observed in the voltammetry measurements. Other electrodes materials could be screened using iron limited PCC7942.

Overall, an enhanced mediatorless exoelectrogenesis in wild-type cyanobacteria is a milestone in the investigation of photo-bioelectricity generation. Iron starvation, which is exacerbated in a CO_2 enriched atmosphere, is set to be a promising strategy to bring PCC7942 cultures to an exoelectrogenic state, which can be used in sustainable mediatorless BPV platforms.

Chapter 8 Future work recommendations

The work presented in this thesis highlights the capacity of the model cyanobacterium PCC7942 to perform high rates of extracellular electron transfer in iron starved conditions. It is imperative that the research move forwards in the identification of the metabolic processes involved in this response. Various iron-deficiency-induced proteins have been identified, with a set of proteins believed to participate in iron uptake (somB1, irpAB and ftr1). The study presented in Appendix C confirmed the overexpression of somB1 and irpA. However, irpB is the cytochrome of the set, which did not appear in the membrane fraction, because is a soluble cytochrome. To study the cellular location of irpB in PCC7942 is important to unveil its participation in ferricyanide reduction. The latter could be achieved by selectively releasing periplasmic proteins, also the knockout of irpAB should be conducted to evaluate the exoelectrogenic activity in absence of irpB. The overexpression in iron limited growth of extracellular proteins with the SLH domain was also observed. Although there is no indication of redox moieties in these proteins, the knockout of their genes should be carried out to study their possible participation in direct electron transfer (mediatorless).

Once the proteins involved in the exoelectrogenic pathway are identified, the development of a strain which is capable of high rates of extracellular electron transfer in iron sufficient conditions can be engineered. However, the engineering of a strain can be an arduous task, besides there are restrictions in using genetically modified microorganisms in field applications. Alternatively, it is also possible to engineer the process by which PCC7942 is fed, conditioning the culture to reach an iron-deficiency state, to then feed iron as ferrous in small quantities in order to keep cellular activity, but without feeding enough for the cells to lose the iron starved state.

Another important continuation of the work presented in this thesis is the screening and identification of other cyanobacterial strain, which can be carried out using cyclic voltammetry and double step potential chronoamperometry. In particular, marine species are of great interest, due to lower ohmic losses associated to the resistivity of the electrolyte (seawater). To screen for strains with the same response to iron limited growth is also a viable approach. The latter can be conducted through genomic studies, searching for strains coding the IrpAB operon.

The efficiency of the BPV platform requires improved design as well. The selection of electrode materials is a critical aspect of the technology and to find cost effective materials is a challenge ahead. The design of the platform should consider inexpensive electrode materials like carbon fibres, however the hydrophobicity of these need to be overcome. Techniques to change the surface

chemistry of carbon materials different to addition of oxygen groups should be explored. Composites with polymers, including redox active polymers, are materials being studied in photo-electricity generation and they should be tested using iron starved PCC7942. An important result presented in this thesis is the electrochemical characterisation of photo-bioanodes fostering PCC7942. The detection of electroactive regions allows an informed decision in selecting the anode material, therefore biofilms in iron limited conditions should be used to screen for suitable electrode materials with lower activation overpotentials.

The integration of bioelectricity generation and mitigation of CO_2 is to be explored in long term studies. The findings expounded in this thesis set a new line of research in utilising high content of CO_2 to trigger PCC7942 exoelectrogenic activity, as well as to generate electricity in the presence of a CO_2 enriched atmosphere. A CO_2 content of 5% is the most promising in terms of biomass growth and cultural pH. The latter can be controlled using CO_2 as the buffering agent. Varying the percentage of CO_2 to maintain the pH at 7.0 would be dependent of the culture biomass density, initially a lower CO_2 content might be necessary, but as the culture grows dense a CO_2 content higher than 5% should be set. The CO_2 feed could be controlled by a plc (programmable logic controller) connected to the cultural pH measurement.

Integrating photo-bioprocesses with exoelectrogenic cyanobacteria will produce photosynthetic biomass alongside energy recovery. High CO_2 content (5%) increases biomass productivity. This biomass can then be harvested to recover valuable products. Particularly, iron starvation in PCC7942 has also been associated to an increment in the lipid content, which are suitable for biodiesel production. Figure 8-1 illustrates the proposed integrated system.

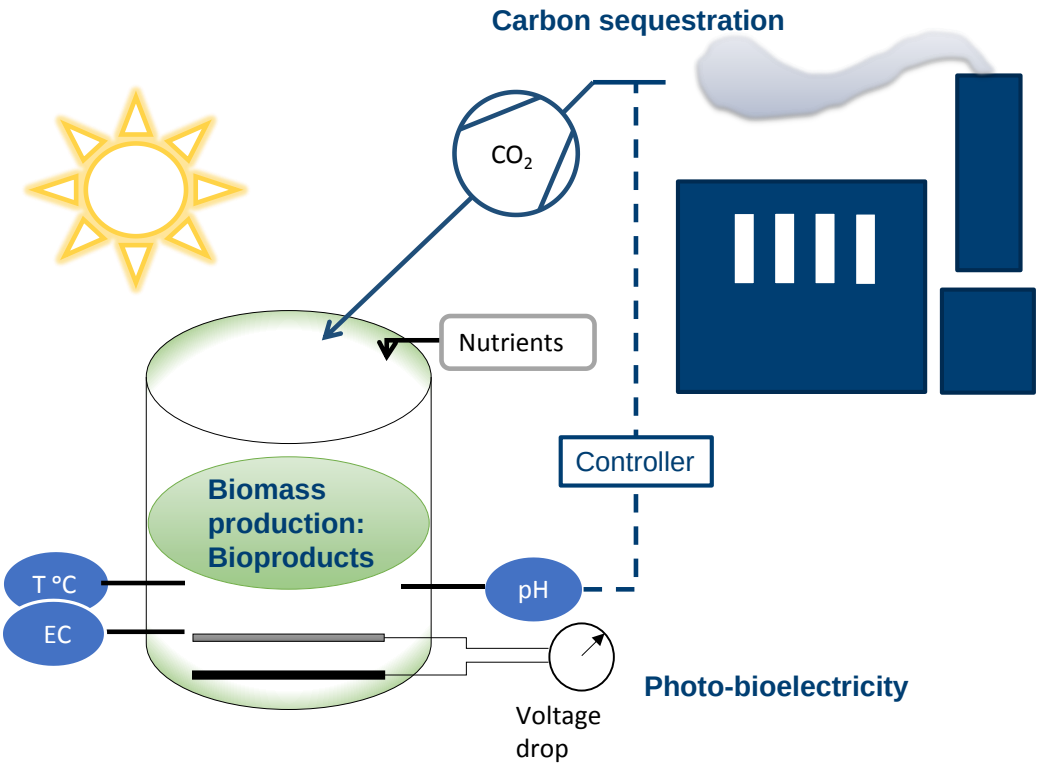

Figure 8-1. Schematics of proposed integrated photo-bioreactor for cyanobacterial biomass growth, CO_2 mitigation and simultaneous electricity generation. Biomass is harvested to extract lipids for biodiesel production. The CO_2 feed is controlled by the cultural pH measurement.

Appendix A Prices of electrode and membrane materials

Table A-1 shows the price of electrode and membrane materials used in the fabrication of the bioelectrochemical cells presented in this thesis.

	Price per cm^2	Supplier
ITO-coated glass	£1.22	Sigma Aldrich
Nafion® membrane	£0.48	Sigma Aldrich
Carbon felt	£0.056	Alfa Aesar
Carbon paper	£0.28	Alfa Aesar
Nitrocellulose membrane	£0.021	Sigma Aldrich
Air cathode	£0.64	Alga Aesar

Table A-1. Prices of materials used for electrode and membranes in the fabrication of the bioelectrochemical devices.

Appendix B Blank and supernatant measurements

The reduction capacity of blanks and supernatants in which the ferricyanide assay and XTT assay were conducted is presented in this Appendix.

Table B-1 and Table B-2 summarise the conversion of ferricyanide in BG11 and modifications and in BG11(-)x3 amended with 10 mM of HEPES (buffer) respectively.

	Ferricyanide conversion %		
Time [min]	**BG11(-)**	**BG11**	**BG11(-)x3**
0	0.00	0.00	0.00
10	0.22	0.00	0.10
30	0.43	0.26	0.00
120	2.48	1.44	-0.83

Table B-1. Ferricyanide reduction in medium BG11 and modifications. BG11(-) lack ferric. BG11(-)x3 lacks ferric, EDTA and citric acid. Ferricyanide was added at time zero at a concentration of 1 mM.

	Ferricyanide conversion %	
Time [min]	**Light**	**Dark**
0	0.00	0.00
10	-0.28±0.20	-0.47±0.67
30	-0.28±0.22	-0.67±0.68
120	0.93±0.13	-1.78±0.76

Table B-2. Ferricyanide reduction in BG11(-)x3 (lacking ferric, EDTA and citric acid) amended with 10 mM of HEPES. Ferricyanide was added at time zero at a concentration of 1 mM.

Table B-3 shows the conversion of ferricyanide in supernatant collected from PCC7942 as part of the iron limitation study.

	Ferricyanide conversion %			
	Day 2		**Day 10**	
Time [min]	**Fe lim**	**Fe suff**	**Fe lim**	**Fe suff**
0	0.00	0.00	0.00	0.00
10	0.25±0.07	0.38±0.06	0.86±0.03	1.12±0.10
30	0.11±0.05	0.21±0.09	1.37±0.03	1.73±0.16
120	0.25±0.24	0.35±0.11	0.85±0.24	1.63±0.37

Table B-3. Ferricyanide reduction in supernatant obtained from PCC7942 cultures in iron limited and iron sufficient growth. Ferricyanide was added at time zero at a concentration of 1 mM.

Table B-4 presents the blank for the XTT assay.

	Formazan (XTT reduction product) [µM]	
Time [min]	**pH 7**	**pH 10**
0	0.00	0.00
10	0.09±0.00	0.23±0.00
30	0.09±0.00	0.23±0.00
120	0.09±0.00	0.21±0.02

Table B-4. XTT reduction in BG11(-)x3 (lacking ferric, EDTA and citric acid) amended with 10 mM HEPES. XTT was added at time zero at a concentration of 150 µM.

Appendix C Plasma membrane and outer membrane proteins in PCC7942

C.1. Outer membrane associated proteins annotation and prediction

The outer membrane (OM) like other biological membranes consists of a bilayer of lipids. Lipid bilayers present little permeability to hydrophilic compounds, thus to most of the nutrients. The permeability of the OM to nutrients and excretes is through porins, protein diffusion channels.[254] About 50% of the OM mass corresponds to integral-membrane proteins, with more than a dozen different outer membrane proteins (OMP) identified in *E. coli*.[255] Within different functions, OMPs are general non-specific porins, substrate-specific porins, membrane-integral enzymes, TonB-dependent receptors, or small membrane anchor proteins.[255]

The lipid bilayer membrane is hydrophobic, consequently membrane integral proteins expose a hydrophobic surface towards the bilayer core, a property which sets them apart from soluble proteins. The hydrophobic environment in the bilayer also implies that maximum hydrogen bonds in the embedded protein segment are formed, therefore only regular secondary structures (α-helices and β-sheets) can occur within the lipid bilayer in order to saturate the entire hydrogen-bonding chain. All membrane integral proteins characterised are accordingly α-helical bundles or β-pleated sheets forming a barrel (β-barrels). These structures correlate with the protein's location, α-helical bundles are found in the plasma membranes, while β-barrels are restricted to the outer membrane. It is believed that this differentiation lies on the biogenesis of OMPs, which have to cross the plasma membrane.[255]

The recent OMPs prediction software PRED-TMBB2[256] has based their model in a HMM architecture, which consists of three sub-models that correspond to periplasmic loops, transmembrane β-strands and extracellular loops, with both the N- and C-terminal in the periplasmic side. It also takes into account the length of the sequence, the number of predicted transmembrane strands, the presence of a signal peptide and the reliability of the prediction, as well as hits to OMPs database.[256,257] The signal peptide sequence is an extension of the N-terminal of newly synthesised secretory and membrane proteins.[258] PRED-TMBB2 offers a balance between sensitivity and specificity, allowing short computing times, thus a whole genome can be processed in only hours. The best methods to predict OMPs are also the slowest available and cannot be used to scan whole genomes in realistic timeframes.[256] HHomp[259] is a bioinformatics toolkit based on homology to a large database of known OMPs using sequence similarity (PSI-BLAST[260]), under the observation that most β-barrel OMPs are

related by common ancestry. HHomp outperforms PRED-TMBB2, however computing times are extensive.

Non-integral proteins associated to the OM cannot be predicted by OMP prediction softwares. The SLH (surface layer homology) domain is present in proteins exposed in the cell surface, thus proteins with the conserved SLH domain are associated to the extracellular side of the OM. SLH domain proteins are non-covalently anchored to the cell surface, specifically anchoring in the wall polysaccharide layers and proteins with SLH domain can be structural and essential for the cell shape, but also present enzymatic activiy.[261,262] The FAS1/BIgH3 domain is an extracellular module involved in cell adhesion (http://www.ebi.ac.uk/interpro/entry/IPR000782). Likewise, in the periplasmic side, there are proteins which are anchored to the OM. The functional/structural annotation of some of these proteins is known, and a list can be extracted from genomic databases. PCC7942 genome can be found in Cyanobase (http://genome.annotation.jp/cyanobase/SYNPCC7942) or alternative UniProtKB (http://www.uniprot.org/taxonomy/1140). Table C-1 presents a list of the annotated proteins in PCC7942, which have been identified as OM associated proteins.

Description	Protein name	Conserved Domain	GO annotation: Cellular component
Probable porin GN=Synpcc7942_1463	SomB1	SLH	integral component of membrane
Probable porin GN=Synpcc7942_1464	SomA1	SLH	integral component of membrane
Probable porin major outer membrane protein GN=Synpcc7942_1607	SomA2	SLH	integral component of membrane
Outer envelope membrane protein GN=Synpcc7942_0928		POTRA	outer membrane
Probable porin major outer membrane protein GN=Synpcc7942_1635	SomB2	SLH	integral component of membrane
Uncharacterized protein GN= Synpcc7942_0443		SLH	
Uncharacterized protein GN=Synpcc7942_1417		SLH	
Extracellular solute-binding protein, family 3 GN=Synpcc7942_0246		PBPb	outer membrane-bounded periplasmic space
Extracellular solute-binding protein, family 3 GN=Synpcc7942_0076		PBPb	outer membrane-bounded periplasmic space
Extracellular solute-binding protein, family 3 GN=Synpcc7942_1276		PBPb	outer membrane-bounded periplasmic space
Sulphate-binding protein GN=Synpcc7942_1681	sbpA		outer membrane-bounded periplasmic space
Thiosulphate-binding protein GN=Synpcc7942_1722			outer membrane-bounded periplasmic space
Thiosulphate-binding protein GN=Synpcc7942_1686			outer membrane-bounded periplasmic space

Description	Protein name	Conserved Domain	GO annotation: Cellular component
Uncharacterized protein GN=Synpcc7942_1695			outer membrane-bounded periplasmic space
ATPase GN= Synpcc7942_0427	sek0043		outer membrane-bounded periplasmic space
Probable membrane-bound lytic transglycosylase A GN=Synpcc7942_0392			outer membrane
Molybdenum ABC transporter, periplasmic molybdate-binding protein GN=Synpcc7942_1531			outer membrane-bounded periplasmic space
General secretion pathway protein D GN=Synpcc7942_2450			outer membrane
Beta-Ig-H3/fasciclin GN=Synpcc7942_1606		FAS1/BIgH3	extracellular space
Uncharacterized protein GN=Synpcc7942_1128		DUF4214 Peptidase-M10	extracellular space

Table C-1. Annotated outer membrane associated protein in PCC7942. Data was obtained from UniProtKB and Cyanobase.

C.2. Outer membrane proteins in PCC7942

It has been seen that mediatorless electron transfer by PCC7942 biofilms occur. To investigate the protein composition of the outer membrane of PCC7942, its genome was analysed with the outer membrane predictor PRED-TMBB2,[256] in order to obtain a list of possible outer membrane proteins. The output was then curated with the more selective outer membrane softer predictor HHomp.[259] Table C-2 summarises the list of possible outer membrane proteins.

Protein ID *Name*	Seq. length	Predicted signal peptide	Beta-barrel score (cut-off is 0.43)	OMPdb family	#TM predicted	Reliability	HHOMP
Synpcc7942_0119	185	1-23	0.477		6	0.703	**No hits found**
Synpcc7942_0317	152	1-26	0.891		4	0.894	**23.49%**
Synpcc7942_0318	151	1-23	0.769		4	0.856	**20.58%**
Synpcc7942_0769	300	1-25	0.450		6	0.807	**51.26%**
Synpcc7942_0904	181	1-21	0.988		8	0.929	**0.48%**
Synpcc7942_0905	180	1-29	0.896		4	0.872	**2.94%**
Synpcc7942_0928	721	1-106	1.000	The OMP Insertion Porin OmpIP/Omp85 Family	16	0.938	**100%**
Synpcc7942_1069	242	1-34	0.541		2	0.842	**No hits found**
Synpcc7942_1195	166	1-20	0.449		2	0.794	**No hits found**
Synpcc7942_1337	1434	1-24	1.000		2	0.962	**0.58%**
Synpcc7942_1463 *SomB*	543	1-23	1.000	The Glucose-selective OprB	18	0.917	**100%**

Protein ID *Name*	**Seq. length**	**Predicted signal peptide**	**Beta-barrel score (cut-off is 0.43)**	**OMPdb family**	**#TM predicted**	**Reliability**	**HHOMP**
				Porin (OprB) Family			
Synpcc7942_1464 *SomA*	531	1-24	1.000	The Glucose-selective OprB Porin (OprB) Family	18	0.925	**100%**
Synpcc7942_1607 *SomA2*	518	1-24	1.000	The Glucose-selective OprB Porin (OprB) Family	18	0.92	**100%**
Synpcc7942_1626	160	1-22	0.690		2	0.891	**No hits found**
Synpcc7942_1632	169	1-26	0.436		4	0.942	**1.28%**
Synpcc7942_1635 *SomB2*	548	1-25	1.000	The Glucose-selective OprB Porin (OprB) Family	16	0.869	**100%**
Synpcc7942_1654	127	1-20	0.841		4	0.867	**No hits found**
Synpcc7942_1706	730	1-84	0.964		6	0.978	**97.40%**
Synpcc7942_1761	576		1.000	The Outer Membrane Factor (OMF) Family	6	0.926	**100%**
Synpcc7942_1788	1568		0.999		6	0.962	**15.27%**
Synpcc7942_1946	159	1-26	0.606		4	0.851	**13.63%**
Synpcc7942_2037	214		0.443		10	0.836	**No hits found**
Synpcc7942_2108	122		0.599		4	0.797	**No hits found**
Synpcc7942_2163	162	1-24	0.611		2	0.846	**34.99%**
Synpcc7942_2281	318	1-50	0.732		10	0.769	**No hits found**
Synpcc7942_2292	754		0.508		24	0.877	**No hits found**
Synpcc7942_2295	367	1-27	0.694		12	0.78	**No hits found**
Synpcc7942_2594	203		0.622		4	0.824	**No hits found**
Synpcc7942_B2635	319	1-26	1.000		14	0.899	**99.26%**

Table C-2. Prediction of outer membrane proteins according to PRED-TMBB2[256] and HHOMP.[259]

Twenty-nine proteins presented admissible beta-barrel scores. Most of them also presented signal peptide domain. Its absence could be due to post-transcriptional modifications. The HHOMP predictor showed eight proteins with a probability over 97%, one in the order of 50% and six between 10% and 35%. There are three OMPs identified for the first time, with a probability >97% (HHomp), these are Synpcc7942_1761, Synpcc7942_1654 and Synpcc7942_B2635. Synpcc7942_1761 was found to be homologous to the outer membrane factor (OMF) family in the output of the prediction software

PRED-TMBB2.[256] Proteins from the OMF family function in conjunction with plasma membrane proteins for substrate export (http://www.tcdb.org/search/result.php?tc=1.B.17). Synpcc7942_1654 is a OstA and DUF3769 domain-containing protein, according to the NCBI conserved domains tool (https://www.ncbi.nlm.nih.gov/Structure/cdd/wrpsb.cgi). OstA-like proteins are mostly uncharacterised. DUF3769 is a superfamily of proteins of unknown function found in bacteria and eukaryotes. Synpcc7942_B2635, also known as ANL06, do not present any conserved domain. Nonetheless, Synpcc7942_B2635 is encoded in the large endogenous plasmid pANL present in PCC7942, which is associated to sulphur metabolism, thus Synpcc7942_B2635 is likely to be related to sulphur uptake.[260] No oxidoreductase domain was found in any of the identified OMPs.

C.3. Proteomics of enriched outer membrane fraction of PCC7942

To analyse the effects of iron limited growth in the plasma membrane and outer membrane of PCC7942, a proteomic study was conducted.

A protocol to separate and purify the three membrane fractions was developed for the cyanobacterium *Synechocystis sp.* PCC6803.[139,263] The latter was conducted in PCC7942 membrane fractions as described in Chapter 2 – Section 2.12, in collaboration with Prof B. Norling and Dr L. Zhang in the School of Biological Sciences, Nanyang Technological University. Only partial separation was achieved. An enriched fraction still contains all membrane proteins, thylakoid, plasma membrane and outer membrane. However, enriching the sample with outer membrane allowed to enlarge the relative abundance of outer membrane proteins to be detected in the proteomics study.

To study differential expression proteins of interest, it was assumed that membrane cross-contamination occurred evenly. Relative abundance of proteins was estimated in proportion to chosen housekeeping proteins (invariant for the condition studied). Due to the experimental error associated to cross-contamination, a cut-off value of 1.5 for overexpression and 0.7 for underexpression were considered as significantly different.

Proteomics was performed in samples from iron sufficient and iron limited cultures (16 days old). For the outer membrane, total protein was normalised in respect to three proteins: SomA1, a porin which was reported to not change under iron starvation,[197] the outer envelope membrane Synpcc7942_0928 and the outer membrane protein Synpcc7942_1761 (OMF). Table C-3 summarises the differential expression of the outer membrane proteins exposed to the extracellular space, and Table C-4 summarises the differential expression of outer membrane associated proteins in the

periplasmic space. Shaded cells correspond to those proteins showing a differential expression change.

Description	Protein name	Fe limited	Fe sufficient	Fold Change Fe(-)/Fe(+)
Probable porin GN=Synpcc7942_1464	SomA1	307.92±12.1	287.88±5.7	1.07
Outer envelope membrane protein GN=Synpcc7942_0928		357.12±6.5	407.61±3.6	0.88
Uncharacterised protein GN=Synpcc7942_1761	OMF	334.96±5.6	304.51±9.3	1.10
Uncharacterised protein GN=Synpcc7942_1706		116.31±8.84	99.29±0.63	1.17
Probable porin GN=Synpcc7942_1463	SomB1	5.62±0.094	2.43±0.001	2.31
Probable porin major outer membrane protein GN=Synpcc7942_1607	SomA2	274.78±13.1	63.03±3.9	4.36
Probable porin major outer membrane protein GN=Synpcc7942_1635	SomB2	122.82±4.8	189.12±2.2	0.65
SLH Uncharacterized protein GN=Synpcc7942_0443		678.59±66.6	388.68±6.3	1.75
SLH Uncharacterized protein GN=Synpcc7942_1417		25.20±1.9	15.16±0.5	1.66
Beta-Ig-H3/fasciclin GN=Synpcc7942_1606		103.83±9.7	50.98±2.1	2.04
Hypothetical protein GN=Synpcc7942_B2635		34.47±3.2	25.51±0.1	1.35
Uncharacterised protein GN=Synpcc7942_1128		23.57±0.25	21.38±0.16	1.10

Table C-3. Differential expression of iron limited PCC7942 outer membrane proteins exposed to the extracellular side.

Description	Protein name	Fe limited	Fe sufficient	Fold Change Fe(-)/Fe(+)
Extracellular solute-binding protein, family 3 GN=Synpcc7942_0246		285.29±31.6	154.04±1.4	1.85
Uncharacterised protein GN=Synpcc7942_1695		117.55±10.3	96.70±6.1	1.22
Thiosulphate-binding protein GN=Synpcc7942_1722		14.10±0.59	17.85±0.13	0.79
Thiosulphate-binding protein GN=Synpcc7942_1686		22.13±0.002	21.26±0.17	1.04
ATPase GN=Synpcc7942_0427	sek0043	7.18±0.63	4.54±0.36	1.58
Sulfate-binding protein GN= Synpcc7942_1681	sbpA	183.87±17.2	137.66±2.7	1.34
Uncharacterised protein GN=Synpcc7942_1128		23.57±0.25	21.38±0.16	1.10
General secretion pathway protein D GN=Synpcc7942_2450		225.68±11.0	203.53±12.4	1.11
Probable membrane-bound lytic transglycosylase A GN=Synpcc7942_0392		30.79±1.3	23.44±0.18	1.31

Table C-4. Differential expression of iron limited PCC7942 outer membrane proteins exposed to the periplasmic side.

Within extracellular exposed proteins (Table C-3), the overexpression of porins SomA2 and SomB1, plus the two uncharacterised SLH proteins and the Beta-Ig-H3/fasciclin protein was determined, while the porin SomB2 was underexpressed. The change in expression of the three porins confirms the changes in the transcriptomic study reported by *Nodop et al*,[197] as well as the overexpression of Beta-

Ig-H3/fasciclin confirms the change reported in the transcriptome study, but changes in the SLH proteins were not described. In the periplasmic side (Table C-4), the overexpression of the extracellular solute-binding protein and the ATPase was also determined, which were not described in the transcriptome study.

Changes in the outer membrane of iron limited PCC7942 cells reveal the adaptation for uptake of extracellular solutes and the energetic requirements for transport (ATPase activity), possibly related to iron complexes. Interestingly, SLH proteins and the Beta-Ig-H3/fasciclin protein were overexpressed. Changes in the extracellular layer of the outer membrane, particularly related to cell adhesion, could be related to the interaction of cells/biofilms with minerals, but also cell-cell communication. Relative protein abundance between SHL proteins shows a large difference. Synpcc7942_0443 is very abundant, very likely a structural SHL protein, while Synpcc7942_1417 have a much lower abundance, thus more likely with a non-structural function.

In the plasma membrane fraction, iron related proteins also experimented changes (Table C-5), but a clear overexpression was only found in futA2 and irpA. PCC7942 is a siderophore producing cyanobacterium and changes in the secretion and uptake capacity of ferric complexes was expected,[201] which is reflected in the overexpression of futA2, while irpA is also thought to participate in iron uptake. However, all iron related proteins in the plasma membrane showed upregulation in Nodop *et al.*[197] transcriptomic study. Table C-5 also shows those plasma membrane proteins (pstB, pacL and mgtE) utilised to normalise the relative abundance of iron related plasma membrane proteins.

Description	Protein name	Fe limited	Fe sufficient	Fold Change Fe(-)/Fe(+)
ATPase GN=Synpcc7942_1406	futC	17.48±0.085	14.80±0.15	1.18
Iron(III) ABC transporter permease protein GN=Synpcc7942_1407	furB	8.84±0.44	6.66±0.38	1.33
Membrane-associated protein GN=Synpcc7942_1408	mapA	4.23±0.25	4.54±0.0064	0.93
Iron transport system substrate-binding protein GN=Synpcc7942_1409	futA2	58.64±1.49	21.08±0.20	2.78
High-affinity iron transporter GN=Synpcc7942_2421	ftr1	2.26±0.034	1.87±0.069	1.21
Iron-regulated protein A GN= Synpcc7942_1462	irpA	3.22±0.19	1.71±0.21	1.88
Phosphate import ATP-binding protein PstB GN=Synpcc7942_2441	pstB	40.68±0.58	38.03±0.41	1.07
Calcium-transporting ATPase GN=Synpcc7942_1082	pacL	38.65±0.019	38.73±0.072	1.00
Magnesium transporter MgtE GN=Synpcc7942_1269	mgtE	20.67±0.60	23.23±0.33	0.89

Table C-5. Differential expression of iron limited PCC7942 plasma membrane proteins participating in iron transport.

Nodop *et al*.[197] transcriptome analysis of iron starved PCC7942 reported upregulation and downregulation of many proteins, including the mentioned transcripts of membrane proteins. The latter are presented in Table C-6 together with the proteomics results obtained in the current investigation. These two separate studies are not entirely comparable as growth conditions were different. The transcriptomics study showed higher growth rates and after 72 hours the growth rate and chlorophyll content of iron limited cultures was considerably lower than the control, showing the symptoms of iron starvation. Iron limited cultures of PCC7942 for the proteomics study were like those presented in Chapter 4. Therefore, growth and chlorophyll content were not significantly diminished in comparison with the iron sufficient condition. Nonetheless, the enhanced exoelectrogenic capacity of iron limited PCC7942 was observed for the conditions studied in this thesis, therefore the proteomics results can be correlated with higher exoelectrogenesis. Furthermore, the transcript expression levels (mRNA) do not necessarily indicate protein abundance due to translation elongation and protein degradation regulation.[264,265]

		Fold Change transcript[197]		**Fold Change protein**
Protein ID	**Protein name**	**24 hrs**	**72 hrs**	**This study**
Synpcc7942_1463	SomB1	22.78	17.87	2.31
Synpcc7942_1607	SomA2	6.11	4.53	4.36
Synpcc7942_1635	SomB2	0.50	0.57	0.65
Synpcc7942_1606	Beta-Ig-H3/fasciclin	2.10	1.08	2.04
Synpcc7942_1406	futC	2.07	1.65	1.18
Synpcc7942_1407	furB	5.46	3.63	1.33
Synpcc7942_1408	mapA	1.37	1.44	0.93
Synpcc7942_1409	futA2	2.50	2.08	2.78
Synpcc7942_2421	ftr1	2.85	3.27	1.21
Synpcc7942_1462	irpA	75.58	62.68	1.88
Synpcc7942_1461	irpB	51.63	46.21	-
Synpcc7942_1870	HlyD	1.95	2.04	1.35

Table C-6. Transcriptome of PCC7942 24 hrs and 72 hrs of iron starvation. Taken from Nodop *et al.*[197] Last column: proteomics of PCC7942 after 16 days of iron limited growth (this thesis).

In Nodop *et al.* [197] studies, SomB1 was the porin undergoing major changes (~20-fold change), which was not seen in the proteomics results with only 2.3-fold change. While the overexpression of SomA2 and the underexpression of SomB2, showed a similar fold change to those in the transcriptomic study. The permeability of the outer membrane was altered, but not to the same extent as suggested by the transcriptomics study. SomB1 is encoded immediately after the operon irpAB and under the same transcriptional factor idiB,[197] with irpA and irpB also showing a substantial change in their transcripts upregulation, ~70-fold and ~50-fold respectively, as reported in the transcriptomics study. The proteomics result for irpA only showed a 1.88-fold change, in accordance to the overexpression of SomB1. The cytochrome irpB was not found in any of the membrane fractions of PCC7942, indicating

that irpB is a soluble cytochrome which is not anchored in any way to the membranes, but it can be inferred from the overexpression of irpA and SomB1 that irpB was overexpressed around the same level.

Ftr1 is also part of this proposed iron acquisition system.[197] However, there was no evident overexpression of this protein. Ftr1 transcripts showed upregulation of ~3-fold change, very low compared with the transcripts of SomB1 and irpA. Ftr1 is regulated under the same transcription factor idiB, explaining that at protein level Ftr1 did not show a differential change. Nonetheless, the presence of ftr1 (ferrous permease) is an important evidence for an iron uptake reductive mechanism.

The function and location of irpB is still to be understood, but its participation in the enhanced exoelectrogenic activity of iron limited PCC7942 could be occurring because it is a protein with oxidoreductase capacity and it is part of an overexpressed operon involved in an iron acquisition system. In the case of such reductive mechanism, a 2-fold increase in cytochrome expression is low compared to the increase in FeCN-R rates (17-fold increase within neutral pH measurements, Chapter 4 – Section 4.2.2.1). Nonetheless, in the long term, photo-bioelectricity generation in mediatorless platforms (Chapter 4 – Section 4.4.2) and in mediated platforms (Chapter 5 – Section 5.3), showed that currents in the light decreased and tended to the magnitude of dark currents.

Changes in the porin composition at the outer membrane are not the cause of the higher electrochemical reactivity, because porins do not present oxidoreductase moieties. Nonetheless, two porins indirectly participate in the extracellular electron transfer observed in *Shewanella oneidensis* MR-1. MtrB is essential for the transfer of electron in the complex MtrABC.[242,243] Omp35 was proven to be necessary for normal growth of *S. oneidensis* grown with ferric complexes as extracellular electron acceptor in anaerobic conditions.[246] Two porins are upregulated by iron starvation in PCC7942. While it is true that these could be participating in ferric-siderophore transport, SomB1 association with irpAB suggest the possibility of a similar function to MtrB or Omp35.

Electrochemical activity in the plasma membrane and in the periplasmic space is a necessary step in cyanobacterial exoelectrogenesis. However, it does not explain the electrochemical activity detected in mediatorless systems.

The difficulty in identifying outer membrane proteins might imply that many proteins of unknown function were disregarded in the analysis, thus more advance prediction softwares, as well as improved outer membrane separation and purification methods, are necessary in order to make progress in the biochemical and electrochemical characterisation of PCC7942 outer membrane.

References

1 R. A. Betts, C. D. Jones, J. R. Knight, R. F. Keeling and J. J. Kennedy, *Nat. Clim. Chang.*, 2016, **6**, 806–810.

2 H. N. Chang, N. J. Kim, J. Kang and C. M. Jeong, *Biotechnol. Bioprocess Eng.*, 2010, **15**, 1–10.

3 *Research&Innovation European Commission*, 2012. At: http://ec.europa.eu/research/bioeconomy/index.cfm?pg=policy

4 F. L. Luo and Y. Hong, in *Renewable Energy Systems: Advance Conversion Technologies and Applications*, CRC Press, Taylor&Francis Group, New York, 2013, pp. 813–814.

5 P. McKendry, *Bioresour. Technol.*, 2002, **83**, 47–54.

6 A. E. Inglesby and A. C. Fisher, *Energy Environ. Sci.*, 2012, **5**, 7996.

7 K. Chandrasekhar, Y. Lee and D. Lee, *Int. J. Mol. Sci.*, 2015, **16**, 8266–8293.

8 N. Quintana, F. Van der Kooy, M. D. Van de Rhee, G. P. Voshol and R. Verpoorte, *Appl. Microbiol. Biotechnol.*, 2011, **91**, 471–90.

9 S. R. Subashchandrabose, B. Ramakrishnan, M. Megharaj, K. Venkateswarlu and R. Naidu, *Biotechnol. Adv.*, 2011, **29**, 896–907.

10 European Commission, Science for Environment Policy, *Futur. Briefs*, 2013.

11 M. Rosenbaum, M. a Cotta and L. T. Angenent, *Biotechnol. Bioeng.*, 2010, **105**, 880–8.

12 B. E. Logan, B. Hamelers, R. Rozendal, U. Schröder, J. Keller, S. Freguia, P. Aelterman, W. Verstraete and K. Rabaey, *Environ. Sci. Technol.*, 2006, **40**, 5181–92.

13 P. Bombelli, R. W. Bradley, A. M. Scott, A. J. Philips, A. J. McCormick, S. M. Cruz, A. Anderson, K. Yunus, D. S. Bendall, P. J. Cameron, J. M. Davies, A. G. Smith, C. J. Howe and A. C. Fisher, *Energy Environ. Sci.*, 2011, **4**, 4690.

14 A. J. McCormick, P. Bombelli, A. M. Scott, A. J. Philips, A. G. Smith, A. C. Fisher and C. J. Howe, *Energy Environ. Sci.*, 2011, **4**, 4699.

15 D. Leech, P. Kavanagh and W. Schuhmann, *Electrochim. Acta*, 2012, **84**, 223–234.

16 N. Lalaoui, K. Elouarzaki, A. Le Goff, M. Holzinger and S. Cosnier, *Chem. Commun.*, 2013, **49**, 9281–9283.

17 J. O. Calkins, Y. Umasankar, H. O'Neill and R. P. Ramasamy, *Energy Environ. Sci.*, 2013, **6**, 1891–1900.

18 H. A. Dewi, F. Meng, B. Sana, C. Guo, B. Norling, X. Chen and S. Lim, *RSC Adv.*, 2014, **4**, 48815.

19 M. Kato, J. Z. Zhang, N. Paul and E. Reisner, *Chem. Soc. Rev.*, 2014, **43**, 6485–97.

20 K. Hasan, R. D. Milton, M. Grattieri, T. Wang, M. Stephanz and S. D. Minteer, *ACS Catal.*, 2017, **7**, 2257–2265.

21 P. Majumdar, D. Pant and S. Patra, *Trends Biotechnol.*, 2017, 285–287.

22 R. Rozendal, H. Hamelers, G. Euverink, S. Metz and C. Buisman, *Int. J. Hydrogen Energy*, 2006, **31**, 1632–1640.

23 R. a. Rozendal, A. W. Jeremiasse, H. V. M. Hamelers and C. J. N. Buisman, *Environ. Sci. Technol.*, 2008, **42**, 629–634.

24 M. Villano, F. Aulenta, C. Ciucci, T. Ferri, A. Giuliano and M. Majone, *Bioresour. Technol.*, 2010, **101**, 3085–90.

25 R. I. Pinhassi, D. Kallmann, G. Saper, H. Dotan, A. Linkov, A. Kay, V. Liveanu, G. Schuster, N. Adir and A. Rothschild, *Nat. Commun.*, 2016, **7:12552**.

26 K. Tanaka, R. Tamamushi and T. Ogawa, *J. Chem. Technol. Biotechnol.*, 1985, **35B**, 191–197.

27 T. Yagishita, T. Horigome and K. Tanaka, *J. Chem. Technol. Biotechnol.*, 1993, **56**, 393–399.

28 M. Torimura, A. Miki, A. Wadano, K. Kano and T. Ikeda, *J. Electroanal. Chem.*, 2001, **496**, 21–28.

29 B. R. Ringeisen, E. Henderson, P. K. Wu, J. Pietron, R. Ray, B. Little, J. C. Biffinger and J. M. Jones-Meehan, *Environ. Sci. Technol.*, 2006, **40**, 2629–34.

30 H. Yi, K. P. Nevin, B.-C. Kim, A. E. Franks, A. Klimes, L. M. Tender and D. R. Lovley, *Biosens.*

Bioelectron., 2009, **24**, 3498–503.

31 R. A. Bouhenni, G. J. Vora, J. C. Biffinger, S. Shirodkar, K. Brockman, R. Ray, P. Wu, B. J. Johnson, E. M. Biddle, M. J. Marshall, L. A. Fitzgerald, B. J. Little, J. K. Fredrickson, A. S. Beliaev, B. R. Ringeisen and D. A. Saffarini, *Electroanalysis*, 2010, **22**, 856–864.

32 Y. Xiong, L. Shi, B. Chen, M. U. Mayer, B. H. Lower, Y. Londer, S. Bose, M. F. Hochella, J. K. Fredrickson and T. C. Squier, *J. Am. Chem. Soc.*, 2006, **128**, 13978–9.

33 D. R. Lovley, *Annu. Rev. Microbiol.*, 2012, **66**, 391–409.

34 H. von Canstein, J. Ogawa, S. Shimizu and J. R. Lloyd, *Appl. Environ. Microbiol.*, 2008, **74**, 615–23.

35 E. Marsili, D. B. Baron, I. D. Shikhare, D. Coursolle, J. a Gralnick and D. R. Bond, *Proc. Natl. Acad. Sci. U. S. A.*, 2008, **105**, 3968–73.

36 T. J. Beveridge, I. S. Chang, B. H. Kim, S. Kim, D. E. Culley, S. B. Reed, F. Margaret, D. A. Saffarini, E. A. Hill, L. Shi, A. Dwayne, Y. A. Gorby, S. Yanina, J. S. Mclean, K. M. Rosso, D. Moyles, A. Dohnalkova, K. S. Kim, M. F. Romine, D. A. Elias and D. W. Kennedy, *Proc. Natl. Acad. Sci.*, 2009, **106**, 9535–9535.

37 M. Y. El-Naggar, G. Wanger, K. M. Leung, T. D. Yuzvinsky, G. Southam, J. Yang, W. M. Lau, K. H. Nealson and Y. a Gorby, *Proc. Natl. Acad. Sci. U. S. A.*, 2010, **107**, 18127–31.

38 J. C. B. Fitzgerald, Lisa A., Emily R. Petersen, Richard I. Ray, Brenda J. Little, Candace J. Cooper, Erinn C. Howard, Bradley R. Ringeisen, *Process Biochem.*, 2012, **47**, 170–174.

39 E. Labelle and D. R. Bond, in *Bio-electrochemical systems: from extracellular electron transfer to biotechnological application*, ed. D. I. P. Lens, Integrated Environmental Technology Series, The Netherlands, 2009, pp. 1–9.

40 Y. Liu and D. R. Bond, *ChemSusChem*, 2012, **5**, 1047–53.

41 K. A. Weber, L. A. Achenbach and J. D. Coates, *Nat. Rev.*, 2006, **4**, 752–764.

42 O. Bretschger, A. Obraztsova, C. a Sturm, I. S. Chang, Y. a Gorby, S. B. Reed, D. E. Culley, C. L. Reardon, S. Barua, M. F. Romine, J. Zhou, A. S. Beliaev, R. Bouhenni, D. Saffarini, F. Mansfeld, B.-H. Kim, J. K. Fredrickson and K. H. Nealson, *Appl. Environ. Microbiol.*, 2007, **73**, 7003–7012.

43 I. Schröder, E. Johnson and S. De Vries, *FEMS Microbiol. Rev.*, 2003, **27**, 427–447.

44 L. E. P. Dietrich, A. Price-whelan, A. Petersen, M. Whiteley and D. K. Newman, *Mol. Microbiol.*, 2006, **61**, 1308–1321.

45 R. W. Bradley, P. Bombelli, S. J. L. Rowden and C. J. Howe, *Biochem. Soc. Trans.*, 2012, **40**, 1302–1307.

46 A. J. McCormick, P. Bombelli, R. W. Bradley, R. Thorne, T. Wenzel and C. J. Howe, *Energy Environ. Sci.*, 2015, **0**, 1–18.

47 R. W. Bradley, P. Bombelli, D. J. Lea-Smith and C. J. Howe, *Phys. Chem. Chem. Phys.*, 2013, **15**, 13611.

48 A. Anderson, Anuphon, I. K. Blaby, P. Bombelli, C. J. Howe, S. S. Merchant, J. M. Davies and A. G. Smith, *Plant Biotechnol. J.*, 2016, **14**, 22–28.

49 F. Zhao, R. C. T. Slade and J. R. Varcoe, *Chem. Soc. Rev.*, 2009, **38**, 1926–1939.

50 Teaching Notes: Applied Electrochemistry, A. C. Fisher. At: http://www.ceb.cam.ac.uk/research/groups/rg-eme/teaching-notes/introduction-403

51 A. J. Bard and L. R. Faulkner, *Electrochemical Methods: Fundamentals and Applications*, John Wiley & Sons, New York, 2nd ed., 2001.

52 R. J. Thorne, K. Schneider, H. Hu and P. J. Cameron, *Bioelectrochemistry*, 2015, **105**, 103–109.

53 H. A. Heering, J. Hirst, L. J. C. Jeuken, F. A. Armstrong, J. P. Mcevoy, A. K. Jones and C. Le, *Faraday Discuss.*, 2000, **116**, 191–203.

54 F. Harnisch and S. Freguia, *Chem. Asian J.*, 2012, **7**, 466–75.

55 E. Marsili, J. B. Rollefson, D. B. Baron, R. M. Hozalski and D. R. Bond, *Appl. Environ. Microbiol.*, 2008, **74**, 7329–37.

56 D. Baron, E. LaBelle, D. Coursolle, J. a Gralnick and D. R. Bond, *J. Biol. Chem.*, 2009, **284**, 28865–73.

57 S. Srikanth, E. Marsili, M. C. Flickinger and D. R. Bond, 2008, **99**, 1065–1073.

58 E. Marsili, J. Sun and D. R. Bond, *Electroanalysis*, 2010, **22**, 865–874.

59 S. M. Strycharz, A. P. Malanoski, R. M. Snider, H. Yi, D. R. Lovley and L. M. Tender, *Energy Environ. Sci.*, 2011, **4**, 896–913.

60 K. Watanabe, *J. Biosci. Bioeng.*, 2008, **106**, 528–36.

61 S. Ishii, K. Watanabe, S. Yabuki, B. E. Logan and Y. Sekiguchi, *Appl. Environ. Microbiol.*, 2008, **74**, 7348–55.

62 C. I. Torres, A. K. Marcus, H.-S. Lee, P. Parameswaran, R. Krajmalnik-Brown and B. E. Rittmann, *FEMS Microbiol. Rev.*, 2010, **34**, 3–17.

63 I. Ieropoulos, J. Greenman and C. Melhuish, *Int. J. Energy Res.*, 2008, **32**, 1228–1240.

64 Y. R. J. Thomas, M. Picot, A. Carer, O. Berder, O. Sentieys and F. Barrière, *J. Power Sources*, 2013, **241**, 703–708.

65 I. Ieropoulos, J. Winfield and J. Greenman, *Bioresour. Technol.*, 2010, **101**, 3520–3525.

66 C. I. Torres, R. Krajmalnik-Brown, P. Parameswaran, A. K. Marcus, G. Wanger, Y. a Gorby and B. E. Rittmann, *Environ. Sci. Technol.*, 2009, **43**, 9519–24.

67 V. J. Watson and B. E. Logan, *Biotechnol. Bioeng.*, 2010, **105**, 489–98.

68 S. Oh, B. Min and B. E. Logan, *Environ. Sci. Technol.*, 2004, **38**, 4900–4904.

69 B. E. Logan, *Nat. Rev. Microbiol.*, 2009, **7**, 375–81.

70 B. E. Logan, M. J. Wallack, K. Y. Kim, W. He, Y. Feng and P. E. Saikaly, *Environ. Sci. Technol. Lett.*, 2015, **2**, 206–214.

71 Y.-F. C. Vanita Roshan Nimje, Chien-Yen Chen, Hau-Ren Chen, Chien-Cheng Chen, Yuh Ming Huang, Min-Jen Tseng, Kai-Chien Cheng, *Bioresour. Technol.*, 2012, **104**, 315–323.

72 Y. Fan, S.-K. Han and H. Liu, *Energy Environ. Sci.*, 2012, **5**, 8273–8280.

73 Z. He, J. Kan, F. Mansfeld, L. T. Angenent and K. H. Nealson, *Environ. Sci. Technol.*, 2009, **43**, 1648–54.

74 D. P. B. T. B. Strik, R. A. Timmers, M. Helder, K. J. J. Steinbusch, H. V. M. Hamelers and C. J. N. Buisman, *Trends Biotechnol.*, 2011, **29**, 41–49.

75 L. Darus, T. Sadakane, P. Ledezma, S. Tsujimura, I. Osadebe, D. Leech, L. Gorton and S. Freguia, *J. Electrochem. Soc.*, 2017, **164**, H3037–H3040.

76 R. Chandra, G. V. Subhash and S. V. Mohan, *Bioresour. Technol.*, 2012, **109**, 46–56.

77 D. Xing, S. Cheng, J. M. Regan and B. E. Logan, *Biosens. Bioelectron.*, 2009, **25**, 105–11.

78 T. Yagishita, S. Sawayama, K. Tsukahara and T. Ogi, *J. Biosci. Bioeng.*, 1999, **88**, 210–214.

79 Y. Wu, Z. Wang, Y. Zheng, Y. Xiao, Z. Yang and F. Zhao, *Appl. Energy*, 2014, **116**, 86–90.

80 K. Nishio, K. Hashimoto and K. Watanabe, *Appl. Microbiol. Biotechnol.*, 2010, **86**, 957–64.

81 M. Helder, D. P. B. T. B. Strik, H. V. M. Hamelers, a J. Kuhn, C. Blok and C. J. N. Buisman, *Bioresour. Technol.*, 2010, **101**, 3541–7.

82 A. E. Kirkwood, C. Nalewajko and R. R. Fulthorpe, *Microb. Ecol.*, 2006, **51**, 4–12.

83 A. J. McCormick, B. Paolo, R. W. Bradley, R. Thorne, T. Wenzel and C. J. Howe, *Energy Environ. Sci.*, 2015, **8**, 1092–1109.

84 L. Darus, P. Ledezma, J. Keller and S. Freguia, *Environ. Sci. Technol.*, 2014, **48**, 14000–14006.

85 D. Xing, Y. Zuo, S. Cheng, J. M. Regan and B. E. Logan, *Environ. Sci. Technol.*, 2008, **42**, 4146–51.

86 J. P. Badalamenti, C. I. Torres and R. Krajmalnik-Brown, *Biotechnol. Bioeng.*, 2013, **110**, 1020–7.

87 X. A. Walter, J. Greenman and I. A. Ieropoulos, *ALGAL*, 2013, **2**, 183–187.

88 I. Gajda, J. Greenman, C. Melhuish and I. Ieropoulos, *Int. J. Hydrogen Energy*, 2013, **38**, 11559–11564.

89 M. Zhou, H. He, T. Jin and H. Wang, *J. Power Sources*, 2012, **214**, 216–219.

90 A. E. Inglesby, D. a. Beatty and A. C. Fisher, *RSC Adv.*, 2012, **2**, 4829.

91 D. P. B. T. B. Strik, H. Terlouw, H. V. M. Hamelers and C. J. N. Buisman, *Appl. Microbiol. Biotechnol.*, 2008, **81**, 659–68.

92 F.-L. Ng, M. M. Jaafar, S.-M. Phang, Z. Chan, N. A. Salleh, S. Z. Azmi, K. Yunus, A. C. Fisher and V. Periasamy, *Sci. Rep.*, 2014, **4**, 7562.

93 N. Schuergers, C. Werlang, C. M. Ajo-Franklin and A. A. Boghossian, *Energy Environ. Sci.*, 2017, **10**, 1102–1115.

94 C.-C. Fu, T.-C. Hung, W.-T. Wu, T.-C. Wen and C.-H. Su, *Biochem. Eng. J.*, 2010, **52**, 175–180.

95 P. Bombelli, M. Thomas, T. W. Herling, C. J. Howe and P. J. Tuomas, *Adv. Energy Mater.*, 2015, **5**, 1--6.

96 K. Nishio, K. Hashimoto and K. Watanabe, *J. Biosci. Bioeng.*, 2013, **115**, 412–7.

97 J. C.-W. Lan, K. Raman, C.-M. Huang and C.-M. Chang, *Biochem. Eng. J.*, 2013, **78**, 39–43.

98 F.-L. Ng, S.-M. Phang, V. Periasamy, K. Yunus and A. C. Fisher, *PLoS One*, 2014, **9**, e97643.

99 N. Sekar, R. Jain, Y. Yan and R. P. Ramasamy, *Biotechnol. Bioeng.*, 2016, **113**, 675–679.

100 A. J. McCormick, P. Bombelli, D. J. Lea-Smith, R. W. Bradley, A. M. Scott, A. C. Fisher, A. G. Smith and C. J. Howe, *Energy Environ. Sci.*, 2013, **6**, 2682.

101 A. E. Inglesby, K. Yunus and A. C. Fisher, *Phys. Chem. Chem. Phys.*, 2013, **15**, 6903–11.

102 Y. Zou, J. Pisciotta, R. B. Billmyre and I. V Baskakov, *Biotechnol. Bioeng.*, 2009, **104**, 939–46.

103 S. Malik, E. Drott, P. Grisdela, J. Lee, C. Lee, D. a. Lowy, S. Gray and L. M. Tender, *Energy Environ. Sci.*, 2009, **2**, 292.

104 J. M. Pisciotta, Y. Zou and I. V Baskakov, *PLoS One*, 2010, **5**, e10821.

105 C.-C. Lin, C.-H. Wei, C.-I. Chen, C.-J. Shieh and Y.-C. Liu, *Bioresour. Technol.*, 2013, **135**, 640–643.

106 C.-C. Fu, C.-H. Su, T.-C. Hung, C.-H. Hsieh, D. Suryani and W.-T. Wu, *Bioresour. Technol.*, 2009, **100**, 4183–6.

107 A. Cereda, A. Hitchcock, M. D. Symes, L. Cronin, T. S. Bibby and A. K. Jones, *PLoS One*, 2014, **9**, 1–8.

108 M. Billini, K. Stamatakis and V. Sophianopoulou, *J. Bacteriol.*, 2008, **190**, 6318–6329.

109 J. E. O'Reilly, *BBA - Bioenerg.*, 1973, **292**, 509–515.

110 R. J. Thorne, H. Hu, K. Schneider and P. J. Cameron, *Phys. Chem. Chem. Phys.*, 2014, **16**, 5810–6.

111 A. Laohavisit, A. Anderson, P. Bombelli, M. Jacobs, C. J. Howe, J. M. Davies and A. G. Smith, *Algal Res.*, 2015, **12**, 91–98.

112 S. Ho, C. Chen and J. Chang, *Bioresour. Technol.*, 2012, **113**, 244–252.

113 J. A. Lynnes, T. L. M. Derzaph and H. G. Weger, *Planta*, 1998, **204**, 360–365.

114 J. K. Middlemiss, A. M. Anderson, C. W. Stratilo and H. G. Weger, *J. Phycol.*, 2001, **37**, 393–399.

115 G. Rabotti and G. Zocchi, *Physiol. Plant.*, 1994, **90**, 779–785.

116 X. Xue, C. M. Collins, H. G. Weger and A. Fecn-r, *J. Phycol.*, 1998, **34**, 939–944.

117 B.D. Lee, W. A. Apel, M.R. Walton. At: https://www.netl.doe.gov/publications/proceedings/04/carbon-seq/179.pdf

118 H. Takano, H. Takeyama, N. Nakamura, K. Sode, J. G. Burgess, E. Manabe, M. Hirano and T. Matsunaga, *Appl. Biochem. Biotechnol.*, 1992, **34–35**, 449–458.

119 T. Sasaki, N. Kurano and S. Miyachi, 1998, **39**, 405–410.

120 C. W. Jin, S. T. Du, W. W. Chen, G. X. Li, Y. S. Zhang and S. J. Zheng, *Plant Physiol.*, 2009, **150**, 272–280.

121 M. Liberton, R. Howard Berg, J. Heuser, R. Roth and H. B. Pakrasi, *Protoplasma*, 2006, **227**, 129–138.

122 B. E. Schirrmeister, M. Gugger and P. C. J. Donoghue, *Palaeontology*, 2015, **58**, 769–785.

123 B. Hankamer, E. Morris, J. Nield, A. Carne and J. B. Y, *FEBS Lett.*, 2001, **504**, 142–151.

124 D. A. Bryant, *The Molecular Biology of Cyanobacteria Volume I and II*, Springer-Science+Business Media. B.V., 1994.

125 D. J. Lea-Smith, P. Bombelli, R. Vasudevan and C. J. Howe, *Biochim. Biophys. Acta - Bioenerg.*, 2016, **1857**, 247–255.

126 D. J. Lea-smith, N. Ross, M. Zori, D. S. Bendall, J. S. Dennis, S. A. Scott, A. G. Smith and C. J. Howe, *Plant Physiol.*, 2013, **162**, 484–495.

127 P. Jordan, P. Fromme, H. T. Witt, O. Klukas, W. Saenger and N. Krauû, *Nature*, 2001, **411**, 909–917.

128 V. Chukhutsina, L. Bersanini, E.-M. Aro and H. van Amerongen, *Sci. Rep.*, 2015, **5**, 1–10.

129 Y. Fujita and A. Murakami, *Plant Cell Physiol.*, 1987, **28**, 1547–1553.

130 A. Satoh, N. Kurano, H. Senger and S. Miyachi, *Plant Cell Physiol.*, 2002, **43**, 440–451.

131 G. Ajlani, J. Verbavatz, I. Vass, C. A. Kerfeld and D. Kirilovsky, *Plant Cell*, 2006, **18**, 992–1007.

132 F. Ferreira and N. A. Straus, *J. Appl. Phycol.*, 1994, **6**, 199–210.

133 J. A. Raven, M. C. W. Evans and R. E. Korb, *Photosynth. Res.*, 1999, **60**, 111–149.

134 H. Lis, C. Kranzler, N. Keren and Y. Shaked, *Life (Basel, Switzerland)*, 2015, **5**, 841–60.

135 B. K. Semin, L. N. Davletshina, A. a Novakova, T. Y. Kiseleva, V. Y. Lanchinskaya, A. Y. Aleksandrov, N. Seifulina, I. I. Ivanov, M. Seibert and A. B. Rubin, *Plant Physiol.*, 2003, **131**, 1756–1764.

136 J. J. Lamb, R. E. Hill, J. J. Eaton-Rye and M. F. Hohmann-Marriott, *PLoS One*, 2014, **9**, e105761.

137 R. J. Ritchie, *Photosynth. Res.*, 2006, **89**, 27–41.

138 M. W. M. W. Sutherland and B. A. B. A. Learmonth, *Free Radic. Res.*, 1997, **27**, 283–289.

139 F. Huang, E. Hedman, C. Funk, T. Kieselbach, W. P. Schröder and B. Norling, *Mol. Cell. Proteomics*, 2004, **3**, 586–595.

140 G. L. Peterson, *Anal. Biochem.*, 1977, **83**, 346–356.

141 I. a. Ieropoulos, J. Greenman, C. Melhuish and J. Hart, *Enzyme Microb. Technol.*, 2005, **37**, 238–245.

142 A. J. Bombelli, P., Zarrouati, M., Thorne, R.J., Schneider, K., Rowden, S.J. L., Ali, A., Yunus, K., Cameron, P.J., Fisher, A.C., Wilson, D.I, Howe, C.J., and McCormick, *Phys. Chem. chem.phys. PCCP*, 2012, **14**, 12221–9.

143 M. Aklujkar, M. V. Coppi, C. Leang, B. C. Kim, M. A. Chavan, L. A. Perpetua, L. Giloteaux, A. Liu and D. E. Holmes, *Microbiol. (United Kingdom)*, 2013, **159**, 515–535.

144 J. N. Roy, K. E. Garcia, H. R. Luckarift, A. Falase, J. Cornejo, S. Babanova, A. J. Schuler, G. R. Johnson and P. B. Atanassov, *J. Electrochem. Soc.*, 2013, **160**, 866–871.

145 D. Coursolle, D. B. Baron, D. R. Bond and J. a Gralnick, *J. Bacteriol.*, 2010, **192**, 467–74.

146 J. C. Biffinger, J. N. Byrd, B. L. Dudley and B. R. Ringeisen, *Biosens. Bioelectron.*, 2008, **23**, 820–6.

147 J. C. Biffinger, R. Ray, B. J. Little, L. a Fitzgerald, M. Ribbens, S. E. Finkel and B. R. Ringeisen, *Biotechnol. Bioeng.*, 2009, **103**, 524–31.

148 E. Hoiczyk and A. Hansel, *J. Bacteriol.*, 2000, **182**, 1191–1199.

149 H. G. Gerken, B. Donohoe and E. P. Knoshaug, *Planta*, 2013, **237**, 239–253.

150 X. Zhang, K. H. Krause, I. Xenarios, T. Soldati and B. Boeckmann, *PLoS One*, 2013, **8**, e58126.

151 N. Sekar, Y. Umasankar and R. P. Ramasamy, *Phys. Chem. Chem. Phys.*, 2014, **16**, 7862–71.

152 S. Kaushik, M. K. Sarma and P. Goswami, *J. Mater. Chem. A*, 2017, **5**, 7885–7895.

153 H.-Y. Wang, A. Bernarda, C.-Y. Huang, D.-J. Lee and J.-S. Chang, *Bioresour. Technol.*, 2011, **102**, 235–43.

154 H. Lee and S. Choi, *Lab Chip*, 2015, **15**, 391–398.

155 *Bioresour. Technol.*, 2013, **142**, 672–682.

156 G. Kim, K. Eom, M. Kim, S. J. Yoo, J. H. Jang, H. J. Kim and E. Cho, *ACS Appl. Mater. Interfaces*, 2015, **7**, 27581–27585.

157 B. Erable, N. M. Duţeanu, M. M. Ghangrekar, C. Dumas and K. Scott, *Biofouling*, 2010, **26**, 57–71.

158 K. J. Kim, S.-W. Lee, T. Yim, J.-G. Kim, J. W. Choi, J. H. Kim, M.-S. Park and Y.-J. Kim, *Sci. Rep.*, 2014, **4**, 6906.

159 M. V. Naseh, A. A. Khodadadi, Y. Mortazavi, F. Pourfayaz, O. Alizadeh and M. Maghrebi, *Carbon N. Y.*, 2010, **48**, 1369–1379.

160 D. Dixon, D. J. Babu, J. Langner, M. Bruns, L. Pfaffmann, A. Bhaskar, J. J. Schneider, F. Scheiba and H. Ehrenberg, *J. Power Sources*, 2016, **332**, 240–248.

161 V. Flexer, M. Marque, B. C. Donose, B. Virdis and J. Keller, *Electrochim. Acta*, 2013, **108**, 566–574.

162 M. Epifanio, S. Inguva, M. Kitching, J. P. Mosnier and E. Marsili, *Bioelectrochemistry*, 2015, **106**, 186–193.

163 H. B. A. Prins and J. T. M. Elzenga, *Aquat. Bot.*, 1989, **34**, 59–83.

164 F. Qian, M. Baum, Q. Gu and D. E. Morse, *Lab Chip*, 2009, **9**, 3076–3081.

165 S. H. Lee, J. Y. Ban, C. Oh, H. Park and S. Choi, *Sci. Rep.*, 2016, **6**, 1–10.

166 J. C. Biffinger, J. Pietron, O. Bretschger, L. J. Nadeau, G. R. Johnson, C. C. Williams, K. H. Nealson and B. R. Ringeisen, *Biosens. Bioelectron.*, 2008, **24**, 900–905.

167 F. C. T. Allnutt and W. D. Bonner, *J. Plant Nutr.*, 1984, **7**, 427–435.

168 L. Liu and S. Choi, *J. Power Sources*, 2017, **348**, 138–144.

169 S. G. Hays, L. L. W. Yan, P. A. Silver and D. C. Ducat, *J. Biol. Eng.*, 2017, **11**, 4.

170 H. Niederholtmeyer, B. T. Wolfstädter, D. F. Savage, P. a Silver and J. C. Way, *Appl. Environ. Microbiol.*, 2010, **76**, 3462–6.

171 S. W. Wilhelm, *Aquat. Microb. Ecol.*, 1995, **9**, 295–303.

172 S. Miyachi, J. Burger, K. Kotzabasis, J. Thielmann and H. Senger, *Z Naturforsch C*, 1996, **51**, 40–46.

173 S. Sandström, A. G. Ivanov, Y.-I. Park, G. Oquist and P. Gustafsson, *Physiol. Plant.*, 2002, **116**, 255–263.

174 I. Iwasaki, Q. Hu, N. Kurano and S. Miyachi, *J. Photochem. Photobiol. B Biol.*, 1998, **44**, 184–190.

175 K. H. Wedepohl, *Geochim. Cosmochim. Acta*, 1995, **59**, 1217–1232.

176 Z. Hu and S. Gao, *Chem. Geol.*, 2008, **253**, 205–221.

177 J. D. Hem, *Geol. Soc. Am. Bull.*, 1972, **83**, 443–450.

178 D. Channei, S. Phanichphant, A. Nakaruk, S. Mofarah, P. Koshy and C. Sorrell, *Catalysts*, 2017, **7**, 45.

179 N. J. Robinson, C. M. Procter, E. L. Connolly and M. L. Guerinot, *Nature*, 1999, **397**, 694–697.

180 J. Rodríguez-Celma and W. Schmidt, *Plant Signal. Behav.*, 2013, **8**, e26116.

181 W. Schmidt, *New Phytol.*, 1999, **141**, 1–26.

182 U. Eckhardt and T. J. Buckhout, *J. Exp. Bot.*, 1998, **49**, 1219–1226.

183 S. W. Wilhelm and C. G. Trick, *Limnol. Oceanogr.*, 1994, **39**, 1979–1984.

184 S. W. Wilhelm, D. P. Maxwell and C. G. Trick, *Limnol. Oceanogr.*, 1996, **41**, 89–97.

185 R. Raghuvanshi, S. Singh and P. S. Bisen, *Indian J. Exp. Biol.*, 2007, **45**, 563–7.

186 C. Kranzler, H. Lis, Y. Shaked and N. Keren, *Environ. Microbiol.*, 2011, **13**, 2990–2999.

187 C. Kranzler, H. Lis, O. M. Finkel, G. Schmetterer, Y. Shaked and N. Keren, *ISME J.*, 2014, **8**, 409–17.

188 H.-B. Jiang, W.-J. Lou, W.-T. Ke, W.-Y. Song, N. M. Price and B.-S. Qiu, *ISME J.*, 2015, **9**, 297–309.

189 M. D. Allen, J. A. Del Campo, J. Kropat and S. S. Merchant, *Eukaryot. Cell*, 2007, **6**, 1841–1852.

190 A. Anderson, J. H. Bothwell, A. Laohavisit, A. G. Smith and J. M. Davies, *Trends Plant Sci.*, 2011, **16**, 579–581.

191 A. L. Rose and T. D. Waite, *Geochim. Cosmochim. Acta*, 2006, **70**, 3869–3882.

192 A. L. Rose, T. P. Salmon, T. Lukondeh, B. a. Neilan and T. D. Waite, *Environ. Sci. Technol.*, 2005, **39**, 3708–3715.

193 M. Fujii, A. L. Rose, T. Omura and T. D. Waite, *Environ. Sci. Technol.*, 2010, **44**, 1980–1986.

194 a. G. Ivanov, Y.-I. Park, E. Miskiewicz, J. a. Raven, N. P. a. Huner and G. Öquist, *FEBS Lett.*, 2000, **485**, 173–177.

195 K. Michel and E. Pistorius, *Physiol. Plant.*, 2004, **120**, 36–50.

196 N. Yousef, E. K. Pistorius and K.-P. Michel, *Arch. Microbiol.*, 2003, **180**, 471–83.

197 A. Nodop, D. Pietsch, R. Höcker, A. Becker, E. K. Pistorius, K. Forchhammer and K.-P. Michel, *Plant Physiol.*, 2008, **147**, 747–763.

198 K.-P. Michel, E. K. Pistorius and S. S. Golden, *J. Bacteriol.*, 2001, **183**, 5015–5024.

199 E. J. Boekema, A. Hifney, a E. Yakushevska, M. Piotrowski, W. Keegstra, S. Berry, K. P. Michel, E. K. Pistorius and J. Kruip, *Nature*, 2001, **412**, 745–748.

200 D. M. Sherman and L. A. Sherman, *J. Bacteriol.*, 1983, **156**, 393–401.

201 C. G. Trick and A. Kerry, *Curr. Microbiol.*, 1992, **24**, 241–245.

202 H. B. Jiang, W. J. Lou, H. Y. Du, N. M. Price and B. S. Qiu, *Plant Cell Physiol.*, 2012, **53**, 1404–1417.

203 E. Alcantara, M. D. De Guardia, F. J. Romera, M. D. Delaguardia, E. Alcántara and M. D. de la Guardia, *Plant Physiol.*, 1991, **96**, 1034–1037.

204 M. S. Davey, D. J. Suggett, R. J. Geider and A. R. Taylor, 2003, **1144**, 1132–1144.

205 W. Schmidt, W. Michalke and A. Schikora, *Plant, Cell Environ.*, 2003, **26**, 361–370.

206 D. M. Rawson, A. J. Willmer and P. F. Turner, 1989, **4**, 299–311.

207 H. G. Weger and G. S. Espie, *Planta*, 2000, **210**, 775–81.

208 J. Yu, M. Liberton, P. F. Cliften, R. D. Head, J. M. Jacobs, R. D. Smith, D. W. Koppenaal, J. J. Brand and H. B. Pakrasi, *Sci. Rep.*, 2015, **5**, 8132.

209 A. G. Ivanov, M. Krol, E. Selstam, P. V. Sane, D. Sveshnikov, Y. Il Park, G. Öquist and N. P. A. Huner, *Biochim. Biophys. Acta*, 2007, **1767**, 807–813.

210 R. E. Hancock, *J. Bacteriol.*, 1987, **169**, 929–933.

211 M. R. Badger and G. D. Price, *J. Exp. Bot.*, 2003, **54**, 609–622.

212 S. Santi and W. Schmidt, *New Phytol.*, 2009, **183**, 1072–1084.

213 E. Yeager, *J. Mol. Catal.*, 1986, **38**, 5–25.

214 C. S. P. Silva, M. E. Silva-Stenico, M. F. Fiore, H. F. De Castro and P. C. M. Da Ros, *Algal Res.*, 2014, **3**, 1–7.

215 L. Rosgaard, A. J. de Porcellinis, J. H. Jacobsen, N.-U. Frigaard and Y. Sakuragi, *J. Biotechnol.*, 2012, **162**, 134–47.

216 A. J. Kaufman and S. Xiao, *Nature*, 2003, **425**, 279–282.

217 R. E. Kopp, J. L. Kirschvink, I. A. Hilburn and C. Z. Nash, *Proc. Natl. Acad. Sci.*, 2005, **102**, 11131–11136.

218 Brian Kahn, *Clim. Cent. - Sci. Am.*, 2017.

219 S. Cha, H.-M. Chae, S.-H. Lee and J.-K. Shim, *PLoS One*, 2017, **12**, 1–19.

220 N. Lotfiomran, M. Köhl and J. Fromm, *Plants*, 2016, **5**, 1–13.

221 U. Riebesell, K. G. Schulz, R. G. J. Bellerby, M. Botros, P. Fritsche, M. Meyerhöfer, C. Neill, G. Nondal, A. Oschlies, J. Wohlers and E. Zöllner, *Nature*, 2007, **450**, 545–548.

222 F. X. Fu, M. E. Warner, Y. Zhang, Y. Feng and D. A. Hutchins, *J. Phycol.*, 2007, **43**, 485–496.

223 A. Wingler, P. J. Lea, W. P. Quick and R. C. Leegood, *Philos. Trans. R. Soc. B Biol. Sci.*, 2000, **355**, 1517–1529.

224 M. R. Badger and G. D. Price, *J. Exp. Bot.*, 2003, **54**, 609–622.

225 M. R. Badger and G. D. Price, *Physiol. Plant.*, 1992, **84**, 606–615.

226 H. Fukuzawa, S. Fujiwara, Y. Yamamoto, M. L. Dionisio-Sese and S. Miyachi, *Proc. Natl. Acad. Sci. U. S. A.*, 1990, **87**, 4383–4387.

227 K. Aizawa and S. Miyachi, *FEMS Microbiol Rev*, 1986, **39**, 215–233.

228 J. Burger, S. Miyachi, P. Galland and H. Senger, *Bot. Acta*, 1988, **101**, 229–232.

229 I. Pesheva, M. Kodama, M. L. Dionisio-Sese and S. Miyachi, 1994, **35**, 379–387.

230 A. Satoh, N. Kurano and S. Miyachi, *Photosynth. Res.*, 2001, **68**, 215–224.

231 D. J. Thomas, S. L. Sullivan, A. L. Price and S. M. Zimmerman, *Astrobiology*, 2005, **5**, 66–74.

232 M. R. Badger, K. Palmqvist and J. ???W Yu, *Physiol. Plant.*, 1994, **90**, 529–536.

233 D. Schwarz, A. Nodop, J. Huge, S. Purfurst, K. Forchhammer, K.-P. Michel, H. Bauwe, J. Kopka and M. Hagemann, *Plant Physiol.*, 2011, **155**, 1640–1655.

234 S. Kajiwara, H. Yamada, N. Ohkuni and K. Ohtaguchi, *Energy Convers. Manag.*, 1997, **38**, 529–532.

235 D. Kuan, University of British Columbia, 2013.

236 K. S. Madiraju, D. Lyew, R. Kok and V. Raghavan, *Bioresour. Technol.*, 2012, **110**, 214–218.

237 T. Sasaki, N. Kurano and S. Miyachi, *Plant Cell Physiol.*, 1998, **39**, 131–138.

238 W. J. Henley and J. Ramus, *Mar. Biol.*, 1989, **103**, 261–266.

239 A. F. Post, R. de Wit and L. R. Mur, *J. Plankton Res.*, 1985, **7**, 487–495.

240 N. Soltani, R. A. Khavari-Nejad, M. T. Yazdi, S. Shokravi and E. Fernández-Valiente, *World J. Microbiol. Biotechnol.*, 2006, **22**, 571–576.

241 J. N. Morris, J. J. Eaton-Rye and T. C. Summerfield, *Front. Plant Sci.*, 2016, **7**, 1–8.

242 C. R. Myers and J. M. Myers, *Appl. Environ. Microbiol.*, 2002, **68**, 5585–5594.

243 A. S. Beliaev and D. A. Saffarini, *J. Bacteriol.*, 1998, **180**, 6292–6297.

244 M. A. Firer-sherwood, N. Ando, C. L. Drennan and S. J. Elliott, *J. Phys. Chem. B*, 2011, **115**,

11208–11214.

245 T. M. Maier, J. M. Myers, C. R. Myers and C. R. Myers, *J. Basic Microbiol*, 2003, **43**, 312–327.

246 T. M. Maier and C. R. Myers, *BMC Microbiol.*, 2004, **4**, 23.

247 K. Hasan, H. Bekir Yildiz, E. Sperling, P. O Conghaile, M. a Packer, D. Leech, C. Hägerhäll and L. Gorton, *Phys. Chem. Chem. Phys.*, 2014, **16**, 24676–80.

248 L. Peng, S.-J. You and J.-Y. Wang, *Biosens. Bioelectron.*, 2010, **25**, 2530–3.

249 E. Environ, D. Pocaznoi, A. Calmet, L. Etcheverry, B. Erable and A. Bergel, *Energy Environ. Sci.*, 2012, **5**, 9645–9652.

250 Y. Zou, J. Pisciotta and I. V Baskakov, *Bioelectrochemistry*, 2010, **79**, 50–6.

251 P. Bombelli, M. Zarrouati, R. J. Thorne, K. Schneider, S. J. L. Rowden, A. Ali, K. Yunus, P. J. Cameron, A. C. Fisher, D. Ian Wilson, C. J. Howe and A. J. McCormick, *Phys. Chem. Chem. Phys.*, 2012, **14**, 12221.

252 C. Leang, X. Qian, T. Mester and D. R. Lovley, *Appl. Environ. Microbiol.*, 2010, **76**, 4080–4084.

253 J. Hirst and F. A. Armstrong, *Anal. Chem.*, 1998, **70**, 5062–5071.

254 H. Nikaido, *Microbiol. Mol. Biol. Rev.*, 2003, **67**, 593–656.

255 R. Koebnik, K. P. Locher and P. Van Gelder, *Mol. Microbiol.*, 2000, **37**, 239–253.

256 K. D. Tsirigos, A. Elofsson and P. G. Bagos, *Bioinformatics*, 2016, **32**, i665–i671.

257 K. D. Tsirigos, P. G. Bagos and S. J. Hamodrakas, *Nucleic Acids Res.*, 2011, **39**, 324–331.

258 G. von Heijne, *J. Membr. Biol.*, 1990, **115**, 195–201.

259 M. Remmert, D. Linke, A. N. Lupas and J. Söding, *Nucleic Acids Res.*, 2009, **37**, 446–451.

260 S. F. Altschul, T. L. Madden, A. A. Schäffer, J. Zhang, Z. Zhang, W. Miller and D. J. Lipman, *Nucleic Acids Res.*, 1997, **25**, 3389–3402.

261 S. Mesnage, T. Fontaine, T. Mignot, M. Delepierre, M. Mock and A. Fouet, *EMBO J.*, 2000, **19**,

4473–4484.

262 A. Kosugi, K. Murashima, Y. Tamaru and R. H. Doi, *J. Bacteriol.*, 2002, **184**, 884–888.

263 B. N. Y, E. Zak, B. Andersson and H. Pakrasi, 1998, **436**, 189–192.

264 J. C. Guimaraes, M. Rocha and A. P. Arkin, *Nucleic Acids Res.*, 2014, **42**, 4791–4799.

265 C. Vogel and E. M. Marcotte, *Nat. Rev. Genet.*, 2013, **13**, 227–232.